UNIVERSITAT POLITÈCNICA
DE CATALUNYA

Ph.D. Thesis

Design of Static Intercell Interference Coordination Schemes for Realistic LTE-based Cellular Networks

Author: David González G

Advisors: Mario García-Lozano, Ph. D.
Associate Professor
Universitat Politècnica de Catalunya (UPC)

Silvia Ruiz, Ph. D.
Associate Professor
Universitat Politècnica de Catalunya (UPC)

Wireless Communications and Technologies Research Group
Department of Signal Theory and Communications
Universitat Politècnica de Catalunya

Barcelona, November 2013

Abstract

Today, 3.5 and 4G systems including Long Term Evolution (LTE) and LTE-Advanced (LTE-A) support packet-based services and provide mobile broadband access for bandwidth-hungry applications. In this context of fast evolution, new and challenging technical issues must be effectively addressed. The final target is to achieve a significant step forward toward the improvement of the Quality of Experience (QoE). To that end, interference management has been recognized by the industry as a key enabler for cellular technologies based on OFDMA. Indeed, with a low frequency reuse factor, intercell interference (ICI) becomes a major concern since the Quality of Service (QoS) is not uniformly delivered across the network, it remarkably depends on user position. Hence, cell edge performance is an important issue in LTE and LTE-A.

Intercell Interference Coordination (ICIC) encompasses strategies whose goal is to keep ICI at cell edges as low as possible. This alleviates the aforementioned situation. For this reason, the novelties presented in this Ph.D. thesis include not only developments of static ICIC mechanisms for data and control channels, but also efforts towards further improvements of the energy efficiency perspective.

Based on a comprehensive review of the state of the art, a set of research opportunities were identified. To be precise, the need for flexible performance evaluation methods and optimization frameworks for static ICIC strategies. These mechanisms are grouped in two families: the schemes that define constraints on the frequency domain and the ones that propose adjustments on the power levels. Thus, Soft- and Fractional Frequency Reuse (SFR and FFR, respectively) are identified as the base of the vast majority of static ICIC proposals.

Consequently, during the first part of this Ph.D. thesis, interesting insights into the operation of SFR and FFR were identified beyond well-known facts. These studies allow for the development of a novel statistical framework to evaluate the performance of these schemes in realistic deployments. As a result of the analysis, the poor performance of classic configurations of SFR and FFR in real-world contexts is shown, and hence, the need for optimization is established. In addition, the importance of the interworking between static ICIC schemes and other network functionalities such as CSI feedback has also been identified. Therefore, novel CSI feedback schemes, suitable to operate in conjunction with SFR and FFR, have been developed. These mechanisms exploit the resource allocation pattern of these static ICIC techniques in order to improve the accuracy of the CSI feedback process.

The second part is focused on the optimization of SFR and FFR. The use of multiobjective techniques is investigated as a tool to achieve effective network-specific optimization. The approach offers interesting advantages. On the one hand, it allows for simultaneous optimization of several conflicting criteria. On the other hand, the multiobjective nature results in outputs composed of several high quality (Pareto efficient) network configurations, all of them featuring a near-optimal tradeoff between the performance criteria. Multiobjective evolutionary algorithms allow employing complex mathematical structures without the need for relaxation, thus capturing accurately the system behavior in terms of ICI. The multiobjective optimization formulation of the problem aims at achieving effective adjustment of the operational parameters of SFR and FFR both at cell level and network-wide. Moreover, the research was successfully extended to the control channels, both the PDCCH and ePDCCH.

Finally, in an effort to further improve the network energy efficiency (an aspect always considered throughout the thesis), the framework of Cell Switch Off (CSO), having close connections with ICIC, is also introduced. By means of the proposed method, significant improvements with respect to traditional approaches, baseline configurations, and previous proposals can be achieved. The gains are obtained in terms of energy consumption, network capacity, and cell edge performance.

Resumen

Actualmente los sistemas 3.5 y 4G tales como *Long Term Evolution* (LTE) y LTE-*Advanced* (LTE-A) soportan servicios basados en paquetes y proporcionan acceso de banda ancha móvil para aplicaciones que requieren elevadas tasas de transmisión. En este contexto de rápida evolución, aparecen nuevos retos técnicos que deben ser resueltos eficientemente. El objetivo último es conseguir un salto cualitativo importante en la experiencia de usuario (QoE). Con tal fin, un factor clave que ha sido reconocido en las redes celulares basadas en *Orthogonal Frequency-Division Multiple Access* (OFDMA) es la gestión de interferencias. De hecho, la utilización de un factor de reuso bajo permite una elevada eficiencia espectral pero a costa de una distribución de la calidad de servicio (QoS) que no es uniforme en la red, depende de la posición del usuario. Por lo tanto, el rendimiento en los límites de la celda se ve muy penalizado y es un problema importante a resolver en LTE y LTE-A.

La coordinación de interferencias entre celdas (ICIC, del inglés *Intercell Interference Coordination*) engloba las estrategias cuyo objetivo es mantener la interferencia intercelular (ICI) lo más baja posible en los bordes de celda. Esto permite aliviar la situación antes mencionada. La contribución presentada en esta tesis doctoral incluye el diseño de nuevos mecanismos de ICIC estática para los canales de datos y control, así como también mejoras desde el punto de vista de eficiencia energética.

A partir de una revisión completa del estado del arte, se identificaron una serie de retos abiertos que requerían esfuerzos de investigación. En concreto, la necesidad de métodos de evaluación flexibles y marcos de optimización de las estrategias de ICIC estáticas. Estos mecanismos se agrupan en dos familias: los esquemas que definen restricciones sobre el dominio de la frecuencia y los que proponen ajustes en los niveles de potencia. Es decir, la base de la gran mayoría de propuestas ICIC estáticas son la reutilización de frecuencias de tipo *soft* y *fraccional* (SFR y FFR, respectivamente).

De este modo, durante la primera parte de esta tesis doctoral, se han estudiado los aspectos más importantes del funcionamiento de SFR y FFR, haciendo especial énfasis en las conclusiones que van más allá de las bien conocidas. Ello ha permitido introducir un nuevo marco estadístico para evaluar el funcionamiento de estos sistemas en condiciones de despliegue reales. Como resultado de estos análisis, se muestra el pobre desempeño de SFR y FFR en despliegues reales cuando funcionan

con sus configuraciones clásicas y se establece la necesidad de optimización. También se pone de manifiesto la importancia del funcionamiento conjunto entre esquemas ICIC estáticos y otras funcionalidades de la red radio, tales como la información que envían los usuarios sobre el estado de su canal *downlink* (*feedback* del CSI, del inglés *Channel State Information*). De este modo, se han propuesto diferentes esquemas de *feedback* apropiados para trabajar conjuntamente con SFR y FFR. Estos mecanismos explotan el patrón de asignación de recursos que se utiliza en ICIC estático para mejorar la precisión del proceso.

La segunda parte se centra en la optimización de SFR y FFR. Se ha investigado el uso de técnicas multiobjetivo como herramienta para lograr una optimización eficaz, que es específica para cada red. El enfoque ofrece ventajas interesantes, por un lado, se permite la optimización simultánea de varios criterios contradictorios. Por otro lado, la naturaleza multiobjetivo implica obtener como resultado configuraciones de red de elevada calidad (Pareto eficientes), todas ellas con un equilibrio casi-óptimo entre las diferentes métricas de rendimiento. Los algoritmos evolucionarios multiobjetivo permiten la utilización de estructuras matemáticas complejas sin necesidad de relajar el problema, de este modo capturan adecuadamente su comportamiento en términos de ICI. La formulación multiobjetivo consigue un ajuste efectivo de los parámetros operacionales de SFR y FFR, tanto a nivel de celda como a nivel de red. Además, la investigación se extiende con resultados satisfactorios a los canales de control, PDCCH y ePDCCH.

Finalmente, en un esfuerzo por mejorar la eficiencia energética de la red (un aspecto siempre considerado a lo largo de la tesis), se introduce en el análisis global el apagado inteligente de celdas, estrategia con estrechos vínculos con ICIC. A través del método propuesto, se obtienen mejoras significativas con respecto a los enfoques tradicionales y propuestas previas. Las ganancias se obtienen en términos de consumo energético, capacidad de la red, y rendimiento en el límite de las celdas.

Resum

Actualment els sistemes 3.5 i 4G tals com *Long Term Evolution* (LTE) i LTE-*Advanced* (LTE-A) suporten serveis basats en paquets i proporcionen accés de banda ampla mòbil per a aplicacions que requereixen elevades taxes de transmissió. En aquest context de ràpida evolució, apareixen nous reptes tècnics que han de ser resolts eficientment. L'objectiu últim és aconseguir un salt qualitatiu important en l'experiència d'usuari (QoE). Amb tal fi, un factor clau que ha estat reconegut a les xarxes cel·lulars basades en *Orthogonal Frequency-Division Multiple Access* (OFDMA) és la gestió d'interferències. De fet, la utilització d'un factor de reús baix permet una elevada eficiència espectral però a costa d'una distribució de la qualitat de servei (QoS) que no és uniforme a la xarxa, depèn de la posició de l'usuari. Per tant, el rendiment en els límits de la cel·la es veu molt penalitzat i és un problema important a resoldre en LTE i LTE-A.

La coordinació d'interferències entre cel·les (ICIC, de l'anglès *Intercell Interference Coordination*) engloba les estratègies que tenen com a objectiu mantenir la interferència intercel·lular (ICI) el més baixa possible en les vores de la cel·la. Això permet alleujar la situació abans esmentada. La contribució presentada en aquesta tesi doctoral inclou el disseny de nous mecanismes de ICIC estàtica per als canals de dades i control, així com també millores des del punt de vista d'eficiència energètica.

A partir d'una revisió completa de l'estat de l'art, es van identificar una sèrie de reptes oberts que requerien esforços de recerca. En concret, la necessitat de mètodes d'avaluació flexibles i marcs d'optimització de les estratègies de ICIC estàtiques. Aquests mecanismes s'agrupen en dues famílies: els esquemes que defineixen restriccions sobre el domini de la freqüència i els que proposen ajustos en els nivells de potència. És a dir, la base de la gran majoria de propostes ICIC estàtiques són la reutilització de freqüències de tipus soft i fraccional (SFR i FFR, respectivament).

D'aquesta manera, durant la primera part d'aquesta tesi doctoral, s'han estudiat els aspectes més importants del funcionament de SFR i FFR, fent especial èmfasi en les conclusions que van més enllà de les ben conegudes. Això ha permès introduir un nou marc estadístic per avaluar el funcionament d'aquests sistemes en condicions de desplegament reals. Com a resultat d'aquestes anàlisis, es mostra el pobre acompliment de SFR i FFR en desplegaments reals quan funcionen amb les seves configuracions clàssiques i s'estableix la necessitat d'optimització. També es posa de manifest la importància del funcionament conjunt entre esquemes ICIC estàtics i

altres funcionalitats de la xarxa radio, tals com la informació que envien els usuaris sobre l'estat del seu canal *downlink* (*feedback* del CSI, de l'anglès *Channel State Information*). D'aquesta manera, s'han proposat diferents esquemes de feedback apropiats per treballar conjuntament amb SFR i FFR. Aquests mecanismes exploten el patró d'assignació de recursos que s'utilitza en ICIC estàtic per millorar la precisió del procés.

La segona part se centra en l'optimització de SFR i FFR. S'ha investigat l'ús de tècniques multiobjectiu com a eina per aconseguir una optimització eficaç, que és específica per a cada xarxa. L'enfocament ofereix avantatges interessants, d'una banda, es permet l'optimització simultània de diversos criteris contradictoris. D'altra banda, la naturalesa multiobjectiu implica obtenir com resultat configuracions de xarxa d'elevada qualitat (Pareto eficients), totes elles amb un equilibri gairebé òptim entre les diferents mètriques de rendiment. Els algorismes evolucionaris multiobjectiu permeten la utilització d'estructures matemàtiques complexes sense necessitat de relaxar el problema, d'aquesta manera capturen adequadament el seu comportament en termes de ICI. La formulació multiobjectiu aconsegueix un ajust efectiu dels paràmetres operacionals de SFR i FFR, tant a nivell de cel·la com a nivell de xarxa. A més, la recerca s'estén amb resultats satisfactoris als canals de control, PDCCH i ePDCCH.

Finalment, en un esforç per millorar l'eficiència energètica de la xarxa (un aspecte sempre considerat al llarg de la tesi), s'introdueix en l'anàlisi global l'apagat intel·ligent de cel·les, estratègia amb estrets vincles amb ICIC. Mitjançant el mètode proposat, s'obtenen millores significatives pel que fa als enfocaments tradicionals i propostes prèvies. Els guanys s'obtenen en termes de consum energètic, capacitat de la xarxa, i rendiment en el límit de les cel·les.

A mis padres, María Teresa y David, y hermana, Lourdes.

Acknowledgements

By writing these lines, I finish an unforgetable journey I started few years ago. What started as an 18-year-old guy's dream, have became the biggest experience of my life. Somebody told me: '*going for a Ph.D. is an act of faith*'. That person was very right. The way has not been easy, it has been full of ups and downs, but I have enjoyed it, and more important, I have grown thorough it (in many senses).

I would like express my deep gratitude and respect to my thesis directors, Professors Silvia Ruiz and Mario García-Lozano at Universitat Politècnica de Catalunya (UPC).

Thank you Silvia for trust on me one day, thanks for allowing me to get into the fantastic world of research, and thanks for all your help and support during these years.

Mario, no doubt, I would attribute the success of this experience to your endless encouragement, inspiring dedication, and continuous pursuing of excellence. Thanks for your patience (which is not a small detail when it comes to me), and thanks for turning every single small situation into a learning experience.

My gratitude is also extended to Prof. Halim Yanikomeroglu (and his students) at Carleton University for receiving me in their group. You made my stay in Ottawa rewarding in every way.

I cannot forget the people in EETAC and the long list of persons (relative and friends) that, in one way or another, in many different places, helped me to close successfully this chapter of my life. I learned a lot from all of you. I want to thank you all for the good moments (and the ones that were not that good) !!

Thanks to my family in Panama, my parents María Teresa and David, and my sister Lourdes, to whom this work is dedicated, for being such an infinite source of inspiration and motivation. You have been the best support system anyone could have. No word is enough to say how much I love you.

Finally, I want to express my gratitude to the Panamanian government, through IFARHU and SENACYT, for funding this investment with a full Ph.D. scholarship.

Contents

Acronyms

2G	Second Generation
3G	Third Generation
4G	Fourth Generation
5G	Fifth Generation
3GPP	Third Generation Partnership Project
ABS	Almost Blank Subframes
AL	Aggregation Level
AMC	Adaptive Modulation and Coding
BER	Bit Error Rate
BLER	Block Error Rate
CA	Carrier Aggregation
CC	Component Carriers
CCE	Control Channel Elements
CDF	Cumulative Distribution Function
CDMA	Code Division Multiple Access
CS-RS	Cell Specific Reference Signal
CSI	Channel State Information
CSO	Cell Switch Off
DCI	Downlink Control Information
DFT	Discrete Fourier Transform
DL-SCH	Downlink Shared Channel
DM-RS	Demodulation Reference Signal
DTCH	Dedicated Traffic Channel
DV	Design Variable
EFFR	Enhanced Fractional Frequency Reuse
eCCE	enhanced CCE

eICIC	enhanced ICIC
ePDCCH	enhanced Physical Downlink Control Channel
FDD	Frequency Division Duplex
FDM	Frequency Division Multiplexing
FeICIC	Further eICIC
FFR	Fractional Frequency Reuse
FOS	Fully Optimized SFR
FR1	Frequency Reuse 1
FR3	Frequency Reuse 3
FTP	File Transfer Protocol
GSM	Global System for Mobile Communications
GPS	Global Positioning System
GUI	Graphical User Interface
HetNet	Heterogeneous Network
HTTP	Hypertext Transfer Protocol
HSPA	High Speed Packet Access
IA	Interference Alignment
ICI	Intercell Interference
ICIC	Intercell Interference Coordination
ICT	Information and Communications Technologies
IEEE	Institute of Electrical and Electronics Engineers
IFR	Incremental Frequency Reuse
IMT	International Mobile Telecommunications
IRC	Interference Rejection Combining
ISD	Inter Site Distance
ITU	International Telecommunication Union
LTE	Long Term Evolution
LTE	LTE-Advanced
M2M	Machine to Machine
MAC	Medium Access Control
MBMS	Multimedia Broadcast Multicast Services
MBSFN	Multicast-Broadcast Single Frequency Network
MCS	Modulation and Coding Scheme
MIESM	Mutual Information Equivalent SINR Mapping

MIMO	Multiple Input Multiple Output
MO	Multiobjective Optimization
MOEAs	Multiobjective Evolutionary Algorithms
MORANS	MObile RAdio Network reference Scenario
MRC	Maximal Ratio Combining
MSE	Mean Square Error
MTCH	Multicast Traffic Channel
NEL	Network Energy Level
NOP	Network Operation Point
NRT	Non Real Time
OAM	Operation and Maintenance
OFDM	Orthogonal Frequency Division Multiplexing
OFDMA	Orthogonal Frequency Division Multiple Access
OPF	Optimal Pareto Front
PAPR	Peak to Average Power Ratio
PDCCH	Physical Downlink Control Channel
PDCP	Packet Data Convergence Protocol
PDSCH	Physical Downlink Shared Channel
PF	Pareto Front
POS	Partially Optimized SFR
PPP	Poisson Point Process
PUCCH	Physical Uplink Control Channel
PUSCH	Physical Uplink Shared Channel
PRB	Physical Resource Block
QoE	Quality of Experience
QoS	Quality of Service
QAM	Quadrature Amplitude Modulation
QPSK	Quadrature Phase Shift Keying
RB	Resource Block
RE	Resource Element
REG	Resource Element Group
RLC	Radio Link Control
RRM	Radio Resource Management
RRC	Radio Resource Control

RT	Real Time
SC-FDMA	Single Carrier FDMA
SFFR	Soft Fractional Frequency Reuse
SFR	Soft Frequency Reuse
SIC	Successive Interference Cancellation
SINR	Signal to Interference plus Noise Ratio
SNR	Signal to Noise Ratio
SIR	Signal to Interference Ratio
SISO	Single Input Single Output
SON	Self Optimizing Networks
TDD	Time Division Duplex
TDMA	Time Division Multiple Access
TTI	Transmission Time Interval
UE	User Equipment
UHF	Ultra High Frequency
UMB	Ultra Mobile Broadband
UMTS	Universal Mobile Telecommunications System
VoIP	Voice over Internet Protocol
WLAN	Wireless Local Area Network

List of Tables

List of Figures

List of Algorithms

Chapter 1

Introduction

1.1 Context and Motivation

The cellular communications industry witnessed a tremendous growth in the past decade. With more than two billion customers, both Global System for Mobile communications (GSM) and Universal Mobile Telecommunications System (UMTS) were a worldwide success, adopted by most countries and mobile network operators.

Although conceived mainly for voice communications, cellular networks experience an exponential growth of data services. According to [1], the main reason behind this trend seems to be the fact that mobile devices are becoming the preferred way to access the Internet. Thus, the increasingly growing market of web-enabled mobile devices including *smarter* smartphones, tablets, and notebooks (1) opens the path towards a wide range of previously unimagined (data-based) applications and, (2) raises the need for ubiquitous availability of Internet (better coverage) and faster broadband connections (more efficiency).

In this context of fast evolution, network operators and standardization bodies would realize that significant enhancements of such systems were required as data-based services demand significantly more network resources than voice communications. Therefore, serious efforts were done in order to improve data transmission capabilities of existing Second and Third Generation (2G and 3G, respectively) technologies. In particular, the Third Generation Partnership Project (3GPP) introduced High Speed Packet Access (HSPA), an enhancement to its 3G technology, the UMTS system, based on Code Division Multiplexing Access (CDMA). In parallel, the Institute of Electrical and Electronics Engineers (IEEE), achieved an important milestone with the introduction of specifications for local and metropolitan (wireless) area networks, the families IEEE 802.11 and IEEE 802.16, respectively. The main novelty was the design of the air interface based on Orthogonal Frequency Division Multiple Access (OFDMA). Similarly, the American counterpart of the 3GPP, the 3GPP2, also evolved towards enhanced systems based on OFDMA, the Ultra Mobile

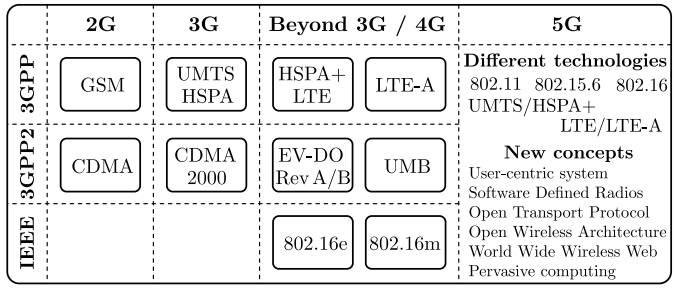

Figure 1.1: Evolution of cellular systems from 2G to 4G and framework for 5G.

Broadband (UMB) system. Nevertheless, since many carriers in Australia, USA, Canada, China, Japan and South Korea announced plans to adopt an OFDMA based solution as their 4G technology, Qualcomm, UMB's lead sponsor, announced in November of 2008 the end of the development of such technology, favoring 3GPP's initiative instead.

Indeed, the 3GPP started the standardization of Long Term Evolution (LTE), a new system also based on OFDMA featuring a simpler IP-based network architecture. LTE and its evolution towards the Fourth Generation (4G), LTE-Advanced (LTE-A), are expected to ensure the competitiveness of the 3GPP for the next 15-20 years and guarantee its presence within the umbrella of the Fifth Generation (5G), which is likely to be around 2020. Figure 1.1 depicts the evolution of cellular systems and some insights about what 5G is supposed to be.

Independently of the technology, a fundamental principle of cellular systems is the concept of frequency reuse where the same bands of frequency are used simultaneously at different places by different base stations. This feature of cellular systems allows boosting the capacity in terms of number of users/km^2 and payload. However, the frequency reuse implies that cells transmitting/receiving over the same frequency bands interfere each other. The problem is known as Intercell Interference (ICI) and it is widely recognized as one of the main capacity-limiting factors in some cellular technologies. Although, interference mitigation techniques have always played a crucial role in the optimization and performance of cellular systems [2], the importance of strategies to deal with ICI in technologies based on OFDMA such as LTE and LTE-A is maximal [3]. In these systems, the aggressive frequency reuse results in poor radio channel quality at cell edges (zones where users receive high levels of ICI and weak signal from their corresponding access points) and hence, a *fairness* issue, i.e., the Quality of Experience (QoE) becomes dependent on the user position as spatial Signal to Interference plus Noise Ratio (SINR) variations imply different performances of multiantenna techniques.

Thus, strategies aiming at improving the Quality of Service (QoS) of mobile terminals in cell edges are mandatory. In the context of OFDMA networks, one approach to accomplish the previous goal is to coordinate (among cells) the radio resources that are going to be allocated to those *unlucky* users in such a way that they receive (1) better signal from their corresponding access points and, (2) less

ICI from neighbor cells. This general framework is called as Intercell Interference Coordination (ICIC) and it is the one over which this thesis is about.

This Ph.D. dissertation provides a contribution to the field of ICIC for cellular systems based on OFDMA. To be precise, *static* ICIC for the downlink of realistic LTE/LTE-A deployments have been investigated and proposed. Static ICIC includes a family of strategies in which the resources available at each cell are determined in a planning-like manner and only smooth variations are performed in time scales of tens of minutes, hours or days. Several open issues were addressed and new methods, guidelines and strategies have been devised accordingly. Throughout the research process, emphasis was placed on achieving not only effective solutions but also feasible innovations and, as far as possible, consider several perspectives of the problem. The main motivation for this work has stemmed from the following factors:

- the optimization of static ICIC techniques in the context of **realistic deployments**, an issue that will be introduced and justified later on. Regarding this particular, the main research objective was to design effective solutions providing network-specific solutions. Real-life networks are all different and hence, these particularities can (and must) be exploited to achieve the maximum benefit.
- the importance of addressing the ICIC problem from **several perspectives**. The well-known tradeoff: efficiency-fairness was always in the center of attention, but in addition, the increasingly important energetic perspective was also considered in the vast majority of the studies presented herein.
- improving the **interworking** between ICIC and other network functionalities. Although many functions of cellular systems are independent (and indeed operate at very different time scales), sometimes the operation of one has a significant impact on the performance of another. This is the case of important static ICIC strategies and some Channel State Information (CSI) feedback schemes in LTE. Consequently, this aspect was investigated and new mechanisms were proposed.

The specific aspects that have been covered concerning the previous research lines are presented in the next section.

1.2 Scope and Structure

The main research objective of this Ph.D. dissertation **is the design of new and advanced schemes to optimize the performance of static ICIC strategies in the context of the downlink of realistic LTE/LTE-A deployments**. As the reader has probably inferred, an important conceptual difference among ICIC proposals is the temporality with which resource coordination is performed. Thus, ICIC schemes can be divided into static and dynamic mechanisms [4]. In static ICIC, there are not *fast* adaptations over time. The main advantage of this approach is

that these schemes require none or little intercell communication and the very low complexity, but on the other hand, there are no means to react to sudden changes in network conditions. In dynamic ICIC, a certain amount (sometimes prohibitive) of intercell signaling is required to be exchanged in time scales of milliseconds or seconds. The ability of tracking network conditions dynamically is clearly the biggest advantage in this type of solutions, but again, this comes at the expense of additional real-time complexity and network resources. It is important to make clear that, by no means, this research aims at presenting a comparison between static and dynamic ICIC mechanisms. As it was commented, both approaches have pros and cons. Instead, the thesis's objective is **to make a solid contribution to the theory and State of the Art of static ICIC**. The results and conclusions of this work clearly suggest that, provided adequate optimization means, static ICIC techniques are a very attractive alternative for mobile operators.

The document is composed of nine chapters and six appendices. The next seven chapters correspond to the core of the Ph.D. dissertation. The final chapter closes the document with final remarks, conclusions and future research lines. Chapters can be grouped in two parts, each one focused in different, but interrelated, strategies to optimize the overall performance of static ICIC schemes in LTE/LTE-A networks.

The first part comprises chapters 2, 3 and 4. It starts with the required background knowledge and it clarifies the motivation and relevance of the research work. In this part, the general framework for ICIC in LTE/LTE-A is also explained, including a description of several mechanisms (the ones relevant to this thesis) defined in the specifications and a survey of the state of the art and current trends. Given this, the work started by investigating the feasibility and performance of static ICIC solutions in realistic networks deployments, i.e., networks in which the propagation conditions vary significantly at different cells and the cellular layout is far from the hexagonal models commonly used. The conclusions pointed out the need for research towards effective static ICIC models that can be applied to those environments/scenarios. During the studies, several perspectives including existing tradeoffs, implementation aspects and interworking in LTE/LTE-A were also considered. The novelties presented were inspired both from analysis of existing proposals and own conclusions. The need for optimization strategies for realistic scenarios was clearly established. In addition, detailed analysis of the interaction between SFR/FFR and other network functionalities revealed that the interworking with the Channel State Information (CSI) feedback mechanisms in LTE can be substantially improved. Thus, novel strategies for CSI feedback are presented to close this part.

The second part, including chapters 5, 6, 7 and 8, begins recovering the need for optimized and network-specific SFR/FFR models suitable for realistic deployments. Several approaches, methodologies and optimization tools were considered. However, taking into account the particularities of this design problem, i.e., the system model, the mathematical structure of the objective functions (performance metrics) and some practical considerations, the use of Multiobjective Evolutionary Algorithms (MOEAs) was proposed and investigated. Novel optimization strategies based on this approach proved their efficacy achieving significant improvements

over baseline configurations and previous proposals. One chapter has been devoted to investigate the adaptation of the new mechanism to ICIC for control channels, a context that shows certain particularities that required a different treatment. Potential extensions to adaptive mechanisms, feasibility/implementation aspects, complexity and convergence properties were also addressed. The studies included not only the effect of every single design variable on performance but also insightful analysis of existing tradeoffs, in which the increasingly important energetic perspective was always taken into account. Indeed, the last chapter of this part, developed during a research visit in Carleton University, Canada, was fully devoted to further enhancements from the energy efficiency point of view. Thus, adaptations of the model used previously for ICIC were successfully extended to the framework of Cell Switch Off (CSO) and interesting innovations were developed.

In this manner, several open issues and research challenges were identified and successfully addressed. The innovations, guidelines and new methodologies of study were obtained by means of studies based on practical engineering considerations, multiobjective optimization techniques and system level simulations. To support the desired flexibility, a LTE system level simulator written in C++ was fully developed by the author during the period of the thesis. A description of this platform is provided in Appendix D. Mathematically speaking, a complete system level analysis of ICIC is very complex without incurring in strong assumptions or simplifications. This is mainly due to the mathematical structure of the performance metrics that need to be studied and the scale of the problem (real-life deployments are composed by hundreds of cells). However, by means of the simulation platform that was developed, it was possible to investigate the ICIC problem accurately and keeping the mathematical rigour required by the theoretical part of the analysis.

Figure 1.2 illustrates the structure of the thesis and several possible reading paths of the document. Thus, some interdependencies that should be respected for better understanding are indicated. Next, a summary of each chapter indicating main research contributions and novelties is provided.

The chapters at a glance

The next chapter explains the need for ICIC in OFDMA based cellular networks. As it will be seen, the use of frequency reuse 1 in systems such as LTE and LTE-A results in poor radio channel quality at cell edges and hence, additional measures need to be taken to compensate that situation. The chapter provides a description of the most relevant approaches to ICIC and the state of the art. The literature about ICIC is extensive and it comprises a wide range of theoretical studies and schemes including heuristic strategies and optimization algorithms, all with different levels of complexity and feasibility. In this thesis, the focus is placed on static ICIC schemes and its performance in LTE/LTE-A deployments. However, dynamic ICIC is also discussed to make explicitly clear the advantages and drawbacks of each type of strategy. From this continuous reviewing process, interesting challenges were identified and research objectives were established accordingly. Next, the chapter continues with an overview of certain functionalities in LTE and LTE-A that are

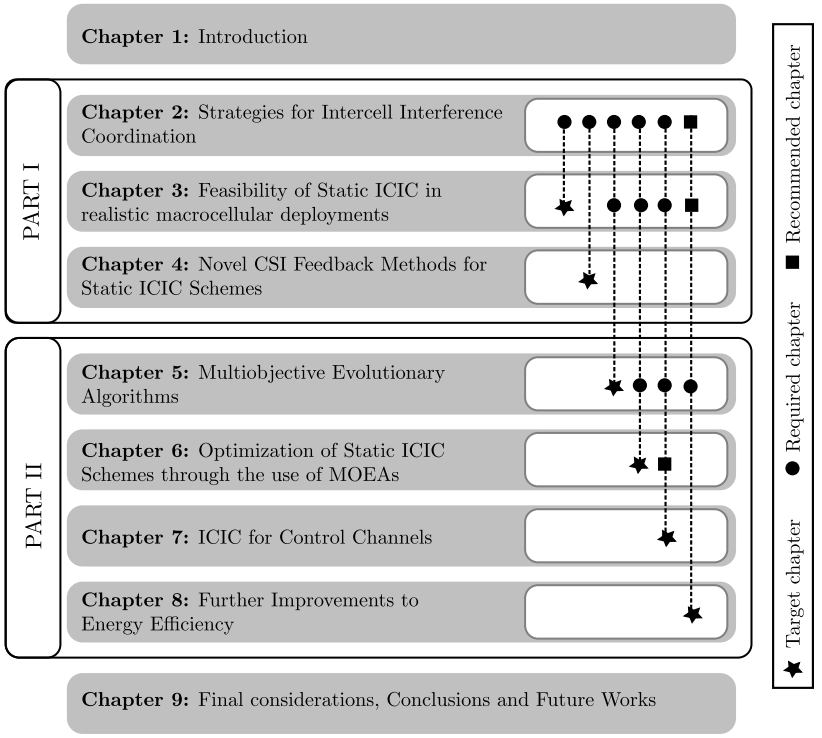

Figure 1.2: Structure of the thesis and interdependencies among chapters.

relevant to this thesis. These include means to implement ICIC, CSI feedback schemes and structure and operation of the data and control channels. This information is required as it allows for a better understanding of the novelties presented throughout the document. In the chapter, great importance is conferred to the way in which ICIC has evolved according to the new features and capabilities that have been incorporated into the 3GPP's specifications. This evolution has raised the need for new frameworks that are trend nowadays such as enhanced ICIC (eICIC), Further eICIC (FeICIC), ICIC for Heterogeneous Networks (HetNets), ICIC for Carrier Aggregation (CA) based systems and ICIC in hyper dense small cell deployments, among others. A discussion about these topics, key in 4G and 5G networks, is also presented.

Chapter 3 presents key studies conducted in order to further investigate the performance, complexity and tradeoffs associated to static ICIC schemes. These analysis remarked the poor performance of static ICIC schemes (SFR and FFR) in realistic cellular deployments. Therefore, the need for schemes achieving simultaneous optimization of several conflicting metrics in those scenarios was established. Besides this important conclusion, it was also pointed out that more efficient methods to evaluate the role and impact of design parameters of SFR and FFR were also required as this particular analysis requires numerous time-consuming system level

simulations. A novel statistical methodology was developed and proposed to that end. By means of this approach, insightful design guidelines were obtained.

The need for improving the interworking between static ICIC and CSI feedback was among the important lessons obtained through the studies focused on the operation and interworking of SFR and FFR. This is the matter of chapter 4. Native CSI feedback mechanisms available in LTE do not take into account the particular resource allocation patterns employed in SFR and FFR, thus resulting in performances that are far from optimal. The proposed mechanisms provide means to adapt the CSI feedback in a way that is more appropriate to SFR and FFR: refining the estimation of the wideband (average) channel quality metric, that is used in turn as reference point to compute the subbands counterparts. Thus, the proposed schemes improve the overall QoS maximizing the number of *satisfied* users. Both Real Time (RT) and Non Real Time (NRT) services were considered along these studies.

Chapter 5 recovers the need for optimization of static ICIC schemes in realistic deployments. The chapter starts introducing the use of metaheuristics in frameworks such as automatic planning and justifies their suitability for a wide range of combinatorial problems similar to SFR and FFR optimization. Next, taking into account the system model employed to study the performance of static ICIC techniques (joint analysis of several conflicting perspectives including spectral/energy efficiency and cell edge performance), the multiobjective approach was considered. In addition, bearing in mind the computational complexity and mathematical structure of the optimization problem, it was concluded that the use of an optimization tool based on stochastic search fitted the research objectives previously defined. Hence, the adaptation of MOEAs to the design of network-specific SFR/FFR models was investigated. The chapter provides an introduction to the theory of multiobjective (global) optimization and a comprehensive description of the evolutionary algorithms employed in this thesis, including quality indicators, calibration guidelines, complexity aspects and convergence properties.

The previous knowledge allows for the understanding of the optimization models presented in chapter 6. The multiobjective algorithms for SFR and FFR based on evolutionary optimization are the heart of the second part of the thesis and they represent a step forward with respect to previous proposals. The algorithms are based on adaptations of two well-known MOEAs, NSGA-II and SPEA-2, to the particularities of the problem under consideration. By means of the Pareto dominance concept, a hybrid scheme able to achieve the best properties of each algorithm was designed and as a result, the performance of the proposed solution is substantially better in terms of the number of resulting network configurations, convergence and distribution. The fundamental idea is to fine tune the operational parameters of SFR and FFR independently at each cell according to local propagation conditions and the mutual impact among cells. Since the core processing is based on average interference conditions, the model does not require neither prohibitive real-time processing nor unfeasible intercell signaling. Moreover, the multiobjective nature of this framework implies that the output is not longer one single network configuration but a set of high quality ones. Thus, this feature enables mobile operators to select among

different operational modes according to their needs or network conditions. In fact, these configurations could be stored in databases and used in adaptive mechanisms. The results show that the novel algorithms outperforms baseline configurations and previous proposals and provide a wider understanding of intrinsic tradeoffs.

Traditionally, ICIC schemes have been focused on data channels, *the user plane*. That is the case of the algorithms presented in chapter 6. However, the operation of LTE and LTE-A strongly rely on information transmitted over control channels, *the control plane*. Although control channels are designed to operate with robust modulation and coding schemes to provide the desired reliability, this additional robustness comes at the expense of consumption of additional radio resources, and hence, under certain circumstances, it has been identified that control channels act as a *capacity bottleneck*. On the one hand, the time-multiplexed design of the control channel in LTE, the Physical Downlink Control Channel (PDCCH), is more rigid than its data counterpart, the Physical Downlink Shared Channel (PDSCH), multiplexed both in time and frequency. Therefore, strategies to reduce the levels of ICI at cell edges and avoid the corresponding excessive resource consumption are required. On the other hand, although the design of the control channel was significantly improved in LTE-A with the addition of a new control channel, the enhanced PDCCH (ePDCCH), no mechanism is specified in the standard to perform ICIC on it. Thus, in the light of these situations and based on the strategies previously developed, suitable ICIC schemes for the PDCCH and the ePDCCH are presented in Chapter 7.

All the analysis and studies presented so far take the increasingly important energetic perspective into account by incorporating energy efficiency and related metrics. Even though the static ICIC solutions based on SFR and FFR minimize energy requirements over the air interface, i.e., the power transmitted in different subcarriers, a further step is considering switch off eNBs completely as the major part of the energy expenditure in these equipments is independent of the power radiated through the antennas. Since base stations are the main contributors to the overall network energy consumption, CSO schemes have attracted enormous attention recently. This is the context of chapter 8. Thus, in order to upgrade this important aspect, several adaptations of the strategies presented so far for ICIC were developed. The resulting schemes and innovations were framed in a research project at Carleton University, Canada, and they constitute the final point to the activities enclosed by this thesis.

The document is closed with a high level assessment of the achievements accomplished through the research presented herein, conclusions and perspectives for future works in chapter 9. Finally, a set of appendices is provided to 1) facilitate the reading and understanding of the document (Appendices A, B, C and D) and, 2) complement the thesis with additional, though relevant, results (Appendix E). The next Section summarizes the research contributions derived from this Ph.D. dissertation.

1.3 Research Contributions

The novel proposals and innovations presented in this thesis have been disseminated through several research contributions[1]. These publications are grouped according to the part of the thesis they correspond to. In addition, several contributions to the European COST Actions 2100 and IC1004 were done and are also indicated.

The publications include:

- **[J]**: 5 journal papers.
- **[P]**: 1 US (provisional) patent.
- **[B]**: 2 book chapters.
- **[LN]**: 2 lecture notes (selected papers from conference proceedings).
- **[C]**: 13 conference papers (two of them granted with the best paper award).
- **[CA]**: 4 contributions to COST Actions.

PART I

Chapters 2, 3 and 4: 2 journal papers, 2 book chapters, 2 lecture notes, 7 conference papers and 3 COST contributions.

[J1] **D. González G**, M. García-Lozano, S. Ruiz, and J. Olmos, "On the Need for Dynamic Downlink Intercell Interference Coordination for Realistic Long Term Evolution Deployments," *Wireless Communications and Mobile Computing*, pp. 1–26, Feb. 2012.

[J2] **D. González G**, M. García-Lozano, S. Ruiz, and J. Olmos, "Improving the Interplay between Periodic Channel State Information Feedback and Static Intercell Interference Coordination in LTE," *Journal of Communications* (Special Issue on Interference Management for 4G Networks), vol. 7, no. 9, pp. 660–675, Sep. 2012.

[B1] N. Cardona, J. Olmos, J. Monserrat, M. García-Lozano (ed.), *3GPP LTE: Hacia la 4G móvil* (in Spanish). Barcelona, Spain: Marcombo, S.A., 1st ed., 2011. Chapter entitled: *Gestión de Recursos Radio* (Radio Resource Management).

[B2] R. Santos, A. Block, and V. Rangel (ed.), *Broadband Wireless Access Networks for 4G: Theory, Application and Experimentation.* Hershey (PA), United States: IGI Global, 1st ed., 2013. Chapter entitled: *Aperiodic ICIC-Oriented CSI Reporting for LTE Networks*.

[LN1] **D. González G**, M. García-Lozano, S. Ruiz, and J. Olmos, "Static Inter-Cell Interference Coordination Techniques for LTE Networks: A Fair Performance Assessment," in *Multiple Access Communications* (A. Vinel, B. Bellalta,

[1]The publications are also listed at the end of the bibliography

C. Sacchi, A. Lyakhov, M. Telek, and M. Oliver, eds.), vol. 6235 of *Lecture Notes in Computer Science*, pp. 211–222, Springer Berlin Heidelberg, 2010.

[**LN2**] **D. González G**, M. García-Lozano, S. Ruiz, and J. Olmos, "On the Performance of Static Inter-cell Interference Coordination in Realistic Cellular Layouts," in *Mobile Networks and Management* (K. Pentikousis, R. Agüero, M. García-Arranz, and S. Papavassiliou, eds.), vol. 68 of *Lecture Notes of the Institute for Computer Sciences, Social Informatics and Telecommunications Engineering*, pp. 163–176, Springer Berlin Heidelberg, 2011.

[**C1**] **D. González G**, S. Ruiz, M. García-Lozano, J. Olmos, and A. Serra, "System Level Evaluation of LTE Networks with Semidistributed Intercell Interference Coordination," in *Proc. of IEEE 20th International Symposium on Personal, Indoor and Mobile Radio Communications (PIMRC 2009)*, Tokyo (Japan), Sep. 13–16, 2009.

[**C2**] **D. González G**, V. Corvino, S. Ruiz, J. Olmos, M. García-Lozano, and R. Verdone, "Downlink Resource Allocation in LTE: Centralized vs. Distributed Approach," in *Proc. of Joint COST2100/NEWCOM++ Workshop on Radio Resource Allocation for LTE*, Vienna (Austria), Sep. 30, 2009.

[**C3**] **D. González G**, M. García-Lozano, V. Corvino, S. Ruiz, and J. Olmos, "Performance Evaluation of Downlink Interference Coordination Techniques in LTE Networks," in *Proc. of IEEE 72nd Vehicular Technology Conference (VTC 2010 Fall)*, Ottawa (Canada), Sep. 6–9, 2010.

[**C4**] **D. González G**, M. García-Lozano, S. Ruiz, and J. Olmos, "Static Inter-Cell Interference Coordination Techniques for LTE Networks: A Fair Performance Assessment," in *Proc. of 3rd Int. Workshop on Multiple Access Communications (MACOM 2010)*, Barcelona (Spain), Sep. 13–14, 2010.

[**C5**] **D. González G**, M. García-Lozano, S. Ruiz, and J. Olmos, "On the Performance of Static Inter-cell Interference Coordination in Realistic Cellular Layouts," in *Proc. of 2nd Int. ICST Conference on Mobile Networks and Management (MONAMI 2010)*, Santander (Spain), Sep. 22–24, 2010.

[**C6**] **D. González G**, M. García-Lozano, S. Ruiz, and J. Olmos, "An Analytical View of Static Intercell Interference Coordination Techniques in OFDMA Networks," in *Proc. of IEEE Wireless Communications and Networking Conference Workshops (WCNCW 2012)*, Paris (France), Apr. 1–4, 2012.

[**C7**] **D. González G**, M. García-Lozano, S. Ruiz, and J. Olmos, "Improving Channel State Information Feedback for Static Intercell Interference Coordination in LTE," in *Proc. of IEEE International Conference on Communications (ICC 2012)*, Ottawa (Canada), Jun. 10–15, 2012.

[**CA1**] **D. González G**, S. Ruiz, J. Olmos, M. García-Lozano, and A. Serra, "Link and System Level Simulation of Downlink LTE," COST 2100, Braunschweig (Germany), Rep. available as TD(09)734, Feb. 16–18, 2009.

[**CA2**] **D. González G**, M. García-Lozano, S. Ruiz, and J. Olmos, "Performance Evaluation of Static Intercell Interference Coordination in Realistic Cellular Layouts," COST 2100, Aalborg (Denmark), Rep. available as TD(10)11053, Jun. 2–4, 2010.

[**CA3**] **D. González G**, M. García-Lozano, S. Ruiz, and J. Olmos, "A Novel ICIC-Oriented Channel State Information Feedback Scheme for Aperiodic Reporting in LTE," COST IC1004, Barcelona (Spain), Rep. available as TD(12)03038, Feb. 8–10, 2012.

PART II

Chapters 5, 6, 7 and 8: 3 journal paper, 1 US patent application, 6 conference papers and 1 COST contribution.

[**J3**] **D. González G**, M. García-Lozano, S. Ruiz, and D. Lee, "Optimization of Soft Frequency Reuse for Irregular LTE Macrocellular Networks," *IEEE Transactions on Wireless Communications*, vol. 12, no. 5, pp. 2410–2423, May. 2013.

[**J4**] **D. González G**, M. García-Lozano, S. Ruiz, and D. Lee, "A Metaheuristic based Downlink Power Allocation for LTE/LTE-A Cellular Deployments," *Wireless Networks*, Accepted for publication, Sep. 2013.

[**J5**] **D. González G**, M. García-Lozano, S. Ruiz, María A. Lema, and D. Lee, "Multiobjective Optimization of Fractional Frequency Reuse for Irregular OFDMA Macrocellular Deployments," *Telecommunication Systems*, Accepted for publication, Oct. 2013.

[**P1**] **D. González G**, H. Yanikomeroglu, and G. Senarath, "A System and Method for a Multiobjective Framework for Cell Switch-Off in Dense Cellular Networks." US Provisional Patent Application, Serial no: 61847403, Filed by Huawei, Canada. Application date: Jul. 2013.

[**C8**] **D. González G**, M. García-Lozano, S. Ruiz, and J. Olmos, "On the Role of Downlink Control Information in the Provision of QoS for NRT Services in LTE," in *Proc. of IEEE 75th Vehicular Technology Conference (VTC 2012 Spring)*, Yokohama (Japan), May. 6–9, 2012.

[**C9**] **D. González G**, M. García-Lozano, S. Ruiz, J. Olmos, and D. Lee, "Optimization of Realistic Full Frequency Reuse OFDMA-based Cellular Networks," in *Proc. of IEEE 23rd International Symposium on Personal, Indoor and Mobile Radio Communications (PIMRC 2012)*, Sydney (Australia), Sep. 9–12, 2012.

[**C10**] **D. González G**, M. García-Lozano, S. Ruiz, and D. Lee, "Improving Soft Frequency Reuse for Realistic OFDMA-based Cellular Deployments," in *Proc. of IEEE Global Telecommunications Conference (GLOBECOM 2012)*, Anaheim (United States), Dec. 3–7, 2012.

[**C11**] **D. González G**, M. García-Lozano, S. Ruiz, M. Lema, and D. Lee, "Adapting Fractional Frequency Reuse to Realistic OFDMA Cellular Networks," in *Proc. of 6th Joint IFIP Wireless and Mobile Networking Conference (WMNC 2013)*, Dubai (United Arab Emirates), Apr. 23–25, 2013. **Paper granted with the 'Best Paper Award'**.

[**C12**] **D. González G**, M. García-Lozano, and S. Ruiz, "Power Allocation for the PDCCH in LTE: A Way to Increase its Capacity in Realistic Deployments," in *Proc. of Wireless Personal Multimedia Communications Symposium (WPMC 2013)*, Atlantic City (United States), Jun. 24–27, 2013.

[**C13**] **D. González G**, M. García-Lozano, and S. Ruiz, "Intercell Interference Coordination for the ePDCCH in LTE-Advanced Macrocellular Deployments," in *Proc. of 9th International Conference on Wireless and Mobile Communications (ICWMC 2013)*, Nice (France), Jul. 21–26, 2013. **Paper granted with the 'Best Paper Award'**.

[**CA4**] **D. González G**, M. García-Lozano, S. Ruiz, and J. Olmos, "Impact of Downlink Signaling Capacity Constraints on the Provision of QoS in LTE," COST IC1004, Lisbon (Portugal), Rep. available as TD(11)02041, Oct. 19–21, 2011.

Apart from publications directly related to the thesis contributions, the author has participated in several other research works that have been carried out during the elaboration of this thesis. In particular, 4 additional contributions to COST Actions and 3 conference papers. These activities will not be explicitly mentioned here for brevity.

Chapter 2

Strategies for Intercell Interference Coordination

2.1 Introduction

In the previous chapter it was indicated the key role of interference management throughout the evolution of cellular systems. Interference, either intracell or intercell, has been always one of the most important performance-limiting factors in the context of cellular communications. In general, interference is any spurious signal on the channel that is being used. These undesired signals can be generated by the use of the own or an adjacent channel either within the same cell or in neighbor ones. OFDMA provides intrinsic orthogonality to the users within the cell, which translates into a almost null level of intracell interference. However, in OFDMA system, intercell interference is created when the same channel is used in neighbor cells and it represents a challenging issue in this type of cellular network, especially for users located at the cell edge due to the frequency reuse 1 that is aimed to meet the ambitious design targets in technologies such as LTE and LTE-A.

This chapter presents, in Section 2.2, a progressive approach to ICI, its impact on OFDMA cellular systems and the need for effective interference mitigation techniques. In the discussion, great attention is paid to the role of frequency reuse, a notion of utmost importance in this context. Building upon this background, Section 2.3 makes a description of the different strategies to deal with ICI. The survey provides a wide perspective of the most important frameworks focused not only on ICI but also related targets, both in the downlink and uplink. Thus, interesting concepts such as Coordinated Multipoint (CoMP), Interference Alignment (IA) and Interference Rejection Combining (IRC) are visited. This discussion aims at contextualizing ICIC within the more general framework of interference mitigation in OFDMA systems. Then, with this wide perspective, the attention is turned to ICIC and Section 2.4 is fully devoted to these strategies with special emphasis on static schemes, the

focus of this Ph.D. dissertation. Classification criteria and operational principles are explained. It will be shown that, the vast majority of ICIC proposals, both dynamic and static, are fundamentally based on the same principles that govern the operation of two important static schemes: SFR and FFR. Consequently, the state of the art of the techniques and strategies based on either SFR or FFR is presented. From this analysis, several important research directions are established, among which, the need for studies about the performance of static ICIC schemes in realistic deployments is the center of attention during the first part of the thesis.

This Ph.D. dissertation is focused on the optimization of static ICIC schemes for the downlink of LTE and LTE-A networks. The downlink of both systems is based on OFDMA, being network performance mainly interference-limited. Nevertheless, throughout Sections 2.3 and 2.4, numerous references to the uplink counterpart of the interference management problem are included. These comments mainly focus on the feasibility of each of these strategies in the uplink. Thus, in order to summarize these aspects and provide a unified perspective of this *parallel* problem, Section 2.5 addresses the adaptability and possible extensions of the aforementioned techniques to the uplink.

Two additional sections complete the chapter. Section 2.6 provides an overview of the framework for ICIC in HetNets and small cell deployments. Section 2.7 includes an introduction to several aspects of LTE: an overview of the air interface, the structure of data and control channels (focusing on ICIC aspects), and a basic description of several ICIC facilitating mechanisms.

2.2 ICI in OFDMA Systems: Background

This section provides a progressive approach to ICI and its management in OFDMA networks by presenting several fundamental theoretical aspects of this problem. These notions will facilitate the understanding of the document and the contributions of the thesis.

2.2.1 OFDM and OFDMA

This theoretical introduction starts discussing the access technology. OFDMA is based on Orthogonal Frequency Division Multiplexing (OFDM), a multicarrier transmission technique that allows the transmission of several data streams in parallel over the same channel. This is accomplished by dividing the available spectrum into K subchannels. Then, K data symbols are transmitted simultaneously during an interval $K\Delta t$ instead of transmitting one data symbol in the whole spectrum during a time Δt. Nevertheless, the key aspect of OFDM is the clever overlapping (the exact location of the subcarriers' nulls) existing in the frequency domain, such that the orthogonality among subcarriers is guaranteed. By doing so, the bandwidth can be used more efficiently, and hence, the spectral efficiency can be increased with respect to traditional Frequency Division Multiplexing (FDM) techniques. OFDMA

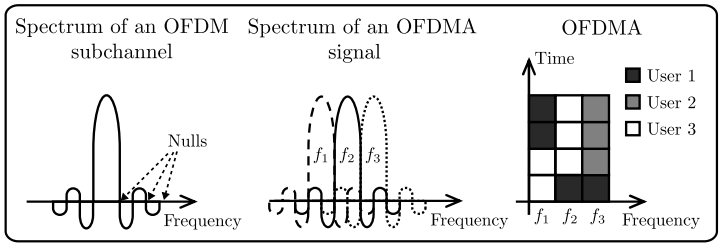

Figure 2.1: Operational principle of OFDMA.

is a multiuser version of OFDM. Multiple access is achieved by assigning subsets of subcarriers to individual users during certain time intervals allowing so simultaneous transmissions. The previous ideas are illustrated in Figure 2.1. The main advantages of OFDMA include:

- ✓ Robustness against inter-symbol interference.
- ✓ OFDM can combat multipath easily.
- ✓ Flexibility of deployment across various frequency bands with minor modifications to the air interface: scalable bandwidth and granularity.
- ✓ Offers frequency diversity by spreading the subcarriers over the total bandwith.
- ✓ No cell size breathing as more users connect.

Some disadvantages include:

- × Higher sensitivity to frequency offsets and phase noise.
- × Dealing with co-channel interference from nearby cells is more complex in OFDM than in CDMA.
- × Larger Peak to Average Power Ratio (PAPR) than other single carrier modulation options.

A detailed description of OFDM and OFDMA can be found in [5].

2.2.2 Fundamental Aspects

Throughout the document, the downlink of a LTE/LTE-A cellular network is considered. However, most of the models and analysis presented herein are perfectly valid for the downlink of any generic OFDMA cellular systems. Thus, the context is a cellular network in which several users receive data through an air interface based on OFDMA. It is always assumed that each user accesses the services provided by the network through one, and only one, base station, i.e., a user receives data from at most one cell. In general, the rate at which the network is able to transmit information to any given user depends on the SINR experienced by that user. Let's consider the scenario depicted in Figure 2.2. According to the Shannon's formula,

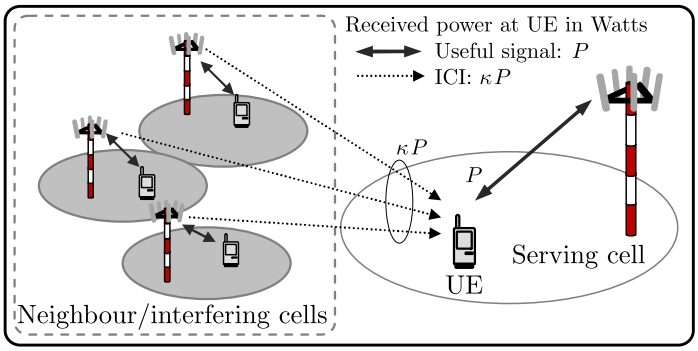

Figure 2.2: Typical ICI scenario.

the spectral efficiency[1] measured in bit/s/Hz of the UE in this non-interference-free system can be written as follows:

$$\eta^{\text{ICI}} = \log_2\left(1 + \frac{\text{Useful signal power}}{\sigma^2 + \text{ICI power}}\right) = \log_2\left(1 + \frac{P}{\sigma^2 + \kappa P}\right). \tag{2.1}$$

Scenarios in which $\kappa P \gg \sigma^2$ are known as interference limited and obviously, these are the cases of interest from the interference management point of view. Note that the amount of ICI power received by the UE has been expressed as κP. Therefore, it can be said that the target of any interference mitigation strategy is to make κ as small as possible. The previous goal becomes evident by looking at the impact of ICI on the spectral efficiency. In this example, the Signal to Noise Ratio (SNR) and Signal to Interference Ratio (SIR) correspond to $\frac{P}{\sigma^2}$ and κ^{-1}, respectively. Thus, the spectral efficiency without ICI can be written in the following manner:

$$\eta^{\text{NoICI}} = \log_2\left(1 + \text{SNR}\right). \tag{2.2}$$

The spectral efficiency loss due to ICI will be given by:

$$\text{Loss} = \frac{\eta^{\text{NoICI}} - \eta^{\text{ICI}}}{\eta^{\text{NoICI}}} = \frac{\log_2\left(\frac{1+\text{SNR}}{1+\left(\frac{1}{SNR}+\kappa\right)^{-1}}\right)}{\log_2\left(1+\text{SNR}\right)}. \tag{2.3}$$

Figure 2.3 clarifies the meaning of (2.1) and (2.3) by showing graphically the relationship among the involved variables. First, Figure 2.3a shows that for moderate to high ICI levels ($\kappa \geq 0.50$), significant increments in the useful signal received power have a negligible effect on the spectral efficiency. Thus, it is clear that ICI is an important capacity limiting factor. Another quantitative perspective of this negative effect is provided in Figure 2.3b. It can be seen that in scenarios with relative low noise (SNR=15 dB), the capacity is reduced between 40% and 80% when the SIR goes from -10 dB to 0 dB ($\kappa^{-1} \in [-10, 0]$ dB). The losses in the heavily interfered region ($\kappa \geq 0$ dB) are above 80%. This example makes evident

[1]The general notation is described in Appendix A.

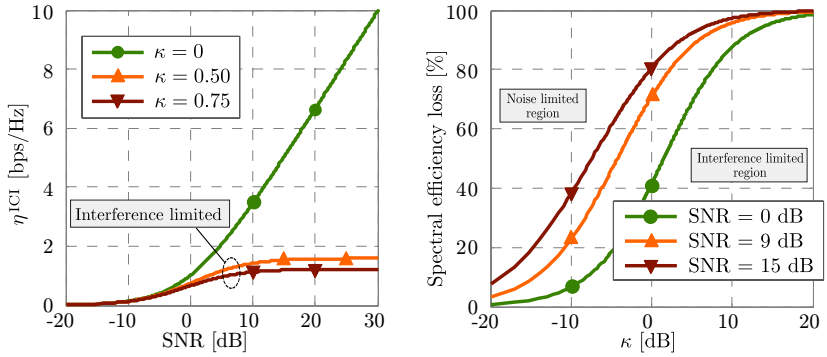

(a) ICI limits capacity. **(b)** Capacity loss due to ICI.

Figure 2.3: Impact of ICI in interference limited scenarios.

the severe impact of ICI on the performance of cellular systems and the need for effective strategies to mitigate its effects.

2.2.3 Practical aspects

In the context of OFDMA cellular networks, ICI management has two main issues. The first fundamental problem appears because ICI is highly non-predictable even in scenarios without mobility due to time varying transmission patterns in interfering cells. On top of this, the effect of the frequency selective fading and the limitations of practical CSI feedback schemes make harder tracking channel quality for narrowband channels (the case of OFDMA subchannels). As a result, obtaining perfect CSI is not feasible, and hence, resource allocation schemes typically relying on such detailed information pose several challenging issues. In addition, even assuming that perfect CSI is available, time scales at which these algorithms operate is often prohibitive due to the computational cost and the amount of intercell signaling that is required. Indeed, and according to [6], ICI management may not have to track fast dynamics. In practice, the impairments caused by the aforementioned issues are typically handled by means of several Radio Resource Management (RRM) mechanisms such as power control, Adaptive Modulation and Coding (AMC), and advanced retransmission schemes. A wider perspective and classification of RRM can be found in [7, 8].

The second issue is related to the fact that SINR levels are not uniformly distributed in the network coverage area. Recall that the wireless channel is basically composed of three nearly independent mechanisms: path loss, shadowing and multipath [9]. The statistics of the loss due to multipath (small scale fading) does not depend on the position, but path loss and shadowing (large scale fading) are position dependent. While multipath and shadowing affect users (statistically) in the same manner, propagation losses are proportional to distance, and hence, users located near to cell edges receive not only weak signals from their serving base stations

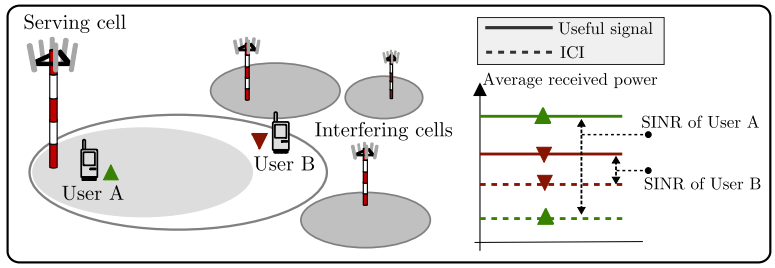

Figure 2.4: Illustration of the cell edge performance issue in OFDMA networks.

but also high ICI. As a result, SINR values are significantly lower than the ones experienced by users close to their transmitters. As it was just illustrated, high ICI penalizes system capacity drastically, and hence, the situation causes an important performance degradation (from the system perspective) and a no less important fairness issue (from the users point of view). The cell edge performance degradation issue is illustrated in Figure 2.4. Consequently, in the context of cellular systems based on OFDMA such as LTE, a fundamental target of any ICI mitigation strategy is to improve the QoS of cell edge users, for which, strategies focused on macroscopic network changes and average interference conditions may represent a good tradeoff between performance and complexity/feasibility.

2.2.4 Impact of Frequency Reuse

The analysis presented so far, although valid for OFDMA systems, did not include into the picture a very important element: the bandwidth. Indeed, it was assumed that a generic resource is used in all cells. The previous assumption is also known as *universal* frequency reuse, *full* frequency reuse, or reuse factor 1. However, a very interesting feature of OFDMA is the possibility of using different portions of the system bandwidth independently at each cell. Thus, this subsection is closed by showing the impact of frequency reuse.

In order to provide an insightful result, the analysis must include the cell edge performance perspective. Let's consider a cellular network featuring hexagonal geometry. Without loss of generality, it is assumed that omnidirectional antennas are located in the center of each cell, each of which has radius R and transmits with the same power P. The analysis is focused on one single cell (the target cell), in which, two users, $\mathrm{UE_{CC}}$ and $\mathrm{UE_{CE}}$, are located in the center and cell edge, respectively. To evaluate the impact of frequency reuse, three different values are considered: 1, 3, and 7. Figure 2.5 depicts the scenario previously described and the frequency reuse patterns. By considering that 1) channel gains are given exclusively by propagation losses, 2) the effect of the background noise is negligible ($\sigma^2 \approx 0$), and 3) δ is a small quantity (δR is significantly smaller than the cell radius); the SINR of each user (ψ_{UE}) can be expressed as function of the distances (d_l) to the different base stations that are reusing the same frequency (according to the reuse pattern) and, the propagation loss exponent ν as follows:

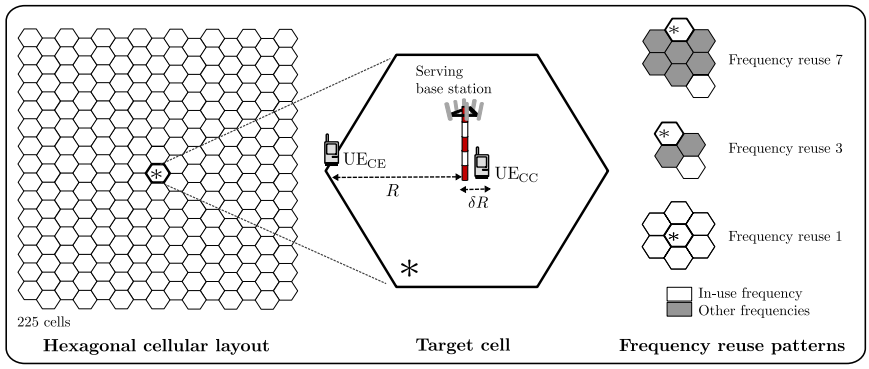

Figure 2.5: Frequency reuse patterns and cell edge performance.

$$\psi_{\mathrm{UE_{CC}}} = \frac{(\delta R)^{-\nu}}{\sum_{l=1, l\neq\hat{l}}^{L} (d_l)^{-\nu}}, \qquad \psi_{\mathrm{UE_{CE}}} = \frac{R^{-\nu}}{\sum_{l=1, l\neq\hat{l}}^{L} (d_l)^{-\nu}}. \tag{2.4}$$

Thus, taking into account the previous expressions and the different frequency reuse patterns, SINR and spectral efficiency values for both users can be obtained and the effect of the propagation loss exponent can be also included into the picture. Figure 2.6 shows the result considering the Shannon's formula for spectral efficiency and $\delta = 0.05$. From Figures 2.6a and 2.6b it can be seen that the improvement on the average SINR experienced by central users ($\mathrm{UE_{CC}}$) due to higher frequency reuse factors (3 and 7) does not compensate the loss in terms of spectral efficiency caused by the bandwidth reduction associated to each reuse pattern. Thus, as a conclusion for central users, frequency reuse factor 1 is the best choice from the capacity point of view. On the other hand, looking at Figures 2.6c and 2.6d, it is evident that frequency reuse factor 3 provides the best performance for cell edge users ($\mathrm{UE_{CE}}$) as it maximizes the capacity. Thus, applying different frequency reuse factor to different groups of users depending on their average channel quality is the fundamental design principle in many ICI mitigation strategies. Whereas some techniques apply certain reuse patterns statically, others apply a frequency reuse factor that is computed based on time varying indicators and/or performance metrics. Consequently, the notion of frequency reuse is key in ICIC. In addition, as the propagation loss exponent growths, SINR figures also increase; an effect that is more pronounced in the cell edge when high frequency reuse factors are employed. This clearly suggests that any *variable* resulting in such effect is advisable from the ICI management perspective. Finally, another aspect to be remarked here is the role of the geometry of the cellular layout. It has a great influence on the best frequency reuse factor, and indeed, as it will be shown in Chapter 3, homogeneous frequency reuse patterns are no longer optimal in realistic deployments where the cellular layout is irregular.

In this manner, having 1) justified the need for ICI mitigation, and 2) introduced several theoretical and practical aspects of this problem, the following section provides a high level perspective of the different approaches that have been proposed so far.

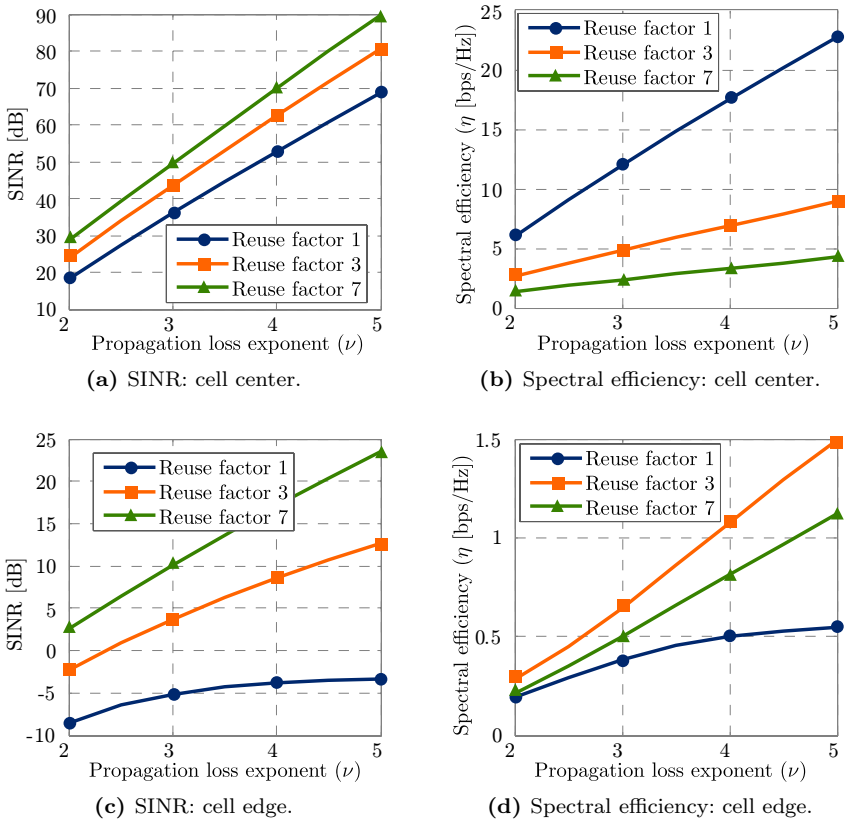

(a) SINR: cell center.

(b) Spectral efficiency: cell center.

(c) SINR: cell edge.

(d) Spectral efficiency: cell edge.

Figure 2.6: Impact of frequency reuse.

2.3 ICI in OFDMA Systems: Strategies

The objective of this section is to provide a wide perspective of the techniques and strategies to deal with ICI in cellular systems based on OFDMA, and so, contextualize ICIC within this broader framework. Given the tremendous impact of the ICI, it is not surprising that other techniques are also focused on minimizing its effects. Although, this thesis is about ICIC, and more precisely about static ICIC, a discussion including all the approaches is needed not only for the sake of completeness but also to understand how ICIC can coexist with several other strategies and evolve to deal with current and future challenges of cellular communications.

In a nutshell, interference mitigation can be done by means of 1) randomization, where the interference is distributed uniformly across the available bandwidth through scrambling, interleaving, or frequency-hopping (spread spectrum), 2) cancellation, where interfering signals can be either subtracted from the received signal or, if Multiple Input Multiple Output (MIMO) is used, the best received signal can be selected, 3) CoMP, a family of novel resource allocation techniques including

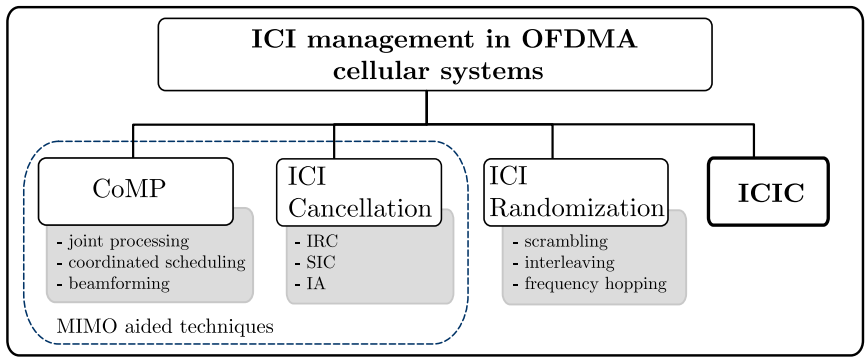

Figure 2.7: General classification of interference mitigation techniques.

joint processing and/or coordinated scheduling/beamforming, and 4) ICIC, where restrictions to the radio resources (bandwidth and power) available at each cell are created to reduce ICI at cell edges. Figure 2.7 provides a panoramic of interference management in OFDMA systems. The previous families of strategies have been identified as key frameworks for interference mitigation within the 3GPP [10, 11], and hence, interference cancellation, interference randomization, and CoMP are briefly described in Subsections 2.3.1, 2.3.2, and 2.3.3, respectively. Then, ICIC is covered in detail in Section 2.4.

2.3.1 ICI Randomization

These strategies aim at randomizing interfering signals, which can be done by using scrambling, applying pseudo-random codes after channel coding/interleaving or by means of frequency hopping. Sometimes a spreading is also included. The randomization makes the interference more uniform so that strong interfering signals, i.e., generated from (or transmitted to) cell edge users, will tend to have a tolerable impact on the rest of users in adjacent cells, rather than a destructive impact on few users (thus increasing outage). ICI randomization achieves good performance in heavily loaded networks since scrambling induces interference fluctuations and this leads to frequency diversity gains [12]. However, it is worth mentioning that, in the context of LTE/LTE-A [13], randomization-based strategies are being preferred for the uplink due to the use of localized Single Carrier Frequency Division Multiple Access (SC-FDMA) in LTE Rel 8 and 9, and up to two clusters of localized subcarriers in LTE Rel 10 and 11. In this manner, frequency hopping allows for the introduction of certain frequency diversity gain. On the other hand, the downlink gets frequency diversity gains directly from frequency distributed scheduling.

Recent contributions in this area include performance evaluations [14], schemes for cell search and synchronization [15, 16], enhancements for the control channels in the uplink [17], and multiple access schemes featuring hopping capabilities [18].

2.3.2 ICI Cancellation

In ICI cancellation, the basic concept is to regenerate the interfering signals and subsequently subtract them from the desired signal [19]. In short, the approach is removing ICI rather than avoiding it. Currently, two major lines are being investigated:

1. *Detection and subtraction*: ICI can be removed by explicitly modeling the interfering symbols. Interfering signals are estimated, for instance, by means of blind detection [20], and their estimates are then subtracted from received signals. However, in order to make ICI cancellation feasible at the receiver side, transmitters must be synchronized.

2. *Spatial suppression*: This approach requires the use of multiple antennas. ICI cancellation can be done without synchronization of the transmitters and the corresponding receiver is usually called Interference Rejection Combining (IRC) receiver [21].

One good feature of interference cancellation is that the implementation at the receiver side can be considered independently of the interference mitigation scheme adopted at the transmitter, and hence, the coexistence with other techniques is not an issue. However, complexity is the major objection associated with these strategies. Thus, interference cancellation techniques including IRC and some types of Interference Alignment (IA) [22] are being considered mostly for the uplink and implemented in the base station receiver. In practice, only certain (interference cancellation) approaches such as Successive Interference Cancellation (SIC) [23] are being considered for the downlink. In the next points, a brief description of these novel strategies is provided.

Interference Rejection Combining

The fundamental concept in IRC is to exploit the correlation (between antennas) of interfering signals. Thus, taking advantage of this spatial correlation, interference can be detected and suppressed by means of multiple antenna techniques. An in-depth treatment can be found in [24]. Basically, the IRC receiver combines signals in such a way that the Mean Square Error (MSE) of the combined signal and the desired signal is minimized. The results presented in [25] indicate that IRC provides significant cell edge performance gains for the uplink of LTE systems.

Successive Interference Cancellation

SIC is a PHY layer capability that allows receivers to decode different packets that arrive simultaneously. This is possible because, aided by signal processing techniques, receivers are able to decode the stronger signal, subtract it from the combined signal, and extract the second stronger one from the residue. Thanks to emerging

software radio platforms, SIC implementations are becoming possible and significant enhancements of MIMO links have been reported. In [26, 27], various strategies based on SIC are evaluated in the context of LTE and its performance has been also tested in conjunction with ICIC techniques as in [28, 29].

Interference Alignment

Interference alignment (IA) is a recent development that reduces the impact of interference. The design concept is to coordinate multiple transmitters so that their mutual interference is aligned at the receivers, thus facilitating interference cancellation. IA can be regarded as a cooperative interference management strategy that exploits the availability of multiple signaling dimensions provided by multiple time slots, frequency blocks, or antennas. The transmitters jointly design their transmitted signals in the multidimensional space such that the interference observed at the receivers occupies only a portion of the full signaling space. A surprising result showed in [30], is that alignment may allow the capacity of the network to grow linearly, and without bound, with the network size. Recall that in TDMA and FDMA, the sum rate is more or less constant independently of the network size as only one pair of users can communicate in a given time/frequency block.

The possibilities opened by this new paradigm are infinite and intensive research is therefore conducted around IA [31–33]. However, IA relies on some assumptions which must be relaxed before it is adopted in practical wireless systems. These include the need for an unfeasible CSI, moderate to high SINR levels, accurate synchronization and self-organization capabilities.

2.3.3 CoMP

CoMP is a family of novel techniques that have been recognized as a key element to deal with intercell interference and increase spectral efficiency within the LTE roadmap after the Release 9. Indeed, CoMP concepts appeared in LTE Release 11. According to [11], CoMP techniques for the downlink can be categorized as:

1. *Joint Processing*: Users' data is available at each point in a CoMP cooperating set[2]. Within joint processing, a special technique called *joint transmission* consists in the transmission from multiple points in the CoMP cooperating set to one single user at a time.

2. *Coordinated Scheduling/Beamforming*: These techniques encompasses a wide range of resource allocation algorithms in which data is only available at serving cell but scheduling/beamforming decisions are made with coordination among cells within the CoMP cooperating set.

[2] A CoMP cooperating set is a set of (geographically separated) base stations directly or indirectly participating in data transmissions to a user.

Preliminary field trials were reported in [34] and thereafter, numerous proposals and contributions have been presented. Recent representative examples include [35–37]. Besides of the theoretical advances that clearly show the potential benefits of CoMP, implementation requires a high capacity/low latency backhaul architecture, efficient cell clustering techniques, accurate synchronization and more detailed CSI feedback schemes. Most of these challenges are being investigated, however it is worth saying that practical implementations are being tested mainly for the uplink [38].

Summarizing...

On the one hand, the strategies for interference management seen so far 1) modify the way the interference is distributed across the system bandwidth (randomization mechanisms), 2) eliminate the interference (cancellation schemes), or 3) make interference signals orthogonal among users by using spatial multiplexing and multicell joint/coordinated scheduling (CoMP strategies). On the other hand, the remaining approach, ICIC, aims at minimizing the impact of ICI on cell edge users by defining the resources (bandwidth and power) that can be used at each cell at any time. In this manner, the levels of ICI at cell edges are reduced, and consequently, the QoS of cell edge users can be improved. The next section is entirely devoted to ICIC.

2.4 Intercell Interference Coordination

The target of this section is to explain the different types of ICIC, their characteristics, advantages and drawbacks, operational principles and discuss how they differ/resemble each other. Then, a survey of ICIC techniques is presented, **with special emphasis on static ICIC and the schemes based thereon**.

Given that ICIC has been recognized as a key piece of 3G, 4G, and future 5G technologies [3, 39], the research around it has been intensive and an uncountable number of works and contributions have been presented in the last few years. A complete compilation and review of such literature is certainly unaffordable, and consequently, this section presents the papers that are more relevant according to the objectives of this thesis.

2.4.1 Baseline schemes

As it was shown in Section 2.2, Frequency Reuse 1 (FR1) and 3 (FR3) are configurations that maximize the throughput at the center and edges of the cell, respectively. These schemes are the common benchmark in the vast majority of ICIC proposals and they provide the basic reference point to assess the merit of any ICIC solution. Therefore, for the sake of completeness, the operational principle of FR1 and FR3 are illustrated in Figure 2.8. Recalling briefly, while in FR1, all cells have access to the whole system bandwidth, in FR3 each cell is only allowed to use one third

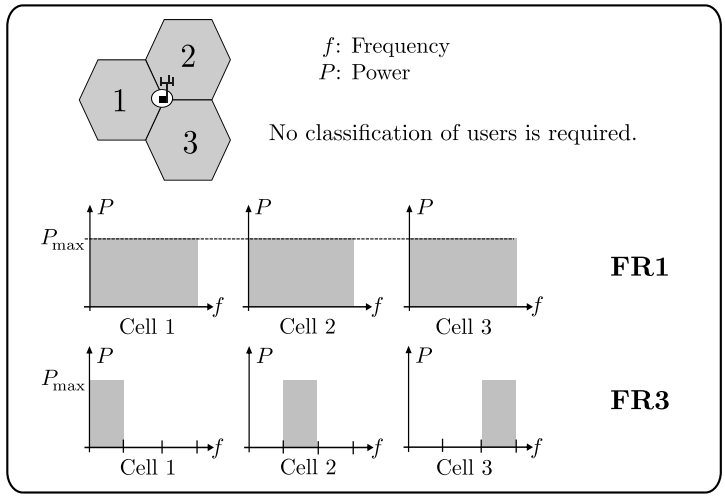

Figure 2.8: Operational principle of FR1 and FR3.

of the system bandwidth. Note that no classification of users is performed, and consequently, all users experience the same frequency reuse factor.

2.4.2 ICIC strategies: Classification

ICIC allows several possible taxonomies. In fact, different classifications and nomenclatures have been presented in surveys about interference mitigation and coordination. Excellent compilations include [19, 39–41], and more recently, [42, 43].

A widely adopted criterion is the temporality with which resource coordination is performed [4, 41, 44]. Thus, ICIC solutions can be classified as static and dynamic schemes.

Static ICIC implies the use of fixed and predefined reuse patterns and power levels levels to different groups of users according to their average SINR. Therefore, the radio resources available at each cell are allocated (and kept fixed) for extended periods of time. To be more precise, the portion of bandwidth and corresponding power that each base station is allowed to use in its cells is defined during the planning process. The static approach has several advantages:

- ✓ No additinal/detailed CSI is required for the operation of the scheme.
- ✓ Intercell signaling does not need to be exchanged.
- ✓ Very low complexity/real-time computational cost.
- ✓ No explicit interworking with other network functionalities is assumed.

The major inconvenience is the lack of adaptability to network dynamics such as traffic variations both in time and space. In addition, static ICIC schemes typically require to define a certain set of *rules* and operational parameters. As it will be

indicated, the performance of these strategies is strongly influenced by the choice of optimal values for such figures, which is not an easy task in many real-life contexts.

On the other hand, dynamic ICIC employs adaptive algorithms to efficiently manage radio resources. Clearly, the main advantage of this approach is the ability to respond to inhomogeneous traffic load distributions and other time varying conditions. Nevertheless, as it will be explained in detail shortly, this dynamism is only achievable at expense of prohibitive complexity and unfeasible practical requirements. Indeed, the feasibility is directly linked to the level of adaptation that is pursued, and consequently, the time scale at which coordination is performed largely determines the complexity. In this line, it is also worth saying that the tradeoff between performance and feasibility is also associated to the architecture that is proposed. While centralized schemes achieve near optimum performance with fairly stable operation and convergence properties, semi distributed and fully distributed solutions, though much more feasible, offer less gains and sometimes, convergence and stability are concerns. The operational principles and design guidelines of several types of dynamic ICIC are covered in subsection 2.4.4

Before going into the details of each type of ICIC, a summary and comparative view is provided in Table 2.1.

2.4.3 Static ICIC

The fundamental idea in static ICIC is to apply different frequency reuse factors to different groups of users based on average SINR measurements[3]. As it was shown in Subsection 2.2.4, different frequency reuse factors are optimal (from the capacity point of view) depending on user position, and consequently, static ICIC techniques are also known as frequency reuse based schemes. SFR and FFR are the most fundamental forms of static ICIC, and so, the discussion is mainly centered in these strategies and the ones derived from them.

The operation of SFR and FFR techniques requires two aspects:

1. *Users classification.* Based on a SINR classification threshold (ψ_{TH}) users are grouped in two classes: central users and cell edge users. Hereafter, central and cell edge users are indicated by the symbols $\mathcal{I}$ (interiors) and $\mathcal{E}$ (exteriors), respectively.

2. *Defining operational parameters.* Both SFR and FFR, need to specify the set of channels (frequency resources) that each cell is allowed to use together with the power and the group of users (either $\mathcal{I}$ or $\mathcal{E}$) associated to them.

Figure 2.9 illustrates the operational principle of SFR and FFR. In the figure, a tri-sectorial site is considered. The design of SFR and FFR is similar in certain aspects, however, there are also important differences. In order to illustrate them, the following convention is adopted.

[3]Average SINR refers to wideband measurements, i.e., considering all frequency resources.

Table 2.1: Classification of ICIC techniques based on the time scale of coordination.

Basic criterion	**ICIC operation** [41]	**Adaptability** [4]	**Time scale** [4]	**Feasibility**
Static	Fixed and potentially modifiable by an external agent	Long term network conditions	Days-weeks	Basic CSI, no intercell signaling, low complexity, no convergence issues. Fixed network planning.
Dynamic	Adaptive	Medium term network conditions	Days	Basic CSI, possible intercell signaling, low complexity, no convergence issues. Flexible network planning.
		Cell load adaptive	Minutes-hours	Basic CSI, intercell signaling required medium complexity, stable operation. Flexibility on uneven traffic distributions.
		User load adaptive	Seconds	Detailed CSI, intercell signaling required medium-high complexity, convergence issues. Flexibility on time varying demand.
	Real time	Synchronized	Miliseconds	Perfect CSI, heavy intercell signaling required high complexity, stability issues. Advanced time-frequency resource allocation.

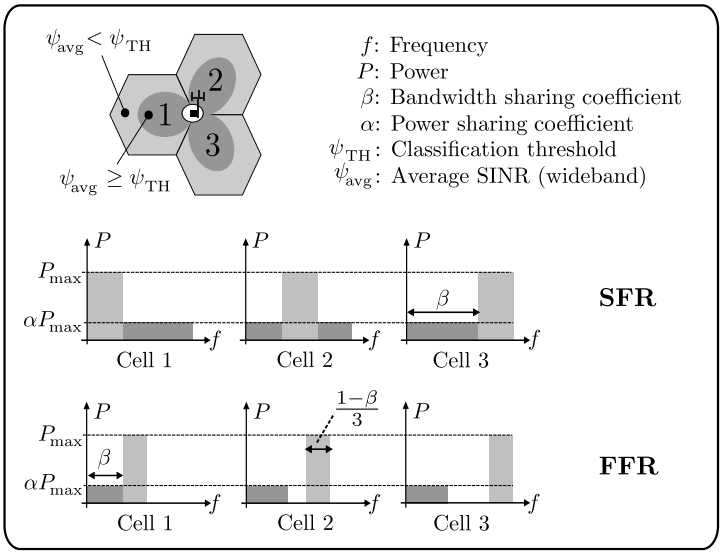

Figure 2.9: Operational principle of SFR and FFR.

- *Active Band*: portion of the system bandwidth in which a cell is allowed to transmit. Hereafter, $\mathcal{B}_l^{\text{A}}$ represents the set of frequency resources (subbands) in which the l^{th} cell is allowed to transmit. $\mathcal{B}_l^{\text{A}} \subseteq \mathcal{B} \ \ \forall l$. Recall that $\mathcal{B}$ is the set of all subbands in the system bandwidth.

- *Reserved Band*: portion of the system bandwidth in which the l^{th} cell is allowed to transmit to either central or cell edge users, $\mathcal{B}_{l,\mathcal{I}}^{\text{R}}$ and $\mathcal{B}_{l,\mathcal{E}}^{\text{R}}$, respectively. Therefore, $\mathcal{B}_l^{\text{A}} = \mathcal{B}_{l,\mathcal{I}}^{\text{R}} \cup \mathcal{B}_{l,\mathcal{E}}^{\text{R}} \ \ \forall l$.

As it is shown in the figure, both SFR and FFR separate users in classes by means of the parameter ψ_{TH}. Each of these classes, $\mathcal{E}$ and $\mathcal{I}$, make exclusive use of its reserved band, whose size and power are determined by the bandwidth sharing coefficient and the power ratio, β and α, respectively. β_l indicates the fraction of the system bandwidth that is assigned to center users in the l^{th} cell. Thus, $\beta_l = \frac{B_{l,\mathcal{I}}}{B} \ \ \forall l$. α_l indicates the power ratio between central and cell edge users in the l^{th} cell. Unless something different is indicated, $\beta_l = \beta$ and $\alpha_l = \alpha \ \ \forall l$. Note that in SFR and FFR, the bandwidth allocated to cell edge users corresponds to $(1-\beta) \cdot B$ and $\frac{(1-\beta) \cdot B}{3}$, respectively. In this manner, users in the cell edge zone enjoy higher frequency reuse and are served with higher power levels than users in the central part (where typically the radio channel is much better). Thus, cell edge users receive significantly less interference, and hence, their average SINR are much better making possible to improve the QoS provided to them.

As it can be easily noticed, in SFR each cell has access to the whole system bandwidth, i.e., $\mathcal{B}_l^{\text{A}} = \mathcal{B}_{l,\mathcal{I}}^{\text{R}} \cup \mathcal{B}_{l,\mathcal{E}}^{\text{R}} = \mathcal{B} \ \ \forall l$. In contrast, in FFR the active band is strictly smaller than the system bandwidth, and hence, $\mathcal{B}_l^{\text{A}} = \mathcal{B}_{l,\mathcal{I}}^{\text{R}} \cup \mathcal{B}_{l,\mathcal{E}}^{\text{R}} \subset \mathcal{B} \ \ \forall l$. In addition, while in SFR the ICI experienced by each class of users is also *interclass*,

in FFR each class of user uses the same subband in different cells, and therefore, ICI is only *intraclass*. The previous makes, in general, SFR notably more sensitive to α than β. The opposite holds for FFR, as shown afterwards.

Another key aspect is about how classify users. This completely depends on the SINR classification threshold (ψ_{TH}). Since this parameter determines the fraction of users belonging to each class, it has a big impact on the performance of these schemes [45]. Note that although this classification is usually regarded as a geographical distinction, in practice it is a radio condition. A detailed analysis of the effect of β, α, and ψ_{TH} is presented in Chapter 3. Based on these analyses, it came out that the classification threshold offers a flexible and feasible way to control the performance of these strategies. The observation turned out to be central in the development of the schemes that are presented in Chapters 6 and 7, where by fine tuning classification thresholds locally at cell level, effective optimization of SFR and FFR to realistic deployments was achieved.

It is important to remark that SFR and FFR are not coupled to scheduling. These schemes only determine the resources that are available at each cell. From this point, different scheduling policies can attain several tradeoffs. This is done by taking advantage of the particular resource allocation patterns, see Figure 2.9. Another important aspect is that the information users must feedback is minimal, only a measure of the wideband SINR is required. This is currently supported by most systems including LTE and LTE-A. As it was indicated, the operation of static ICIC schemes is fully distributed and only a very low amount of intercell signaling could be needed (only in cases where the network configuration needs to be changed).

As studied afterwards, a tradeoff appears between the gains in fairness and spectral efficiency. This tradeoff can be adjusted by means of the operational parameters previously introduced, however, the sensitivity strongly depends on other factors such as the scheduling policy, the performance metrics' definition and the network geometry. Thus, the need for an evaluation methodology completely decoupled from this type of assumptions was identified, and consequently, a novel parametric/statistical performance assessment procedure was developed. This methodology is presented in Chapter 3.

Finally, it is worth saying that, applying the fundamental design concepts found in SFR and FFR, i.e., frequency reuse 1 and low transmission power for central users and frequency reuse greater than 1 with high transmission power for cell edges, several other static ICIC strategies that introduce minor modifications have been proposed. Given that all of them are basically based on SFR and FFR, the discussion presented so far suffices to achieve the objectives of this chapter. Instead, only the particularities of those schemes are explained qualitatively in the following points.

Performance evaluations and methodologies

This type of contributions focus on the impact of the operational parameters and other context variables such as the type of network, mobility, and traffic model. Examples of this type of study include [46–49]. However, the merit and performance

of these schemes (including SFR and FFR) are mainly evaluated through system level simulations. So conclusions cannot be generalized since simulations are subject to the previous context variables.

In the light of this situation, analytical models have been also proposed. Interesting examples include [45, 50–52]. However, this methodology applied to complex technologies such as LTE simply require many simplifications to make the task affordable. Thus, the vast majority of these works strongly rely on synthetic (perfectly hexagonal) layouts. According to [53], this assumption is quite optimistic from the cell edge performance degradation point of view. Indeed, SINR figures found in realistic deployments can be much worse than the SINR generated from idealistic models.

Thus, it was identified the need for new and efficient performance evaluation methodologies to study the complex relationships between operational parameters and performance metrics. In this manner, useful guidelines and better understanding of the underlying tradeoffs can be obtained. In addition, the methodology should not be rigid in the sense that any possible network geometry can be taken into account.

Static ICIC schemes derived from SFR and FFR

In the literature, a wide range of static ICIC models based on SFR, FFR, or hybrid schemes have been proposed. Both SFR and FFR succeed in increasing the sum rate of users at cell edges, however, this is obtained by paying a price in terms of overall system spectral efficiency. While the penalty with SFR is smaller than the one with FFR due to the full frequency reuse, the latter achieves higher SINR values as a result of the higher frequency reuse factor, which is, on the other hand, desirable for some certain techniques such as interference cancellation [29]. Thus, research efforts have been made to enhance the performance of SFR and FFR. The operational principles of these schemes are explained in the following points and illustrated in Figure 2.10.

- *Soft FFR* (SFFR). This scheme was originally proposed in [54]. Basically, the difference with respect to conventional FFR is that this model allows the use of the subbands allocated to cell edge users for central users, although with less power. Variations of SFFR were also investigated in [55, 56]. The idea behind these modifications is to exploit the fact that cell edge users typically operate at low SINR regimes, and hence, they are more sensitive to interference (power), while central users are more sensitive to bandwidth increments [57]. Thus, by increasing the bandwidth allocated to central users, the cell throughput can be increased. However, in cases where users get concentrated at cell edges, the performance of SFFR will be clearly poor even if the new bands of central users are switched off.

- *Incremental Frequency Reuse* (IFR). The motivation of incremental frequency reuse is to improve the efficiency of conventional SFR. Since in SFR cell edge users have a maximum of one third of the system bandwidth, situations where

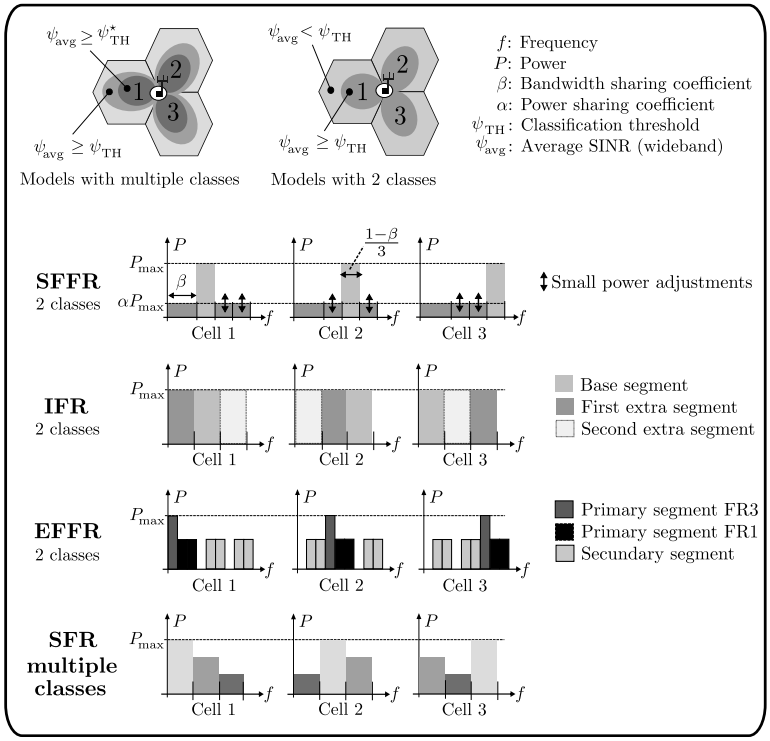

Figure 2.10: Operational principle of some schemes derived from SFR and FFR.

users are mainly concentrated at cell edges result in poor efficiency as many subchannels would be idle. IFR was introduced in [58] to address this issue. The idea is to divide the system bandwidth into segments, i.e., groups of subchannels. Each cell has its own *base segment* in which resource allocation can be done arbitrarily. If the subchannels in the base segment are exhausted, the cell can start using subchannels of their second extra segment, next third extra segment, and so on. If more than one segment is required, cell edge users have priority in the base segment. The number of segments obviously would depend on the cluster size or the target frequency reuse for low loading factors. Clearly, this scheme achieves effective ICIC if the traffic is low, however, in moderate to high load conditions, the operation tends to FR1, and hence, cell edge users cannot be protected effectively.

- *Enhanced Fractional Frequency Reuse* (EFFR). In the light of the drawbacks of IFR, a variation of FFR was proposed in [59]. The novel EFFR scheme divides the system bandwidth in two segments. A primary segment, orthogonal among cells, and a secondary segment that is not orthogonal among cells. Moreover, the primary segment is further divided in two parts with FR1 and FR3. Similarly to IFR, each cell gives priority to the primary segment being the access to the secondary one conditioned to a monitoring process. This scheme outperforms FR1, FR3, and IRF in terms of cell edge capacity.

- *Static ICIC with multiple classes.* The authors in [60] considered the use of more than two classes in static ICIC based on FFR. The idea is to divide the coverage area of each cell into more than one region and control the amount of ICI. This approach can help to increase fairness at expenses of additional complexity as the classification process is based on more thresholds. Moreover, there is also a frequency diversity loss that implies a reduction in the spectral efficiency.
- *Classification based on Soft Handover.* Although the preferred approach to classify users is according to the average SINR, another interesting alternative was proposed in [61]. In this work, users are classified as cell edge users if there are more than 2 neighbor cells in the handover list. Thus, this methodology leverages the information obtained from the handover algorithm. Results showed that cell edge performance gains are achievable with a low soft handover overhead.
- *Optimization models and heuristics.* A common pattern found in static ICIC is that most of the previous models are designed and evaluated considering perfectly hexagonal layouts. However, from the ICIC point of view, the situation is much worse in realistic deployments with irregular cellular layouts according to [53, 62]. In those scenarios, propagation conditions vary significantly from one cell to another, and hence, an homogeneous frequency reuse applied uniformly to all cells results in poor performances. Indeed, no reuse pattern can be easily derived. This was initially pointed out in [63, 64], where optimization algorithms for SFR and FFR were proposed to improve their performance in realistic large scale networks. The same conclusions were also obtained in [62]. Other examples in this category are [65–68]

Table 2.2 shows a comparative analysis of the static ICIC solutions presented so far showing their main features. At a glance, it turns out on the one hand, that simulation is the preferred research methodology, and on the other hand, that the vast majority of proposals and studies consider synthetic (hexagonal) layouts, thus making limited their contributions from a practical point of view. The issue of the performance of static ICIC schemes in realistic deployments was initially addressed by the contributions of Chen and Yuan in [63, 64], where this problem was identified and heuristics were proposed to alleviate the situation. However, some aspects of these contributions were subject to substantial improvements. First, in their work, Chen and Yuan only consider the achievable rate at cell edge as performance indicator for their algorithm, and so, in cases when some SFR setting improves this metric, the throughput of the users that contribute the most to the average spectral efficiency is penalized. Second, defining common network-wide parameters clearly leads to suboptimal performances, since in realistic deployments cells are quite different in terms of ICI and coverage; in fact, the algorithms proposed in [63, 64] does not give any clue about how to select such operational parameters (α, β, and ψ_{TH}), and therefore, a huge number of trials need to be done in order to find useful results. Finally, but no less important, the need for more than one network configuration is also advisable as static ICIC does not provide means for adaptation. Thus, a feasible approach based on static ICIC that leaves the door open to straightforward

Table 2.2: Comparison of static ICIC contributions.

Ref.	Type	Irregular traffic patterns	LTE feasibility	QoS and fairness	Layout	Research Methodology
[45]	PE	×	×	✓	Irregular	Analytical
[46]	PE	×	✓	✓	Synthetic	Simulations
[47]	PE	×	✓	P	Synthetic	Simulations
[48]	PE	×	×	P	Synthetic	Simulations
[49]	PE	×	✓	✓	Irregular	Simulations
[50]	PE	×	×	×	Synthetic	Analytical
[51]	PE	×	×	✓	Synthetic	Analytical
[52]	PE	×	✓	P	Synthetic	Analytical
[55]	DS	P	×	✓	Synthetic	Simulations
[56]	DS	×	×	✓	Synthetic	Both
[58]	DS	×	×	✓	Synthetic	Simulations
[59]	DS	P	×	✓	Synthetic	Simulations
[60]	DS	×	×	P	Synthetic	Simulations
[61]	DS	×	×	✓	Synthetic	Simulations
[63]	DS	×	×	✓	Irregular	Simulations
[64]	DS	×	×	✓	Irregular	Simulations
[65]	DS	P	×	✓	Synthetic	Simulations
[66]	DS	P	×	✓	Synthetic	Simulations
[67]	DS	×	×	×	Synthetic	Simulations
[68]	DS	×	×	P	Synthetic	Simulations

PE: Performance Evaluation DS: Derived from SFR and FFR P: Partially

extensions to achieve a certain level of dynamism is highly desirable. On top of this, only few schemes based on static ICIC cover aspects related to LTE feasibility and irregular traffic distributions. These observations, together with the results presented in Chapter 3, inspired the first part of the research work presented in this thesis.

Curiously, no significant research efforts have been placed on improving the performance of static ICIC strategies, although these schemes are the most suitable ones for implementation in real systems such as LTE. In general, previous works were focused on dynamic mechanisms that in their vast majority, present serious feasibility challenges. Here it is important to recall that in real systems such as LTE and LTE-A, other RRM functionalities are responsible for coping with the effects of bursty traffic and fast fading. This was remarked in [6], where the authors showed that around 50%–60% of the typical gains obtained by means of (hardly feasible) dynamic resource allocation algorithms that determine optimal configurations can also be obtained by means of ICIC schemes following only macroscopic (medium-to-long term) conditions. Thus, the author focused on the idea of taking the way of improving static ICIC schemes rather than go over, theoretically attractive but unfeasible, dynamic strategies. As it was mentioned, dynamic ICIC will be visited in the next subsection for the sake of completeness.

2.4.4 Dynamic ICIC

In essence, dynamic ICIC tries to provide some dynamism to the process of ICIC. Since traffic load patterns are neither constant over time nor uniformly distributed spatially, static configurations that perform correctly, on average, may be underusing network resources in smaller time scales. Therefore, dynamic mechanisms attempt to cover this gap by adapting the ICIC process to short term variations.

Dynamic ICIC schemes can be classified according to several criteria. In this survey, the objective is to provide a complete and wide picture of the advantages and drawbacks of this approach, and consequently, several classification criteria are considered:

1. *Model type*. In general terms, dynamic mechanisms can be grouped in two sets: models based on static ICIC schemes (either SFR or FFR) and models based on generic resource allocation formulations.
2. *Time scale of coordination*. As it was shown, several time scales can be identified. Accordingly, the classification based on adaptive and real time schemes as proposed in [41] (see Table 2.1) is adopted.
3. *Architecture*. According to the way in which the operation is performed, proposals can be centralized, semidistributed, or distributed [43].

The three previous classification criteria result in non disjoint sets of contributions, and hence, certain works can appear repeatedly along the following descriptions that illustrate the basic characteristics of each group. Again, the goal is to offer several perspectives of dynamic ICIC rather than a detailed description of each contribution, which obviously is out of scope herein. In any case, a unified/comparative view of all these works is presented along the following points.

Model type

Basically, the models based on static ICIC propose different types of bandwidth and power reallocations starting from the patterns defined in SFR or FFR. These strategies aim at making use of the experience with static schemes by means of heuristic algorithms. A clear example is [69], where cells assign resources orthogonally to cell edge users by means of a scheme termed dynamic major group allocation that follows the SFR principle. The final resource allocation is performed by a kind of centralized proportional fair scheduler. The authors in [70] proposed a two level semidistributed dynamic algorithm that can coexist with classical SFR and FFR to achieve further cell edge performance gains. The work is notorious because it analyzes the effects of scheduling on throughput and fairness for a given amount of resources. Other relevant contributions following this approach include adaptations of the previously introduced IFR [71], EFFR [72], and SFR and FFR [73–75].

There is a large number of contributions in which a certain level of ICIC has been obtained by developing solutions to optimization problems based on generic

resource allocation formulations. This category encompasses the vast majority of dynamic ICIC mechanisms. According to [42], performance objectives typically include maximization of sum rate capacity and minimization of ICI and/or power subject to one or more constraints to include energy efficiency, QoS, and practical aspects. As ICI involves transmission in different cells, this type of approach inherently requires some sort of network-wide opportunistic scheduling and power control. Interesting heuristic algorithms have been presented in [76–81]. This type of solutions are inspired on a wide range of models including collisions [82], cross-layer designs [83], and interference graphs [84]. Tools commonly used to solve these generic ICIC formulations encompass game theory [85–89], programming techniques [90–93], and learning algorithms [94, 95].

Given that the general problem of ICIC (closely related to dynamic channel assignment) in wireless network is, in general, NP-Complete [96], efficient metaheuristics[4] for solving combinatorial problems have also been employed. Thus, several contributions have applied techniques such as simulated annealing [97] and genetic algorithms [98]. Machine learning methods such as neural networks [99] are also typical options. Moreover, irregular traffic patterns distributions have been considered as a very important aspect in many adaptive ICIC solutions. Representative examples incorporating these aspects can be found in [6, 100–107].

Time scale of coordination

Adaptive ICIC provides flexible resource allocation according to different network requirements in terms of user-load and cell-load traffic demands. The degree of flexibility depends on the ICIC time scale, which varies from hundreds of milliseconds to days. In general, the basic mechanisms consist in adjusting the frequency reuse at each cell to satisfy traffic demand. So, the usage of the resources devoted to cell edge users is coordinated. Nevertheless, this requires that different cells exchange information. ICIC proposals featuring this degree of adaptation can be found in [74, 105, 108, 109].

Real time ICIC is able to achieve near-optimum performance in terms of sum rate and cell edge performance. These strategies operate at time scales of milliseconds and full synchronization is required. Moreover, in order to exploit the channel diversity, full and perfect CSI is assumed to be known at each cell. This information (or the data derived from it) needs to be transmitted to other cells. The assumption of global knowledge and the need for a certain level of joint scheduling at such small time scale impose challenging issues from the implementation point of view [13]. Excellent contributions falling into this category include [70, 110–114].

Architecture

In centralized schemes, ICIC is typically modeled as an optimization problem that is solved in a central entity that collects all the required information through

[4] A more formal introduction to the matter is presented in Chapter 5.

intercell signaling. After the processing of this information, each cell receives resource allocation commands or guidelines. In practice, the implementation of centralized schemes represents a difficult task since a high capacity and fast transmission infrastructure is needed. For this reason, modern technologies such as LTE and LTE-A avoid such control entity and feature flat architectures, in which, coordination is possible through intercell interfaces. Examples of centralized schemes are [112, 115–117].

In semidistributed schemes, coordination is typically performed at two (temporal) levels. The higher level is still performed in a centralized entity while the lower level, at smaller time scale, is executed independently at each cell. In this manner, semidistributed solutions are able to deal with practical limitations of cellular systems, i.e., processing load and signaling delay. However, an efficient and reliable infrastructure is required, and more important, a sort of central entity is still needed. Thus, the vast majority of semidistributed solutions are not practical for implementation in systems such as LTE and LTE-A. Examples of semidistributed schemes include [70, 79, 109, 110, 118–121]

In distributed solutions, commonly known as fully distributed, the whole processing and decisions are made independently at each cell. However, intercell signaling is allowed. Due to this selfish behavior, distributed solutions typically suffer conflicts among cells, and so, convergence and stability are often serious concerns. Given its nature, non-cooperative game theory represents a suitable framework to solve distributed ICIC formulations [85, 87, 114]. However, heuristics focused on self-organization are also a popular approach as it can be seen in [103, 111, 122, 123].

In order to provide a comparative perspective of the contributions previously commented, several criteria have been considered:

- *The type of resource allocation*. Several classification can be considered.
  - According to the time scale of coordination, dynamic ICIC schemes can be classified as real-time or adaptive, see Table 2.1.
  - Three different objectives are commonly used in optimization formulations: interference minimization, transmit power minimization, and throughput maximization.
  - According to the architecture, the proposals can be: centralized, semidistributed, and distibuted.
- *LTE feasibility*. It indicates if LTE implementation aspects have been considered. This aspects include the need for detailed CSI, intercell signaling, and the required interaction with other functionalities such as AMC, power control, and scheduling.
- *Solution approach*. It indicates the type of approach employed in the ICIC scheme. As it was shown, heuristic algorithms are a popular method, however, proposals based on mathematical programming (optimization techniques) have also been presented.

- *Complexity*. A numerical scale from 1 to 5 have been used to measure the complexity. The value '5' means very high complexity, a '1' corresponds to very low complexity. The scale takes into account the level of intercell overhead, the type of CSI, and the computational cost required to perform the ICIC process.

- *The research methodology*. It indicates the type of method used in performance assessments.

Table 2.3 shows a comparative analysis of the dynamic schemes commented so far taking into account the previous criteria. As it can be seen, a common approach is to formulate optimization problems and solve them by means of programming methods and/or heuristic algorithms. As it happened with static ICIC, simulation is the preferred evaluation methodology because cellular systems are too complex. So it is extremely complicated to capture all elements and factors through analytical (closed-form) models. Note also that almost invariably, feasibility aspects are not completely addressed. Some authors simply provide certain insights and guidelines about how their proposals can be implemented, but, to the best of the author's knowledge, no contribution is fully compatible with the current features of commercial systems such as LTE and LTE-A. The previous statement does not imply, by any means, that the contribution of those works is limited. Instead, excellent works have shed light on several aspects describing the complex operation of cellular systems, and in particular, the interference coordination process. Finally, note that all these schemes feature a moderate to high complexity (values from 3 to 5). For instance, the scheme presented in [100] is assigned a 5 because it 1) requires perfect CSI, 2) features a centralized architecture requiring high a significant amount of intercell signaling exchange and, 3) proposed the online solution of an optimization problem whose complexity is proportional to the number of users. However, the work presented in [81] assumes a limited CSI and proposes a semidistributed architecture to solve an heuritic algorithm that achieves suboptimal performances. Consequently [81] receives a 3.

2.4.5 Remarks from the state of the art

This section has presented a detailed introduction to ICIC. Besides explaining the main features of the two approaches, static and dynamic, an updated review of the literature was also discussed. The structure showing the classification criteria considered so far is depicted in Figure 2.11. It was shown that ICIC represents today, one of the most promising alternatives to improve cell edge performance in OFDMA based cellular systems. From the results reported in the literature, some guidelines and conclusions can be drawn.

Static ICIC

1. The threshold used to classify users is a parameter of utmost importance as it has an immediate impact on scheduling decisions.

Table 2.3: Comparison of dynamic ICIC contributions.

Ref.	Type	LTE feasibility	Solution approach	Complexity [1-5]	Research Methodology
[6]	AD/SD/T	Partially	Heuristics	5	Simulations
[69]	AD/CE/T	×	Heuristics	3	Simulations
[70]	RT/SD/I	Partially	Heuristics	4	Simulations
[71]	AD/SD/T	Partially	Heuristics	3	Simulations
[72]	AD/CE/T	×	Heuristics	3	Simulations
[73]	AD/CE/T	×	Heuristics	3	Simulations
[74]	AD/CE/T	Partially	Heuristics	4	Simulations
[76]	RT/CE/T	×	Programming	4	Simulations
[77]	RT/CE/T	×	Heuristics	4	Simulations
[78]	RT/SD/T	×	Both	5	Simulations
[79]	AD/SD/T	×	Heuristics	4	Simulations
[79]	AD/SD/T	×	Heuristics	3	Simulations
[81]	AD/SD/T	×	Heuristics	3	Simulations
[82]	N/A	×	N/A	3	Analytical
[83]	RT/CE/T	×	Programming	5	Both
[84]	AD/SD/I	×	Heuristics	3	Simulations
[85–89]	AD/DI/I	×	Heuristics	5	Simulations
[90–93]	RT/CE/T	×	Programming	5	Simulations
[94]	AD/SD/T	×	Heuristics	3	Simulations
[95]	AD/SD/I	×	Heuristics	3	Simulations
[99]	AD/CE/P	×	Metaheuristics	3	Simulations
[97]	AD/CE/T	×	Metaheuristics	3	Simulations
[98]	AD/CE/T	×	Metaheuristics	3	Simulations
[100]	RT/CE/T	×	Programming	5	Simulations
[101]	AD/CE/T	×	Programming	5	Both
[102]	AD/SD/T	Partially	Heuristics	4	Simulations
[103]	AD/DI/T	Partially	Heuristics	4	Simulations
[104]	AD/SD/P	×	Heuristics	4	Simulations
[105, 106]	AD/SD/T	×	Heuristics	4	Simulations
[107]	AD/DI/T	Partially	Heuristics	3	Simulations
[108]	AD/SD/T	Partially	Heuristics	4	Simulations
[109]	AD/SD/T	Partially	Heuristics	5	Simulations
[110]	RT/SD/T	×	Heuristics	5	Simulations
[111]	RT/DI/T	Partially	Programming	5	Simulations
[112, 113]	RT/CE/T	×	Heuristics	5	Simulations
[114]	RT/DI/P	×	Heuristics	4	Simulations
[115–117]	RT/CE/T	×	Programming	5	Simulations
[118]	AD/SD/I	Partially	Heuristics	4	Simulations
[119]	RT/SD/T	Partially	Heuristics	5	Simulations
[120, 121]	AD/SD/T	×	Heuristics	4	Simulations
[120]	AD/SD/T	×	Heuristics	4	Simulations
[122]	AD/DI/T	×	Heuristics	3	Simulations
[123]	AD/DI/T	×	Heuristics	5	Simulations

RA: Resource allocation — DS: Derived from SFR and FFR — P: Partially
AD: Adaptive — RT: Real time
CE: Centralized — SD: Semidistributed — DI: Distributed
T: Maximize throughput — P: Minimize power — I: Minimize interference

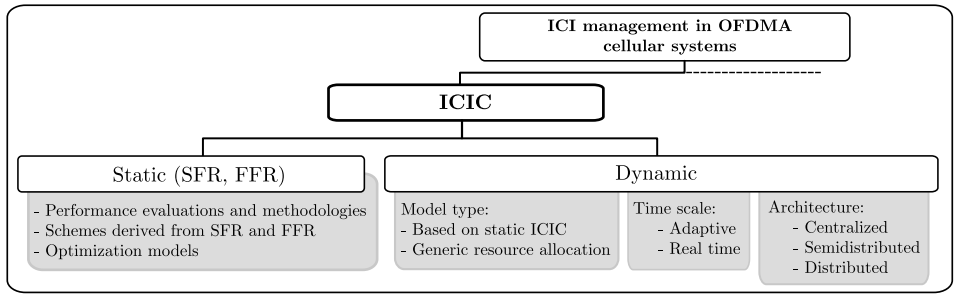

Figure 2.11: General classification of ICIC strategies.

2. In general, the spectral efficiency of the system is proportional to the power allocated to central users, while fairness strongly depends on the amount of resources allocated to cell edge users. This is a fundamental tradeoff in ICIC.
3. Increasing the number of classes is another way to improve fairness, although at expense of spectral efficiency.
4. Interclass interference can be avoided by reducing the bandwidth available at each cell. Avoiding interclass interference is key to achieve high SINR values, but again, at the expense of spectral efficiency.
5. Network geometry strongly affects the optimal frequency reuse to be used at cell edges and hence, the performance of any static ICIC strategy.

Dynamic ICIC

1. In dynamic ICIC, higher gains come from centralized schemes where a central *coordinator* has a global knowledge and takes decisions accordingly.
2. The general problem of resource allocation is NP-hard and hence, optimal solutions are basically unfeasible.
3. Semidistributed and distributed require *cooperation* among cells. Thus, adaptive schemes should minimize the amount of signaling overhead.
4. The coordination time scales is directly related to the ability to exploit the channel diversity gain. However, faster adaptation implies higher complexity.

In conclusion...

After reviewing the contributions in the state of the art, it was concluded that significant research opportunities exist in the field of static ICIC. Static mechanisms are, by the moment, the most feasible approach to ICIC. However, significant research efforts on this area was required. To be precise, contributions in the following aspects are needed:

1. *Performance assessment*. The need for efficient and insightful evaluation methodologies was identified.

2. *Performance in realistic deployments*. The need for optimization techniques to make SFR and FFR (and in general techniques derived from both of them) suitable to realistic networks was remarked by several authors in previous contributions.
3. *Control channels capabilities*. Control channels are shown to be quite sensitive to ICI. Thus, feasible mechanisms to alleviate this problem in such a critical component of cellular systems are required. For the sake of clarity, details on existent works explicitly dealing with control channels are presented in Chapter 7.
4. *Interworking*. An interesting aspect of ICIC is the close relationship with other network functionalities such as CSI feedback schemes. Another way to improve the overall network performance is by improving such interactions. In Chapter 4, the interworking between the CSI feedback schemes available in LTE and SFR/FFR is analyzed, and consequently, several mechanisms are proposed to improve the performance of ICIC.
5. *Flexibility and scalability*. A static ICIC based framework should have means for easy extensions to decision-making entities in a scalable manner, i.e., whose complexity during real time operation neither depends on the network size/load nor requires unfeasible knowledge.
6. *Energy efficiency*. The increasingly important concern about energetic aspects also encompasses ICIC. Implementing energy-efficient ICIC schemes is not easy because cell edge users require high transmission power and typically their spectral efficiency is low. Therefore, the maximization of the number of bits per Joule, the main energy efficiency metric, is a challenging task. Interestingly, and according to [43], only few works have included this important perspective into their ICIC formulations. Thus, all novelties resulting in more energy efficiency are welcome and highly valuable for mobile operators.

All the previous aspects were addressed in this thesis and will be detailed throughout the following chapters. In this manner, the general objective of making a solid contribution to the theory of static ICIC by means of feasible strategies that optimize their performance in realistic LTE/LTE-A deployments was clearly accomplished. Although this thesis is about the downlink, the extension and adaptability of these strategies to the uplink is an interesting topic. The next section covers this matter.

2.5 Interference Management in the Uplink

The management of ICI in the uplink has remarkable similarities and differences with respect to the downlink. In both problems, the main concern is about cell edge users. Nevertheless, while in the downlink these users receive high levels of ICI, in the uplink they interfere severely with the transmission of other users in neighboring cells. The scenario is depicted in Figure 2.12.

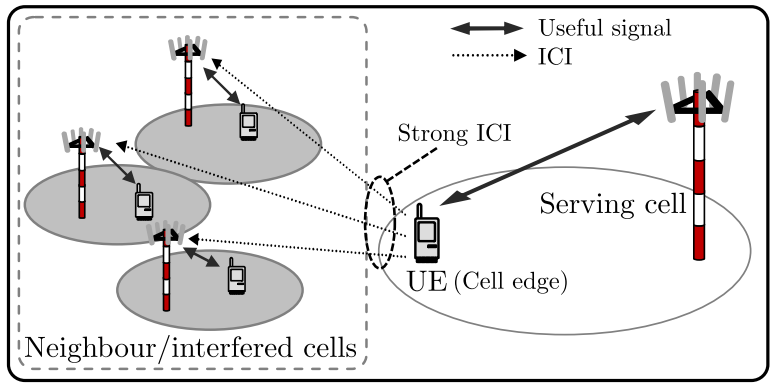

Figure 2.12: Typical ICI scenario in the uplink.

Another fundamental difference in the context of LTE/LTE-A is the access technology. While the downlink is based on OFDMA, the uplink is based on Single-Carrier FDMA (SC-FDMA), a frequency-division multiple access scheme. SC-FDMA can be regarded as a linearly precoded OFDMA mechanism because it includes a Discrete Fourier Transform (DFT) before the conventional OFDMA processing. A detailed description can be found in [13, 124]. Its adoption is due to the low PAPR requirement needed to benefit users in terms of transmit power efficiency and cost since the power amplifier used in SC-FDMA is simpler than in OFDMA.

The management of ICI in the uplink is especially complicated due to the strong burstiness of interference patterns caused by users mobility and random variations in transmitted power. Indeed, ICI is more uniformly distributed both in time and space in the downlink than in the uplink. To cope with this particularity, power control is preferred over schemes based on resource restrictions that are more complicated in SC-FDMA as users have to transmit in contiguous subchannels or at most use two clusters of contiguous subcarriers (LTE Rel 10) [125]. In LTE, the power transmitted by UE is dynamically adjusted by an intracell power control scheme [126].

According to [21], the techniques for interference management in the uplink can be grouped in schemes based on: fractional power control, frequency reuse, and interference cancellation. A brief description is provided in the following points.

- *Fractional Power control.* The basic principle is compensating the path loss in the uplink based on downlink measurements or average received power levels at the base station. With this approach, a mean ICI level in neighbor cells can be guaranteed regardless of user position. However, target SINR values need to be reduced proportionally to the distance to serving cells. Examples can be found in [127–130].
- *Frequency reuse.* This category encompasses strategies similar to SFR and FFR (and dynamic schemes derived from them) applied to the uplink. Proposals following this approach include [131–133]. However, given that in LTE/LTE-A, resource allocation is more rigid in the uplink than in the downlink, a more

promising approach is the usage of these techniques in conjunction with interference suppression schemes as in [28].

- *Interference cancellation.* ICIC for the uplink based on interference cancellation is gaining popularity. The reason is the intensive research activity around strategies such as IRC [21], SIC [23], IA [22], and the significant performance gains that has been reported in several recent studies [24, 25, 27, 33]. These techniques suit perfectly to several features of the problem in the uplink. To be precise, on the one hand, much higher processing power can be allocated in base stations than in user devices, and on the other hand, interference cancellation is inherently robust to bursty transmissions patterns (received power variations).

- *CoMP.* Strategies based on CoMP [134] can be used at base stations to collect uplink signals received by serving and neighboring cells and demodulate them jointly to reduce the Bit Error Rate (BER). This method mitigates interference, and hence, the cell edge experience is substantially improved [36]. Representative contributions include [135–137]

Thus, based on the conclusions that can be drawn from recent contributions, and according to the results shown in [138], the following remarks can be made:

1. The use of conventional ICIC based on frequency reuse is possible for the uplink. However, their efficacy is not as high as in the downlink where resource allocation is more flexible than in the uplink. Moreover, the omnipresence of power control schemes in the uplink makes ICI much more variable than in the downlink. Thus, reducing the gains that can be achieved by means of frequency reuse based strategies that are inherently more useful in the mid-to-long run.
2. Strategies based on CoMP and interference cancellation such as IRC and SIC have proven to be effective and feasible approaches for the uplink. Uplink CSI is available without resource-consuming CSI reporting, and hence, UE need almost no modification to become uplink CoMP ready. Indeed, in contrast to the downlink, it is easy to implement CoMP in the uplink [134]. Similarly, compared with other algorithms, IRC ensures high network performance and significantly improves user experience.

2.6 ICIC in HetNets and Small Cell Deployments

Currently, mobile operators have the challenge of answering to the exponential growth of traffic in cellular networks. HetNets are hierarchical network topologies in which a combination of macro, micro, pico, and femto cells are deployed all together as shown in Figure 2.13. HetNets are considered one of the most promising solutions to enhance the spectral efficiency of the network per area unit, and consequently, ICIC for HetNets has become an active research field. Another important advantage of HetNets is that they significantly improve indoor coverage. From a practical perspective, two major issues must be addressed in HetNets. First, determining

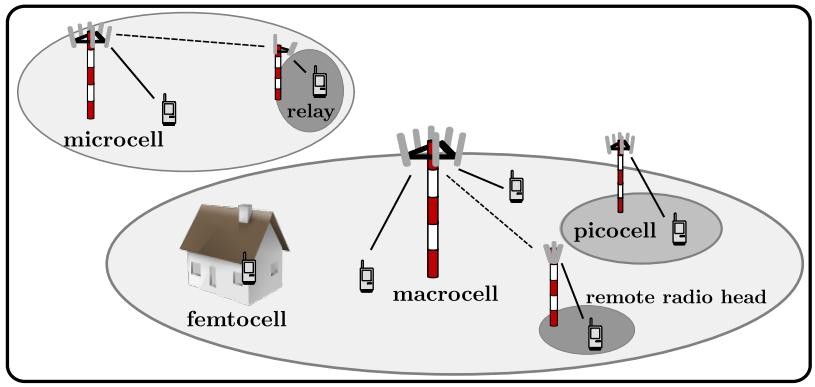

Figure 2.13: Example of a HetNet deployment.

the amount of radio resources that one layer can grant to others, and second, implementing association rules to decide which users have to get connected to each layer [139]. In addition to that, effective interference mitigation is another aspect that needs to be solved in HetNets.

The frameworks for eICIC and FeICIC addressed interference mitigation issues within the 3GPP starting from the Release 10 (LTE-A). The techniques that have been proposed and evaluated so far in the context of HetNets include ABS [140, 141]. ABSs are introduced in time domain to reduce the ICI in severly interfered cells. In these subframes (ABSs), interfering cells (typically macro ones) mute their transmissions, and *this time* is used by interfered cells (typically femto ones) to provide service for its users. Moreover, dynamic cell range expansion [142], specialized power control mechanisms [143], static ICIC based strategies [144], and hybrid techniques with interference cancellation [145] have been proposed.

Carrier Aggregation has been included in LTE-A to increase the operational bandwidth [146]. This multiband implementation, i.e., the addition of several Component Carriers (CC), offers interesting ICIC possibilities to *separate* interfering and interfered cells. Interesting ICIC formulations for carrier aggregation can be found in [147–149].

One step forward in HetNets is small cell deployments, this constitutes the natural approach to bring the network even closer to the user and not only in hotspots or cell edge areas. They are key in boosting network capacity by means of a *highly aggressive* frequency reuse and they are becoming popular among mobile operators. The idea behind this access network architecture is a hyperdense deployment of low power nodes. In addition, strong interworking with other low power based technologies such as Wireless Local Area Networks (WLANs) is expected. With such a high number of smaller cells, ICI also increases, and hence, interference mitigation is certainly a critical aspect to be effectively addressed [150].

Intensive research is being reported and several flavors of interference mitigation techniques are being studied, among which, ICIC has been also identified as a key

enabling technique for these hyper-dense cell deployments. Representative proposals include [151–153].

Finally, it is worth mentioning that Massive MIMO is, in the context of hyper-dense cell deployments working at frequencies beyond the Ultra High Frequency (UHF). This constitutes a novel approach in which the high number of antennas (due to the high number of cells) is used to provide service to users simultaneously in the same frequency resource. Its importance from an ICIC point of view resides in the fact that with such a high number of antennas, the aperture of the array grows and therefore, the resolution also does. As a result, the power can be concentrated into very small areas, reducing the required transmission power (and hence ICI) significantly. Further details can be found in [154].

The increasingly important framework of Self Organizing Networks (SON) [39, 155] rises the need for self organizing ICIC. This framework is a necessity in HetNets, where a large number of access points can be 1) deployed in an ad hoc manner and 2) switched on/off at any time. In the same manner, SONs is also important in the context of small cell deployments to help simplifying the management of network with high number of nodes. However, self organizing strategies for ICIC must be scalable, feasible, stable, and agile. Interesting examples of this emerging parading can be found in [95, 156, 157].

2.7 ICIC in LTE

This section introduces the mechanisms available in LTE and LTE-A that allow for ICIC. Thus, a description of several aspects of LTE are required for a better understanding of the rest of the document.

It is worth saying LTE and LTE-A are complex systems whose complete description is certainly unaffordable. An excellent description of every single aspect of these technologies can be found in [96, 158], and the references therein. Instead, given that this thesis is about ICIC in the downlink, the goal is to provide the reader with the basic LTE terminology and a general description of the access technology (OFDMA) and the air interface. The description is mainly based on LTE (Release 8/9), however some aspects of LTE-A (Release 10/11), are also required.

2.7.1 Introduction to the LTE Downlink Air Interface

Before describing the air interface of LTE, it is important to indicate that there are 3 different types of channels in LTE: *logical*, *transport* and *physical* channels. The general function of these channels is described in the following points:

- *Logical channels*. These channels are defined between the Radio Link Control (RLC) and the Medium Access Control (MAC). They indicate **what** type of information, either data (payload) or control (signaling) is transmitted.

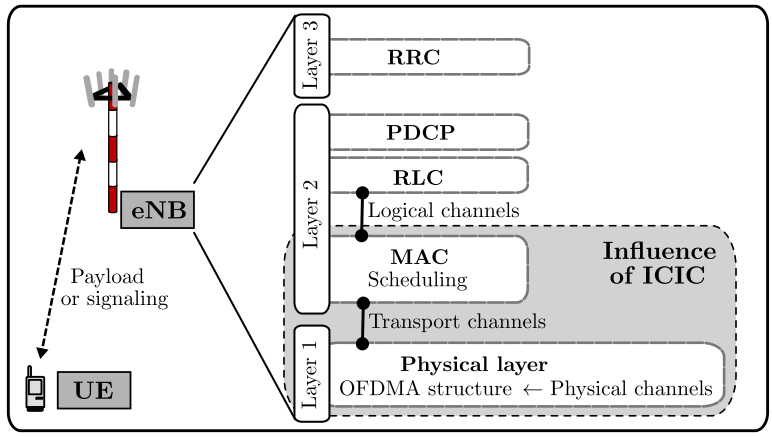

Figure 2.14: Representation of the radio interface protocol architecture in LTE.

- *Transport channels*. These channels are defined between the Medium Access Control (MAC) and the physical layer. They determine **how** the information has to be transmitted.

- *Physical channels*. These channels carry the information over the air interface. They define **where** the information is transmitted within the OFDMA structure, i.e., what time and frequency resources are used.

As it is shown in Figure 2.14, these channels are defined within the radio interface, composed of the layers 1, 2, and 3, between the UE and the network [159, 160]. The figure illustrates the action ambit of ICIC policies. It can be therefore said that, what ICIC does is to determine how the information of different users should be transmitted within the OFDMA structure (where the physical channels are defined over) in order to avoid excessive ICI for cell edge users. In the context of this thesis, it is enough to focus on the physical channels. In particular, 3 different physical channels are of interest, the Physical Downlink Shared Channel (PDSCH) that conveys user payload, and the control channels, the Physical Downlink Control Channel (PDCCH) and the enhanced PDCCH (ePDCCH) defined for LTE-A. In order to show how these physical channels are defined, the OFDMA structure and some basic LTE terminology must be introduced.

Frame structure and resource grid

In LTE, two duplexing modes are supported: Frequency Division Duplex (FDD), with radio frame structure type 1, and Time Division Duplex (TDD), with radio frame structure type 2. Thus, LTE supports operation in paired and unpaired spectrum. The following description is mainly focused on the downlink and it corresponds to the operation mode considered in the studies of this thesis, i.e., FDD with normal

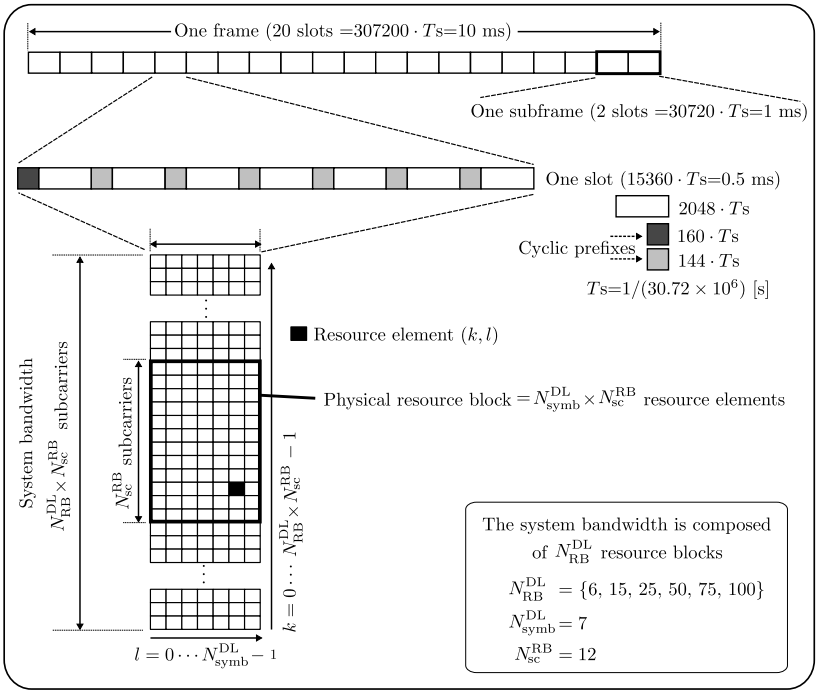

Figure 2.15: Downlink frame and OFDMA grid structure in LTE/LTE-A.

cyclic prefix and single-antenna port scheme[5]. Additional modes and configurations are detailed in [161].

The radio frame has a duration of 10 ms and it is composed of 20 slots of 0.5 ms. Independent transmissions are scheduled in Transmission Time Intervals (TTIs) or subframes of 1 ms (2 slots). All time intervals are defined in terms of the sampling period $T_s = 1/f_s$, where $f_s = 30.72 \times 10^6$ samples per second. A slot is composed of 7 OFDM symbols plus a cyclic prefix of $160 \cdot T_s$ in the first OFDM symbol and $144 \cdot T_s$ in the last 6 ones as it is shown in Figure 2.15. The figure depicts the structure of the OFDM resource grid. On it, Resource Elements (REs) are the most fundamental resource unit comprising one subcarrier in one OFDM symbol.

In order to allow for several bandwidth configurations, the physical layer is defined in terms of Resource Blocks (RBs). Thus, the system bandwidth is formed by N_{RB}^{DL} RBs each of which is composed of N_{sc}^{RB} consecutive subcarriers of 15 kHz. A Physical Resource Block (PRB) is defined as $N_{symb}^{DL} = 7$ OFDM symbols in the time domain and $N_{sc}^{RB} = 12$ subcarriers (one RB) in the frequency domain. Therefore, one PRB contains $N_{symb}^{DL} \times N_{symb}^{DL} = 84$ resource elements.

[5]Transmission with multiple antennas are also supported with configurations in the downlink with two or four transmit antennas and two or four receive antennas.

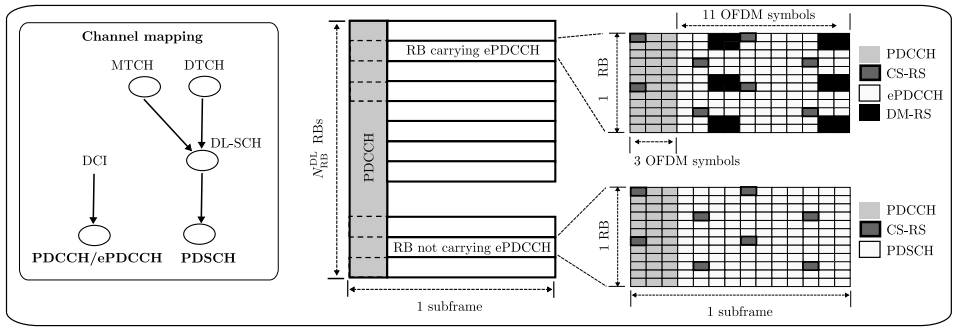

Figure 2.16: Channel mapping and structure of the PDSCH, PDCCH and ePDCCH.

The user plane and the control plane

There are two logical channels dedicated to convey user (traffic) information. The Dedicated Traffic Channel (DTCH) and the Multicast Traffic Channel (MTCH). The former is a point-to-point channel dedicated to one single user and the latter is a point-to-multipoint channel for transmission to users receiving Multimedia Broadcast Multicast Services (MBMS). Broadly speaking, all the information transmitted by means of the DTCH is called *the user plane*. At the transport level, these two channels are mapped into the versatile Downlink Shared Channel (DL-SCH)[6]. This channel supports several mechanisms including AMC, HARQ, power control, semi-static and dynamic resource allocation, discontinuous reception, MBMS transmission, and multi-antenna technologies. The DL-SCH is finally transported by means of the PDSCH that is transmitted in the last $((2 \cdot N_{\text{symb}}^{\text{DL}}) - n)$ OFDM symbols of each subframe. Note that $n \leq 4$ [160]. Figure 2.16 illustrates the case where $n = 3$.

An aspect of the PDSCH of interest here is the AMC scheme. The PDSCH can be transmitted using 3 different modulation schemes and several coding rates to provide different levels of reliability that are selected according to user radio channel quality. The modulation schemes are QPSK, 16-QAM and 64-QAM. Different coding rates can be applied to each modulation scheme resulting in 28 possible Modulation and Coding Schemes (MCSs) that are defined in [162] and shown in Table C.1.

It is worth nothing that a certain control information is also transmitted through the DL-SCH/PDSCH. This information include paging messages, broadcast and multicast control information, and common and dedicated control channels. However, in this thesis, the attention is placed on the control channel that informs each user where and how its data is located within the PDSCH[7]. This information is transmitted as the Downlink Control Information (DCI) and it represents *the control plane*. The DCI is mapped into the PDCCH. As it can be seen in Figure 2.16, the PDCCH is time-multiplexed and it is allocated in the first n ($n \leq 4$) OFDM symbols of each subframe. The DCI includes MCS information, HARQ messages, and power control commands, among other things. Because of the importance of such information, a

[6]Other traffic channels are also mapped to the DL-SCH, see [160] for a complete description.
[7]The impact of this critical information on the performance of LTE is explained in Chapter 7.

target Block Error Rate (BLER) of 1% is pursued for the PDCCH. The transmission formats used for the PDCCH are shown in Table C.2.

2.7.2 X2 Interface and ICIC Signaling

Interference management policies, from an intercell point of view, are basically signaled by means of the X2 interface [163, 164]. This interface allows peer-to-peer communication between different cells facilitating ICIC tasks. Other functions of the X2 interface and its protocol, the X2 Application Protocol, are mobility and load management and certain operation and maintenance procedures.

The mechanisms defined in the X2 interface to allow ICIC are:

- *Relative Narrowband Transmit Power* (RNTP). By means of this message, basic ICIC oriented measures can be taken in the downlink. Basically, each cell notifies to its neighbors about the power that is going to be used in each RB. The message is a bit map where each bit corresponds to one single RB. If a bit is '0', the cell guarantees that the power used in that RB is below a certain threshold, otherwise no guarantees are given. The threshold can be changed but it is common to all RBs. In this manner, each cell knows the RBs in which high ICI is likely to occur, and hence, those resources should not be assigned to cell edge users.

- *Interference Overload Indicator* (IOI). With this message, each cell informs to its neighbors about the ICI levels that is receiving in the uplink in each RB. Three different ICI levels are defined: high, medium, and low.

- *High Interference Indicator* (HII). This message is equivalent to the RNTP in the uplink. The message is also based on a bit map where the cell indicates what are the RBs that are going to be used by users transmitting with high power (cell edge users), thus helping the ICIC process in the uplink.

2.7.3 LTE Control Channels and ICIC

The framework to deal with ICI in the context of HetNets is commonly known as eICIC. These mechanisms were developed in the Release 10 (LTE-A). They can be classified in schemes that operate in the frequency and time domain. In the the frequency domain, CA and cross-scheduling capabilities have been defined [146]. In the time domain, Almost Blank Subframes (ABS) have been created to protect victim layers of excessive ICI [140] by *muting* transmission in certain subframes.

Thus, the framework for ICIC in LTE/LTE-A comprises techniques that can be implemented by means of the messages defined in the X2 Application Protocol (RNTP, IOI, and HII), the so-called Frequency Domain based ICIC (Releases 8 and 9) and the strategies more focused on HetNets (Releases 10 and 11), eICIC and FeICIC.

The strategies that have been introduced so far provided protection for data channels. However, control channels are also highly sensitive to ICI not only in macro- and microcellular deployments [53] but also in HetNets [39]. In LTE the PDCCH is time multiplexing (operating with full reuse), and hence, frequency domain ICIC cannot be applied. Thus, the degradation of the PDCCH at cell edges is significant. The situation worsen in HetNets where one cell interferes severly another one. In the light of this situation, ICIC for control channels becomes an important research item.

LTE-A provides means to protect the PDCCH. The first option, in the frequency domain, is based on carrier aggregation [147] and cross carrier scheduling [146]. However, **it is not an option for legacy users**. The second approach is in the time domain, the use of ABSs. Nevertheless, this alternative severely penalizes the capacity, and hence, it is a solution reserved for HetNets [140, 141].

Given that the capacity of the PDCCH was shown to be a limiting factor in scenarios with a large number of users using low-rate services such as Voice over Internet Protocol (VoIP) [165], a new enhanced PDCCH, the ePDCCH, was introduced in the Release 11 [166]. The ePDCCH employs Frequency Division Multiplexing (FDM) and it can be allocated dynamically within the PDSCH as it is illustrated in Figure 2.16. In this manner, the ePDCCH provides additional flexibility to apply ICIC and exploit conveniently the frequency diversity gain. Similarly to the PDCCH, a target Block Error Rate (BLER) of 1% is pursued for the ePDCCH. The transmission formats used for the ePDCCH are shown in Table C.3. However, given its recent appearance, few research effords and ICIC schemes for the ePDCCH have been presented.

A complete description of the matter together with a survey of recent proposals is presented in Chapter 7, where novel ICIC optimization strategies to enhance the performance of the control channels in LTE and LTE-A (PDCCH and ePDCCH, respectively) are presented.

Summarizing...

Clearly, the research on ICIC is far from being finished. The framework is rich and, in the light of the continuous evolution of cellular systems, it requires big efforts to fulfill the challenges that have been just described. This chapter has presented a review of the different approaches to interference mitigation, among which ICIC stands out not only as an effective solution but also as a feasible alternative for mobile operators. This thesis contributes with solid arguments and novel optimization schemes to make static ICIC more attractive. The next chapter starts a chronicle detailing the work that was required to accomplish the previous target.

Chapter 3

Feasibility of Static ICIC in Realistic Deployments

3.1 Introduction

In the previous chapter, a complete picture of the techniques for interference management in OFDMA networks was provided. It was shown that cell edge performance is a major concern in technologies such as LTE and LTE-A since ICI affects drastically the QoE of users located in cell boundaries. ICIC encompasses a family of solutions aiming at alleviating this problem. While significant research efforts are being placed on dynamic strategies, the implementation of most of them in real-world systems is far from a being an easy task due to the complexity of these mechanisms and the practical limitations of current technologies.

LTE is being deployed at a pace never seen before while in parallel, mobile operators are looking for ICIC mechanisms that can be integrated without delay in their networks to maximize performance. Since standards do not provide specific strategies or algorithms for interference management, static ICIC schemes stand out for their low complexity and its inherent feasibility. However, the static nature of these strategies implies the need for a very careful adjustment to make them effective solutions. As it was shown before, the efforts focused on static ICIC have been limited, and consequently, important research gaps have been identified. One of them is the need for more appropriate evaluation models and studies that shed light on the merit of these algorithms in contexts where it is really important: realistic deployments.

This chapter looks deeper into the theory of static ICIC by looking at different analytical models that try to characterize the complex interdependencies between operational parameters and performance metrics. The discussion about existing analytical models is presented in the next section. Interestingly, a close gaze to those frameworks reveals that new evaluation methods are required. In particular to be

applied in the context of real deployments. As an answer to this, a new framework is presented in Section 3.3. The proposal aims at getting a good balance between accuracy and feasibily and this is done in such a way that it can be used to study and characterize the performance of SFR and FFR in any arbitrary network topology.

Based on this methodology, the performance of SFR and FFR is investigated in the context of realistic deployments. Section 3.4 is fully devoted to such analysis. The results clearly point to the need for *additional measures* in order to make SFR and FFR attractive and feasible for real-world networks. As it will be seen in Chapters 6 and 7, the knowledge generated through these initial studies establishes the foundations of the multiobjective optimization models presented therein.

Finally, the conclusions close the chapter in Section 3.5.

3.2 Deepening into the Theory of Static ICIC

Up to now, not so many analytical models to characterize the performance of the strategies for static ICIC have been presented. The studies can be grouped in two categories:

1. Using the stochastic geometry framework. Here, one of the most relevant contributions is the work by Novlan in [45], which extends to SFR and FFR the coverage model originally proposed in [167].

2. Using the fluid model. Most works basically adapt the model developed in [168], which dealt with CDMA networks. In this case, relevant contributions are the works presented in [50] and [169].

The review of these evaluation models is illustrative and complements the theoretical introduction presented in Subsection 2.4.3. Moreover, it justifies the need for the statistical framework presented herein. Therefore, the target of the discussion is to analyze the advantages and disadvantages of each of them.

3.2.1 Analysis of Static ICIC based on Stochastic Geometry

In [167], the long-standing problem of analytically model the downlink of cellular systems is addressed. The authors conceived that, instead of assuming fixed locations for the sites, their location was modeled as an stochastic process. For the sake of completeness, and in order to make the subsequent discussion clear, the most fundamental concepts of this framework are explained. An interested reader is referred to [170, 171] for an in-depth discussion.

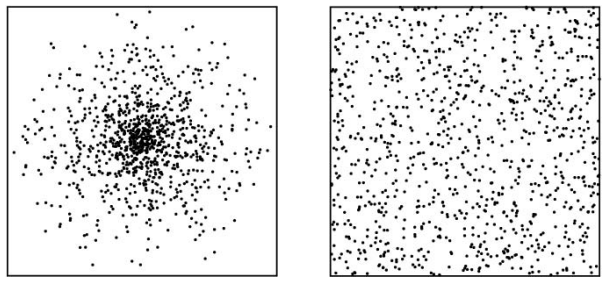

(a) A Gaussian-like point process.

(b) Poisson Point Process.

Figure 3.1: Point processes in two dimensions.

A bird's eye view of Stochastic Geometry

A point process is basically a random collection of points in the space as shown in Figure 3.1. More formally, a point process is a mapping $\mathbf{\Phi}$ from a probability space of point measures to another space $\mathcal{K}$ of point measures. Each of these measures can be represented as a sum of Dirac measures on $\mathcal{K}$. Thus, $\mathbf{\Phi} = \sum_i \delta X_i$, where the X_i's are the random points of $\mathbf{\Phi}$ that take their values in $\mathcal{K}$. In this context, $\mathcal{K}$ is the Euclidian plane ($\mathbb{R}^2$).

A particular type of point process is relevant to this discussion, the homogeneous Poisson Point Process (PPP). A PPP with density κ is a random set of points for which the number of points for any bounded area $\mathcal{A} \subset \mathbb{R}^2$ follows a Poisson distribution with mean equal to $\kappa \times \text{Area}(\mathcal{A})$. Moreover, the number of points in disjoint and independent sets $\mathcal{A}_1$ and $\mathcal{A}_2$ are also independent. PPPs have interesting mathematical properties including complete independence, superposition and the fact that the PPP can be completely characterized by means of the Laplace functional of the process. This stochastic model is very convenient due to its mathematical tractability and availability of several interesting theorems. However, when used to model the position of base station in a mobile communications networks, unrealistic assumptions are required. These limitations are explained subsequently.

Characterization of Cellular Networks in Terms of PPPs

The work presented in [45] aims at determining coverage probabilities, i.e., the probability that a user experience an SINR greater than a minimum SINR requirement ($\psi_{\min}$). The assumptions in this model include:

1. Base stations are distributed according to a PPP with density κ. Note that as a consequence of the PPP assumption, the distances (d's) between (uniformly distributed) users and base stations are Rayleigh distributed random variables.

2. Small scale fading is modeled as Rayleigh fading, and hence, the received power

is a random variable exponentially distributed with mean μ.

3. Lognormal shadowing is not considered. Only path loss has been taken into account, being this factor proportional to the path loss exponent (ν). According to [167], more realistic assumptions for the distribution of received power result in some loss of tractability.

4. As it is usually done in static ICIC, users are classified according to their average SINR by means of a classification threshold (ψ_{TH}). The frequency reuse factors applied to interior and exterior users are $RF_{\mathcal{E}}$ and $RF_{\mathcal{I}}$, respectively.

Relaying on the previous set of assumptions, the authors in [167] showed that the coverage probability (p_{c}) of an arbitrary user in a network with reuse factor RF, where each cell transmits a power level P is given by:

$$p_{\text{c}}\left(\psi_{\min},\kappa,\nu,RF\right) \triangleq P\left(\text{SINR}\geq\psi_{\min}\right), \tag{3.1}$$

$$p_{\text{c}}\left(\psi_{\min},\kappa,\nu,RF\right) = \pi\kappa\int_{0}^{\infty} e^{-\pi\kappa x\left(1+\frac{1}{FR}\rho(\psi_{\min},\nu)\right)} e^{-\mu\psi_{\min}\frac{\sigma^2}{P}x^{\nu/2}}dx, \tag{3.2}$$

where

$$\rho\left(\psi_{\min},\nu\right)=\left(\psi_{\min}\right)^{\frac{2}{\nu}}\int_{\left(\psi_{\min}\right)^{\frac{-2}{\nu}}}^{\infty}\frac{1}{1+y^{\frac{\nu}{2}}}dy. \tag{3.3}$$

Note that, in (3.2), σ^2 corresponds to the noise power. Thus, by extending this model to analyze SFR and FFR, the authors in [45] derived analytical expressions for coverage probabilities for interior and exterior users both for SFR and FFR. However, for the sake of clarity and brevity, only the expressions corresponding to SFR are presented and analyzed here. Similar expressions were obtained for FFR.

Essentially, in SFR users are classified according to ψ_{TH}, and based on such classification, a new resource allocation pattern is applied as it is indicated in Subsection 2.4.3. Thus, in order to obtain the coverage probability for exterior users, authors in [45] determined the probability that the resulting SINR, once SFR is applied (ψ_{SFR}), is greater than a minimum requirement in terms of SINR ($\psi_{\min}$). Of course this probability is conditioned to the user being classified as exterior. This means its average SINR before classification (ψ_{avg}) is smaller than ψ_{TH}. Note that ψ_{avg} is measured under reuse 1 conditions, for example, in LTE, over the Cell Specific Reference Signals (CS-RSs).

$$\begin{aligned} p_{\text{c}}^{\text{SFR},\mathcal{E}}\left(\psi_{\min}\right) &\triangleq P\left(\psi_{\text{SFR}}>\psi_{\min}\mid\psi_{\text{avg}}<\psi_{\text{TH}}\right), \\ p_{\text{c}}^{\text{SFR},\mathcal{E}}\left(\psi_{\min}\right) &= \frac{p_{\text{c}}\left(K\alpha\psi_{\min},\kappa,\nu,RF=3\right)}{1-p_{\text{c}}\left(\psi_{\text{TH}},\kappa,\nu,RF=3\right)} \\ &- \frac{\pi\kappa\int_{0}^{\infty}e^{-\pi\kappa x(1+2\zeta(\psi_{\min},\psi_{\text{TH}},\nu,K,\alpha))}e^{-\mu K(\alpha\psi_{\min}+\psi_{\text{TH}})\frac{\alpha\sigma^2}{P}x^{\nu/2}}}{1-p_{\text{c}}\left(\psi_{\text{TH}},\kappa,\nu,RF=3\right)}dx. \end{aligned} \tag{3.4}$$

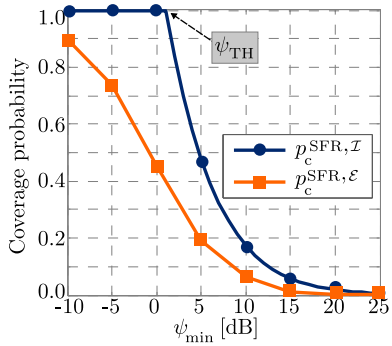

Figure 3.2: Coverage probability for SFR.

Recall that α is the power control ratio used in SFR, see Subsection 2.4.3. The function $\zeta\left(\psi_{\mathrm{min}}, \psi_{\mathrm{TH}}, \nu, K, \alpha\right)$ is defined as follows:

$$\zeta\left(\psi_{\mathrm{min}}, \psi_{\mathrm{TH}}, \nu, K, \alpha\right) = \int_0^{\infty} \left(1 - \frac{1}{1 + K\psi_{\mathrm{TH}} x^{-\nu}} \frac{1}{1 + K\alpha\psi_{\mathrm{min}} x^{-\nu}}\right) x dx. \tag{3.5}$$

Given that ICI is also interclass in SFR, the parameter K is a power factor consolidating the interference coming from the subbands devoted to exterior and interior users in neighbor cells and it defined as follows:

$$K = \frac{RF - 1 + \alpha^{-1}}{RF}. \tag{3.6}$$

Analogously, for interior users:

$$p_{\mathrm{c}}^{\mathrm{SFR},\mathcal{I}}\left(\psi_{\mathrm{min}}\right) \triangleq P\left(\psi_{\mathrm{SFR}} > \psi_{\mathrm{min}} \mid \psi_{\mathrm{avg}} \geq \psi_{\mathrm{TH}}\right), \tag{3.7}$$

$$p_{\mathrm{c}}^{\mathrm{SFR},\mathcal{I}}\left(\psi_{\mathrm{min}}\right) = \frac{p_{\mathrm{c}}\left(K \cdot \max\{\psi_{\mathrm{min}}, \psi_{\mathrm{TH}}\}, \kappa, \nu, RF = 1\right)}{p_{\mathrm{c}}\left(K\psi_{\mathrm{TH}}, \kappa, \nu, RF = 1\right)}. \tag{3.8}$$

In order to provide a more graspable perspective of the previous expressions, (3.5) and (3.8) have been evaluated numerically. Figure 3.2 shows results for $\psi_{\mathrm{TH}} = 1$ dB, SNR $= 25$ dB, $\alpha = 0.25$, and $\nu = 4$. The stochastic geometry approach captures well the behaviour of SFR. As expected, exterior users perform worse than interiors in terms of coverage. It was also expected that coverage probability was inversely proportional to ψ_{min}.

However, as it is analysed in Section 3.4, once SFR is applied it turns out that a certain fraction of interior users worsen their SINR figures as a result of the change in frequency reuse and power level that is applied. Note that this effect is not captured by the stochastic geometry analysis since from (3.8), it becomes evident that if $\psi_{\mathrm{min}} < \psi_{\mathrm{TH}}$, then $p_{\mathrm{c}}^{\mathrm{SFR},\mathcal{I}}\left(\psi_{\mathrm{min}}\right) \to 1$, this is confirmed graphically.

In this manner, the stochastic nature of this model provides a valuable tool to evaluate the relative merit of SFR and FFR. However, the framework is far

from being a tool to evaluate the performance of a particular configuration in a practical network (especially if the configuration is different from cell to cell). As it is analyzed in Section 3.4, the performance resulting from a certain SFR configuration is network-specific, and hence, the model would provide performance figures valid for global features such as site density. But the framework cannot be used by an operator as an approach for the optimization of static ICIC.

Beyond the previous remarks, the main results from the stochastic geometry approach shed light on the following aspects:

1. The merit of FFR as a strategy providing the highest interference reduction and, the excellent resource efficiency of SFR.
2. The utmost role of the classification threshold (ψ_{TH}) and its impact on the performance of SFR and FFR.

3.2.2 Analysis of Static ICIC based on Fluid Models

Another interesting approach to evaluate the performance of different frequency reuse schemes, including SFR and FFR, in terms of resulting SINR figures is by means of fluid models. A contribution following this approach can be found in [50]. Similarly to the framework presented previously, closed-form expressions can be derived relying on a set of assumptions about the network geometry. Key assumptions in these models include:

1. Instead of considering base stations as discrete entities, base stations are modeled as a continuum.
2. Large scale fading is only function of the distance between transmitters and receivers and the path loss exponent ν. Lognormal shadowing is not taken into account.
3. Noise power is neglected, and hence, SINR=SIR.
4. The power transmitted by each base station is the same, i.e., P.

The model basically replaces a finite number of base stations by an equivalent continuum of transmitters that are uniformly distributed in the coverage area. Therefore, the transmitted power is modeled as a continuum field and both base stations and users are characterized by means of constant densities, ρ_{BS} and ρ_{UE}, respectively. The radius of the total area covered by the network and the inter-site-distance ISD are d_{net} and d_{isd}, respectively. The distance between a generic user and its serving base stations is d_u. Thus, for the case of full frequency reuse, given that base stations are uniformly distributed, the interference (I) coming from each area element expressed in circular coordinates is $P\kappa z^{-\nu}\rho_{\mathrm{BS}} z dz d\theta$, where κ is a constant. Thus, to compute the ICI, the integration is approximated by a ring (with the user in the center) whose inner and outer radius given by $d_{\mathrm{isd}} - d_u$ and $d_{\mathrm{net}} - d_u$, respectively. Such integration limits are illustrated in Figure 3.3. Therefore, the

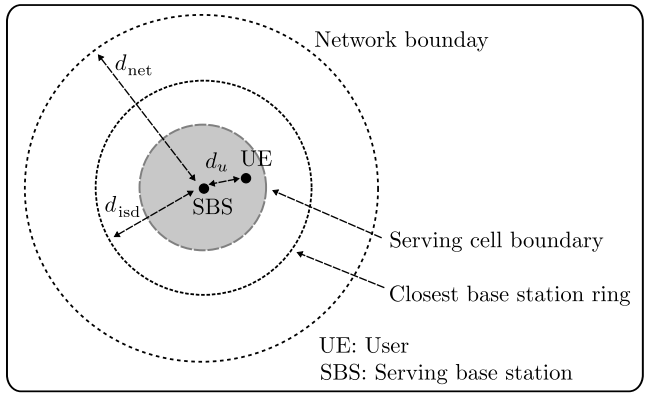

Figure 3.3: Integration limits in the fluid model.

amount of ICI can be estimated by means of the following expression:

$$I = \int_0^{2\pi} \int_{d_{\text{isd}}-d_u}^{d_{\text{net}}-d_u} P\kappa z^{-\nu} \rho_{\text{BS}} z dz d\theta, \tag{3.9}$$

$$I = \frac{2\pi\kappa P \rho_{\text{BS}}}{\nu - 2} [(d_{\text{isd}} - d_u)^{2-\nu} - (d_{\text{net}} - d_u)^{2-\nu}]. \tag{3.10}$$

Given that the SINR is equal to $\frac{\kappa P d_u^{-\nu}}{I}$, the SINR of the user ($\psi_u$) can be estimated by means of the following expression:

$$\psi_u = \frac{d_u^{-\nu}(\nu - 2)}{2\pi\rho_{\text{BS}}[(d_{\text{isd}} - d_u)^{2-\nu} - (d_{\text{net}} - d_u)^{2-\nu}]}. \tag{3.11}$$

It is important noting that, under the assumption of equal power at each cell, ψ_u becomes independent of P, and indeed, it only depends on d_u similarly to Equation 2.4 in Section 2.2.4. As typically $d_{\text{net}} \gg d_u$, Equation 3.11 can be approximated to:

$$\psi_u = \frac{d_u^{-\nu}(\nu - 2)}{2\pi\rho_{\text{BS}}(d_{\text{isd}} - d_u)^{2-\nu}}. \tag{3.12}$$

Equation 3.12, derived under the assumption of full frequency reuse, can be easily extended to higher reuse factors by simply modifying distances of co-channel base stations. Thus, for a reuse factor RF, ρ_{BS} and d_{isd} must be properly scaled by $(RF)^{-1}$ and $\sqrt{RF}$, respectively. According to [50], taking into account the hexagonal geometry, the density of base stations becomes:

$$\rho_{\text{BS}} = \frac{1}{2RF\sqrt{3}\left(\frac{1}{2}d_{\text{isd}}\right)^2}. \tag{3.13}$$

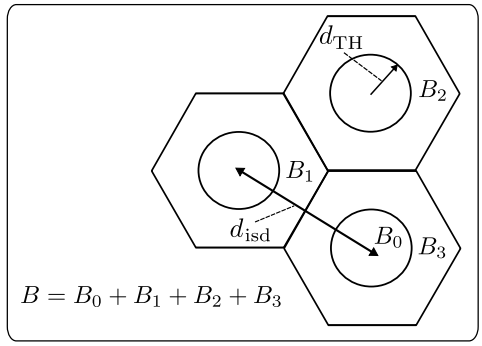

Figure 3.4: FFR applied to a cluster of three cells.

Thus, introducing a normalized distance ($x = \frac{d_u}{\frac{1}{2}d_{\mathrm{isd}}}$), Equation 3.12 can be generalized as follows:

$$\psi_u\left(x, RF\right) = \frac{RF\sqrt{3}}{\pi}\left(\nu - 2\right)\left(\frac{1}{\left(2\sqrt{RF} - x\right)^2}\right)\left(\frac{2\sqrt{RF}}{x} - 1\right)^{\nu}. \tag{3.14}$$

The capacity in bps/Hz, according to the Shannon's formula, is given by:

$$\eta\left(x, RF\right) = \log_2\left(1 + \psi_u\left(x, RF\right)\right). \tag{3.15}$$

Given that SFR was considered in the previous model (Subsection 3.2.1), the case of FFR is presented here. The extension to SFR follows a very similar path, see [50] for details.

As it can be seen from Figure 2.9 (case FFR), the bandwidth (B) is divided into four subbands, one of size $\beta \cdot B$ (that operates with full reuse) and three subbands of size $((1-\beta)/3) \cdot B$ (that operates with reuse factor 3).

However, in [50], the authors considered onmidirectional antennas and a cluster of 3 cells as it is shown in Figure 3.4. Note that B_0 corresponds to the full reuse subband, while B_1, B_2, and B_3 are the ones with reuse factor 3. Moreover, user classification is done considering a circle with radius d_{TH}, and thus, for interior and exterior users it holds that $d_u \leq d_{\mathrm{TH}}$ and $d_u > d_{\mathrm{TH}}$, respectively.

Assuming a scheduler that guarantees fairness allocation, i.e., the same rate (R) is allocated to each user, it is clear that users at different distances of the serving base station require different bandwidths. Let $B_u(x)$ be the bandwidth requirement of user u at a distance x. It is assumed that N_{UE} users are uniformly distributed in each cell, and hence, the user density becomes:

$$\rho_{\mathrm{UE}} = \frac{N_{\mathrm{UE}}}{2\sqrt{3}\left(\frac{1}{2}d_{\mathrm{isd}}\right)^2}. \tag{3.16}$$

Given that, $R = \eta\,(x, RF) \cdot B_u(x)$, it is possible to show that:

$$B_0 = 2\pi \int_0^{d_{\mathrm{TH}}} B_u(r)\rho_{\mathrm{UE}} r dr, \tag{3.17}$$

$$B_1 = 12 \int_0^{\frac{\pi}{6}} \int_0^{\frac{d_{\mathrm{isd}}}{2\cos(\theta)}} B_u(r)\rho_{\mathrm{UE}} r dr d\theta, \tag{3.18}$$

Since $B = B_0 + B_1 + B_2 + B_3$ and $B_1 = B_2 = B_3$, then,

$$B = B_0 + (3 \times B_1)\,. \tag{3.19}$$

Finally, combining (3.17), (3.18), and (3.19), and taking into account that the N_{UE} users receive the same rate (R), the total cell data rate under FFR (C_{FFR}) becomes:

$$C_{\mathrm{FFR}} = \frac{\sqrt{3}B}{\pi \int_0^{\kappa} \frac{x}{\eta(x,1)} dx + 18 \int_0^{\frac{\pi}{6}} \int_{\kappa}^{\frac{1}{\cos(\theta)}} \frac{x}{\eta(x,3)} dx d\theta}, \tag{3.20}$$

where $\kappa = 2d_{\mathrm{TH}}/d_{\mathrm{isd}}$. Note that in this model, C_{FFR} does not depends either on N_{UE} or d_{isd}, which is a very nice feature of the model because makes the analysis independent of system load and network size.

Figure 3.5 shows graphical representations of some relationships that can be drawn from (3.20). Figure 3.5a illustrates the prediction for the spectral efficiency as a function of the distance to serving base station. The model clearly captures the behavior of FFR for the regions below and above of the classification threshold (in this case d_{TH}). As expected, interior users, at distances smaller than d_{TH}, will perceive spectral efficiencies of a full reuse (reuse 1) system, while exterior users enjoy a higher reuse factor. The model also indicates that there is a region in which interior users obtain worse SINR than exterior users. This observation is key because it shows that, in the context of static ICIC, **it is necessary to analyze cell edge performance not only in terms of cell edge users but also in terms of interior ones**. Several recent works including [45] and [63] focus almost exclusively on the performance of exterior users. Moreover, the work presented in this Ph.D. thesis evidences that, when analyzing irregular deployments, considering the whole set of users is key to optimize SFR and FFR. Figure 3.5b illustrates the impact of the classification metric (d_{TH}) on the performance of FFR. Although the model helps to find an optimum value from the capacity point of view, it does not provide a clear vision of how does this optimum impacts other performance metrics. Moreover, the optimum is not valid for irregular layouts where the inter-site distance is not regular. Finally, but not less important, it is important to say that existing tradeoffs such as efficiency-fairness can not be analyzed completely by means of this model.

Summarizing...

Analytical methods are an alternative to study the performance of static ICIC schemes without the need for computationally-heavy and time-consuming system

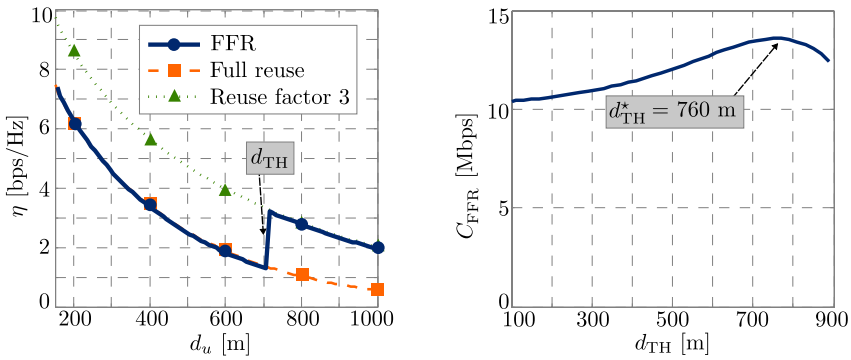

(a) Capacity vs. distance to transmitters. **(b)** Capacity vs. classification distance.

Figure 3.5: Performance of FFR: fluid model.

level simulations. To date, only few research efforts have been done in this direction. Two analytical models resulting in closed-form expressions have been introduced and discussed in this section.

These models provide insightful perspectives of the relative merit of different configurations and the impact of operational parameters in SFR and SFR, being in these sense, excellent and valuable theoretical contributions. However, a set of idealistic assumptions and simplifications are required to make the mathematical analysis tractable. Clearly, this limits the possibility of employing such evaluation methods in realistic deployments, that are obviously far from those assumptions. In practice, there are two aspects of interest for mobile operators regarding static ICIC:

1. *Regarding the performance of SFR and FFR in realistic deployments, how can it be efficiently characterized?*
2. *Is it possible to further customize SFR and FFR to achieve cell edge performance gains in such contexts?*

The rest of the chapter (and the thesis) is about the previous questions.

3.3 Statistical Analysis of Static ICIC Schemes

In this section, a statistical framework for the analysis of SFR and FFR is presented. A fundamental difference between this model and previous ones is that no assumption need to be made on the network topology. Instead the model relies on the radio characterization of the network in terms of the statistic of the average SINR. Based on this information, a network-specific performance pattern for SFR and FFR can be obtained.

It is worth saying that this statistical approach can be considered complementary

to system level simulations. In this Ph.D. thesis, both methods have been combined conveniently according to the research objectives.

3.3.1 General Setting

The system model is described in Appendix C, Section C.1. The total available power per cell ($P_{\max}$) is distributed according to the resource allocation pattern of SFR and FFR (see Figure 2.9), i.e., governed by the operational parameters α, β, and ψ_{TH}. Recall that α is the ratio of the power assigned to interior and exterior users, β is the fraction of bandwidth allocated to the class of interior users, and ψ_{TH} is the classification threshold. It is assumed that users are classified based on their average SINR under the assumption of universal frequency reuse. Let's call to this figure ψ_{u}. The assumption is consistent with the manner in which average SINR values are computed in LTE/LTE-A, i.e., based on always-on reference signals that are distributed over the whole system bandwidth at each cell [162].

Thus, according to the system model, if the a^{th} area element (pixel) has an average SINR ψ_{u}, then the average SINR of any user in that pixel is also equal to ψ_{u}, and consequently, the users within that pixel will be classified accordingly. For the sets of interior ($\mathcal{I}$) and exterior ($\mathcal{E}$) users, $\psi_{\text{u}} \geq \psi_{\text{TH}}$ and $\psi_{\text{u}} < \psi_{\text{TH}}$, respectively.

As in previous models, it is also considered that common values of α, β, and ψ_{TH} are applied at each cell. Hereafter, this type of configurations are referred to as *baseline designs*.

Performance Metrics

The following metrics have been considered to characterize the performance of SFR and FFR:

1. *Average spectral efficiency* (η [bps/(Hz·cell)]): This system-oriented metric provides a direct measure of the effectiveness with which radio resources are employed and it is proportional to the overall network capacity. In the study of this section, the Shannon's formula is considered as link performance model.

2. *Percentile 5 of users rate r* ($r_{5\%}$ [bps]): This user-oriented metric is used as a measure of the performance of users at cell edges, and hence, it is very important in the context of ICIC. It is defined as the value of r when $F_r = 5\%$. Recall that F_r is the empirical CDF of r.

3. *Jain's index* ($\jmath$): This metric measures the ability of the system to deliver similar rates to users, i.e., *fairness*. It is defined in [172] and it is computed based on user rates. The Jain's index is defined as follows:

$$\jmath(r_1, r_2, \cdots, r_n) = \frac{\left(\sum_{i=1}^{n} r_i\right)^2}{n \cdot \sum_{i=1}^{n} (r_i)^2}, \tag{3.21}$$

where there are n users and r_i is the throughput of the i^{th} connection.

Merit Assessment Methodology

In order to establish a strict order among the different configutations of SFR and FFR, linear aggregation (weighted sum) is employed in this study. In this manner, the fitness value (θ) of each configuration is computed as the scalar product between performance metrics (normalized) and corresponding weights:

$$\theta = \mathbf{y} \cdot \mathbf{w}^{\mathrm{T}}, \tag{3.22}$$

Note that $\mathbf{w}$ is defined by the operator and the vector $\mathbf{y}$ contains the normalized performance metrics. Thus,

$$\mathbf{y} = [\ \hat{\eta}\ \ \hat{r}_{5\%}\ \ \hat{\jmath}\ ], \tag{3.23}$$

$$\mathbf{w} = [\ w_{\eta}\ \ w_{r_{5\%}}\ \ w_{\jmath}\ ], \qquad \mathbf{w} \cdot \mathbf{1} = 1. \tag{3.24}$$

Given that normalized values are always positive, $\theta \in [0, 1]$.

In the context of static ICIC, a Network Operation Point (NOP) is defined as any given configuration of SFR or FFR. Such settings are specified in terms of their operational parameters (α, β, and ψ_{TH}). Thus, a NOP is a vector $\mathbf{x} \in \mathbb{R}^3$ defined as follows:

$$\mathbf{x} \triangleq [\ \alpha\ \ \beta\ \ \psi_{\text{TH}}\ ]. \tag{3.25}$$

In this manner, for each NOP ($\mathbf{x}$), a fitness value (θ) can be obtained according to the following flow:

$$\mathbf{x} \longrightarrow \mathbf{y} \xrightarrow{\mathbf{w}} \theta.$$

The search space ($\mathcal{X}$) is defined as the Cartesian product of the sets of possible values of β, α, and ψ_{TH}, i.e., the sets $\mathcal{U}_{\beta}$, $\mathcal{U}_{\alpha}$, and $\mathcal{U}_{\psi_{\text{TH}}}$, respectively. Thus:

$$\mathcal{X} \triangleq \mathcal{U}_{\alpha} \times \mathcal{U}_{\beta} \times \mathcal{U}_{\psi_{\text{TH}}}. \tag{3.26}$$

3.3.2 Statistical Analysis

The results and conclusions that can be drawn from the analytical models previously introduced (Subsections 3.2.1 and 3.2.2), clearly suggest that the operation of SFR and FFR **can be described in terms of two independent, though interacting, sub-systems**: the subsystems of interior ($\mathcal{I}$) and exterior ($\mathcal{E}$) users/pixels. Thus, the statistical model presented here exploits and investigates this intuition.

The key element of the analysis is estimating separately the SINR distributions of each class of users ($\mathcal{I}$ and $\mathcal{E}$), which are completely determined by the operational parameters α, β, and ψ_{TH}. The statistical model requires determining the achievable rate at pixel, obviously taking into account the resource allocation pattern of SFR and FFR. The proposed methodology is explained along the following points:

Average SINR

According to the system model, the vector $\mathbf{\Psi}_{\mathrm{u}} \in \mathbb{R}^{A}$ that indicates the average SINR (ψ_{u}) of each pixel, can be computed as follows:

$$\mathbf{\Psi}_{\mathrm{u}} = \left[(\mathbf{S} \odot \mathbf{G}) \cdot \mathbf{p}_{\text{CS-RS}}\right] \oslash \left[\left[(\mathbf{S}^{\mathrm{c}} \odot \mathbf{G}) \cdot \mathbf{p}_{\text{CS-RS}}\right] \oplus \sigma^{2}\right], \tag{3.27}$$

where the operators $\odot$, $\oslash$ and $\oplus$ indicate Hadamard (pointwise) operations. Recall that the a^{th} pixel is classified based on its value of ψ_{u}, i.e., $\mathbf{\Psi}_{\mathrm{u}}(a)$.

Server Classification

Taking advantage of the trisectorial sectorization, cells are divided into three subsets based on their antenna azimuth ($\phi \in [0, 359]$) to allow efficient processing. Therefore, a cell belongs to the set $\mathcal{C}_j$ ($j \in \mathcal{J} = \{0, 1, 2\}$) according to the rule:

$$j = \lfloor \phi / 120 \rfloor \tag{3.28}$$

Analogously, pixels are also divided into three subsets ($\mathcal{A}_j$, $j \in \{0, 1, 2\}$), such that, a pixel is element of the set $\mathcal{A}_j$ if it is served by a cell of type j. Recall that the pixel-to-cell association is stored in the matrix $\mathbf{S}$ and that, $\sum_{\forall j \in \mathcal{J}} |\mathcal{A}_j| = A$ and $\sum_{\forall j \in \mathcal{J}} |\mathcal{C}_j| = L$. In this manner, the type of the server of each pixel ($j \in \{0, 1, 2\}$) is stored in the vector $\mathbf{t} \in \{0, 1, 2\}^{A}$.

Classification of Pixels

The classification of each pixel is stored in the matrix $\mathbf{C} \in \mathbb{R}^{A \times 2}$. The matrix indicates the class (either $\mathcal{I}$ or $\mathcal{E}$) to which each pixel belongs to. The value '1' in the column 0 indicates that the pixel belongs to $\mathcal{E}$. A '1' in the column 1 indicates that the pixel belongs to $\mathcal{I}$.

Coverage per Class and Cell

The matrix $\mathbf{\Phi} \in \mathbb{R}^{2 \times L}$ contains the inverse of the number of pixels classified as $\mathcal{I}$ or $\mathcal{E}$ at each cell according to the classification threshold (ψ_{TH}) as it was explained previously. The first and second rows correspond to the classes $\mathcal{E}$ and $\mathcal{I}$, respectively. Each column corresponds to a cell.

Characteristic Matrices

The matrices $\mathbf{P}_{\text{ser}} \in \mathbb{R}^{L \times 2}$ and $\mathbf{P}_{\text{int}} \in \mathbb{R}^{L \times 6}$ are used to compute the average SINR values corresponding to the PDSCH [161]. The structure of these matrices exploits the trisectorial layout[1].

[1]The extension to cases in which other sectorization pattern is used is straightforward.

Let's consider that the maximum power per subcarrier, $P_{\max}^{\mathrm{SC}}$, is calculated according to the following expression:

$$P_{\max}^{\mathrm{SC}} = P_{\max} / \left(N_{\mathrm{RB}}^{\mathrm{DL}} \cdot N_{\mathrm{sc}}^{\mathrm{RB}} \right). \tag{3.29}$$

The power levels applied to the classes of exterior and interior users ($p_{\mathcal{E}}$ and $p_{\mathcal{I}}$, respectively), are given as a function of the power ratio (α) as follows:

$$p_{\mathcal{E}} = P_{\max}^{\mathrm{SC}}, \tag{3.30}$$

$$p_{\mathcal{I}} = \alpha \cdot P_{\max}^{\mathrm{SC}}. \tag{3.31}$$

The matrix $\mathbf{P}_{\mathrm{ser}}$ is defined as follows:

$$\mathbf{P}_{\mathrm{ser}} = \begin{bmatrix} p_{\mathcal{E}}^{(1)} & p_{\mathcal{E}}^{(2)} & \cdots & p_{\mathcal{E}}^{(L)} \\ p_{\mathcal{I}}^{(1)} & p_{\mathcal{I}}^{(2)} & \cdots & p_{\mathcal{I}}^{(L)} \end{bmatrix}^{\mathrm{T}}. \tag{3.32}$$

The matrix $\mathbf{P}_{\mathrm{int}}$ is defined in terms of the submatrix $\mathbf{P}_{\mathrm{int}}^{\mathrm{base}} \in \mathbb{R}^{3\times 6}$. $\mathbf{P}_{\mathrm{int}}^{\mathrm{base}}$ depends on the type of static ICIC, either SFR or FFR, and it is defined as it is shown below:

$$\mathbf{P}_{\mathrm{int}}^{\mathrm{base}} = \begin{bmatrix} p_{\mathcal{E}} & p_{\mathcal{I}} & p_{\mathcal{I}} & p_{\mathcal{E}} & p_{\mathcal{I}} & p_{\mathcal{I}} \\ p_{\mathcal{I}} & p_{\mathcal{I}} & p_{\mathcal{E}} & p_{\mathcal{I}} & p_{\mathcal{I}} & p_{\mathcal{E}} \\ p_{\mathcal{I}} & p_{\mathcal{E}} & p_{\mathcal{I}} & p_{\mathcal{I}} & p_{\mathcal{E}} & p_{\mathcal{I}} \end{bmatrix} \quad \text{for SFR,} \tag{3.33}$$

$$\mathbf{P}_{\mathrm{int}}^{\mathrm{base}} = \begin{bmatrix} p_{\mathcal{E}} & p_{\mathcal{I}} & 0 & p_{\mathcal{I}} & 0 & p_{\mathcal{I}} \\ 0 & p_{\mathcal{I}} & p_{\mathcal{E}} & p_{\mathcal{I}} & 0 & p_{\mathcal{I}} \\ 0 & p_{\mathcal{I}} & 0 & p_{\mathcal{I}} & p_{\mathcal{E}} & p_{\mathcal{I}} \end{bmatrix} \quad \text{for FFR.} \tag{3.34}$$

Therefore,

$$\mathbf{P}_{\mathrm{int}} = \left[(\mathbf{P}_{\mathrm{int}}^{\mathrm{base}})^{\mathrm{T},\,(1)} (\mathbf{P}_{\mathrm{int}}^{\mathrm{base}})^{\mathrm{T},\,(2)} \cdots (\mathbf{P}_{\mathrm{int}}^{\mathrm{base}})^{\mathrm{T},\,(L/3)} \right]^{\mathrm{T}}. \tag{3.35}$$

The matrices $\mathbf{P}_{\mathrm{ser}}$ and $\mathbf{P}_{\mathrm{int}}$ contain the power levels transmitted from serving and interfering cells according to the resource allocation pattern of SFR and FFR. These structures allow efficient matrix-based operations to obtain the resulting SINR distributions as it will be indicated shortly.

Segmentation

This procedure pulls out from the matrices $\mathbf{G}$, $\mathbf{C}$, $\mathbf{S}$, and $\mathbf{S}^{\mathrm{c}}$, the rows whose corresponding value in $\mathbf{t}$ is equal to j, $\forall j \in \mathcal{J}$. In other words, each of these matrices is segmented in $|\mathcal{J}|$ submatrices, one for each type of cell according to the rule given

by (3.28). In this manner, $\forall j \in \mathcal{J}$,

$$\begin{aligned} \mathbf{C}_j &\in \{0,1\}^{|\mathcal{A}_j|\times 2}, \\ \mathbf{S}_j \text{ and } \mathbf{S}_j^{\mathrm{c}} &\in \{0,1\}^{|\mathcal{A}_j|\times L}, \\ \mathbf{G}_j &\in \mathbb{R}^{|\mathcal{A}_j|\times L}. \end{aligned}$$

Link performance

The spectral efficiency of each pixel is stored in the vector $\mathbf{H} \in \mathbb{R}^A$, which is obtained by computing a non-decreasing function of the SINR. To capture the level of sensitivity with respect to the SINR variations, the Shannon's formula is considered. This model allows for mathematical tractability. However, any practical AMC scheme can be used. In system level simulations, the MCSs defined for LTE are considered.

Given a vector of SINR values ($\mathbf{\Psi}$), the spectral efficiency (η_a) of each element ($\psi_a \in \mathbf{\Psi}$) is bounded by:

$$\eta_a \leq \log_2(1+\psi_a), \tag{3.36}$$

and hence, allowing a certain abuse of notation, the following expression can be written:

$$\mathbf{H} = \log_2\left(1+\mathbf{\Psi}\right). \tag{3.37}$$

Bandwidth computation

The vector $\mathbf{B} \in \mathbb{R}^2$ indicates the bandwidth allocated to each class. This depends on the static ICIC scheme, and hence, it is computed as a function of β as follows:

$$\mathbf{B} = \left[\ (1-\beta)\cdot B \quad \beta \cdot B\ \right] \qquad \text{for SFR,} \tag{3.38}$$

$$\mathbf{B} = \left[\ \frac{(1-\beta)}{3}\cdot B \quad \beta \cdot B\ \right] \qquad \text{for FFR.} \tag{3.39}$$

The first and second element correspond to the bandwidth allocated to the class of exterior ($\mathcal{E}$) and interior ($\mathcal{I}$) users, respectively (see Figure 2.9).

Pixels rate

The rate at each pixel is calculated under the assumption that the bandwidth allocated to each class (at each cell) is equally divided among the pixels belonging to that class. This improves the fairness in the long run similarly to the proportional fairness policy that tends to share the resources equally among users as time passes.

The computation of the vector $\mathbf{r} \in \mathbb{R}^A$ that contains the rate of each pixel is obtained by means of the following operations that must be done for each group of

pixels. Thus, for each $j \in \{0, 1, 2\}$,

$$\tilde{\mathbf{P}}_{\text{int}} = \mathbf{P}_{\text{int}}(:,\ 2j : 2j+1\ ), \tag{3.40}$$

$$\mathbf{\Psi}_j = \left[[(\mathbf{S}_j \odot \mathbf{G}_j) \cdot \mathbf{P}_{\text{ser}}] \oslash \left[\left[(\mathbf{S}_j^{\text{c}} \odot \mathbf{G}_j) \cdot \tilde{\mathbf{P}}_{\text{int}} \right] \oplus \sigma^2 \right] \right] \odot \mathbf{C}_j, \tag{3.41}$$

$$\mathbf{H}_j = \log_2 (1 + \mathbf{\Psi}_j), \tag{3.42}$$

$$\mathbf{r}_j = \left[\left[\mathbf{S}_j \cdot (\mathbf{\Phi}^{\text{T}} \cdot \text{diag}(\mathbf{B})) \right] \odot \mathbf{H}_j \right] \cdot \mathbf{1}. \tag{3.43}$$

Note that $\tilde{\mathbf{P}}_{\text{int}} \in \mathbb{R}^{L \times 2}$ is created by selecting two columns (the columns with indexes $2j$ and $2j+1$) of the matrix $\mathbf{P}_{\text{int}}$. Once the previous operations are performed for each j, the vector $\mathbf{r}$ is built as follows:

$$\mathbf{r} = \left[\begin{array}{ccc} \mathbf{r}_1^{\text{T}} & \mathbf{r}_2^{\text{T}} & \mathbf{r}_3^{\text{T}} \end{array} \right]^{\text{T}}. \tag{3.44}$$

Having $\mathbf{r}$, the empirical CDF of r (F_r) can be obtained. Note that, although the dependence of $\mathbf{r}$ on α, β, and ψ_{TH} is not explicitly indicated, the vector $\mathbf{r}$ strongly depends on these parameters, and hence, it captures the essence of each static ICIC scheme. The results presented in Section 3.4 confirm the previous asseveration. Therefore, for the sake of clarity, the dependence of $\mathbf{r}$ on α, β, and ψ_{TH} is omitted.

Performance metrics

The performance metrics (η, $r_{5\%}$, and $\jmath$) are defined in terms of the vector $\mathbf{r}$ and the spatial traffic distribution, $\mathbf{\Gamma} \in \mathbb{R}^A$ (see Appendix C, Section C.1) according to the following expressions:

$$\eta = \frac{A \cdot (\mathbf{r}^{\text{T}} \cdot \mathbf{\Gamma})}{B \cdot L}, \tag{3.45}$$

$$r_{5\%} = F_r^{-1}(0.05), \tag{3.46}$$

$$\jmath = \frac{(\mathbf{r} \cdot \mathbf{1})^2}{((\mathbf{r} \odot \mathbf{r}) \cdot \mathbf{1})^2}. \tag{3.47}$$

Equations 3.45, 3.46, and 3.47 provide the required (accurate) characterization of SFR and FFR in terms of spectral efficiency, cell edge performance and fairness among users, respectively.

The next section is devoted to study and characterize the performance of these schemes by means of the aforementioned statistical model.

3.4 Performance of Static ICIC Schemes

In order to study the performance of SFR and FFR in the context of hexagonal (synthetic) and irregular (realistic) layouts, different cellular scenarios were considered. The test cases are the scenarios: 'Synthetic' and 'MORANS', which are defined in Appendix B, Section B.1.

The analysis is based on the statistical method presented in the previous section. In addition, results obtained from LTE-based system level simulations are also provided to complement the study and validate the conclusions from a practical point of view.

3.4.1 Statistical Analysis

The analysis focuses on two different aspects:

1. The impact of the operational parameters (α, β, and ψ_{TH}) on the average radio channel quality of each user class: interior ($\mathcal{I}$) and exterior ($\mathcal{E}$). This part of the study shows the utility of the proposed framework to 1) capture the inter-dependencies among design variables and performance metrics, and 2) analyze the operation of SFR and FFR based on the performance of each class of users.

2. A high level performance assessment based on linear aggregation. This method aims at providing a network-specific performance evaluation tool that can be suitably tuned to the operators' preferences/needs. This method provides mobile operators with means to perform a fast visual analysis by comparing and/or crossing variable-maps subject to different weights in a convenient fashion. Based on this part of the analysis, it will be shown (from a theoretical point of view) the poor performance of baseline design configurations in the context of realistic deployments.

Impact of α, β, and ψ_{TH} on SINR distributions

In this first part, the impact of the operational parameters on the resulting SINR distributions is studied. The scenario 'Synthetic' is considered in this initial part of the analysis.

The study presented herein investigates the impact of the parameters α and ψ_{TH} on the performance of SFR, and the impact of the parameters β and ψ_{TH} on the performance of FFR.

On the one hand, for the case of SFR, β is kept fixed to 1/3, the maximum value that avoids overlapping among cell edge subbands in trisectorial layouts. Note that from the cell edge viewpoint, $\beta = 1/3$ maximizes the bandwidth allocated to cell edge users, and hence, it is the logical choice from the ICIC perspective. Thus, two degrees of freedom are explored in the context of SFR: α and ψ_{TH}. On the other hand, in case of FFR, α is kept constant as the performance of this scheme is independent of it as long as 1) it is applied globally in the network (as in baseline design configurations), and 2) average ICI levels are significantly higher than the noise power (as in interference-limited systems). In this manner, $\alpha = 0.40$ was used in numerical evaluations[2]. Thus, two degrees of freedom are explored in the context

[2]This figure guarantees a minimum received power of -123 dBm in the coverage area of both test cases.

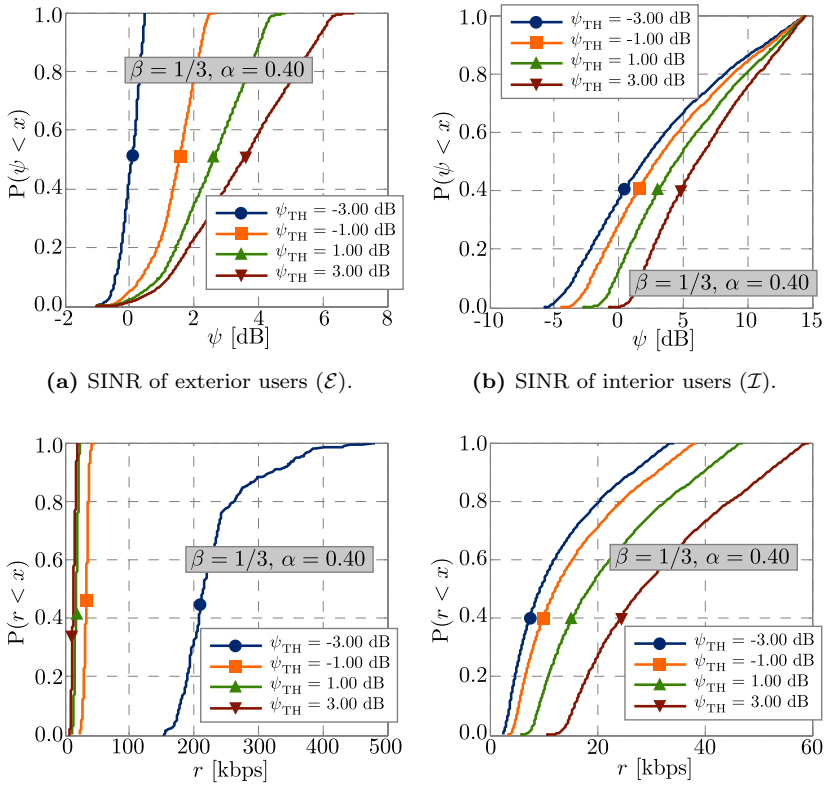

(a) SINR of exterior users ($\mathcal{E}$).

(b) SINR of interior users ($\mathcal{I}$).

(c) Rate of exterior users ($\mathcal{E}$).

(d) Rate of interior users ($\mathcal{I}$).

Figure 3.6: Impact of ψ_{TH} on the performance of SFR.

of FFR: β and ψ_{TH}. As it will be shown shortly, two dimensions are enough to adjust both SFR and FFR and attain a wide range of values for the performance metrics with the joined advantage that it simplifies the analysis significantly.

The study starts with the analysis of the impact of each parameter. For the sake of clarity, the remaining degree of freedom is kept fixed in each case.

Figure 3.6 illustrates the impact of ψ_{TH} on SFR. As classification threshold, ψ_{TH} determines the size of the sets $\mathcal{E}$ and $\mathcal{I}$. The larger the value of ψ_{TH}, the larger the number of exterior pixels and the smaller the number interior pixels. Figures 3.6a and 3.6b show how this parameter affects the SINR distribution of each class. Clearly, increasing ψ_{TH} makes the set $\mathcal{E}$ larger by adding users with better SINR figures, and hence, the upper tail of the SINR distribution of the set $\mathcal{E}$ moves to the right (good SINR values) as it is shown in Figure 3.6a. In a similar way, decreasing ψ_{TH} makes the set $\mathcal{I}$ larger by adding more worse users, and consequently, the lower tail of the SINR distribution of the set $\mathcal{I}$ moves to the left (bad SINR values) as it is shown in Figure 3.6b. Note that adding more pixels to the sets $\mathcal{I}$ or $\mathcal{E}$ tends to reduce the per-pixel bandwidth as the bandwidth of each class is

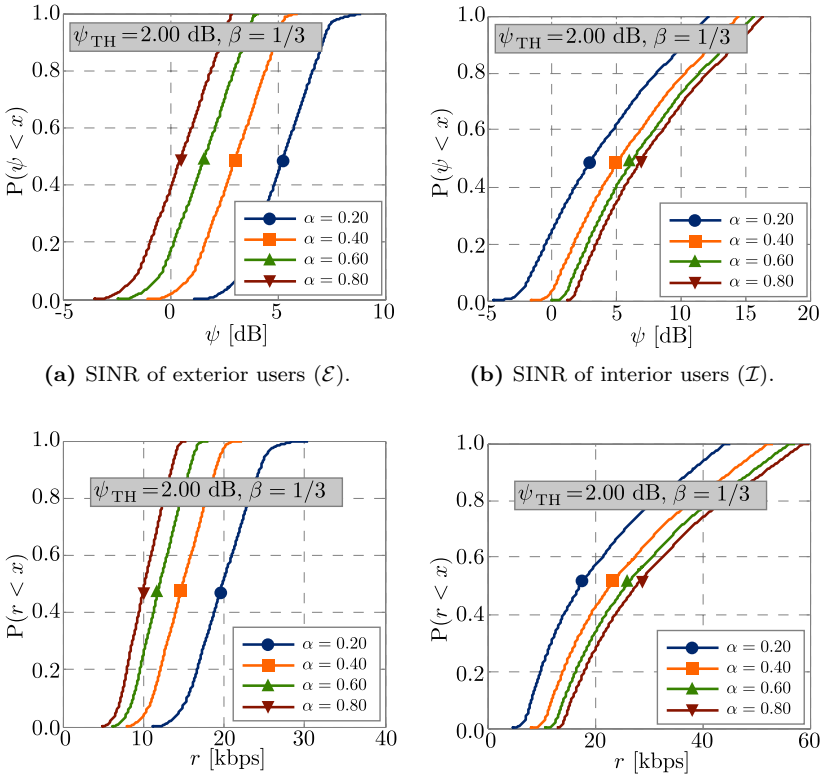

(a) SINR of exterior users ($\mathcal{E}$).

(b) SINR of interior users ($\mathcal{I}$).

(c) Rate of exterior users ($\mathcal{E}$).

(d) Rate of interior users ($\mathcal{I}$).

Figure 3.7: Impact of α on the performance of SFR.

fixed. This obviously has an impact on the rates at pixel level as it is shown in Figures 3.6c and 3.6d. Thus, individual rates in the set $\mathcal{E}$ are expected to be reduced if ψ_{TH} growths and the opposite holds for the set $\mathcal{I}$. Note that the type and amount of pixels belonging to each class for different values of ψ_{TH} also explains the way in which the distribution of r varies in each class, i.e., while increasing ψ_{TH} results in notorious changes in the set $\mathcal{I}$ and small variations in the set $\mathcal{E}$, decreasing ψ_{TH} results in notorious changes in the set $\mathcal{E}$ and small variations in the set $\mathcal{I}$.

Figure 3.7 illustrates the impact of α on SFR. Recall that α determines the power level of the subbands devoted to the set $\mathcal{I}$. Thus, increasing α results in a degradation of the SINR distribution of the set $\mathcal{E}$ and the corresponding improvement on the set $\mathcal{I}$ as it is shown in Figures 3.7a and 3.7b, respectively. Given that ψ_{TH} is fixed, the size of the sets $\mathcal{I}$ and $\mathcal{E}$ is also constant, and thus, for a fixed per-class bandwidth allocation, a better SINR distribution results in a better rate distribution and viceversa. The previous is shown in Figures 3.7c and 3.7d, where, in addition, it can be seen that the variations in the rate distributions are always proportional to the variations of the SINR distributions for both sets. Nevertheless, it is worth

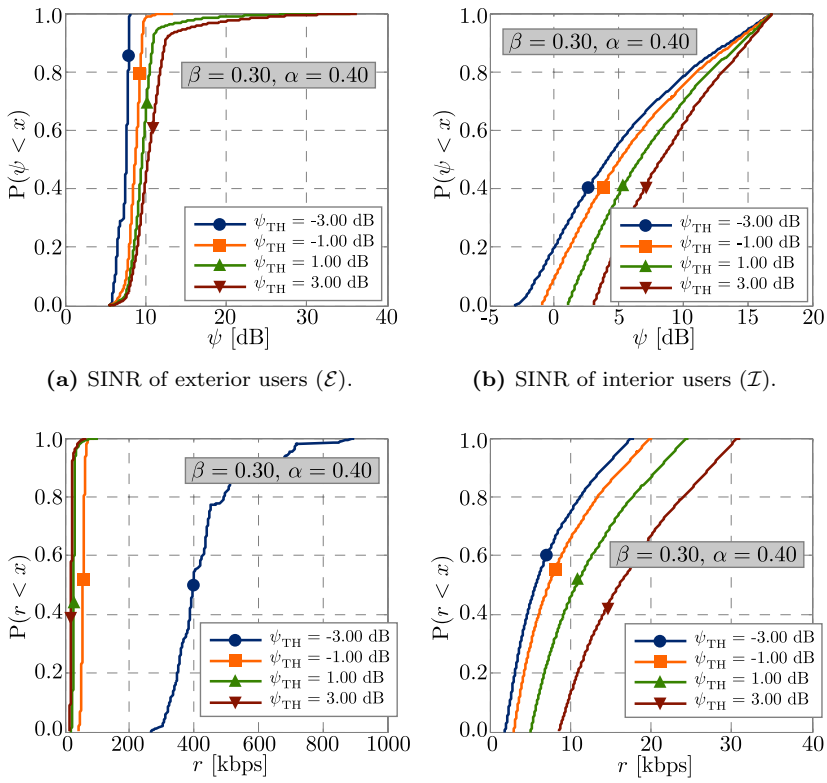

(a) SINR of exterior users ($\mathcal{E}$).

(b) SINR of interior users ($\mathcal{I}$).

(c) Rate of exterior users ($\mathcal{E}$).

(d) Rate of interior users ($\mathcal{I}$).

Figure 3.8: Impact of ψ_{TH} on the performance of FFR.

saying that in this case, both SINR and rate distributions are more sensitive to decrements of α than increments of it. The previous is explained because if $\alpha \to 1$, the system tends asymptotically to full reuse in terms of ICI, although with the separation of users into classes. If $\alpha \to 0$, the system becomes frequency reuse 3 but only for the set $\mathcal{E}$ (the one more sensitive to ICI), and hence, decrements of α result in increasingly improvements of the SINR distribution. Note that for $\alpha \to 0$, the SINR distribution of the set $\mathcal{I}$ would disappear.

Figure 3.8 illustrates the impact of ψ_{TH} on FFR. The effect is exactly the same as in SFR, i.e., ψ_{TH} controls the size of the sets $\mathcal{I}$ and $\mathcal{E}$, thus modifying the resulting SINR distributions as it can be seen in Figures 3.8a and 3.8b. Similarly to SFR, increasing ψ_{TH} makes the set $\mathcal{E}$ larger by adding users with better SINR figures, and hence, the upper tail of the SINR distribution of this set moves to the right (good SINR values) as it is shown in Figure 3.8a. Decreasing ψ_{TH} makes the set $\mathcal{I}$ larger by adding more worse users, and consequently, the lower tail of the SINR distribution of this set $\mathcal{I}$ moves to the left (bad SINR values) as it is shown in Figure 3.8b. As expected, varying the size of each set of pixels also affects the resulting pixel

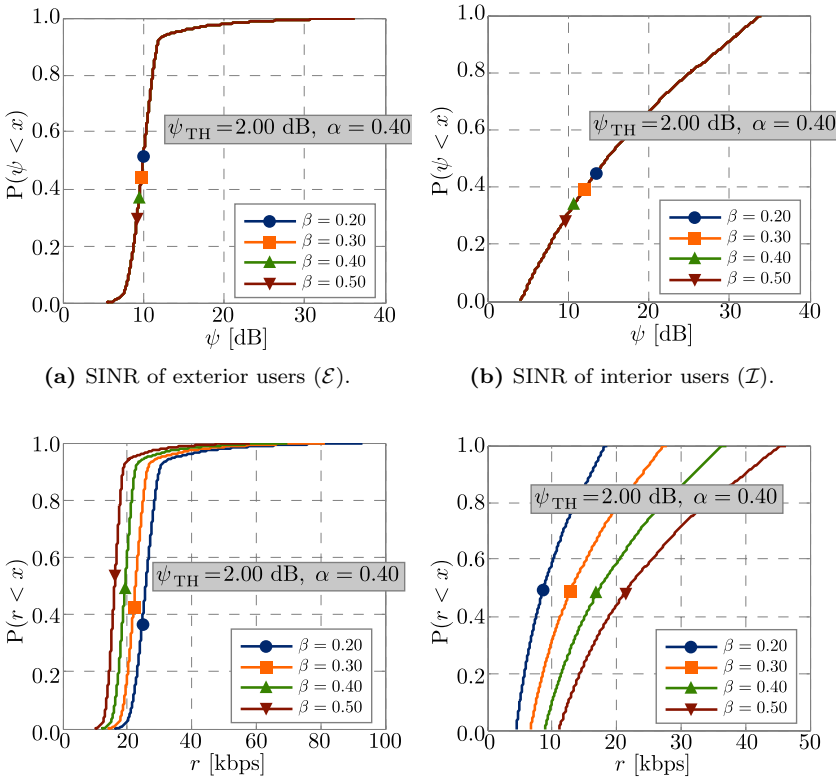

(a) SINR of exterior users ($\mathcal{E}$).

(b) SINR of interior users ($\mathcal{I}$).

(c) Rate of exterior users ($\mathcal{E}$).

(d) Rate of interior users ($\mathcal{I}$).

Figure 3.9: Impact of β on the performance of FFR.

rates as it is shown in Figures 3.8c and 3.8d. The same analysis about the impact of ψ_{TH} on pixel rates for SFR also holds in this case. Note the similarity among Figures 3.6c and 3.6c, and Figures 3.8c and 3.8d.

Finally, Figure 3.9 illustrates the impact of β on FFR. The impact of this parameter on the resulting SINR distributions is illustrated in Figures 3.9a and 3.9b. As it was mentioned before, in FFR ICI is intra-class, meaning that each type of users makes exclusive use of the same set of subbands at each cell. Thus, the sets $\mathcal{E}$ and $\mathcal{I}$ operate independently with reuse factor 3 and full reuse, respectively. For this reason, once the sets $\mathcal{E}$ and $\mathcal{I}$ are fixed (by means of ψ_{TH}), the variations of β have no effect on the distributions of the resulting SINR as it can be appreciated. However, varying β modifies the bandwidth available to each class, and therefore, pixel rates are affected by such changes. This can be seen in Figures 3.9c and 3.9d. In addition, note that such bandwidth variations are more noticeable in the set $\mathcal{I}$ (on average, from 8 to 22 kbps, +175%), precisely the set of pixels that is more sensitive to bandwidth than interference, while the impact on the set $\mathcal{E}$ is less remarked (on average, from 25 to 15 kbps, -40%) as this set is more sensitive to interference.

However, the impact is almost linear with respect to the variations of β in both cases.

Based on the previous analysis, the following conclusions can be drawn:

1. In SFR, α controls the amount of ICI in the system by modifying the power allocated to the set $\mathcal{I}$. Its impact on the resulting SINR and rate distributions is quasi-linear for $\alpha \in (0.6, 1.0)$ and non-linear for $\alpha \in (0, 0.6)$. However, an issue with the use of this parameter is that varying α (even in one single cell) modifies ICI conditions in the network.

2. Both in SFR and FFR, the classification thresholds (ψ_{TH}) has a significant impact on the SINR and rate distributions with the joined advantage that this parameter can be adjusted both globally in the network or locally at each cell without impact on the levels of ICI affecting neighboring cells.

Up to now, the analysis has been focused on the impact of the operational parameters on the performance of each user class. Let's have a look at the performance of SFR and FFR from a system point of view.

Operation of SFR and FFR

Figure 3.10 illustrates the operation of SFR and FFR from a network perspective. The resulting SINR distribution of each user class is shown in Figure 3.10b. The system performance in terms of user rates is illustrated in Figure 3.10a. In addition, the case of full reuse is also included as a reference. Note how SFR clearly tends to homogenize the SINR distributions of each user class with respect to full reuse. In addition, and more important from the ICIC point of view, the lower bound of each of these distributions are approximately 4 dB above the reference scheme. This is translated in an improvement of around 50% in terms of the percentile 5 of r ($r_{5\%}$). The case of FFR is illustrated in Figures 3.10c and 3.10d. Note that the SINR levels are substantially better than in SFR due to the higher reuse factor. However, as only part of the system bandwidth is used at each cell, the spectral efficiency is penalized. Despite of this, a significant improvement of more than 80% is attained for the percentile 5 of r.

Note that in both cases (SFR and FFR, Figures 3.10b and 3.10d, respectively), the resulting pixel rate distribution, indicated with the upside-down triangle, is not necessarily the mean point between the rate distributions of each user class. This is due to the fact that the amount of pixels in each class is different (it is determined by ψ_{TH}), and hence, the relative importance of each class is not always the same.

Up to now, the impact of the operational parameters and the operation of SFR and FFR have been analyzed by employing the statistical framework presented in Subsection 3.3.2. It is evident that the performance evaluation methodology provides a very convenient approach to study the interactions in SFR and FFR by means of an independent analysis of each class ($\mathcal{E}$ and $\mathcal{I}$).

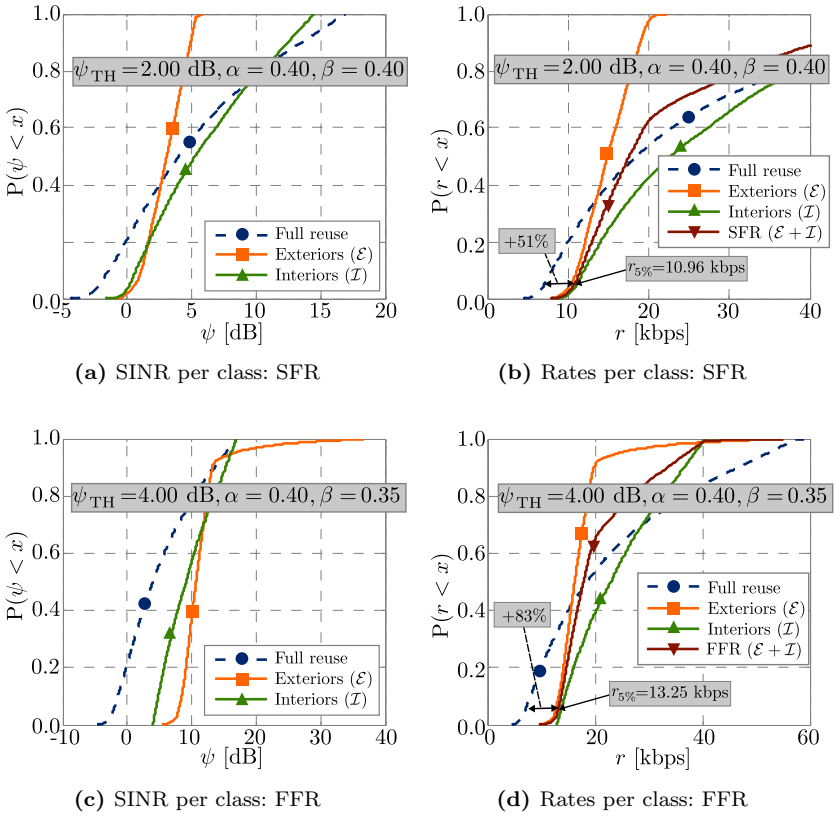

(a) SINR per class: SFR

(b) Rates per class: SFR

(c) SINR per class: FFR

(d) Rates per class: FFR

Figure 3.10: Operation of static ICIC schemes.

Nevertheless, nothing has been said about how to select appropriate values for α, β, and ψ_{TH}. The proposed model can also be used as a performance assessment tool to explore the search space ($\mathcal{X}$) of the operational parameters, as it is defined in (3.26). This can be done in a very efficient manner without the need for computationally-heavy and time-consuming system level simulations. This part of the study is presented next.

Performance Assessment based on Linear Aggregation

The system is evaluated by means of different linear aggregations of the metrics η, $r_{5\%}$, and $\jmath$. This allows selecting different levels of priority for each indicator and pointing out the tradeoffs among them.

For numerical purposes, the search space is defined as follows:

$$\mathcal{U}_{\alpha} = \{\ 0.025,\ 0.050,\ 0.075,\ \cdots,\ 1.000\ \}, \tag{3.48}$$
$$\mathcal{U}_{\beta} = \{\ 0.050,\ 0.075,\ 0.100,\ \cdots,\ 0.975\ \}, \tag{3.49}$$
$$\mathcal{U}_{\psi_{\mathrm{TH}}} = \{\ -3.00,\ -2.75,\ -2.50,\ \cdots,\ 6.00\ \}\quad [\mathrm{dB}], \tag{3.50}$$
$$\mathcal{X}_{\mathrm{SFR}} = \mathcal{U}_{\alpha} \times \mathcal{U}_{\psi_{\mathrm{TH}}}, \tag{3.51}$$
$$\mathcal{X}_{\mathrm{FFR}} = \mathcal{U}_{\beta} \times \mathcal{U}_{\psi_{\mathrm{TH}}}. \tag{3.52}$$

Three different criteria ($\mathbf{w}$), as defined in (3.24), have been considered:

$$\mathbf{w}_1 = [\ 0.34,\ 0.33,\ 0.33\ ], \tag{3.53}$$
$$\mathbf{w}_2 = [\ 0.80,\ 0.10,\ 0.10\ ], \tag{3.54}$$
$$\mathbf{w}_3 = [\ 0.10,\ 0.80,\ 0.10\ ]. \tag{3.55}$$

Each of these criteria reflects different preferences among the metrics (η, $r_{5\%}$, and $\jmath$). The criterion $\mathbf{w}_1$ assigns the same importance to the three metrics. The second and third one ($\mathbf{w}_2$ and $\mathbf{w}_3$) prioritize spectral efficiency and cell edge capacity, respectively.

In order to investigate the performance of SFR and FFR both in regular and irregular layouts, this study is conducted in the context of synthetic and realistic cellular layouts, i.e., the scenarios 'Synthetic' and 'MORANS' defined in Appendix B. Without loss of generality, in this study, it was considered that the traffic is uniformly distributed in the coverage area, i.e., $\mathbf{\Gamma}(a) = 1/A,\ \forall a = 1, 2, \cdots, A$. Recall that $\mathbf{\Gamma}$ is the spatial traffic distribution.

Figures 3.11 and 3.12 show the characterization of SFR. Figures 3.13 and 3.14 illustrate the resulting pattern for FFR.

The performance of SFR in terms of each metric for the scenario 'Synthetic' is shown in Figures 3.11a, 3.11b, and 3.11c. The figures show the cross-impact of the parameters α and ψ_{TH} on each indicator. In the maps, red tones indicate better values. Note that, while the pattern of η is fairly monotone with α and ψ_{TH}, the variations of $r_{5\%}$ and $\jmath$ are clearly convex. As it can be seen, certain configurations favor more one metric than others. In general, higher values of α tend to favor the spectral efficiency, while the value of α that maximizes the percentile 5 of r depends on the classification threshold. Consequently, the selection of an appropriate NOP strongly depends on the needs or priorities of the network operator that should consider the weighted result by means of a predefined criterion as it is shown in Figures 3.11d, 3.11e, and 3.11f. The figures illustrate the three cases: $\mathbf{w}_1$, $\mathbf{w}_2$, and $\mathbf{w}_3$, respectively. As it can be seen, the statistical model allows an fast and easy identification of the configurations that provide the best results according to each criterion. However, it is important to take into account that the final selection could include additional factors such as the minimum value of α to guarantee the required coverage. The parametric sweep shown in the figures is complete for illustrative purposes. Note the high correlation between the patterns shown in Figures 3.11a and 3.11e, and Figures 3.11b and 3.11f.

The tradeoff between the different metrics can be visually assessed by looking at the distance between yellow and red zones in the maps corresponding to different indicators. Thus, the methodology allows for a fast assessment of SFR and FFR based on network-specific patterns (maps).

The pattern of each metric for SFR in the scenario 'MORANS' is shown in Figures 3.12a, 3.12b, and 3.12c. Clearly, the red zones are not only more separated among the maps but also the transitions between red and blue area are more pronounced. This can be interpreted as a much worse tradeoff between the metrics, i.e., the penalty in terms of any variable to improve another is much higher in this context of irregular layouts. For instance, the selection of a NOP that is optimal in the synthetic scenario, could result in a poor performance if that setting is applied in a realistic deployment. This situation remarks the importance of obtaining accurate network-specific characterizations. The same conclusion was also pointed out in [63, 64]. As the figures illustrate, the method employed here not only allows for efficient computation of such patterns but also provides intuitive representations of them.

The same analysis and conclusions presented so far for SFR also hold for FFR. Thus, the same analysis is omitted for brevity. The performance characterization of this scheme for the scenarios 'Synthetic' and 'MORANS' is presented in Figures 3.13 and 3.14, respectively.

In order to provide additional perspectives about the previous results, Figure 3.15 shows the distribution of the average SINR per-cell in the test cases previously considered. Based on this, it can be inferred that the *good* rsults of SFR and FFR in hexagonal layouts is due to the homogeneity among cells in terms of SINR distributions as it is shown in Figure 3.15a. Given this, it makes sense that common values of α, β, and ψ_{TH} can be applied uniformly to the network and it results in acceptable performances. In contrast, the situation is quite different in realistic deployments because propagation conditions and ICI levels vary significantly from cell to cell as it is shown in Figure 3.15b. Therefore, it is expected that the same setting applied to each cell results in suboptimal (indeed poor) achievements.

In order to validate the previous reasoning, LTE-based system level simulations are presented. The study is presented next.

3.4.2 System Level Simulations

The evaluation setting has been embedded in the LTE system level simulator described in Appendix D, which carefully models all the relevant aspects of LTE such as HARQ and the actual structure of the OFDMA frame and transport/physical channels according to [159, 161, 162]. This simulation environment is calibrated according to guidelines given in [175, 176].

The system level simulations are based on Monte Carlo experiments with uniform randomly spread users. The results compile statistic from 500 independent experiments each of which has a duration of 900 s (9×10^5 TTIs). Recall that the

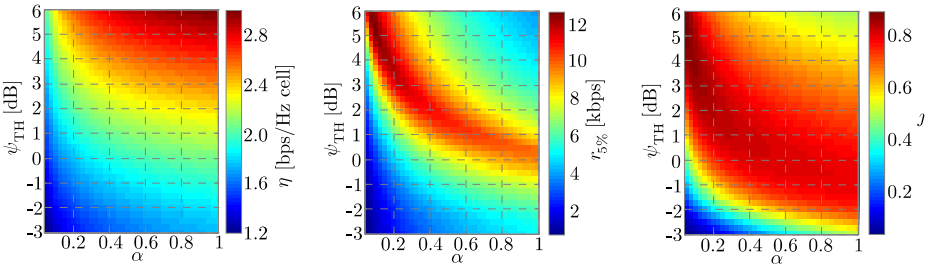

(a) Spectral efficiency: η. **(b)** Percentile 5 of r: $r_{5\%}$. **(c)** Jain's index: $\jmath$.

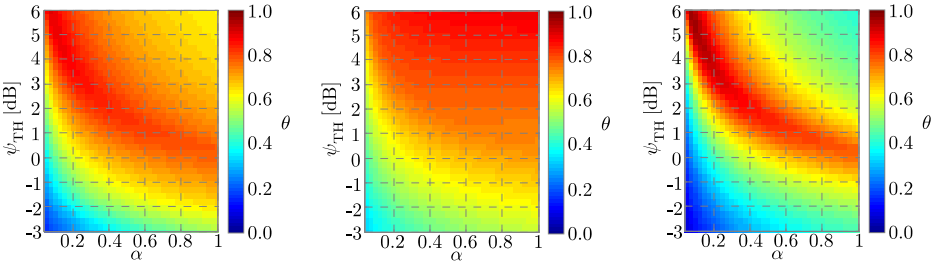

(d) θ considering $\mathbf{w}_1$. **(e)** θ considering $\mathbf{w}_2$. **(f)** θ considering $\mathbf{w}_3$.

Figure 3.11: Performance characterization of SFR: scenario 'Synthetic'.

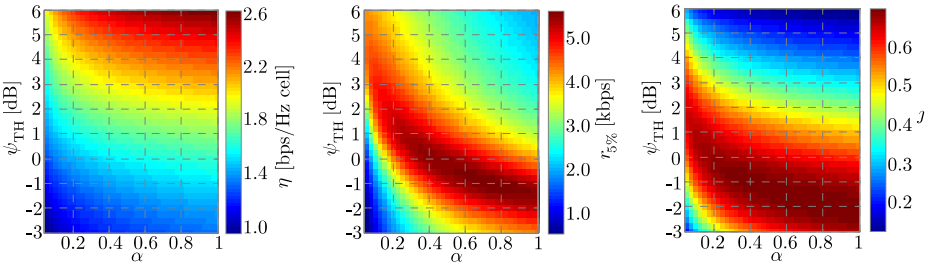

(a) Spectral efficiency: η. **(b)** Percentile 5 of r: $r_{5\%}$. **(c)** Jain's index: $\jmath$.

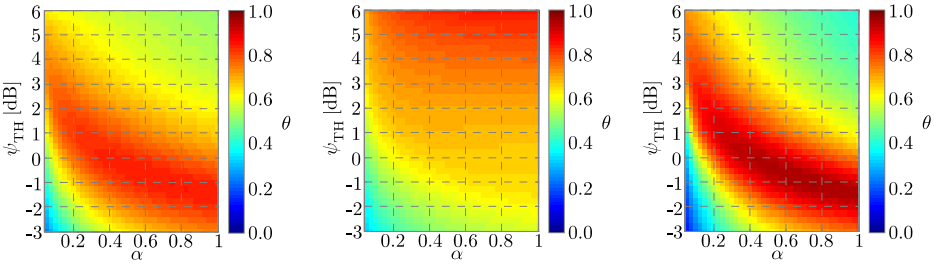

(d) θ considering $\mathbf{w}_1$. **(e)** θ considering $\mathbf{w}_2$. **(f)** θ considering $\mathbf{w}_3$.

Figure 3.12: Performance characterization of SFR: scenario 'MORANS'.

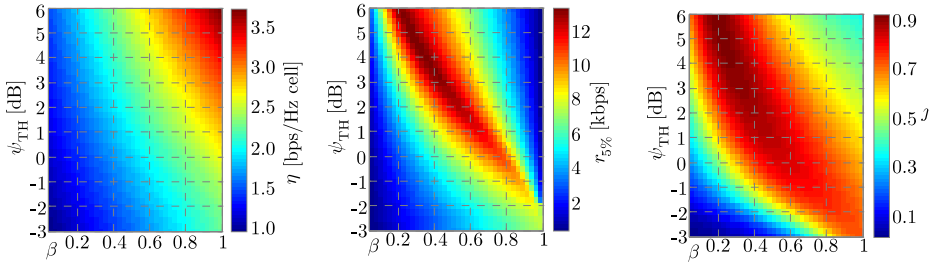

(a) Spectral efficiency: η. **(b)** Percentile 5 of r: $r_{5\%}$. **(c)** Jain's index: $\jmath$.

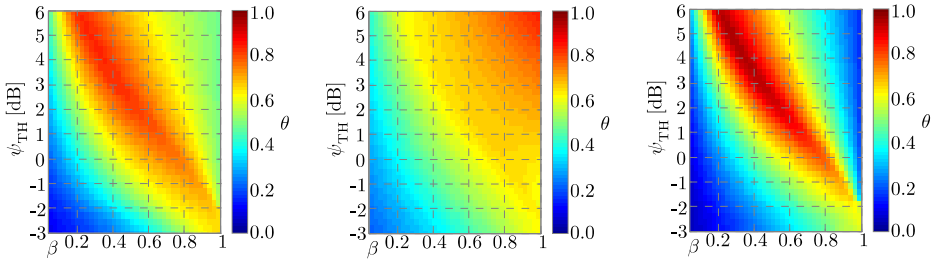

(d) θ considering $\mathbf{w}_1$. **(e)** θ considering $\mathbf{w}_2$. **(f)** θ considering $\mathbf{w}_3$.

Figure 3.13: Performance characterization of FFR: scenario 'Synthetic'.

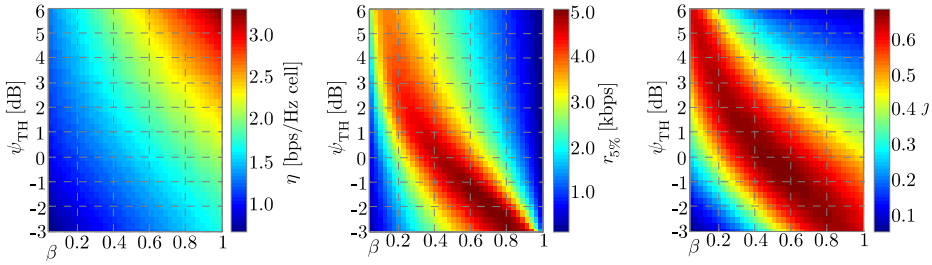

(a) Spectral efficiency: η. **(b)** Percentile 5 of r: $r_{5\%}$. **(c)** Jain's index: $\jmath$.

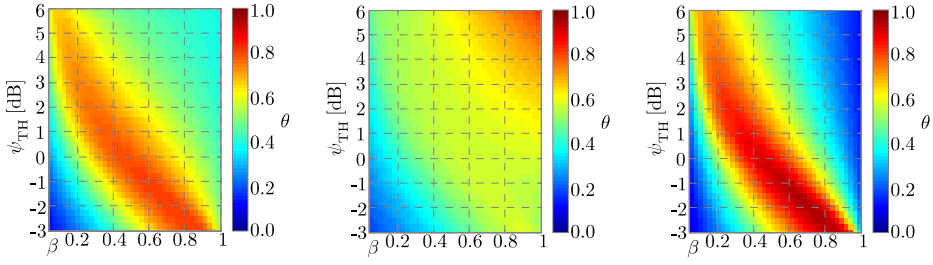

(d) θ considering $\mathbf{w}_1$. **(e)** θ considering $\mathbf{w}_2$. **(f)** θ considering $\mathbf{w}_3$.

Figure 3.14: Performance characterization of FFR: scenario 'MORANS'.

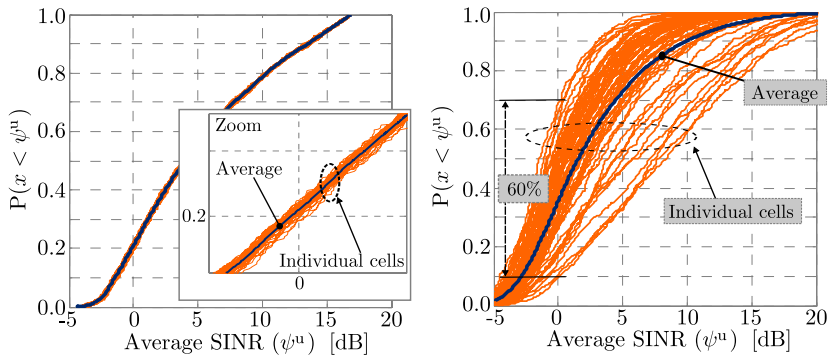

(a) Sce. 'Synthetic' **(b)** Sce. 'MORANS'

Figure 3.15: Average SINR distribution per cell.

Table 3.1: Simulation Parameters and Evaluation Setting.

Parameter	**Value/assumption**
Test cases (scenarios)	'Synthetic', 'MORANS' (see Section B.1).
System bandwidth (B)	5.4 MHz.
System load	$30 \times L$ users (30 users per cell (on average)).
User distribution	Random/uniform.
Scheduler	Proportional fair.
Traffic model	Full Buffers.
CSI feedback	CQI-based, one CQI per RB.
Mobility model	Urban vehicular [173]
Link Abstraction	Mutual Information Equivalent SINR Mapping [174].
Transmission mode	Single-antenna port.
SFR @ 'Synthetic'	$\mathbf{x} = [\ 0.250 \quad 0.33 \quad 4.00\ \text{dB}\ ]$. ($\mathbf{x}$ is defined in (3.25))
FFR @ 'Synthetic'	$\mathbf{x} = [\ 0.400 \quad 0.40 \quad 4.25\ \text{dB}\ ]$.
SFR @ 'MORANS'	$\mathbf{x} = [\ 0.475 \quad 0.33 \quad 0.25\ \text{dB}\ ]$.
FFR @ 'MORANS'	$\mathbf{x} = [\ 0.400 \quad 0.60 \quad -0.75\ \text{dB}\ ]$.

simulation parameters common to all scenarios are indicated in Table B.2. Additional parameters and assumptions considered in this study are shown in Table 3.1. Both synthetic and realistic scenarios are considered: the test cases 'Synthetic' and 'MORANS' that are described in Appendix B.

In order to assess an accurate BLER prediction, the system level is fed by look-up tables obtained through detailed link level simulations according to [174, 177]. Results from link level include means to map effective SINR figures subject to different transport block sizes, modulation and coding schemes, and redundancy version into transmission error probabilities. In this manner, BLER is modeled similarly as in the actual LTE operation.

The mobility model is vehicular for urban scenarios as defined in [173]. In order

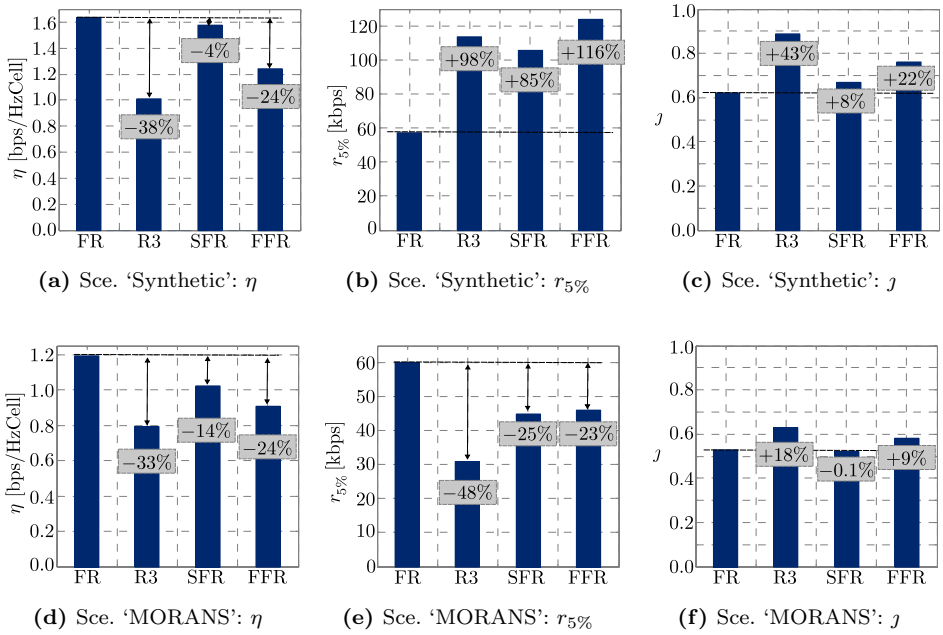

(a) Sce. 'Synthetic': η **(b)** Sce. 'Synthetic': $r_{5\%}$ **(c)** Sce. 'Synthetic': $\jmath$

(d) Sce. 'MORANS': η **(e)** Sce. 'MORANS': $r_{5\%}$ **(f)** Sce. 'MORANS': $\jmath$

Figure 3.16: Performance comparison of different resource allocation schemes.

to emulate low/moderate conditions, pedestrian speed of 3 km/h was assumed. The channel model is the Extended ITU Pedestrian B defined in [178], which features a 32.55 ns sampling grid that matches the LTE sampling rate of 30.72 MHz.

In order to investigate the operation of SFR and FFR from an ICIC point of view, several configurations with the best values of θ for $\mathbf{w}_3$ are tested. Recall that the criterion $\mathbf{w}_3$ gives high priority to the performance at cell edges ($r_{5\%}$).

The results presented here correspond to the configurations with the best results in system level simulations, i.e., calculating θ based on results coming from system level trials. Such setting are also indicated in Table 3.1. In addition, the performance of full reuse (FR) and reuse factor 3 (R3) are included as reference.

Figure 3.16 shows the results. The results for the scenario 'Synthetic' are shown in Figures 3.16a, 3.16b, and 3.16c. The corresponding figures for the scenario 'MORANS' are provided in Figures 3.16d, 3.16e, and 3.16f. The gains (or losses) are always indicated with respect to the performance of full reuse. On the one hand, in the context of the scenario 'Synthetic', both SFR and FFR provide significant gains in terms of the percentile 5 of user rates ($r_{5\%}$), 85% and 116%, respectively. However, the gains come at the expense of losses in terms of spectral efficiency. In addition, these static ICIC schemes also improve the fairness among users. On the other hand, looking at the results in the context of the scenario 'MORANS', it is evident the very poor performance of SFR and FFR. Besides the noticeable loss in terms of spectral efficiency, neither SFR nor FFR are able to provide gains in terms of $r_{5\%}$, indeed

losses of around 25% are obtained in both cases. Moreover, fairness levels decrease for all the schemes. These results can be analyzed from two different points of view. First, in terms of absolute values. All the metrics are worsened in the context of the scenario 'MORANS', being these losses more pronounced for the schemes R3, SFR, and FFR. In other words, the schemes that relies on the fact that reuse 3 is optimal at cell edges (an assumption valid for regular layouts) are the ones with the worst performance. However, in irregular layouts, several factors cause different levels of ICI at each cell. Examples of them are antenna azimuths not perfectly aligned as in the synthetic case, the different levels of dominancy among cells due to the terrain orography, irregular intersite distances, propagation conditions, in some cases strongly guided through streets, and so on. The combined effect of these elements cause that the amount of ICI received by each cell is different, and hence, the size of cell edges and the SINR distributions are also different. This essentially explains the poor performance of baseline designs in the context realistic (irregular) deployments, and thus, the need for **a certain degree of local optimization (at cell level) is mandatory in the context of irregular layouts to compensate such unbalances**.

3.5 Concluding Remarks

A statistical analysis of SFR and FFR by means of a model that can be used without assumptions on the network topology has been presented in this chapter. The need for such methodology has stemmed from drawbacks found in analytical models previously introduced. More precisely, the fact that such models cannot be used as a performance assessment tool in cellular deployments featuring an arbitrary network topology.

The proposed statistical model captures all the complex interactions between the operational parameters of SFR and FFR and the most important performance metrics from the ICIC point of view, i.e., cell edge performance and spectral efficiency. However, the analysis goes beyond well known facts and tradeoffs and it explores the relationship between the performance of each class of users and the overall system performance.

The results clearly indicate that the proposed scheme is suitable to be applied to any realistic network. In this manner, convenient performance patterns in the form of 2D maps that are specific to every single network can be obtained efficiently without the need for computationally-heavy system level simulations. These patterns allow to the mobile operator an easy visual-assessment of the configuration that can be applied to the network. Moreover, different criteria can also be defined in a flexible manner.

Based on this tool, the impact of the operational parameters in SFR/FFR (α, β, and ψ_{TH}) represents the first set of results presented in this chapter, and thus, the main conclusions are summarized next:

- The operation of SFR and FFR can be described in terms of two subsystems,

namely the class of exterior and interior users. The performance of them is largely influenced by the selection of the parameters α, β, and ψ_{TH}.

- A proper calibration of such parameters implies achieving a proper balance between these two classes in terms of all performance metrics. Otherwise one class would be severely penalized, and hence, the performance from a system point of view would be poor. However, finding such set of values is far from being an easy task since the impact of each parameter is strongly conditioned by the values of the other ones.

- The classification threshold (ψ_{TH}) arises as a firm candidate to tune the performance of SFR and FFR as it can be adjusted independently at each cell without impact on neighboring ones.

- Conversely, local adjustments of the parameters α and β convey practical difficulties from an implementation point of view.

  - On the one hand, increasing α locally originates more ICI in neighbouring cells, which in turn, could tend to do the same, creating in this manner a sort of undesirable positive feedback. On the other hand, decreasing α could result in coverage holes due to the requirements of mobile devices in terms of received power.
  - Similarly, adjusting β (even globally) requires precise coordination in order to guarantee the required reuse factor for each class of users.

The second set of results presented in this chapter is devoted to investigate the performance of SFR and FFR in the context of realistic deployments. This was done by means of two different approaches: 1) the statistical analysis (using the model previously introduced), and 2) system level simulations. The main conclusions can be summarized as follows:

- In the context of hexagonal layouts, baseline designs of SFR and FFR provide convenient means to adjust the well known tradeoff between spectral efficiency and cell edge performance. This is somehow, expected as it was shown that a reuse factor 3 is optimal for the cell edges and in this type of layout azimuths are perfectly aligned, thus minimizing ICI.

- In realistic networks featuring irregular cell layouts, the performance of baseline designs of SFR and FFR is poor. This is a direct consequence of the fact that SINRs distributions and cell edge sizes vary significantly from one cell to another. Thus, the need for optimization in such contexts was justified and established.

- The results suggest that a certain level of local optimization (at cell level) is required to compensate such unbalances and improve the performance of SFR and FFR, being ψ_{TH} (as it was previously mentioned) a good candidate for design variable in such optimization problem.

In the light of these conclusions, the following chapters focus on investigating schemes and optimization models to enhance the performance of static ICIC schemes. The description of such novelties begins in the next chapter, where mechanisms to improve the interplay between CSI feedback and static ICIC are presented.

Chapter 4

Novel CSI Feedback Methods for Static ICIC Schemes

4.1 Introduction

Along the previous chapters, the need for additional research efforts to improve the performance of static ICIC schemes was shown. Mechanisms based on static ICIC are feasible candidates to deal with ICI due to their low complexity and ease of implementation. However, ICIC schemes are not standardized in LTE, which just provides a certain support so that every vendor/operator configures its particular ICIC option. Hence, the interworking of ICIC with other important network functionalities such as CSI feedback is not considered within the specifications. This chapter provides a description of the relationship between ICIC and CSI in LTE and it introduces novel mechanisms to improve such interworking.

Whereas ICIC is in charge of determining the resources to be used at each cell by each class of users (exteriors and interiors, $\mathcal{E}$ and $\mathcal{I}$, respectively) in the mid and long term, scheduling deals with resource allocation at the very short term scale. In this sense, CSI feedback is a key functionality whose role is of utmost importance because updated and free of errors CSI allows taking opportunistic decisions, and thus, making the most of each user channel conditions. LTE specifications do include several CSI feedback methods comprising periodic and aperiodic mechanisms suitable for Real Time (RT) and Non Real Time (NRT) traffic, respectively. However, such in-built schemes are quite generic and they do not take into account the presence of ICIC techniques. Hence, the operation of these native CSI feedback mechanisms is not optimized to operate in conjunction with static ICIC techniques. Both ICIC and CSI feedback have been investigated independently, nevertheless, it is desirable a design in which the joint operation is efficient. As it will be shown later on, this particular interworking deserves special attention as the performance of native LTE CSI reporting schemes is poor in cases where static ICIC policies are applied.

This chapter introduces two novel CSI feedback schemes: a periodic scheme and an aperiodic one. Both mechanisms are suitable to operate in conjunction with SFR and FFR. The design of these schemes exploit the typical per-class resource allocation in SFR and FFR. In this manner, UE only feedback to their serving base stations the quality of the subbands in which they are allowed to be transmitted, thus reducing the signaling overhead and improving the accuracy of the CSI feedback process.

The Chapter is organized as follows: the next section introduces the required LTE background, i.e., a general description of the mechanisms available in LTE for CSI feedback. The problem statement is also presented. Next, Section 4.3 contains a survey of related works, where it is shown that the interworking between static ICIC and CSI feedback has not been explicitly considered before.. In the light of this situation, novel schemes are proposed and presented in Section 4.4. Section 4.5 describes the system model and the QoS assessment methodology used to evaluate the performance of these schemes. Finally, the chapter is closed with the analysis of the numerical results and conclusions in Sections 4.6 and 4.7, respectively.

4.2 CSI Feedback in LTE

There are two different mechanisms to perform CSI feedback in LTE: *Periodic* and *Aperiodic* schemes [162].

1. *Periodic CSI feedback*: UE reports periodically through the Physical Uplink Control Channel (PUCCH) channel quality measurements. The reporting interval is configured by higher layers.

2. *Aperiodic CSI feedback*: The feedback is performed on-demand and it is transmitted over the Physical Uplink Shared Channel (PUSCH).

Periodic CSI feedback is recommended for traffic patterns having constant or near constant bit rate such as conversational or streaming services. Aperiodic CSI feedback is more appropriate for bursty traffic patterns in which a more detailed reporting is needed (from time to time). It is worth noting that both types of reporting can be used together, in such cases aperiodic reporting has priority.

Before describing the CSI schemes defined in LTE, it is important to provide some details about Channel Quality Indicators (CQI), the main format in which LTE manages the CSI[1].

[1]Precoding Matrix Indicator (PMI) and Rank Indicator (RI) are required for additional transmission modes including transmit diversity, open- and closed- loop spatial multiplexing and multiuser MIMO [162].

4.2.1 Cell Specific Reference Signals and Channel Quality Indicators

A CQI is a 4-bit integer calculated from SINR measurements. Reported CQI values are used together with additional UE capabilities to select the optimum MCS index for transmission. In order to allow for SINR estimations, CS-RS are embedded into the overall signal bandwidth at certain REs. The position of the CS-RS at each cell is determined taking into account the cell's identity [162]. Figure 2.16 shows a possible allocation of the CS-RS within the OFDMA grid.

Lets consider the SINR at subcarrier level. The corresponding expression is as follows:

$$\psi_m^{n,sc} = \frac{P_{\hat{l}}^{n,sc} \cdot g_{m,\hat{l}}^{n,sc}}{\sum\limits_{l=1,\, l\neq\hat{l}}^{L} P_l^{n,sc} \cdot g_{m,l}^{n,sc} \;+\; \sigma^2}, \tag{4.1}$$

where the indices $m \in \{1, 2, \ldots, M\}$, $n \in \{1, 2, \ldots, N_{\text{RB}}^{\text{DL}}\}$ and $sc \in \{1, 2, \ldots, N_{\text{sc}}^{\text{RB}}\}$ indicate the user, RB, and subcarrier, respectively.

Let's consider the vector $\mathbf{\Psi} \in \mathbb{R}^{N_{\text{CS-RS}}^{\mathcal{P}}}$, whose elements ψ_i (i=1, 2, ..., $N_{\text{CS-RS}}^{\mathcal{P}}$) correspond to the SINR values of the CS-RS in an arbitrary set of PRBs ($\mathcal{P}$). Thus, taking into account that SINR values are computed according to (4.1), the *effective* SINR [179] is obtained from the following expression:

$$\psi_{\text{eff}} = a_1 I^{-1}\left(\frac{1}{N_{\text{CS-RS}}^{\mathcal{P}}} \sum_{i=1}^{N_{\text{CS-RS}}^{\mathcal{P}}} I\left(\frac{\psi_i}{a_2}\right)\right). \tag{4.2}$$

The parameters a_1 and a_2 adapt to different MCS. The function $I(\cdot)$ maps each SINR value (ψ_i) to a performance metric that is averaged over all the samples. In this thesis, the Mutual Information Equivalent SINR Mapping (MIESM) or modulation constrained capacity [174] is employed. Therefore:

$$I(\psi_i) = \log_2(Q) + \frac{1}{2\pi Q} \sum_{q=1}^{Q} f(\psi_i, q), \tag{4.3}$$

$$f(\gamma_i, q) = \int e^{-\psi_i (y - x_q)^2} \log_2\left(\frac{e^{-\psi_i (y-x_q)^2}}{\sum_{k=1}^{Q} e^{-\psi_i (y-x_k)^2}}\right) dy, \tag{4.4}$$

where Q is the size of the modulation alphabet, y is the channel output and x_q are the modulation symbols. The reader is referred to [174] for further details. Note that each element of $\mathcal{P}$ represents a PRB whose index (n) univocally identifies the PRB in the system bandwidth, and hence, $n \in \{1, 2, \ldots, N_{\text{RB}}^{\text{DL}}\}$.

Thus, the equivalent CQI index ($\Theta \in \{0\ 1\ 2\ ...\ 15\}$) indicating the MCS that can be supported for transmissions over $\mathcal{P}$, with an arbitrary BLER (see Table C.4), is obtained by means of a non-decreasing function ($\Lambda(\cdot)$) of the effective SINR (ψ_{eff})

as follows:

$$\Theta_{\mathcal{P}} = \Lambda\left(\psi_{\text{eff}}\right). \tag{4.5}$$

LTE subbands and bandwidth parts

Before describing the CSI feedback schemes in LTE, two LTE definitions/notations are required:

- *Subbands*: The system bandwidth, composed of $N_{\text{RB}}^{\text{DL}}$ RBs, is divided into N_{SB} subbands, where $\lfloor N_{\text{RB}}^{\text{DL}}/k \rfloor$ subbands are of size k and one is of size $N_{\text{RB}}^{\text{DL}} - k \cdot \lfloor N_{\text{RB}}^{\text{DL}}/k \rfloor$. The subband size ($k$) depends on the system bandwidth ($N_{\text{RB}}^{\text{DL}}$) as it is specified in [162] and it is shown in Table C.5. Thus, $\mathcal{P}_s$ represents the set of (consecutive) PRBs within the s^{th} subband.

- *Bandwidth parts*: N_{J} consecutive subbands in a total of J bandwidth parts span the system bandwidth. The value of J also depends on $N_{\text{RB}}^{\text{DL}}$ as it is specified in [162] and it is shown in Table C.6. For $J > 1$, $N_{\text{J}} = \lceil N_{\text{RB}}^{\text{DL}}/k/J \rceil$ or $N_{\text{J}} = \lceil N_{\text{RB}}^{\text{DL}}/k/J \rceil - 1$ depending on the values of $N_{\text{RB}}^{\text{DL}}$, k, and J. In this manner, $\mathcal{P}_{i,j}$ represents the i^{th} subband within the j^{th} bandwidth part, where $i \in \{1,\ 2,\ \ldots,\ N_{\text{J}}\}$ and $j \in \{1,\ 2,\ \ldots,\ \text{J}\}$.

The different CSI feedback schemes available in LTE are explained in the following points. Please note that Δ and δ are the CQI-based CSI report content and uplink signaling overhead associated to each scheme, respectively.

4.2.2 Aperiodic CSI feedback schemes in LTE

- *Wideband feedback* (LTE-WB). The UE reports one wideband CQI (Θ_{WB}), i.e., a value indicating the average channel quality observed in the whole system bandwidth. To compute this metric, all the CS-RS must be considered in the CQI estimation process: from (4.1) to (4.5).

$$\begin{aligned} \Delta_{\text{LTE-WB}} &= \Theta_{\text{WB}}, & (4.6)\\ \delta_{\text{LTE-WB}} &= 4 \text{ [bits per report]}. & (4.7) \end{aligned}$$

- *Cell-configured subband feedback* (LTE-HLC)[2]. One single *differential* CQI value is reported for each subband within the whole system bandwidth. A 2 bits differentially encoded CQI, with respect to the wideband CQI (Θ_{WB}), is used as defined in [162] and it is shown in Table C.8.

$$\begin{aligned} \Delta_{\text{LTE-HLC}} &= \{\, \Theta_{\text{WB}},\, \vec{\boldsymbol{\Theta}} \in \mathbb{N}^{N_{\text{SB}}} \,\}, & (4.8)\\ \delta_{\text{LTE-HLC}} &= 4 + 2 \cdot N_{\text{SB}} \text{ [bits per report]}. & (4.9) \end{aligned}$$

[2]The suffix 'HLC' stands for higher layers configured.

- *UE-selected subband feedback* (LTE-USa)[3]. The UE reports one differential CQI value reflecting the channel quality over the best M subbands. The position of such M subbands is reported using a combinatorial index (w) composed of x bits. The wideband CQI (Θ_{WB}) is also reported. The differential encoding uses 2 bits as it is defined in [162] and it is shown in Table C.9.

$$\Delta_{\text{LTE-USa}} = \{\, \Theta_{\text{WB}},\, w,\, \vec{\boldsymbol{\Theta}} \in \mathbb{R}^M \,\}, \tag{4.10}$$

$$\delta_{\text{LTE-USa}} = 4 + x + 2 \text{ [bits per report]}, \tag{4.11}$$

$$x = \left\lceil \log_2 \left(\begin{array}{c} N_{\text{SB}} \\ M \end{array} \right) \right\rceil. \tag{4.12}$$

4.2.3 Periodic CSI feedback schemes in LTE

- *Wideband feedback* (LTE-WB). See wideband feedback in aperiodic mode.
- *UE-selected subband feedback* (LTE-USp). The UE selects the single subband with the best CQI out of N_{J} subbands of the j^{th} bandwidth part, and then, it feeds back the corresponding CQI together with a label (w) of x bits to identify the best subband within the current bandwidth part. The reporting period is $N_{\text{p}} \in \{\, 2,\, 5,\, 10,\, 16,\, 20,\, 32,\, 40,\, 64,\, 80,\, 128,\, 160 \,\}$ ms. The index j of the bandwidth part does not need to be fed back since the cell can compute it directly by means of an internal counter N_{SF} as follows: $j = \text{mod}(N_{\text{SF}}, J)$. The size of the label is given by $x = \lceil \log_2(\lceil N_{\text{RB}}^{\text{DL}}/k/J \rceil) \rceil$).

  It is worth saying that with this approach, there is a high risk of having outdated CSI if the reporting frequency is larger than the coherence time of the channel [9]. Moreover, CQI is encoded differentially using 3 bits with respect to the wideband CQI that is measured every $H \cdot N_{\text{p}}$ ms, where $H = J + 1$. The differential encoding is defined in [162] and it is shown in Table C.9.

$$\Delta_{\text{LTE-USp}}(t) = \Theta_{\mathcal{P}^*} + w, \tag{4.13}$$

$$j = t \bmod (J+1), \tag{4.14}$$

$$\mathcal{P}^* = \begin{cases} \underset{\mathcal{P}_{i,j}}{\text{argmax}}\ \psi_{\text{eff}} \quad \forall i, & j \neq 0, \\ \Theta_{\text{WB}}, & j = 0, \end{cases} \tag{4.15}$$

$$\delta_{\text{LTE-USp}} = 4 + x, \text{ or } 2 \text{ [bits per report]}. \tag{4.16}$$

4.2.4 Problem Statement

As it has been shown, both periodic and aperiodic CSI feedback are coded differentially with respect to the wideband CQI (Θ_{WB}). Note that the highest granularity that can be reported is at subband level, which is a set of contiguous PRBs, and as it was indicated, the subband size depends on the system bandwidth ($N_{\text{RB}}^{\text{DL}}$).

[3]The scheme LTE UE-selected subband feedback can operate both in periodic and aperiodic mode with minor differences. To make the distinction explict, the letters 'p' and 'a' have been used as suffixes.

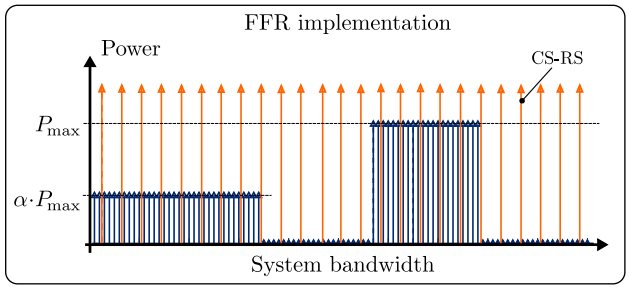

Figure 4.1: Wideband CQI estimation issue.

Both differential encoding and subband reporting are needed to reduce the uplink CSI feedback overhead. Thus, given that 1) Θ_{WB} is computed by considering all the CS-RSs in the system bandwidth, and 2) the resource allocation used in SFR and FFR assigns different power levels (or even no power) to different portions of the system bandwidth, it is clear that Θ_{WB} only provides a very rough estimate of the actual average radio channel quality from the perspective of each class of users ($\mathcal{E}$ or $\mathcal{I}$). Since subband CQIs are differentially encoded with respect to this figure, when static ICIC is applied, Θ_{WB} will be under- and over- estimated for exterior ($\mathcal{E}$) and interior ($\mathcal{I}$) users, respectively. The situation is illustrated in Figure 4.1 for the case of FFR.

The situation previously described results in suboptimal performance of the LTE CSI feedback schemes, and consequently, additional measures need to be taken to alleviate this issue. Before presenting the proposed CSI reporting schemes, a survey of related works is provided.

4.3 Related Work

The literature about CSI feedback in LTE is extensive since it is 1) a very important aspect affecting the performance of wireless systems [180], and 2) especially useful in case of multicarrier based access methods such as OFDMA [181]. This section provides an overview of important works about CSI feedback.

4.3.1 Work within the 3GPP

The work related to CSI feedback is mainly discussed in the meetings of the Technical Specification Group (TSG) Radio Access Network (RAN), specifically by the Working Group 1 (WG1). During the final phase of the standardization of LTE (2007 and 2008), discussions and proposals about CSI feedback were mainly focused on CQI definition, measurement, and reporting methodologies [182–187]. From the very beginning, especial emphasis was placed on the amount of uplink signaling overhead and the overall complexity involved in the different reporting mechanisms. Subsequent

discussions addressed other important aspects such as overhead analysis, feedback compression, CQI computation, and the interplay with retransmissions [188–191].

With the advent of LTE-A, during 2010 and 2011, discussions on aperiodic reporting schemes and their adaptation to new features such as CA and eICIC have also taken place [192–198]. More recently, as CoMP [34] has become a very active research field, further improvements are being discussed in that direction as well [199–202].

4.3.2 Contributions from the Research Community

According to [203], CSI feedback is an element that needs to be taken into greater consideration when wireless systems are investigated. However, the way in which this is done is rather diverse and, in general, it depends on the research objectives in each case. Bearing this in mind, it is possible to distinguish the following groups:

- *Group 1*: works implementing existing reporting mechanisms as a complementary functionality to study other aspects, rather than CSI feedback, such as ICIC or scheduling.
- *Group 2*: studies presenting performance evaluation and/or analysis of one or more existing feedback schemes either analytically or by means of system level simulations.
- *Group 3*: contributions introducing new reporting strategies.

Group 1: Modeling CSI Feedback

One common assumption found in the literature is considering full and perfect channel knowledge both in frequency and time domain. In the frequency domain, this implies that channel quality information is available with an arbitrary small resolution, i.e., at subcarrier level, at PRB level, or in groups of PRBs. In the time domain, full knowledge implies that channel measurements are available instantaneously to the transmitter. Perfect knowledge implies that channel quality estimations are done without errors, which is rather arguable in practical systems. In addition, it is worth noting that the performance of several RRM algorithms relying on such detailed CSI could be significantly different if erroneous or delayed channel estimations are considered.

An interesting example is [107], where the authors proposed a set of interference avoidance schemes for the particular case of light load conditions. In this study, channel information was available for each PRB (full knowledge in the frequency domain), but 2 ms reporting delay was assumed (partial knowledge in the time domain). Measurement error was also introduced through a log-normal random variable, thus imperfect knowledge was assumed. Channel quality information was represented by means of SINR levels with 1 dB resolution to emulate the discrete nature of realistic reporting schemes such as the ones in LTE. This way, the assumptions are perfectly

valid for the context of the study since small variations on them would not affect the conclusions qualitatively speaking. The work eventually shows the importance of an accurate and realistic CSI feedback modeling.

Group 2: Performance Analysis of CSI Feedback Strategies

Although analytical treatment is in general advisable, evaluating analytically the performance of CSI feedback schemes in the context of cellular networks requires incurring in analytical approximations and modeling simplifications, as it has been pointed out in [203]. In [203], closed-form expressions measuring the merit of different reporting schemes available in LTE were obtained. Nevertheless, Donthi and Mehta remarked 1) the complementary nature of their work with respect to the need for detailed/accurate system level simulations, and 2) the fact that their findings should be understood as independent theoretical references that can provide additional insights to system design and optimization. Additional aspects such as the impact of estimation errors were identified as open issues. Given this, the study presented in this chapter addresses these and other related issues by means of detailed system level simulations. Other interesting analytical performance assessments have been presented recently in [204, 205], although for more generic CSI feedback mechanisms and OFDMA settings.

Group 3: Previous Proposals

One of the first practical CSI feedback schemes was proposed by Su et al. in [206]. Their reporting scheme is mainly based on two ideas: first, reporting CQIs only for subbands featuring the best channel conditions, and second, using a hierarchical structure to divide the system bandwidth into levels with different granularities. According to [207], where this structure was initially introduced, by iterating through these levels, it is possible to roughly estimate a fading profile of the whole bandwidth. However, this would require certain reporting periodicity that indeed does not exist for several types of services.

Another practical approach was proposed in [81]. In this work, the authors employed a Modified Top-M scheme, in which, UE only feedbacks the average channel quality of the best M subbands. However, in this scheme the value of M depends on traffic load and type. When system load increases, the value of M is decreased in order to keep the uplink overhead mostly constant.

The previous works realistically deal with the LTE specifications and its constraints, however, the vast majority of works about CSI with limited feedback are proposals mainly oriented to generic OFDMA systems, whose LTE-feasibility would require important changes in the system design. In practice, new proposals must be, as far as possible, in compliance with the standards. Moreover, no previous proposal has addressed ICIC aspects explicitly.

A brief overview of other recent generic works (that are not compatible with LTE) are also presented. The work in [208] identifies interesting aspects of the CSI

feedback problem: the need for efficient low-rate strategies and the question on how accurate CSI should be transmitted to achieve near optimum performances. Nevertheless, a pitfall of the system model in [208] is that it only considers one single access point, and hence, the random nature of ICI is not taken into account.

The contribution in [209] extended the analysis presented in [208] to OFDMA. This work is important because it introduces a feedback scheme that allocates feedback resources depending on the status of buffers and channel conditions. However, the model used in this study assumes that the transmissions are always done with the same format, and that the number of required subbands per user is constant. These assumptions are hardly justified for complex multiservice modern cellular systems.

Recently, a joint feedback-scheduling scheme, similar to [209], was proposed in [210]. The authors also highlighted the importance of considering the impact of CSI feedback on the performance of queuing systems with realistic traffic models. Other feedback schemes providing partial CSI for the downlink of generic OFDMA systems include [211–213].

In order to provide a comparative perspective, Table 4.1 shows a summary of these contributions highlighting the following aspects:

- ✓ *CSI estimation errors*. Given that channel quality measurements are based on CS-RS, CSI is partial. In addition, this information is subject to other sources of error such as delay processing, quantization, and measurement impairments.
- ✓ *LTE feasibility*. Any CSI feedback proposal must be, as far as possible, in compliance with the technical specifications, meaning that only minor changes would be required for implementation.
- ✓ *Uplink capacity*. As mentioned before, the limited capacity of uplink feedback channels is an important practical constraint in real systems.
- ✓ *Overhead analysis*. Given the previous point, the required uplink overhead is an indicator that must be considered as a performance metric.
- ✓ *Realistic traffic*. Aperiodic feedback schemes are especially useful for NRT traffic patterns, where CSI is more likely to be requested on-demand. Considering realistic traffic patterns is required to consistently evaluate the performance and merit of CSI reporting schemes.
- ✓ *System model*. This aspect is particularly important in the context of interference limited systems. If only one access point is considered, radio channel quality can only be expressed in terms of SNR, instead of SINR, and therefore, the inherent randomness of intercell interference cannot be taken into account.
- ✓ *ICIC aspects*. As it was shown, the resource allocation pattern in static ICIC techniques can have a significant effect on the performance of the CSI feedback schemes. Hence, it is important to highlight this aspect within this survey.

From Table 4.1, it can be seen that no ICIC-oriented CSI feedback scheme has been investigated so far. In addition, the lack of a realistic performance assessment considering a multi-cell system, in which ICI and CSI can be jointly modeled is

Table 4.1: Summary of CSI feedback proposals and contributions

Ref.	CSI errors	LTE feasibility	Uplink capacity	Overhead analysis	Realistic traffic	Model	ICIC
[81]	✓	✓	✓	×	✓	Multi-cell	×
[206]	×	✓	✓	✓	×	Multi-cell	×
[208]	×	×	✓	✓	×	Single-cell	×
[209]	×	×	✓	×	✓	Single-cell	×
[210]	×	×	✓	✓	✓	Single-cell	×
[214]	×	×	×	×	✓	Single-cell	×
[212]	×	×	✓	✓	×	Single-cell	×
[211]	×	×	✓	×	×	Single-cell	×
[213]	×	×	×	✓	×	Single-cell	×

notorious. A fair performance assessment must take all the aspects shown in Table 4.1 into account. Thus, the main novelties presented in this chapter can be summarized as follows:

1. The introduction of periodic and aperiodic CSI feedback schemes for LTE aiming at optimizing both user QoS and system performance when static ICIC is considered. This is done by employing realistic traffic patterns and an independent QoS oriented scheduling policy.

2. The proposed schemes incorporate all the aspects shown in Table 4.1. The channel quality definition and SINR measurements are done according to the LTE specifications, i.e., CSI is based on CQI reports obtained by means of SINR values of CS-RS, and subject to delay and estimation errors.

3. Additional notorious aspects include:

   - The performance of the proposed CSI feedback schemes has been evaluated by considering both FFR and SFR.
   - The impact of the novel strategies on user satisfaction ratio has been analyzed by means of the joint system capacity notion [215], which provides good insights into the actual impact on the QoS.

4.4 Description of the Proposed Schemes

In this section, a description of the proposed CSI feedback schemes is provided. As it was explained, two fundamental aspects of the design of CSI feedbacks schemes in LTE are 1) the wideband CQI (Θ_{WB}) is computed by each UE taking into account the whole system bandwidth, and 2) the CQI of different subbands (see Table C.4) is encoded differentially with respect to Θ_{WB} (see Tables C.8 and C.9). Recall that

the differential encoding aims at reducing the amount of CSI feedback overhead in the uplink.

Nevertheless, despite this design is effective in the vast majority of cases, it is counter-productive if static ICIC is employed. This is because the estimation of the wideband CQI (Θ_{WB}) takes into account parts of the system bandwidth in which the user will not be allocated due to 1) the resource allocation pattern of SFR and FFR, and 2) the current classification of the user (either $\mathcal{E}$ or $\mathcal{I}$). Even worse is the fact that the channel quality in those subbands changes significantly as a result of the variation of the reuse factor and power level.

In this manner, the design of the CSI feedback schemes presented herein relies on **refining the estimation of $\Theta_{\mathbf{WB}}$**. This can be done by focusing the computation of this figure only on the subbands assigned to the class ($\mathcal{E}$ or $\mathcal{I}$) each UE belongs to. This has another advantage, the estimation of Θ_{WB} is simpler (it requires less processing) because the user equipment does not have to sweep the whole system bandwidth.

Given that for the vast majority of scenarios, Θ_{WB} does not change significantly over time, it can be fedback every few seconds, i.e., at a very low frequency from the CSI feedback point of view. In any case, the update interval of Θ_{WB} can be adjusted conveniently by higher layers (RRC protocols) and it can be combined with the classic Θ_{WB} definition to let the proposed schemes to be aware of potential classification changes (from $\mathcal{E}$ to $\mathcal{I}$ or vice versa).

The operation of the proposed schemes is explained next.

4.4.1 Periodic CSI feedback for static ICIC: ICIC-SEQ

The operation of the proposed periodic scheme (ICIC-SEQ)[4] is illustrated in Figure 4.2 for the case of SFR. The operation is exactly the same for FFR.

The approach requires transmitting a very small amount of information in the downlink (Step 1 in Figure 4.2), the vector $\mathbf{m}$ that indicates the subbands in which the user can be allocated in virtue of the class it belongs to ($\mathcal{E}$ or $\mathcal{I}$). The size of the vector is $\lceil N_{\mathrm{RB}}^{\mathrm{DL}}/k \rceil$ bits, where k depends on the system bandwidth ($N_{\mathrm{RB}}^{\mathrm{DL}}$) as it is indicated in Table C.5. Note that the worst case, $N_{\mathrm{RB}}^{\mathrm{DL}} = 110$, gives $|\mathbf{m}| = 14$ bits. In any case, this information only needs to be transmitted once, unless the user changes its classification which typically either does not happen during the session time or it happens only a few times[5]

Having the vector $\mathbf{m}$, the UE focuses the estimation of the wideband CQI (Θ_{WB}) on the subbands of interest (Step 2 in Figure 4.2), for which, it is required less processing than in the normal case. Then, at every CSI feedback interval[6], the UE

[4]The suffix 'SEQ' stands for sequential.

[5]Assuming a very pessimistic case in which a user changes its classification every 20 s, the required downlink overhead is, again in the worst case ($N_{\mathrm{RB}}^{\mathrm{DL}} = 110$), equal to $14/20 = 0.70$ bps.

[6]In periodic CSI feedback, the feedback interval is transmitted to the user by means of user-specific signaling.

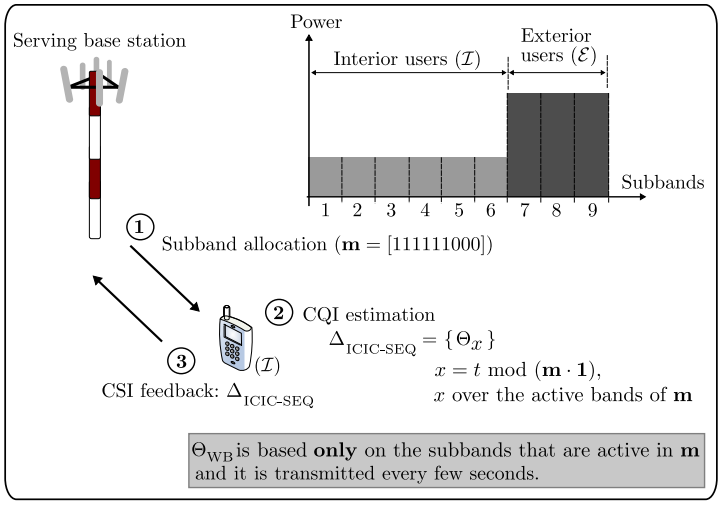

Figure 4.2: Description of the proposed periodic scheme: ICIC-SEQ.

feedbacks sequentially the CQIs of the subbands indicated by $\mathbf{m}$. In particular, it transmits one differentially encoded CQI to its serving base station (Step 3 in Figure 4.2). In this manner, the proposed scheme accomplishes the design targets: improving the accuracy of the CSI, while keeping both computational effort and uplink overhead to minima.

The CQI-based CSI report content (Δ) and uplink signaling overhead (δ) associated to the proposed mechanism are indicated next:

$$\Delta_{\text{ICIC-SEQ}}(t) = \Theta_i \quad (i \text{ over the active subbands in } \mathbf{m}), \tag{4.17}$$

$$i = t \bmod (|\mathbf{m} \cdot \mathbf{1}|), \tag{4.18}$$

$$\delta_{\text{ICIC-SEQ}} = 2 \text{ [bits per report]}. \tag{4.19}$$

4.4.2 Aperiodic CSI feedback for static ICIC: ICIC-LOC

The operation of the proposed aperiodic scheme (ICIC-LOC)[7] is illustrated in Figure 4.3 for the case of SFR. The operation is exactly the same for FFR.

The operation is similar to the periodic scheme ICIC-SEQ. The information that is transmitted by the serving base station (Step 1 in Figure 4.3) in the downlink is exactly the same as in ICIC-SEQ, i.e., a vector $\mathbf{m}$ indicating the subbands in which the user will be allocated in virtue of the class it belongs to ($\mathcal{E}$ or $\mathcal{I}$).

However, there are some differences. When aperiodic feedback is required over the PUSCH (Step 2 in Figure 4.3), the UE computes and feedbacks (Steps 3 and 4 in Figure 4.3), based on the vector $\mathbf{m}$, the wideband CQI (Θ_{WB}), plus one differentially encoded CQI for the subbands marked with '1' in $\mathbf{m}$. Note that similarly to the

[7] The suffix 'LOC' stands for localized.

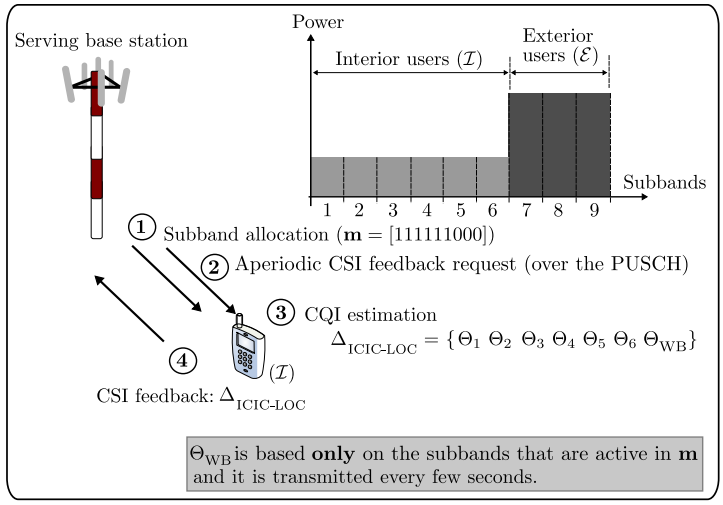

Figure 4.3: Description of the proposed aperiodic scheme: ICIC-LOC.

schemes defined for LTE, aperiodic feedback provides more precise CSI. Thus, the proposed scheme improves the accuracy of such information by focusing exclusively on the subbands of interest for each user.

The CQI-based CSI report content (Δ) and uplink signaling overhead (δ) associated to the proposed mechanism are indicated next:

$$\Delta_{\text{ICIC-LOC}} = \Theta_{\text{WB}} + \Theta_i \quad \text{(For all index } i \text{ marked as '1' in } \mathbf{m}\text{)}, \tag{4.20}$$

$$\delta_{\text{ICIC-LOC}} = 4 + [2 \times (\mathbf{m} \cdot \mathbf{1})] \text{ [bits per report]}. \tag{4.21}$$

4.5 System Model

In order to investigate the impact of the CSI feedback schemes previously introduced on system performance, the downlink of an LTE network was considered. The interworking considered for this study between different network functionalities such as CSI feedback, scheduling, and HARQ is illustrated in Figure 4.4. As it can be seen, the scheduler allocates radio resources and shapes future transmissions to different users taking into account the resource allocation pattern of the static ICIC scheme, the status of the buffers, and several operator-defined policies. However, as the figure suggests, the focus is placed on the role of the CSI feedback scheme, while the rest of functionalities are kept fixed.

In this study, QoS is measured in terms of the number of *satisfied* users. A user is said to be satisfied, if it mets a certain service-dependent criterion. In this manner, in order to provide a quite realistic perspective of the merit of the proposed schemes, different services have been considered. For the service s, the user satisfaction ratio

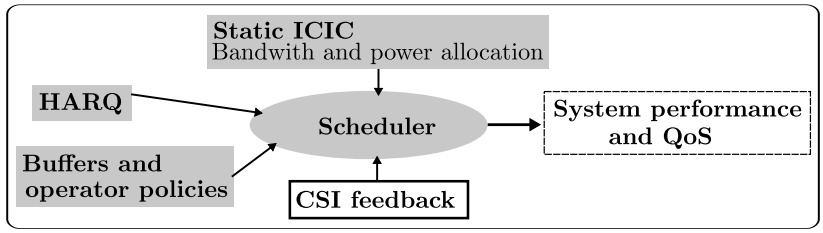

Figure 4.4: System interworking used to study the impact of CSI feedback.

(Q_s) is given by:

$$Q_s = \hat{\mu}_s / \mu_s, \tag{4.22}$$

where μ_s is the number of users of the service s, and $\hat{\mu}_s$ is the number of satisfied users in the service s. In this work, it has been considered both RT and NRT services in single-service scenarios, i.e., scenarios in which all the users employ the same application, and hence, the subindex s is omitted for the sake of clarity.

The traffic models used in this study are VoIP, FTP, and HTTP. They are defined in Appendix B, Section B.2.

The MAC scheduler allocates radio resources in such a way as to satisfy QoS requirements and to optimize system performance. However, despite its importance, the design of the MAC scheduler is not specified within the LTE specifications. As different schedulers may result in significantly different levels of user satisfaction and system performance, mobile operators implement vendor-specific solutions according to their needs. In this study, the scheduler implementation corresponds to the Capacity-driven Resource Allocation (CRA) scheduler proposed in [215]. The CRA scheduler dynamically controls the resource sharing among flows of different services such as delay-sensitive and rate demanding ones. The authors in [215] claim that the CRA scheduler improves the *joint system capacity* [216], defined as the maximum total offered load in which all provided services fulfill a certain user satisfaction ratio. In case of NRT services such as HTTP and FTP, a user is said to be satisfied if a target bit rate (r_{T}) is met. In case of RT services such as VoIP, a user is said to be satisfied if the BLER is below a certain threshold. Other parameters such as delay and jitter are indirectly considered due to the operation of the CRA scheduler.

Thus, the joint system capacity concept fits perfectly the research objectives of this study since it captures all the relevant aspects of multiservice environments such as per-service QoS requirements, while it allows to assess how different CSI feedback schemes affect the QoS provisioning. In addition, it is worth saying that the CRA scheduler by itself does not apply any restriction to users based on classes ($\mathcal{E}$ or $\mathcal{I}$), i.e., such constraints come from the static ICIC policy, which determines the resources assigned to each class of users at each cell.

4.6 Performance evaluation

In order to obtain accurate and realistic performance figures, this study is conducted by means of detailed LTE-based system level simulations. This approach allows taking into account all the elements affecting the performance of CSI feedback schemes such as realistic ICI, fading effects, estimation errors, and processing delay. In addition, more insights can be obtained about the actual impact of the feedback mechanisms previously described on the QoS experienced by users.

The simulation conditions are the ones described in Subsection 3.4.2 with minor differences. Such details are indicated next. Experiments were also conducted by means of Monte Carlo simulations and the results were obtained from 500 independent experiments with uniform randomly spread users. Each experiment simulates 60 s (6×10^4 TTIs) to account with traffic features and let enough time to the scheduler to converge to a stable regime. The test case is the scenario 'Synthetic' described in Appendix B, Section B.1.

Channel model and users mobility deserve especial attention because the these elements have an important influence on the performance of CSI feedback mechanisms, and hence, on the results and conclusions. The mobility model is vehicular for urban scenarios as defined in [173]. In order to emulate low/moderate conditions, pedestrian speed of 3 km/h was assumed. The channel model is the Extended ITU Pedestrian B defined in [178], which features a 32.55 ns sampling grid that matches the LTE sampling rate of 30.72 MHz. Additional implementation details and parameters used in numerical evaluations are shown in Tables 4.2 and B.2.

4.6.1 Benchmarks

The performance of the proposed periodic scheme (ICIC-SEQ) is compared with the native CSI feedback schemes in LTE, i.e., UE-selected subband feedback (LTE-USp) and Wideband feedback (LTE-WB).

The performance of the proposed aperiodic scheme (ICIC-LOC) is also compared with LTE schemes, i.e., Wideband feedback (LTE-WB), Cell-configured subband feedback (LTE-HLC), and UE-selected subband feedback (LTE-USa). In addition, two additional aperiodic reporting mechanisms previously proposed have been also included as benchmarks. The hierarchical selective (HI-SEL) scheme presented in [206], and the modified Top-M reporting mechanism (MOD-TOPM) introduced in [81].

Moreover, in order to obtain a sort of optimality gap in each case, an ideal reporting scheme (IDEAL), where one CQI is fedback for each RB is also considered both for periodic and aperiodic CSI feedback. The remaining benchmarks are described next.

Table 4.2: Simulation Parameters and Evaluation Setting.

Parameter	Value/assumption
Test cases (scenarios)	'Synthetic', 'MORANS' (see Section B.1).
System bandwidth (B)	18 MHz.
User distribution	Random/uniform.
Scheduler	CRA [215].
Mobility model	Urban vehicular [173].
PDCCH Capacity	8 scheduling grants per TTI.
CSI processing delay	3 TTIs.
CS-RS power boost	0 dB.
Resource allocation	Type 1 [162].
Link Abstraction	Mutual Information Equivalent SINR Mapping [174].
Transmission mode	Single-antenna port.
Services	VoIP, HTTP, and FTP. (see Section B.2).
Target BLER: VoIP	$\leq 1\%$.
Target rate (r_{T}): HTTP	$\geq$600 kbps.
Target rate (r_{T}): FTP	$\geq$400 kbps.
Periodic reporting interval	5 TTIs.
Aperiodic reporting interval	$\geq$5 TTIs.
SFR setting	$\alpha = 0.40$, $\beta = 0.33$, and $\psi_{\mathrm{TH}} = 1.00$ dB.
FFR setting	$\alpha = 0.40$, $\beta = 0.40$, and $\psi_{\mathrm{TH}} = 1.00$ dB.

Ideal CSI feedback: IDEAL

In this scheme, one perfectly estimated (without error) CQI is fedback and instantaneously known for each RB. The CQI-based CSI report content (Δ) and uplink signaling overhead (δ) associated to this scheme are indicated next:

$$\Delta_{\mathrm{IDEAL}} = \Theta_i \quad (i = 1, , 2, \cdots, N_{\mathrm{RB}}^{\mathrm{DL}}), \tag{4.23}$$

$$\delta_{\mathrm{IDEAL}} = 4 \times N_{\mathrm{RB}}^{\mathrm{DL}} \text{ [bits per report]}. \tag{4.24}$$

Hierarchical selective CSI feedback: HI-SEL

In this scheme, proposed in [206], the system bandwidth is divided into different levels with different granularities. For $N_{\mathrm{RB}}^{\mathrm{DL}} = 100$ (the case of study herein), the implementation defines 5 levels. The number of subbands in the l^{th} level (N_{SB}^{l}) is: 1, 2, 4, 20, and 100, for $l = 1, 2, 3, 4$, and 5, respectively. Correspondingly, the subband size (S^l) and the number of suboptimal subbands (q^l) in the level l is 100, 50, 25, 5, and 1, and 0, 1, 2, 3, and 4, respectively. Note that the notion of subband in the context of this strategy is not the same as in LTE, and hence, the size of each of them depends on both the hierarchical level and the system bandwidth. The algorithm transmits, for each level, a CQI value for the best subband together with another CQI representing the average quality in the next q best subbands (the suboptimal subbands). In addition to the pair of CQIs, the positioning of the

best and suboptimal subbands at each level must be indicated to the network by means of a combinatorial index (w) composed of x bits. The CQI-based CSI report content (Δ) and uplink signaling overhead (δ) associated to this mechanism are indicated next:

$$\Delta_{\text{HI-SEL}} = \{\Theta_{\text{Best}},\, \Theta_q,\, w\}, \tag{4.25}$$

$$\delta_{\text{HI-SEL}} = 4 + 4 + x \text{ [bits]}, \tag{4.26}$$

$$x = \left\lceil \log_2 \left(\sum_{l=2}^{5} \left(\binom{N_{\text{SB}}^l}{1} \cdot \binom{N_{\text{SB}}^l - 1}{q^l} \right) \right) \right\rceil. \tag{4.27}$$

Modified TOP-M CSI feedback: MOD-TOPM

This scheme was proposed in [81] and it operates similarly to LTE-USa with some differences. The UE reports a 4-bit CQI representing the average quality observed within the best M subbands. Thus, instead of using differential encoding, 4-bit CQIs are employed, and so, wideband CQI is not required. However, the value of M is adjusted depending on the load (the number of users at each cell). The positioning of the best M subbands must be informed to the transmitter by means of a combinatorial index w composed of x bits. The CQI-based CSI report content (Δ) and uplink signaling overhead (δ) associated to this mechanism are indicated next:

$$\Delta_{\text{MOD-TOPM}} = \{\Theta_{\text{BestM}},\, w\}, \tag{4.28}$$

$$\delta_{\text{MOD-TOPM}} = 4 + x \text{ [bits]}, \tag{4.29}$$

$$x = \left\lceil \log_2 \binom{N_{\text{SB}}}{M} \right\rceil. \tag{4.30}$$

4.6.2 Numerical Results

The impact of the CSI feedback schemes on the overall user satisfaction ratio is shown in Figure 4.5 for the periodic CSI feedback strategies.

Figures 4.5a and 4.5b show the impact of the periodic CSI feedback schemes on the satisfaction ratio for VoIP users when SFR and FFR are applied, respectively. The figures indicate the resulting satisfaction ratio for different cell loads. As it can be seen, the amount of satisfied users (the ones with BLER $< 1\%$) is quite similar in both static ICIC schemes (SFR and FFR). Actually, for low load conditions, FFR tends to improve the system capacity (especially for LTE-WB and LTE-USp) due to the higher levels of SINR that are obtained by means of this strategy. In terms of the VoIP capacity, ICIC-SEQ outperforms both LTE-WB and LTE-USp in a range that varies from 3% to 12%. These gains represent (on average) between 6 and 40 more satisfied VoIP users per cell. The figures also show the performance of the scheme IDEAL, which can be regarded as an upper bound from the performance point of view. Recall that this scheme is unfeasible for practical systems due to the extremely high amount of overhead in the uplink and the computational cost at UE

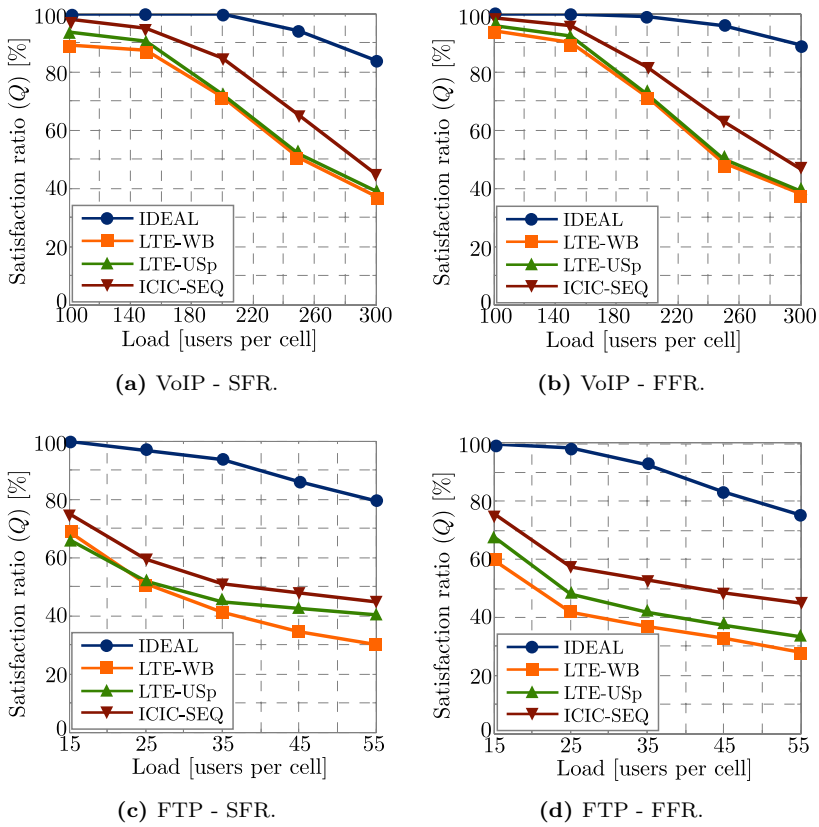

(a) VoIP - SFR. **(b)** VoIP - FFR.

(c) FTP - SFR. **(d)** FTP - FFR.

Figure 4.5: Impact of periodic CSI feedback schemes on QoS.

side. As it was mentioned before, this scheme was included in order to provide a perspective of the optimality gap between practical schemes and the ideal case.

Figures 4.5c and 4.5d show the users satisfaction ratio in the FTP scenario for different cell loads. Focusing first on the ICIC strategies, it can be seen that, in general, the performance of the schemes is similar for both SFR and FFR. Despite that, theoretically, SFR provides higher levels of spectral efficiency. This is due to the fact that the CRA scheduler strictly tries to provide users with the target rate (r_{T}).

Looking at the results from a comparative perspective, the proposed periodic CSI feedback scheme (ICIC-SEQ) clearly improves the QoS provided by the system with respect to the native LTE schemes. The gains in case of SFR range from 5% to 8%, while in case of FFR the improvement goes from 7% to 13% in terms of the number of satisfied users, i.e., users with $r \geq r_{\mathrm{T}}$. Note that the optimality gap (with respect to the scheme IDEAL) ranges from 22% to 35%, but as it was mentioned before, this gain comes at the expense of a prohibitive increase of around $\times 100$ times in the required uplink overhead. A per-scheme overhead analysis is shown later on.

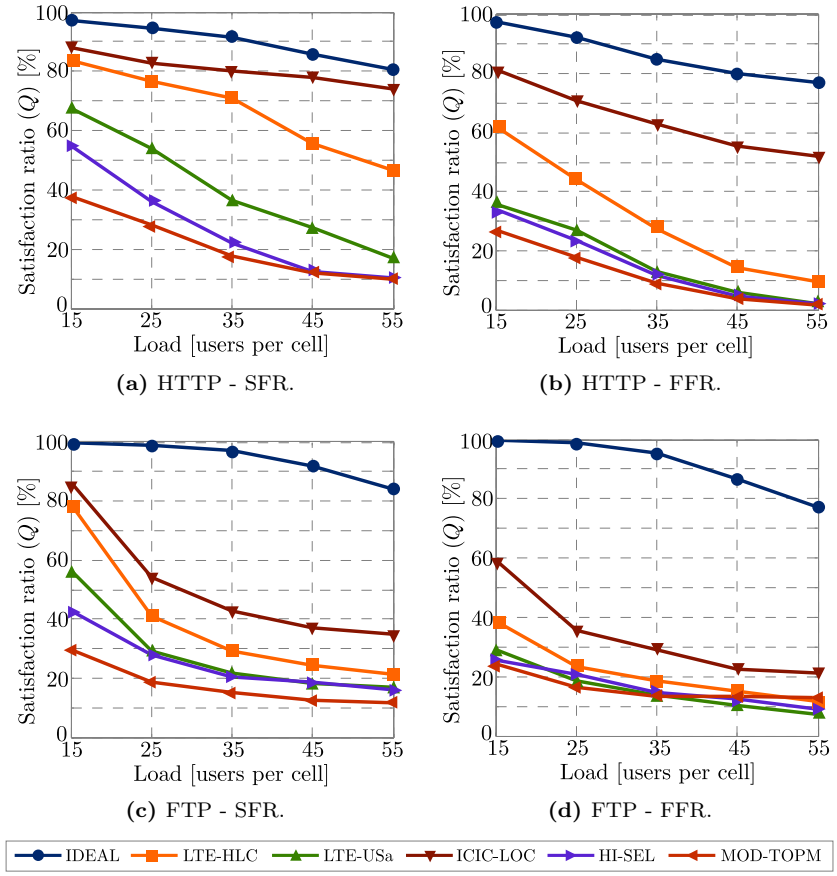

Figure 4.6: Impact of aperiodic CSI feedback schemes on QoS.

Figure 4.6 shows the performance comparison of the aperiodic CSI feedback schemes. Figures 4.6a and 4.6b present the results corresponding to the scenarios with HTTP users. As it can be quickly noticed, the proposed aperiodic CSI feedback scheme (ICIC-LOC) clearly improves the overall QoS with respect to the LTE schemes and existing approaches from the literature. The significant improvement is due to the fact that more accurate wideband CQI estimations in ICIC-LOC allows for a more precise MCS selection. Of particular interest is always the case where the system load is high (45 and more active users per cell). ICIC-LOC provides gains with respect to the closest LTE scheme (LTE-HLC) ranging from 5% to 28% (in case of SFR), and gains from 20% to 45% (in case of FFR). These gains can be explained by the bursty nature of the HTTP traffic that leaves more room for retransmission, from which ICIC-LOC can be especially benefited from. As it will be shown, ICIC-LOC features a less conservative MCS selection than the schemes in LTE, which are more *pessimistic* in that sense. In case of bursty traffic, HARQ can effectively handle the errors resulting of such *aggressive* MCS selection, and hence,

the less conservative (but more accurate) channel estimation in ICIC-LOC results in gains from the QoS point of view.

Figures 4.6d and 4.6d show the results corresponding to the FTP scenarios for SFR and FFR, respectively. In case of FTP traffic, the optimality gap with respect to the case IDEAL is greater meaning that the spectral efficiency loss due to HARQ retransmissions is more pronounced. In any case, the proposed scheme also outperforms all the benchmarks although with smaller gains than in cases of HTTP traffic. The gains range from 5% to 15% in case of SFR, and from 8% to 20% in case of FFR.

It is worth mentioning that in the context of FTP traffic (a model that is similar to the full buffer assumption), the results presented herein confirm and complement the theoretical findings shown in [203], in the sense that LTE-HLC clearly outperforms LTE-USa. The results presented herein confirm that this is also true in the context of static ICIC. However some clarifications need to be remarked. In [203], the comparison was presented in terms of the average throughput subject to 'synthetic' scheduling policies such as greedy and proportional fair that have a clear asymptotic behavior under the full/infinite buffer assumption. The CRA scheduler employed herein is multiservice and QoS oriented [215]. This means that the scheduler, on the one hand, tries to allocate the minimum amount of resources to meet the QoS (target bit rate) of each user, and on the other hand, it tries to maximize the number of satisfied flows meaning that under heavy load conditions it focuses on users more likely to be satisfied, jeopardizing *unlucky* users. For these reasons, the study presented in this chapter is both required and relevant as it extends previous theoretical findings to cases where analytical treatment is impossible, but that have great interest from a practical viewpoint.

The performance of HI-SEL [206] and MOD-TOPM [81] is especially poor in the context of static ICIC (Figure 4.6), being even below of 3GPP baselines. Both HI-SEL and MOD-TOPM showed acceptable performances in [206] and [81], respectively. However, it is worth saying that these strategies were tested under the full frequency reuse assumption, for which they were explicitly designed. Moreover, no comparison with LTE reporting schemes was presented therein, and hence, their relative merit with respect to these important baselines was not clarified. The introduction of static ICIC schemes sketches a completely different picture from the CSI point of view. Indeed, some of the strengths in HI-SEL and MOD-TOPM become important drawbacks in this new scenario. For instance, both HI-SEL and MOD-TOPM just report the best subbands. On the one hand, MOD-TOPM is a variation of LTE-USa without neither wideband CQI nor differential encoding. To some extent, wideband estimates are good in the sense that, as they favor conservative estimations, it makes possible to limit other error sources such as reporting/processing delay. On the other hand, HI-SEL always reports the quality of the best M subbands at each level, but, in static ICIC the bandwidth portion reserved for exterior users receives significantly less ICI, and hence, without an explicit mechanism to deal with this, these subbands are always the ones reported no matter the current UE classification.

Figure 4.7 provides a user-oriented perspective of the performance of the CSI

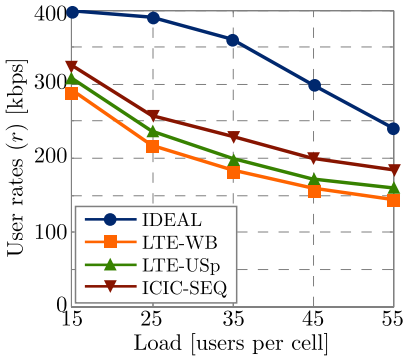

(a) Periodic reporting: r (FTP - FFR).

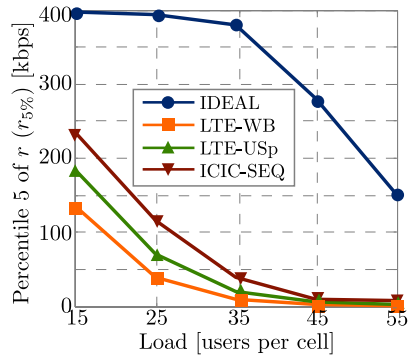

(b) Periodic reporting: $r_{5\%}$ (FTP - FFR).

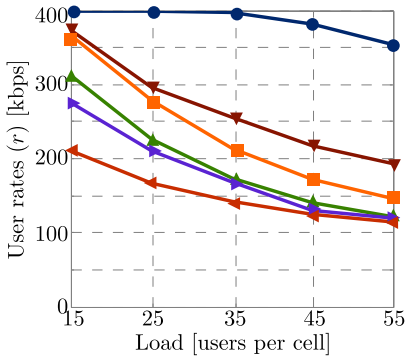

(c) Aperiodic reporting: r (FTP - SFR).

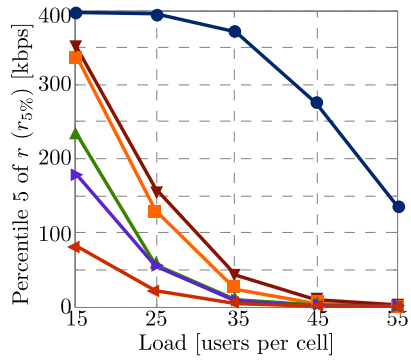

(d) Periodic reporting: $r_{5\%}$ (FTP - SFR).

(e) Legend for aperiodic reporting: (c) and (d).

Figure 4.7: Impact of reporting schemes on users rates and cell edge performance.

feedback schemes. To be precise, Figures 4.7a and 4.7b show the impact of the periodic reporting mechanisms on the average user rates (r) and percentile 5 of r ($r_{5\%}$), respectively, for the scenario FTP/FFR. A similar performance pattern was also found for rest of periodic scenarios. As it can be seen, ICIC-SEQ achieves gains in terms of users rate ranging from 5% to 16%. Given that the overall spectral efficiency is proportional to the average value of r, it can be concluded that ICIC-SEQ also helps to improve the spectral efficiency of the system, which is a consequence of the accurate CSI estimation and its corresponding BLER reduction. Equally important, and even more in the context of ICIC, is the cell edge performance. The results shown in Figure 4.7b clearly indicate that ICIC-SEQ also improves the percentile 5 of r for low to moderate levels of load. For instance, the improvement ranges from 27% (in case of 15 users per cell) to 100% (in case of 35 users per cell). In case of heavy load conditions (45 and 50 users per cell), the gains are significantly reduced due to the fact that under such circumstances, the CRA scheduler tends to block the

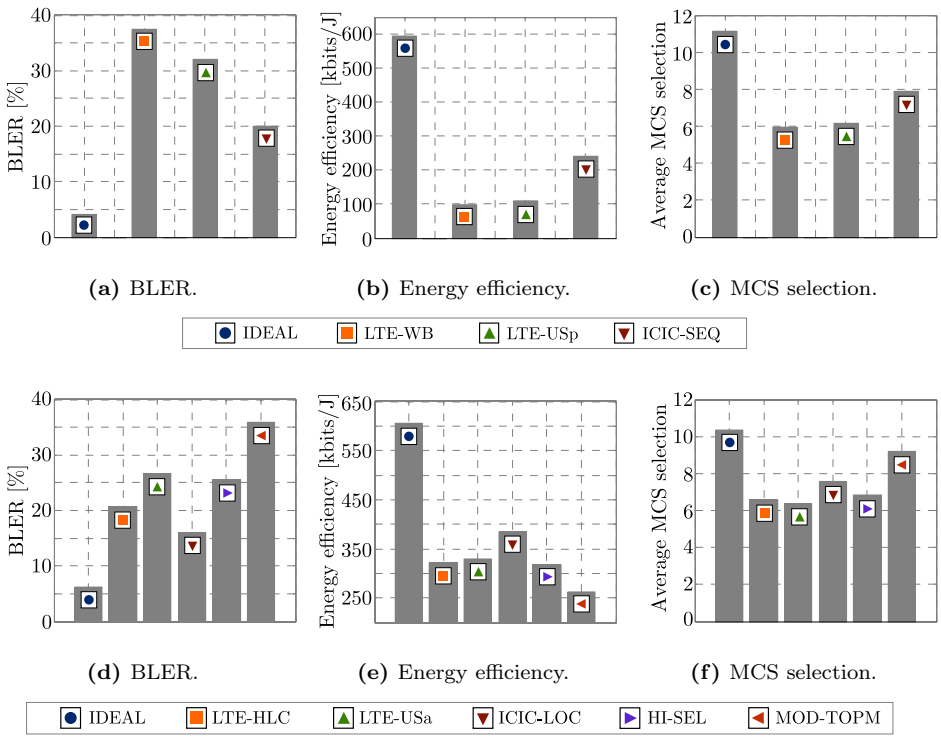

Figure 4.8: Additional performance metrics.

worst users as it has been designed to maximize the number of satisfied connections (users with $r \geq r_{\mathrm{T}}$). However, the level of fairness can be adjusted as in many other scheduling algorithms, in this case, by reducing the overall satisfaction ratio (Q).

The same results are also found for the aperiodic proposal, ICIC-LOC (Figure 4.7) with gains that go up to 33% for r and between 2% and 21% for the percentile 5.

Given the previous paragraphs, it can be stated that ICIC-SEQ and ICIC-LOC are excellent companion for the static ICIC schemes.

Additional performance metrics

In order to provide additional insights, Figure 4.8 shows a comparison among schemes in terms of BLER, energy efficiency, and MCS selection. BLER provides a measure of the accuracy of the CSI provided by each reporting mechanism. The energy efficiency provides an indication of the effectiveness of the transmissions over the air interface. It is defined as the ratio of the total (successfully) transmitted payload and the energy expenditure required to do that. The MCS selection indicates the transmission format that is selected (on average) by the scheduler based on the CSI, thus providing an idea of how conservative the CSI is, i.e., low values of this

Table 4.3: Uplink signaling overhead of CSI feedback schemes.

Periodic Schemes	**Overhead [kbps] (Reporting period: 5 TTIs)**
IDEAL	80.00
LTE-WB	0.50
LTE-USp	1.00
ICIC-SEQ	1.2 (Assuming that Θ_{WB} is always transmitted)
Aperiodic Schemes	**Overhead [bits/report] ($N_{\mathbf{RB}}^{\mathbf{DL}} = 100$)**
IDEAL	400
LTE-HLC	30
LTE-USa	17
ICIC-LOC	20 (SFR), 14 (FFR)
HI-SEL	29
MOD-TOPM	17

figure indicate a more conservative channel quality estimation. The figure shows the comparative for both periodic (Figures 4.8a, 4.8b, and 4.8c) and aperiodic schemes (Figures 4.8d, 4.8e, and 4.8f).

The results indicate that the proposed schemes (ICIC-SEQ and ICIC-LOC) improve the BLER with respect to LTE schemes and previous proposals (Figures 4.8a and 4.8d). This is very important for two main reasons. First, less erroneous transmissions imply less ICI in the system, and hence, less impact on cell edge users as it was shown before. Second, the need for less transmissions also implies that less energy is required to transmit the same amount of information, and thus, energy efficiency can also be enhanced as it can be seen in Figures 4.8b and 4.8e. Finally, Figures 4.8c and 4.8f confirm what it was mentioned before, the more accurate channel state estimation of ICIC-SEQ and ICIC-LOC, which is reflected not only by the lower BLER but also the higher MCS selection.

Uplink overhead and complexity

From the complexity point of view, the proposed schemes require less computational effort at UE side. Recall that in ICIC-SEQ and ICIC-LOC, less subcarriers need to be processed to estimate the wideband CQI (Θ_{WB}).

Regarding the required signaling overhead in the uplink, Table 4.3 shows the comparison. Although the proposed scheme requires a small increment of signaling overhead with respect to LTE schemes, it is affordable since it only represents 0.2 kbps of additional overhead than in LTE-USp, but substantial gains as previously shown. Similarly, the required overhead of ICIC-LOC is fairly in the same order of magnitude as the other options and much lower than IDEAL.

Feasibility in LTE

Finally, some implementation aspects in LTE are discussed. As it was commented before, any proposal must be, as far as possible, standard-compatible, otherwise implementation would be unfeasible. This aspect has been considered in the design of ICIC-SEQ and ICIC-LOC. They do not require additional functionalities at UE level since wideband CQI estimation and differential encoding, both used in LTE, are preserved. Besides, the new feedback solutions can coexist with legacy devices without problems. The only aspect to be considered is the bit stream $\mathbf{m}$, introducing minimal extra overhead as previously quantified. Such information could be transmitted by means of the 'RRC connection reconfiguration' message from the network to UE [217]. Through this control signaling, LTE provides means to send user-specific information associated to their connections. As the amount of information is at most 13 bits, it can be allocated easily in any of the several available optional fields such as the 'pdsch-ConfigDedicated' within the 'radioResourceConfigDedicated' subtree. Indeed, this message is transmitted to users in 'RRC CONNECTED' state, and hence, it fits perfectly the operational principle of ICIC-SEQ and ICIC-LOC.

In the light of the previous discussion, it is clear that ICIC-SEQ and ICIC-LOC can be implemented by vendors in their mobile terminals and base stations without the need for significant changes in their equipment.

4.7 Concluding Remarks

QoS refers to the ability of the network to provide a desired level of service for selected traffic on the network. Typically, service levels are described in terms of throughput, latency, jitter, and packet error rate and these figures are specified for different types or streams of traffic. Designing QoS policies for evolving packet-based applications is a fundamental requirement in modern multiservice cellular systems as QoS impacts directly the Quality of Experience (QoE) of the users. In this chapter, novel periodic and aperiodic CSI feedback schemes have been proposed for LTE.

The solutions have been designed bearing in mind the objectives of the dissertation. Therefore they are suitable to work in conjunction with static ICIC techniques requiring minimal signaling with respect to current LTE mechanisms. The novel strategies allow QoS improvements when static ICIC techniques are introduced.

After describing the operation of ICIC-SEQ and ICIC-LOC, they have been evaluated and compared with 3GPP schemes and several existing proposals. For this purpose, scenarios with different types of traffic have been considered and the main conclusions can be summarized as follows:

- Numerical results indicate the importance of designing CSI feedback considering and adequate interworking with other network functionalities. Both ICIC-SEQ and ICIC-LOC provide significant gains in terms of overall QoS, average user rates, and cell edge performance. Thus, the proposed CSI feedback schemes

are good candidates to work in conjunction with static ICIC strategies and they are suitable for practical implementation in LTE systems.

- The performance of the proposed schemes is especially good with bursty traffic, where retransmissions can be easily allocated. In this sense, the following design guidelines are obtained:
  - In scenarios with FTP (full buffers like patterns) channel quality estimations based on average figures are recommended in order to minimize the number of retransmissions.
  - In scenarios with bursty traffic, a small amount of transmissions errors can be afforded and compensated by retransmission capabilities such as HARQ, without a negative impact on the overall QoS. Thus, narrow band estimations (based on short term samples) can be used.
- The solutions can be implemented in LTE networks without substantial modifications. Indeed, UE featuring these new reporting capabilities can coexist transparently with legacy users.
- Theoretical findings about the performance of LTE schemes presented in previous studies were confirmed also in the context of static ICIC. Moreover, the results presented herein point out that the way to improve the performance of CSI feedback schemes is not necessarily through more uplink overhead. Instead, a more accurate and better localized channel quality estimations suffice to achieve desired results.
- The schemes presented in this chapter represents by themselves a contribution that is well aligned with the objectives of this Ph.D. dissertation, i.e., provided a solid contribution and significant improvements to the theory and operation of static ICIC schemes. In this sense, the importance of effective CSI feedback in the context of static ICIC was shown and quantified.

Chapter 5

Multiobjective Evolutionary Algorithms

5.1 Introduction

In Chapter 3, the need for optimization for the static ICIC schemes (SFR and FFR) in the context of realistic cellular deployments was shown. It was explained that the poor performance of baseline design configurations in such scenarios is mainly due to the irregular network topologies (far from the commonly assumed hexagonal layout) and the significantly different propagation conditions that can be found from one cell to another. These factors result in very different SINR distributions at each cell. Recall that baseline designs are configurations in which the same values of the operational parameters (α, β, and ψ_{TH}) are applied to all cells of the network.

Based on those findings, it was concluded that a certain level of adjustment at cell level needs to be done. Moreover, previous studies also showed the importance of focusing not only on cell edge performance (the main design goal of ICIC), but also looking at other performance metrics such as spectral and energy efficiency. As it was shown in Chapter 2, this interesting research problem has gone almost unnoticed despite the unquestionable importance of the strategies for static ICIC and their potential as feasible solutions to address the cell edge performance issue in cellular networks based on OFDMA.

Bearing in mind the previous context, and taking into account the existing literature, the research was directed towards investigating the use of multiobjective optimization techniques as a novel approach to address the design of SFR and FFR. In this framework, several conflicting objectives are required to be jointly satisfied. This contrasts with single objective options. In this case the problem could be posed 1) as the optimization of a linear combination of individual objectives, and 2) the transformation of all but one objective into constraints. Note that the first option was used in the performance assessment method presented in Section 3.3.

On the other hand, tackling the problem under a multiobjective perspective offers several advantages as for example:

1. The possibility to study the problem as it is, without the need for incurring in system simplifications or assumptions to make the mathematical treatment feasible. In this manner, by capturing all the relationships among design variables and performance metrics, better insights and more design guidelines can be obtained.

2. Provides a complete picture of the tradeoffs among objective functions: The analysis of such dependencies allows detecting very sensitive variations. This for example is useful when a slight loss in one objective allows very high gains in others. Thus, final solutions can be chosen in a smarter way.

3. Rather than getting one single solution, multiobjective optimization brings as output several network configurations, all of them representing different tradeoffs among the objectives. Thus, the multiobjective approach provides more flexibility to mobile operators to select different network settings (solutions) according to criteria that can change over time.

Today, multiobjective optimization is both a rich matter from the theoretical point of view and a very active research field. This paradigm encopassess a broad set of strategies and algorithms whose individual consideration would require a complete Ph.D. dissertation [218]. In this chapter, based on the features of the optimization problem that is required for static ICIC and practical considerations, evoluationary algorithms are investigated. These constitute a type of metaheuristic highly suitable for multiobjective optimization.

This chapter presents the most relevant concepts of the theory of multiobjective optimization and it explains the motivation behind the use of evolutionary algorithms. The chapter should be regarded as a transition point to the Chapters 6, 7, and 8, where this approach has been successfully applied.

The chapter is organized as follows: the next section presents some background theory and general concepts of multiobjective optimization. Section 5.3 introduces the metaheuristics and it clarifies their use in static ICIC optimization. Next, two important Multiobjective Evolutionary Algorithms (MOEAs) that were employed in the studies presented in this Ph.D. thesis, the algorithms NSGA-II and SPEA 2, are explained in Sections 5.4 and 5.5, respectively. Readers that are already confident with these two approaches can directly jump to Section 5.6 where the conclusions are presented.

5.2 Multiobjective Optimization

Many fields of science have to deal with large scale problems in which acceptable solutions involve simultaneous optimization of several conflicting criteria or objectives.

Multiobjective optimization (MO) is the discipline that focuses on the resolution of these problems [219].

The target of MO is to find a subset of *good* solutions ($\mathcal{X}^\star$) from a set $\mathcal{X}$ according to a set of criteria $\mathcal{F}$, with cardinality greater than one, typically expressed as mathematical functions, the so-called objective functions. Thus,

$$\mathcal{F} = \{\ f_i(\mathbf{x})\ :\ \mathbb{R}^n \to \mathbb{R},\ i = 1, 2, \cdots, m\ \}, \tag{5.1}$$

where, f_i represents the i^{th} objective function and $\mathbf{x} \in \mathbb{R}^n$ is the optimization vector containing the n design variables (DVs). Therefore, every single $\mathbf{x} \in \mathcal{X}$ is a solution of the multiobjective problem, that in general, is defined by:

- A set of n DVs (x_1, x_2,$\cdots$, x_n) subject to optimization such that $\forall\ \mathbf{x} \in \mathcal{X}$, $\mathbf{x} = [\ x_1,\ x_2,\ \cdots,\ x_n\ ]$.
- The domain of each DV ($\mathcal{X}_1$, $\mathcal{X}_2$,$\cdots$, $\mathcal{X}_n$) such that $x_i \in \mathcal{X}_i$ and $\mathcal{X} = \mathcal{X}_1 \times \mathcal{X}_2 \times \cdots \times \mathcal{X}_n$. The set $\mathcal{X}$ is also known as search space or feasible set.
- Constraints among DVs.
- An objective space defined by a function $\mathbf{f} : \mathcal{X} \to \mathbb{R}^m$, such that for each $\mathbf{x} \in \mathcal{X}$, $\mathbf{f}(\mathbf{x}) = [\ f_1(\mathbf{x}),\ f_2(\mathbf{x}), \cdots,\ f_n(\mathbf{x})\ ]$.

It might well happen that the objectives are in conflict. In this case, improving one of them implies worsening another. It makes no sense talking about a signle global optimum, and for this reason, the notion of an optimum set ($\mathcal{X}^\star$) acquires especial relevance in the context of MO.

A central element in the theory of MO is the concept of Pareto efficiency. A solution $\mathbf{x}^\star$ is element of the set $\mathcal{X}^\star$, i.e., it is Pareto efficient, if and only if, there does not exist a solution $\mathbf{x} \in \mathcal{X}$, such that $\mathbf{x}$ dominates to $\mathbf{x}^\star$ in the Pareto sense. A solution $\mathbf{x}_1$ dominates in the Pareto sense (is preferred to) another solution $\mathbf{x}_2$, ($\mathbf{x}_1 \succ \mathbf{x}_2$), if $\mathbf{x}_1$ is better than $\mathbf{x}_2$ in at least one criterion (objective function) and no worse with respect to the remaining ones[1]. Thus,

$$\mathbf{x}_1 \succ \mathbf{x}_2,\ \Longleftrightarrow\ f_i(\mathbf{x}_1) \leq f_i(\mathbf{x}_2)\ \ \wedge\ \ \exists\ j\ \ |\ \ f_j(\mathbf{x}_1) < f_j(\mathbf{x}_2). \tag{5.2}$$

In this manner, the notion of optimality in the multiobjective context can be formalized as follows: a solution $\mathbf{x}^\star$ features Pareto efficiency (is Pareto optimal), and hence, element of $\mathcal{X}^\star$, if and only if, there does not exist a solution $\mathbf{x} \in \mathcal{X}$, such that $\mathbf{x}$ dominates $\mathbf{x}^\star$. Thus,

$$\mathbf{x}^\star \in \mathcal{X}^\star\ \Longleftrightarrow\ \nexists\ \mathbf{x} \in \mathcal{X}\ \ |\ \ \mathbf{x} \succ \mathbf{x}^\star. \tag{5.3}$$

The set $\mathcal{X}^\star$ of Pareto optimal solutions is called optimal nondominated set and its image is known as the Optimal Pareto Front (OPF). When a multiobjective problem

[1] In global optimization, it is a convention that optimization problems are defined as minimizations problems [220], and hence, if one criterion f needs to be maximized, then f is redefined as $-f$. The same convention is adopted in this document.

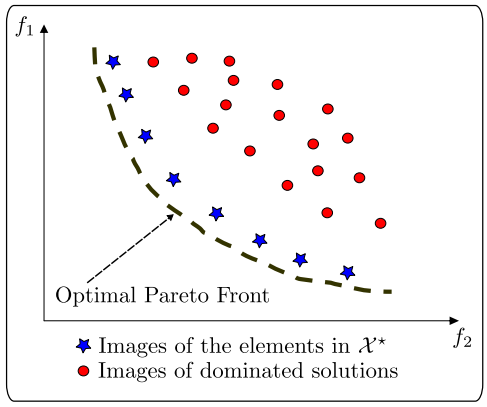

Figure 5.1: A representation of the Pareto Front.

is solved, it is unusual to obtain the OPF due to problem complexity, instead a set of near-optimal solutions is found. Hereafter, for the sake of clarity, it should be understood that the set $\mathcal{X}^\star$ contains such near-optimal solutions, and hence, its image, the corresponding Pareto Front (PF), is an estimation of the OPF. These ideas are illustrated in Figure 5.1 for the case where $\mathbf{f} = [\ f_1(\mathbf{x}),\ f_2(\mathbf{x})\ ]$.

Any solution in $\mathcal{X}^\star$ is optimal in the sense that no improvement can be made on a component of $\mathbf{f}$ without worsen at least another of its components. Given this, **the estimation of the set $\mathcal{X}^\star$ provides a complete picture of the tradeoffs among objective functions**, which is desirable in problems such as the optimization of static ICIC techniques, where improving cell edge performance always comes at the expense of spectral efficiency.

Multiobjective optimization problems, in general, can be expressed in the following form:

$$\text{minimize} \quad \mathbf{f}(\mathbf{x}) = [\ f_1(\mathbf{x}),\ f_2(\mathbf{x}), \cdots,\ f_n(\mathbf{x})\ ], \tag{5.4a}$$

$$\text{subject to:} \quad \mathbf{x} \in \mathcal{X}. \tag{5.4b}$$

Solving problems such as 5.4 is very difficult for the following reasons:

1. As it was shown, the definition of optimality in MO only allows establishing a partial order [221] between the solutions, which complicates the design of resolution algorithms.

2. The vast majority of multiobjective problems are NP-hard [96].

3. The cardinality of the set $\mathcal{X}^\star$ grows exponentially with the number of objectives.

Problem 5.4 can be solved encoding the solutions either with real-valued variables (continuous optimization problems) or discrete variables (combinatorial optimization problems). The following discussion applies to both types of problems.

The approaches to solve (5.4) can be classified as follows:

- *Pareto approaches*. The search and selection of solutions is based on the concept of Pareto efficiency. This chapter focuses on this strategy because MOEAs are also based on this approach.
- *Non-Pareto and non-scalar approaches*. These methods use operators to deal with the objective functions separately. Few works have employed this approach. Examples include parallel [222] and lexicographic [223] selection.

Why Multiobjective Evolutionary Optimization in Static ICIC Design?

As it was shown in Chapter 3, the performance of baseline designs of SFR and FFR is poor in cellular scenarios where the network geometry is irregular. Based on the analysis presented therein, it was suggested that a way to improve the performance of such strategies is by means of local adjustments at each cell. In other words, by tuning the configuration (the operational parameters α, β, and ψ_{TH}) of SFR and FFR locally at each cell. Thus, the optimization of static ICIC schemes could be posed as a MO problem where the design variables correspond to the parameters of different cells and the objectives include cell edge performance and network capacity, among others. The optimization formulation can be done, as it will be shown in Chapter 6, by means of discrete- or real-valued design variables.

However, as previously mentioned, multiobjective (combinatorial or not) optimization problems typically belong to the class NP-Complete [96], and hence, optimality cannot be guaranteed in polinomial time[2]. Therefore, deterministic methods for finding optimal solutions are not an option. Moreover, multiobjective problems with objective functions depending on many (independent) design variables often results in large n-dimensional objective spaces, full of local optima and discontinuities [220]. In the particular case of static ICIC optimization, n would be proportional to the network size (the number of cells), which is considerably high even in deployments covering small cities. In addition, discontinuities could occur on objectives such as aggregate cell edge rate due to variations of ψ_{TH}, when a certain (integer) number of pixels changes its classification from $\mathcal{E}$ to $\mathcal{I}$ or vice versa.

Certain algorithms such as gradient based methods are susceptible to be trapped in local optima, while other optimization techniques such as Sequential Quadratic Programming based methods [224] require convexity (a very strong assumption in this context) to guarantee convergence. In addition, traditional constrained optimization, in which only one objective function is optimized subject to a set of constraints on the remaining ones, has the drawbacks of 1) limiting the *visibility* of the whole objective space, and 2) reducing the output to one single network configuration.

Summarizing, the problem under consideration requires of an optimization tool fulfilling the following features:

[2]An optimization (decision) problem is NP-Complete if the computational time required to find the answer to a worst case instance grows faster with the size of the problem than any polynomial function [218].

- ✓ It must be able to find good (near-optimal) solutions by efficiently exploring the search space.

- ✓ It should operate in an effective manner with multiple criteria and a large number of design variables.

- ✓ It should not require strong assumptions on the objective functions such as linearity, convexity, continuity, or differentiability.

MOEAs [225] fulfill the previous requirements, and hence, their use in static ICIC optimization for large and irregular networks is investigated. MOEAs are population-based metaheuristics that simulate the process of natural evolution. Two well-known algorithms have been used: The Nondominated Sorting Genetic Algorithm II (NSGA-II) [226] and The Strength Pareto Evolutionary Algorithm 2 (SPEA 2) [227][3]. The main advantages of these algorithms are: 1) their black box nature makes them suitable to deal with many practical problems as only few assumptions need to be made on the objective functions, and 2) they incorporate important features such as *elitism*, *convergence*, and *distribution*. The next section provides an introduction to metaheuristics and evolutionary optimization. Interested readers are refereed to [225] for an in-depth treatment of the matter. The algorithms NSGA-II and SPEA 2 are described in Sections 5.4 and 5.5, respectively.

5.3 Metaheuristics and Evolutionary Algorithms

The solution of multiobjective optimization problems has always been of great interest for scientist and engineers working on operations research. Several exact methods have been proposed for solving problems involving two objectives and a small number of design variables such as *branch and bound* [229] and *dynamic programming* [230]. However, these methods are not effective for large scale problems with more than two criteria and a high number of design variables. Indeed, for more than two criterion, there are not useful procedures due to the multiobjective nature of the problems and the NP-Complete difficulty [225].

Thus, heuristic methods have become a very popular approach to solve problems involving a large number of design variables and multiple objective functions. These strategies do not guarantee to find the OPF, but a good approximation of it. In this context, the methods can be grouped into two types: on the one hand, the heuristic based algorithms that are problem-specific (heuristics), and on the other hand, high level strategies that can be applied to a large number of multiobjective problems (metaheuristics).

[3]These two algorithms are widely accepted as reference in the field of Evolutionary multiobjective optimization and their performance has been shown to be superior to other MOEAs [228].

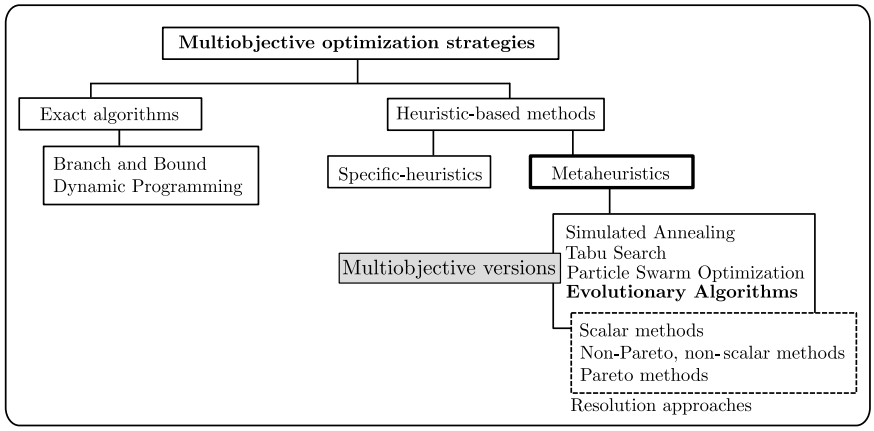

Figure 5.2: Methods for solving multiobjective optimization problems.

5.3.1 On the Use of Heuristic-based Methods

An heuristic can be considered as a part of an iterative optimization algorithm that uses available information to determine 1) which solution candidate should be tested in each iteration, and 2) how next candidates must be produced [220]. However, as heuristics are problem type dependent, they have been used as means to solve specific problems.

A metaheuristic is a method for solving more general classes of problems. They combine objective functions and heuristics in an abstract and hopefully efficient way, usually without utilizing deeper insight into their structure, i.e., by treating them as black-box-procedures [220]. Due to this versatility, metaheuristics have become a very active research area and several algorithms have been proposed. Popular ones include adaptations of classic (single objective) schemes such as Tabu Search [231], Simulated Annealing [232], Particle Swarm Optimization [233], and Evolutionary Algorithms [225]. For instance, a simulated annealing based multiobjective optimization algorithm can be found in [234]. A summary of the methods for solving MO problems is shown in Figure 5.2. A complete and in-depth discussion of metaheuristics and evolutionary computation can be found in [218] and [225].

In this chapter, the attention is placed on evolutionary algorithms, and more precisely, on MOEAs, the approach used in static ICIC optimization. The next subsection provides an introduction to evolutionary algorithms.

5.3.2 Essentials of Evolutionary Algorithms

According to [235], "*evolutionary algorithms are algorithms that perform optimization or learning tasks with the ability to evolve.*". The evolutionary algorithms have three main characteristics:

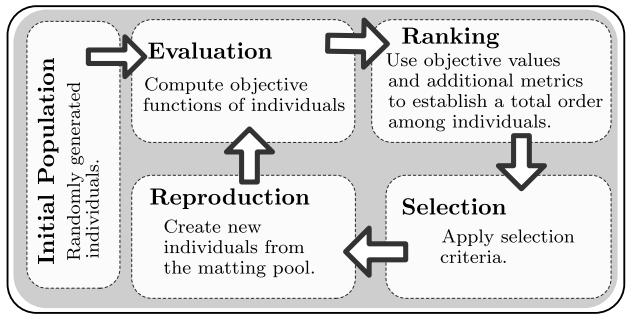

Figure 5.3: Main cycle of evolutionary algorithms.

1. *Population-based.* In evolutionary algorithms, a set of solutions, called 'population', is processed to optimize the design variables and learn from the problem structure.

2. *Fitness-oriented.* Every single solution in the population is called 'an individual', and each individual is codified by means of a genotype, i.e., the particular values of the design variables. The corresponding performance of each genotype (obtained through the objective functions) is referred to as its *fitness*. Thus, the target of evolutionary algorithms is to improve progressively (generation by generation) *the quality* of the individuals in the population by means of certain selection and fitness assignment schemes.

3. *Variation-driven.* The individuals of the population are subject to some mechanisms to mimic the process of natural evolution. This principle is key to explore efficiently the search space (the set $\mathcal{X}$).

Thus, in MOEAs, a population of individuals (candidate solutions) is iteratively modified by means of two basic principles: selection and variation. While selection tries to imitate the battle for reproduction among living beings, variation mimics their inherent ability of creating new (better adapted) individuals through recombination and mutation. The overall cyclic process followed by MOEAs is depicted by Figure 5.3. A description of the different steps stages is provided in the following points:

- *Initial Population.* An initial population of individuals or solutions, the $\mathbf{x}$'s, is created. Such elements can be created either randomly or (if possible) by means of a predefined algorithm to further exploit the structure of the problem.

- *Evaluation.* Each solution is assigned with a fitness value that is based on the objective function values. Typically, in Pareto-based approaches, the fitness is based on Pareto dominance, i.e., the number of solutions each $\mathbf{x}$ dominates to.

- *Ranking.* It consists in establishing a strict order [221] among the individuals of the population. This sorting procedure is typically based on the fitness values previously assigned, however, it can include other variables, by which certain desired traits can be preserved.

- *Reproduction.* Reproduction involves the process of selecting well-adapted (good fitness) individuals and combining their genes in order to create new offsprings with high probability of achieving good (or even better) fitness figures. In this manner, the evolution (convergence of the algorithm) of the population is improved. The process of combining two solutions is performed by means of *crossover* operators [220]. In addition, mutating some genes of some individuals is also a mechanism to introduce diversity in the population and to favor faster convergence.

- *Selection.* Selection is the process to determine which individuals pass to the next generation and which ones are discarded. The criterion is typically based on fitness values.

- *Termination criterion.* Although not shown in Figure 5.3, a termination criterion is verified after each generation to determine whether the evolutionary process should stop. This criterion is typically context-specific and depends on convergence criteria and/or computational cost that can be afforded.

As it was mentioned, the main advantage of MOEAs is their black box nature that makes them suitable to deal with many practical problems as only few assumptions need to be done on the objective functions. However, there are three important features that any good MOEA must incorporate.

- ✓ *Elitism.* It refers to the ability of MOEAs to preserve good individuals. Its role has been shown to be crucial in the performance of genetic algorithms [228]. To be precise, not only it speeds up the convergence, but also to avoid losing good solutions once they are found.

- ✓ *Convergence.* MOEAs should implement mechanisms to find (or estimate) the set $\mathcal{X}^\star$ as soon as possible. In problems with one objective, the direction is clear because there is only one objective. However, in multiobjective problems, a good algorithm should determine different *paths* in such a way that the exploration of the set $\mathcal{X}$ allows for finding solutions that 1) feature Pareto efficiency, and 2) are well distributed in the Pareto Front.

- ✓ *Distribution.* It is related to the ability to provide the largest possible set of nondominated solutions and keep them as evenly distributed as possible along the Pareto Front.

Another interesting aspect in MOEAs is how to measure performance. The literature in this particular case is large and a compilation of quality measures is certainly unaffordable. Instead, the quality indicators used in this dissertation are explained.

- *Hypervolume indicator* (υ). This measure reflects the size of volume dominated by the estimated Pareto Front [236, 237]. Formally, the hypervolume indicator is defined for a given set of nondominated points $\mathcal{X}^\star$ and a reference point

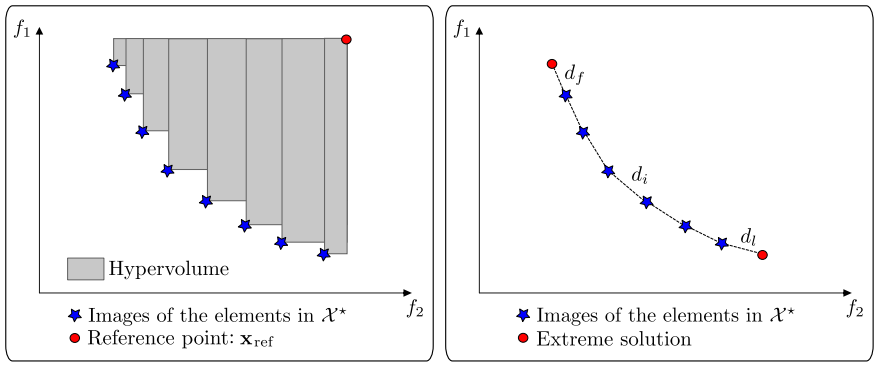

(a) The hypervolume indicator (υ). **(b)** The nonuniformity index (ϱ).

Figure 5.4: Quality measures in multiobjective optimization.

$\mathbf{x}_{\text{ref}} \in \mathbb{R}^m$ as follows:

$$\upsilon(\mathcal{X}^\star, \mathbf{x}_{\text{ref}}) = \Lambda\left(\bigcup_{\mathbf{x}\in\mathcal{X}} \hat{\mathbf{x}} \mid \mathbf{x} \prec \hat{\mathbf{x}} \prec \mathbf{x}_{\text{ref}}\right), \qquad \mathcal{X}^\star \subseteq \mathbb{R}^m, \tag{5.5}$$

where Λ denotes the Lebesgue measure [238]. Note that $\mathbf{x}_{\text{ref}}$ should be dominated by all the elements of $\mathcal{X}^\star$. Since it has been shown that maximizing the hypervolume measure is equivalent to finding the OPF [239], higher values of υ indicate better convergence. As it can be seen in Figure 5.4a, each single element in the set $\mathcal{X}^\star$ contributes to the hypervolume, and hence, having more solutions (belonging to the same front) implies improving the hypervolume.

- *Nonuniformity index* (ϱ). This metric measures how well distributed the elements of the estimated Pareto Front are [226]. Thus, for any given distribution of solutions, the non-uniformity index is defined as follows:

$$\varrho = \frac{d_f + d_l + \sum_{i=1}^{N-1} |d_i - \bar{d}|}{d_f + d_l + \bar{d}\,(N-1)}, \tag{5.6}$$

where the parameters d_f and d_l are the Euclidean distances between the extreme solutions (optimal values of each metric, in case they are known) and the boundary solutions of the estimated nondominated set, as it is illustrated in Figure 5.4b. In problems where the extreme solutions are not known, they can be replaced by the best values found for each metric. The figures d_i correspond to the distances between consecutive solutions. The parameter $\bar{d}$ is the average of all distances d_i ($i = 1,\ 2,\ \cdots,\ (N-1)$), under the assumption that the set $\mathcal{X}^\star$ is composed of N solutions. Note that if all the distances d_i are equal, and the estimated Pareto Front includes the extreme solutions, $d_f = d_l = 0$ and the sumation in the numerator of (5.6) is also zero. Thus, for this ideal case $\varrho = 0$. Higher values of ϱ indicate worse distributions.

5.3.3 Calibration Aspects

An important aspect of evolutionary (genetic-based) algorithms is that a calibration is required for the parameters that control the algorithm. The goal of this subsection is to provide insights into this particular by 1) indicating the main parameters subject to calibration, and 2) presenting certain (empirical) rules of thumb for an easy adjustment. The following paragraphs aim at highlighting some practical calibration guidelines:

- *Population size*: There is a general consensus about the number of individuals in the population in approaches based on genetic algorithms (such as NSGA-II and SPEA-2). The range to consider during calibration is [20,100] and beyond 100, extra gains are hardly achieved and the same global convergence is obtained [240]. Since computation time grows exponentially with this input, the final population size also depends on the problem scale and the computational complexity that can be afforded. However, in the context of study of this thesis, greater populations allow a smoother Pareto Front (better characterization of the tradeoffs among the performance metrics), and hence, operators could choose *alternatives* from a denser/bigger set of solutions.

- *Termination criterion*: The number of generations depends on a predefined termination criterion that can be defined in several ways. Note that more than one single termination criterion can be used simultaneously.

  - Direct termination criteria. For instance, defining a maximal number of generations or execution time. Another option is to stop the algorithm when one or more objective functions surpass a predefined bound(s). In practice, this approach is not very recommended unless the termination criterion guarantees (a priori) the desired convergence level. Hence, this method is only suitable in very particular contexts.
  - Derived termination criteria. This approach considers the definition of termination criteria that can be problem-specific. For instance, the relative progress of one or more objective functions after a certain number of generations or the relative improvement in a convergence measure such as the hypervolume indicator.

- *Parameters in genetic operators*: Genetic operators include crossover, mutation, and selection. The calibration of these *internal* procedures of evolutionary algorithms has a great impact on the performance of them, and therefore, it requires special attention. However, the operation of these operators depends on several factors such as the type of design variables (continuous or discrete) or problem-specific features, and hence, the calibration process varies accordingly.

  Crossover is a fundamental process when genetic algorithms preserve elitism. It guarantees exploring the search space in regions where *good* solutions are more likely to be found, by combining individuals with good fitness. The crossover rate determines the probability of combining such solutions to preserve their genes in future generations. Values close to one are suggested in the related

literature [226]. In addition, the way in which the combination is performed can also be adjusted according to the needs of each particular problem, see [241, 242] for further details.

Mutation is another important source of diversity in MOEAs [241]. The mutation rate determines the probability of of changing each gene (generate a new random value for the gene or modify its value according to a certain rule). However, high mutation rates would result in random search. A practical rule of thumb is to select a mutation rate equal to $1/n$, where n is the number of design variables [226].

In practice, it is advisable to perform some calibration trials in order to determine appropriate values, and so, avoid the evolutionary algorithm to operate with wrong (highly suboptimal) settings. This can be done by means of parametric sweeps to study the performance of the algorithm by looking at metrics such as the hypervolume indicator.

5.4 Description of the Algorithm NSGA-II

In 2002, Deb *et al.* [226] presented improvements of their Nondominated Sorting Genetic Algorithm (NSGA) that was originally introduced in 1994 [243]. The algorithm NSGA was based on the *Pareto rank* method, in which the individuals in the population are ranked taking into account a domination count, i.e., the number of solutions that dominates to each individual. Thus, the solutions with rank 1 are nondominated solutions. Rank 2 implies that an individual is only dominated by another solution, rank 3 means that a solution is only dominated by two individuals, and so on. The individuals with the same rank share the same fitness. In this manner, individuals with lower rank gain advantage in the selection procedure, thus including increasingly better solutions and favoring the convergence of the algorithm. In [226], the algorithm NSGA-II introduced the following improvements:

1. *Lower complexity*. The complexity of the algorithm NSGA is $\mathcal{O}(MN^3)$, where M and N are the number of objective functions and population size, respectively. By adding an improved nondominated sorting approach, the complexity of the algorithm NSGA-II becomes $\mathcal{O}(MN^2)$.

2. *Elitism*. The algorithm NSGA does not implement elitism, a feature that, as it was indicated before, is useful to speed up the convergence of genetic algorithms [228] by preventing the loss of good solutions once they are found. NSGA-II implements an archive-based mechanism to introduce elitism.

3. *Improved distribution*. In NSGA-II, the need for a diversity-controlling parameter, the sharing figure (σ_{share}) in NSGA, was eliminated.

Improved Nondominated Sorting

The pseudo-code describing the fast nondominated sort in NSGA-II is shown in Algorithm 5.1. Basically, for each element p, the number of individuals that dominates p (n_p) is calculated. The variable n_p is referred to as nondomination count. In addition, the set of elements dominated by p ($\mathcal{S}_p$) is also computed. Therefore, the individuals in the first front ($\mathcal{F}_1$) will have $n_p = 0$. Next, for each solution p with $n_p = 0$, the value of n_p of the individuals in the set $\mathcal{S}_p$ is reduced by one. If n_p in an element of $\mathcal{S}_p$ becomes zero, it is moved to a separate list $\mathcal{Q}$, the members of the second front. The previous procedure is now executed for the members of $\mathcal{Q}$ and so, the third front is also created. The loop goes until all fronts are created. Note that all the elements in the i^{th} front have rank i.

Algorithm 5.1 is an important novelty presented in [226]. This algorithm is the main responsible for the gain in terms of computational cost with respect to NSGA.

Crowding Distance

The method used in NSGA to preserve diversity based on a user-defined parameter (σ_{share}) has two main drawbacks:

× the performance of the sharing function strongly depends of σ_{share}, and

× the complexity of the sharing function approach is $\mathcal{O}(N^2)$.

Thus, in NSGA-II the sharing function is replaced by a crowding distance assignment procedure that does not require any user-defined parameter. The definition and computation of crowding distances in a set of nondominated individuals is given in Algorithm 5.2. Basically, the procedure computes the crowding distance for each solution in a nondominated set $\mathcal{F}$. In the pseudo-code, $\mathcal{F}[i]_m$ corresponds to the value of the m^{th} objective function of the i^{th} individual in the set $\mathcal{F}$. The parameters $f_m^{\max}$ and $f_m^{\min}$ are the maximum and minimum values of the m^{th} objective function. The complexity of Algorithm 5.2 is $\mathcal{O}(MN\log(N))$.

Thus, by means of this density metric and the previously introduced nondomination rank, NSGA-II uses the following *crowded comparison* operator ($\prec_n$) to establish a partial order between different solutions as follows:

$$p \prec_n q \;\text{ if }\; (p_{\text{rank}} < q_{\text{rank}}) \;\text{ or }\; ((p_{\text{rank}} = q_{\text{rank}}) \;\text{ and }\; (p_{\text{distance}} > q_{\text{distance}}))\,. \quad (5.7)$$

According to the partial order $\prec_n$, $p \prec_n q$ means that p is preferred over q. Therefore, the algorithm always prefers solutions 1) with lower rank (better domination count), and 2) located in lesser crowded regions to favor a better distribution.

Algorithm 5.1: Fast Nondominated Sort in NSGA-II

Input : A set of individuals ($\mathcal{R}$).
Output : Efficient nondominated sorting of the elements of the set $\mathcal{R}$.

```
1  for each p ∈ R do
2      S_p = ∅, n_p = 0;
3      for each q ∈ R do
           // If p dominates q;
4          if (p ≺ q) then
5              S_p = S_p ∪ q;        /* Add q to the set of solutions dominated by p */
6          end
7          else if (q ≺ p) then
8              n_p = n_p + 1;        /* Increment the domination counter of p */
9          end
10         if (n_p = 0) then
11             p_rank = 1;           /* p belongs to the first front */
12             F_1 = F_1 ∪ {p};
13         end
14     end
15 end
16 i = 1;                            /* Initialize the front counter */
17 while F_i ≠ ∅ do
18     Q = ∅;                        /* Used to store the members of the next front */
19     for each p ∈ F_i do
20         for each q ∈ S_p do
21             n_q = n_q − 1;        /* Decrement the domination counter of q */
22             if (n_q = 0) then
23                 q_rank = i + 1;   /* q belongs to the next front */
24                 Q = Q ∪ {q};
25             end
26         end
27     end
28     i = i + 1, F_i = Q;           /* Updates the next front */
29 end
```

Elitism

In NSGA-II, elitism is introduced by comparing (using the operator $\prec_n$) each new generation with the best nondominated solutions of the previous generation. The best solutions are stored in a separate archive.

Algorithm 5.2: Crowding distance assignment in NSGA-II

Input : A set of nondominated individuals ($\mathcal{F}$).
Output : Crowding distance assignment to the elements of the set $\mathcal{F}$.

```
1  l = |F|;                                          /* Number of solutions in F */
2  for each i ∈ F do
3  |  F[i]_distance = 0;                                  /* initialize distance */
4  end
5  for each m do
6  |  F = sort(F, m);                                 /* sort using each objective value */
7  |  F[1]_distance = F[l]_distance = ∞;   /* boundary points are always selected */
8  |  for each i = 2:(l − 1) do
9  |  |  F[i]_distance = F[i]_distance + (F[i+1]_m − F[i−1]_m) / (f_m^max − f_m^min)
10 |  end
11 end
```

NSGA-II Procedure

The pseudo-code of the algorithm NSGA-II is shown in Algorithm 5.3. The evolving process in the t^{th} generation is graphically illustrated in Figure 5.5. In the pseudo-code, the set $\mathcal{R}_t$ contains the initial (combined) population of the t^{th} generation. Recall that the population size is N, and therefore, $|\mathcal{R}_t| = 2N$. Initially, the combined population is created by merging the previous generation ($\mathcal{P}_t$, $|\mathcal{P}_t| = N$) and the offsprings ($\mathcal{Q}_t$, $|\mathcal{Q}_t| = N$). Next, the nondominated sorting (Algorithm 5.1) takes place. The elitism is guaranteed because current and previous population members are all included in $\mathcal{R}_t$. Then, the whole population is sorted again by means of the crowded comparison operator $\prec_n$ (5.7), and finally the best N individuals according to the partial order established by $\prec_n$ are selected to pass to the next generation ($\mathcal{P}_{t+1}$). The offsprings of the new generation ($\mathcal{Q}_{t+1}$) are obtained from the elements in $\mathcal{P}_{t+1}$ by means of binary (pairwise) tournament selection based on $\prec_n$, crossover, and mutation. Note that diversity is promoted by using the crowding comparison procedure as it is indicated in 5.7, which is employed both in selection and population reduction.

The schemes for convergence, distribution, and elitism are implemented in the algorithm NSGA-II by means of the nondominated sorting (Pareto rank) and selection ($\prec_n$), the crowding distance assignment (Algorithm 5.2), and the introduction of an archive (of size equal to the baseline population), respectively. Thus, the algorithm NSGA-II obtains a good balance between these three important requirements.

Algorithm 5.3: Algorithm NSGA-II

input :
$|\mathcal{P}|$: Population size (the same figure is used for the archive).
$\mathcal{C}$: Calibration parameters (genetic operators).
T: Binary termination criterion.

output :
$\mathcal{F}_1$: Set of nondominated solutions (referred to as $\mathcal{X}^\star$ in the document).

```
1  t = 0, Q_t = ∅, T = 0;                                   /* Initial generation */
2  P_t = Create-Random-Generation(|P|);
3  while T ≠ 1 do
4      R_t = P_t ∪ Q_t;      /* combine parent (P_t) and offspring (Q_t) population */
5      F = Nondominated-Sort(R_t);                          /* Algorithm 5.1 */
6      P_{t+1} = ∅, i = 1;
7      while |P_{t+1}| + |F_i| ≤ N do
8          Crowding-Distance-Assignment(F_i);               /* Algorithm 5.2 */
9          P_{t+1} = P_{t+1} ∪ F_i;     /* include the i^th nondominated front in P_{t+1} */
10         i = i + 1;                    /* check the next front for inclusion */
11     end
12     Sort(F_i, ≺_n);                   /* sort in descending order using ≺_n */
13     P_{t+1} = P_{t+1} ∪ F_i[1 : (N − |P_{t+1}|)]; /* first (N − |P_{t+1}|) elements of F_i */
14     Q_{t+1} = Offsprings(P_{t+1});    /* selection, crossover and mutation */
15     t = t + 1;                        /* increment the generation counter */
16     Check-Termination-Criterion(P_{t+1});                /* Check T */
17 end
```

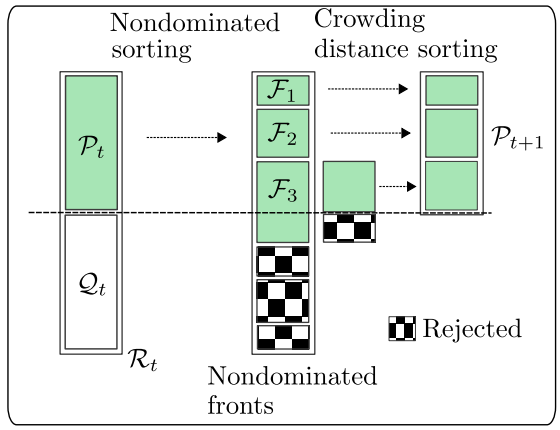

Figure 5.5: The evolving process in one generation of the algorithm NSGA-II.

5.5 Description of the Algorithm SPEA 2

In 1998, Zitzler and Thiele introduced its Strength Pareto Approach for multiobjective optimization [244]. The algorithm SPEA showed its potential by outperforming existing (non-elitist) alternatives at that time, including the algorithm NSGA [243]. However, further advances in the theory of multiobjective optimization were made and subsequent proposals, including NSGA-II, clearly outperform SPEA on certain test cases.

Taking advantage of new insights into the theory and design of evolutionary algorithms, the authors of SPEA introduced several improvements to SPEA in 2001. The novel algorithm (SPEA-2) [227] differs from its predecessor in the following aspects:

1. The fitness assignment takes into account not only the number of individuals dominating each solution but also the number of individuals each solution dominates to.

2. The density estimation approach is largely based on the distances to the nearest neighbors.

3. An archive is introduced to keep boundary solutions and improve the distribution of the Pareto Front.

During the design stage of SPEA 2, its authors considered the following aspects: why does the size of the archive need to be the same than in the population? In addition, in NSGA-II, the rank is somehow considered twice (in the nondominated sorting and crowded comparison operator). Thus, the authors also investigated whether these process can be shorten into a single one. Finally, the authors were specially concerned with the selection procedure.

Fitness Assignment and Density Estimation

A novel aspect of SPEA 2 (with respect to SPEA) is that individuals that are dominated by the same number of solutions in the archive (elitist group) do not have the same fitness. Thus, in SPEA 2, both dominating and dominated solutions are considered. Let's consider that the sets $\mathcal{A}_t$ and $\mathcal{P}_t$ are the archive and the population in the t^{th} generation. The *strength* ($S(i)$) of an individual p is the number of solutions it dominates to. Therefore,

$$S(p) = |\{\ q \mid q \in (\mathcal{A}_t + \mathcal{P}_t)\ \ \wedge p \prec q\}|. \tag{5.8}$$

Based on the strength measure, the raw fitness ($R(p)$) of the individual p is calculated as follows:

$$R(p) = \sum_{q \in (\mathcal{A}_t + \mathcal{P}_t),\ q \prec p} S(q). \tag{5.9}$$

The raw fitness tells how good an individual p is because it tells how many individuals dominate p. Note that 1) the term 'raw' suggests that the fitness needs to be further refined, and 2) the fitness should be minimized, i.e., $R(p) = 0$ means that p is a nondominated individual.

Given that the raw fitness could fail in cases where most individuals do not dominate each other, SPEA 2 uses additional density information to refine the measure. The density estimation in SPEA 2 is an adaptation of the k^{th} nearest neighbor method [245]. In this method, the density at any point is a decreasing function of the distance to the k^{th} nearest point. In SPEA 2, the inverse of such distance is considered as the density estimation. In [227], Zitzler and Thiele suggest using $k = \sqrt{|\mathcal{A}| + |\mathcal{P}|}$. Thus, the density of the individual p ($D(p)$) is computed as a function of the distance of p to k^{th} nearest neighbor ($\rho^k(p)$). Thus, $D(p)$ is given by the following expression:

$$D(p) = \frac{1}{2 + \rho^k(p)}. \tag{5.10}$$

The two in the denominator of (5.10) ensures that $D(p) \in (0,\ 0.5]$. Thus, the fitness of the individual p (used for selection purposes) is obtained according to:

$$F(p) = D(p) + R(p). \tag{5.11}$$

The computational complexity of the fitness assignment procedure is $\mathcal{O}(M^2 \log(M))$, where $M = |\mathcal{A}| + |\mathcal{P}|$.

Environmental Selection based on Archive Truncation

The clustering strategy used in SPEA was able to reduce the nondominated set without destroying its features, however, boundary solutions are often lost. The novel truncation method in SPEA 2 guarantees keeping those individuals, and hence, it improves the spread of the Pareto Front.

How does SPEA 2 handle the situation when the number of nondominated solutions in $(\mathcal{A} \cup \mathcal{P})$ is not equal to $|\mathcal{A}|$ (the size of the archive)? Let's consider that the set $\mathcal{B}$ is the set of nondominated solutions in $(\mathcal{A} \cup \mathcal{P})$. If $|\mathcal{B}| < |\mathcal{A}|$, more dominated solutions are added according to the fitness given by (5.11). If $|\mathcal{B}| > |\mathcal{A}|$, the individuals with the smallest distance (ρ^1) to others are deleted, then individuals with the smallest second distance (ρ^2), and so on, until $|\mathcal{B}| = |\mathcal{A}|$.

Basically, for dominated individuals, their raw fitness (several times greater than their densities, which is smaller than 0.5) predominates. For nondominated solutions, their raw fitness is always zero, and hence, sparser solutions are preferred. Elitism is guaranteed because individuals that are far from others in the estimated Pareto Front will never be lost, which at the same time achieves an excellent distribution.

Algorithm 5.4: Algorithm SPEA 2

input :
$|\mathcal{P}|$: Population size.
$|\mathcal{A}|$: Archive size.
$\mathcal{C}$: Calibration parameters (genetic operators).
T: Termination criterion.
output:
$\mathcal{X}^\star$: A set of nondominated solutions.

```
1  t = 0, T = 0, A_t = ∅;                                   /* Initial generation */
2  P_t = Create-Random-Generation(|P|)
3  while T ≠ 1 do
4  |  Fitness(P_t ∪ A_t);                                   /* According to 5.11 */
5  |  Environmental-Selection(P_t ∪ A_t);                   /* Fitness-based sorting */
6  |  A_{t+1} = Archive-Truncation(|A|, P_t ∪ A_t);          /* Archive truncation */
7  |  P_{t+1} = Offsprings(A_{t+1});                        /* selection, crossover and mutation */
8  |  X* = Nondominated-individuals(P_{t+1} ∪ A_{t+1});     /* Pareto Front */
9  |  Check-Termination-Criterion(X*);                      /* Check T */
10 |  t = t + 1;                                           /* increment the generation counter */
11 end
```

SPEA 2 Procedure

The pseudo-code of SPEA 2 is shown in Algorithm 5.4. The evolving process in the t^{th} generation is graphically illustrated in Figure 5.6. As a genetic algorithm, the overall procedure is quite similar to NSGA-II, with differences in the form of fitness calculation. These particular mechanisms of SPEA 2 have been already explained, and hence, the pseudo code is self-explanatory. However, it is important to highlight some points. In SPEA 2, the size of the archive is not specified. The authors in [227] claim that increasing the size of the archive favors a better distribution but less pressure is done towards the OPF.

The convergence, distribution, and elitism mechanisms are implemented in SPEA 2 by means of the raw fitness assignment, density, and the introduction of an archive, respectively.

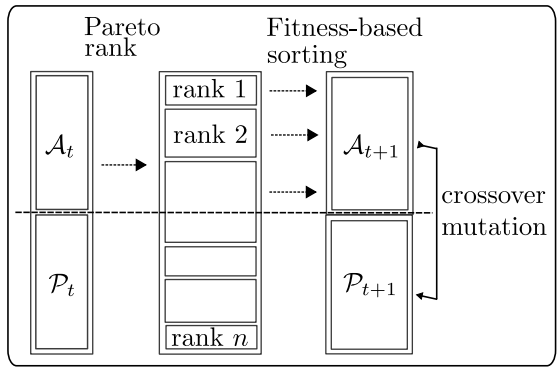

Figure 5.6: The evolving process in one generation of the algorithm SPEA 2.

5.6 Concluding Remarks

In this chapter, the most fundamental aspects of the theory of multiobjective optimization have been presented. In addition, a discussion of the most relevant methods and approaches to address problems involving several objectives has been provided.

In contrast to single objective optimization formulations, multiobjective problems do not have a single optimal solution. There exist several solutions that cannot be sorted following a single total order. Thus, the notions of Pareto dominance and optimal set play a crucial role in the design of suitable optimization strategies. This particularity of multiobjective problems can be regarded as a *two-edge sword* because, on the one hand, these are features that are very difficult to model mathematically. But, on the other hand, having multiple solutions allows to capture tradeoffs among objective functions. This certainly is a highly desirable feature in many practical contexts and in ICIC design in particular, as shown in the next chapter.

Multiobjective problems usually are very hard to solve due to its complexity (typically NP-hard), and hence, exact procedures to determine optimal solutions are not available. In the chapter, it was shown the advantages of heuristic-based schemes when facing such problems and the increasing interest on the use of metaheuristics.

A particular class of metaheuristic, evolutionary algorithms, has demonstrated its effectiveness in solving problems whose mathematical structure is not suitable for traditional methods. Evolutionary algorithms designed for multiobjective problems dealing with several (more than two) objective functions and a high number of design variables have been successfully employed by scientists and engineers in the last 20 years. These strategies are generically known as MOEAs and they have the distinguished feature that a population of individuals evolve together to explore the search space efficiently, i.e., finding regions of the domain in which solutions featuring Pareto efficiency are likely to be found.

Thus, by revisiting the characteristics and needs previously shown for static

ICIC optimization (Chapters 2 and 3), the suitability of MOEAs was discussed and analyzed. As it was seen, the optimization of static ICIC schemes in realistic deployments require adjustments in the operational parameters of these schemes at cell level. This implies that a potentially high number of design variables need to be considered. Moreover, given the conflicting nature between cell edge performance and overall spectral efficiency in OFDMA based cellular networks, the multiobjective approach arises as an attractive alternative to investigate the matter. In addition, the stochastic nature of MOEAs **eliminates the need for system simplifications**, and hence, expressions capturing all the relevant aspects of the problem could be considered as they are.

The next chapters of this thesis prove that the use MOEAs in the context of static ICIC optimization is not only effective but also it conveys several remarkable advantages from a practical point of view. Two MOEAs were used to conduct the research presented next: the algorithms NSGA-II and SPEA 2, both of them presented and explained in this chapter.

Thus, having introduced this important background, multiobjective optimization schemes to improve the performance of static ICIC strategies, both for data and control channels, are presented in Chapters 6 and 7, respectively.

Chapter 6

Optimization of Static ICIC Schemes through the use of MOEAs

6.1 Introduction

In Chapter 2, it was shown that, in the context of OFDMA based cellular systems, the low SINR levels at cell edges have a very negative impact on the QoE of users located in such areas. Thus, the techniques for interference management, and more precisely the schemes for ICIC, have attracted the attention of the industry and research community.

SFR and FFR, the static ICIC techniques *par excellence*, have the following advantages: 1) their low complexity, thus making implementation almost straightforward, and 2) they do not require either unrealistic CSI feedback from users or prohibitive intercell signaling exchange. As it is detailed in Chapters 2 and 3, both SFR and FFR aim at reducing the amount of ICI and increasing the reuse factor of cell edge users. By means of these principles, and under the assumption of regular layouts, the aggregate capacity of cell edge users can be increased at the expense of a reasonable price in terms of spectral efficiency.

However, in-depth studies about the operation of SFR and FFR, such as the one presented in Section 3.4, show that relaxing the hexagonal geometry condition results in severe performance degradations. This conclusion is also pointed out in related research works including [62–64].

Indeed, the analysis presented in Chapter 3 about the impact of the operational parameters of SFR and FFR clearly suggests that the reason of such poor performance in realistic deployments is twofold. On the one hand, an irregular layout implies that cell edge size and SINR distribution at different cells vary significantly (see

Figure 3.15b). On the other hand, the SINR levels found at cell edges (assuming the same propagation conditions) are worse than the ones obtained in hexagonal models [53]. Thus, the following hypothesis is formulated:

> *The performance of SFR and FFR can be optimized for any arbitrary cellular layout by adjusting locally (at each cell) the configuration of these schemes (the parameters α, β, and ψ_{TH}) in such a way that the unbalances created by the layout irregularities can be compensated.*

This chapter presents the work developed around the previous idea. It represents one of the central contributions of this Ph.D. dissertation: the introduction of multiobjective optimization algorithms to make SFR and FFR feasible and useful in the context of realistic deployments. As it was discussed in the previous chapter, the multiobjective approach is, by itself, an interesting novelty in the context of ICIC. It has some interesting advantages:

1. It provides a better view of the tradeoffs among conflicting criteria such as cell edge performance and spectral efficiency.
2. It makes possible to obtain an output composed of many near-optimal solutions (network settings). Thus, additional flexibility is provided to mobile operators to select configurations according to their needs.
3. It allows including additional perspectives to the problem such as the energy consumption.

However, as it is analyzed in the previous chapter, the complexity involved in the optimization (at cell level) of SFR or FFR cannot be addressed by means of exact (deterministic) procedures. Thus, this study investigates a metaheuristic approach based on stochastic search, in which MOEAs are considered and successfully applied to static ICIC optimization.

The next section presents practical considerations and it describes the proposed multiobjective formulation. The system model is explained in Section 6.3. The description of the novel multiobjective strategy and the results corresponding to performance evaluations are presented in Sections 6.4 and 6.5, respectively. In Section 6.6, additional aspects including calibration, complexity, and LTE-feasibility are discussed. Finally, the chapter is closed with conclusions in Section 6.7.

6.2 Multiobjective Problem Design

The optimization of SFR and FFR is, from a practical point of view, a problem in which the interest is placed not only in guaranteeing certain levels of QoS to users but also avoiding severe penalties in terms of spectral efficiency.

Indeed, the attention of this study is not only placed on the tradeoff between the cell edge performance and spectral efficiency. Recently, an increasingly interest on

energy efficiency and *green* communications [246–248][1] has appeared. Consequently, this important aspect has also been included not only for its relevance, but also for the intuition that transmitting less power implies introducing less ICI in the system.

Therefore, the performance assessment presented in this study is based on the following criteria:

1. Maximization of the **average cell capacity** (f_1): This metric is proportional to the overall system spectral efficiency, and hence, the system-oriented perspective is captured by means of this criterion.
2. Maximization of the **aggregate capacity of the worst percentile 5** of the coverage area (f_2): With this metric, ICIC's main objective, cell edge performance, is considered. Note that the area corresponding to this percentile can be geographically distributed among the coverage of different cells, and hence, it introduces a certain level of fairness among cells.
3. Minimization of the **power transmitted over the air interface** (f_3): By considering this metric, the proposed algorithms contribute not only to reduce the Operation Expenditures (OPEX), but also to improve the network energy efficiency [249].

6.2.1 Practical Insights

According to the hypothesis presented previously, the design target of the proposed strategy is to optimize SFR and FFR not only from a global (network) perspective, but also from a local point of view. These local adjustments would make possible to compensate *the unbalances* found in realistic deployments.

In order to 1) decouple the analysis from assumptions such as scheduling policies, and 2) obtain reliable results (from an statistical point of view), the framework presented herein focuses on the optimization of expected values. To be precise, the minimization of average ICI conditions. This approach was suggested in [6], where it is indicated that ICIC **may not have to track fast dynamics** such as small scale fading. These elements can be handled more efficiently by other RRM functionalities such as instantaneous power control and retransmissions.

The authors in [6] showed that around 60% to 70% of the gains achieved by dynamic (but often impractical) schemes can be obtained by means of ICIC schemes following only macroscopic network changes such as average channel conditions. Thus, in the light of these observations, a similar approach is followed in Chapter 3 (Section 3.3), and it is also suggested and applied by other researchers (see [45, 50, 63, 64]) working on static ICIC.

Bearing in mind the previous considerations, and aiming at keeping a reasonable complexity, the proposed multiobjective optimization framework is based on the following idea:

[1] A complete discussion about the matter is presented in Chapter 8.

Defining cell edges independently at each cell by means of cell-local thresholds ($\psi_{\text{TH}}^{l},\ l = 1, 2, \cdots, L$), subject to an additional network-wide (global) parameter common to all cells. This global adjustment is done by means of the parameters α and β, in case of SFR and FFR, respectively. The rationale of the previous design stems from the following facts:

- ✓ Local adjustments of α or β result in a significant increment of the computational cost (basically $2\times$), whereas treating them as global design variables allows the use of easy-to-build matrices to characterize the ICI (see (3.32) and (3.35)). This is done by leveraging both the trisectorial topology and resource allocation pattern in SFR and FFR. Moreover, previous studies such as [63, 64], in which optimization is based on adjustments of α and β, only achieve cell edge capacity improvements at the expense of significant (more than 60%) spectral efficiency degradations. As it is shown in the next chapter, local adjustments of α only provide small gains, and hence, the additional computational cost is not worth.

- ✓ As it was shown in Chapter 3, local adjustments of ψ_{TH} are a convenient way to deal with the tradeoff between cell edge performance and spectral efficiency at each cell, without modifying the levels of ICI at neighbor ones. Moreover, by adding α and β as global design variables, the genetic search is also aided. Simultaneous and uncoordinated variations of α and ψ_{TH} (in SFR), and β and ψ_{TH} (in FFR), are counterproductive because the effects of one could be neutralized by the other. Thus, the novel strategy aims at performing a sort of parallel optimization for the different values of the global design variable (α or β), and so, a desirable *equilibium* between local and global goals is achieved. On the one hand, in case of SFR, the use of the global design variable (α) is justified because cell edge users are more sensitive to interference than bandwidth [45], and hence, exploring different values of α is mandatory from an ICIC point of view. On the other hand, in case of FFR, it was shown that the effect of α is almost negligible, whereas β provides a convenient way to include the required network-wide component.

- ✓ In case of SFR, β is set to 2/3. Given a trisectorial topology, the figure $(1 - \beta)$ is restricted to the interval (0, 1/3] in order to avoid overlapping of cell edge subbands in adjacent sectors. Thus, from the cell edge viewpoint, $\beta = 2/3$ is the logical global choice as this value is the one assigning more bandwidth to the class $\mathcal{E}$, and hence, it helps to localize the exploration in regions of the search space ($\mathcal{X}$) boosting the cell edge capacity.

- ✓ In case of FFR, the value of α must be set taking into account coverage criteria, i.e., it should be selected such that a minimum received power can be provided in the coverage area both for interior and exterior pixels.

By means of the previous strategy, a convenient tradeoff between local and global goals is accomplished. The proposed scheme aims at optimizing the network configuration that is represented by the optimization vector $\mathbf{x}$ (similarly to $\mathbf{x}$ in (3.25)). However, $\mathbf{x}$ is codified by means of $L + 1$ design variables as depicted in Figure 6.1.

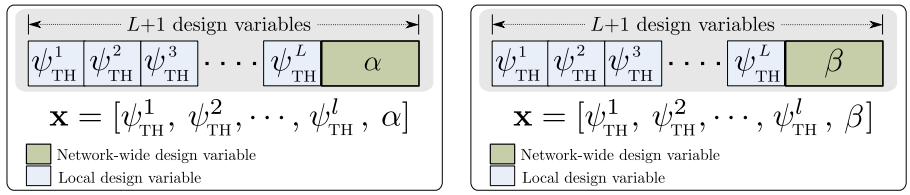

(a) SFR. **(b)** FFR.

Figure 6.1: Codification of solutions in multiobjective optimization of static ICIC.

Note that this approach guarantees a complexity (in terms of the number of design variables) linear with respect to the network size. Recall that L is the number of cells in the network.

6.2.2 Problem Formulation

The multiobjective optimization problem is formulated as follows:

$$\text{minimize} \quad \mathbf{f}(\mathbf{x}) = [\, -f_1(\mathbf{x}), \;\; -f_2(\mathbf{x}), \;\; f_3(\mathbf{x}) \,], \tag{6.1a}$$

subject to:

$$\mathbf{x}(l) \;\in\; [\psi_{\text{low}}, \; \psi_{\text{up}}], \quad l = 1, 2, \cdots, L, \tag{6.1b}$$

$$\mathbf{x}(L+1) \;\in\; [\alpha_{\text{low}}, \; \alpha_{\text{up}}], \quad \text{case SFR}, \tag{6.1c}$$

$$\mathbf{x}(L+1) \;\in\; [\beta_{\text{low}}, \; \beta_{\text{up}}], \quad \text{case FFR}. \tag{6.1d}$$

In the optimization problem (6.1), $\mathbf{f}(\mathbf{x})$ determines the objective space that includes the performance criteria previously introduced: average cell capacity (f_1), cell edge capacity (f_2), and transmitted power (f_3). The constants ψ_{low}, ψ_{up}, α_{low}, α_{up}, β_{low}, and β_{up} are used to define the domain of the design variables, and hence, the set $\mathcal{X}$.

The connection of the objective functions and design variables is as follows: the classification threshold (ψ_{TH}) (optimized at each cell) controls the tradeoff between f_1 and f_2. In general, an increment of ψ_{TH} increases the network spectral efficiency (f_1) but reduces fairness among users, and hence, the capacity of worst regions, thus penalizing f_2. In both cases (SFR and FFR) f_3 is strictly linked to the global design variable (α or β). While an increment of α or β favors f_1, decrementing such variables tend to favor f_2. Therefore, there is a close interconnection among objective functions and design variables. The mathematical definition of the objective functions is provided in the next section.

6.3 System Model

The system model is the one presented in Appendix C, Section C.1. Moreover, it includes most of the formulations corresponding to the statistical framework explained in Section 3.3.2.

For the sake of modularity, a functional nomenclature is used. Thus, the following functions, summarized in Table 6.1, are defined:

- *Average SINR.* The function `AvgSINR()` determines average SINR figures and it is represented by the operation corresponding to (3.27).
- *Type of Server.* The process of determining the type of serving cell of each pixel is done according to (3.28) and it is performed by the function `TypeOfServer()`.
- *Pixel Classification.* The process of determining the class of each pixel is done as it is described in Section 3.3.1. Thus, a pixel is classified as exterior ($\mathcal{E}$) if its average SINR (ψ_{u}) is smaller than the classification threshold (ψ_{TH}), i.e., $\psi_{\mathrm{u}} < \psi_{\mathrm{TH}}$, otherwise, the pixel is classified as interior ($\mathcal{I}$). Recall that in the framework presented herein, the classification threshold is cell-specific and it is indicated in the optimization vector $\mathbf{x}$ (see Figure 6.1). This process is defined in 'Classification of Pixels' (Subsection 3.3.2), and it is represented by the function `Class()`.
- *Relative Coverage.* This process is described in 'Coverage per Class and Cell' (Subsection 3.3.2), and it is represented by the function `RelCov()`.
- *Characteristic Matrices.* The function `CharacMat()` determines the characteristic matrices according to (3.32) and (3.35).
- *Segmentation.* The function `Segmentation()` performs the segmentation procedure as described in 'Segmentation' (Subsection 3.3.2).
- *Link Performance.* The function `LinkPer()` applies the link performance model according to (3.37) as it is described in 'Link performance' (Subsection 3.3.2).
- *Bandwidth allocation.* The function `Bandwidth()` determines the bandwidth allocation of each class according to (3.38) and (3.39), as it is described in 'Bandwidth computation' (Subsection 3.3.2).
- *Pixels rate.* The function `PixRate()` determines the rate obtained by each pixel (3.44) according to the iterative process described in 'Pixels rate' (Subsection 3.3.2), i.e., computing (3.40), (3.41), (3.42), and (3.43) for each $j \in \{0, 1, 2\}$.
- *Sorting.* The function `Sort()` sorts a vector that is passed as argument in ascending order.
- *Sum of the first k elements.* The function `Sum()` determines the sum of the first k elements of a vector that is passed as argument.

Table 6.1: Summary of the functions used in Static ICIC optimization.

Function	Reference
`AvgSINR()`	Eq. 3.27 in 'Average SINR' (Subsection 3.3.2).
`TypeOfServer()`	Eq. 3.28 in 'Server Classification' (Subsection 3.3.2).
`Class()`	Section 3.3.1 and 'Classification of Pixels' (Subsection 3.3.2).
`RelCov()`	'Coverage per Class and Cell' (Subsection 3.3.2).
`CharacMat()`	Eq. 3.32 and 3.35 in 'Characteristic Matrices' (Subsection 3.3.2).
`Segmentation()`	'Segmentation' (Subsection 3.3.2).
`LinkPer()`	Eq. 3.37 in 'Link performance' (Subsection 3.3.2).
`Bandwidth()`	Eq. 3.38 and 3.39 in 'Bandwidth computation' (Subsection 3.3.2).
`PixRate()`	Eq. 3.40, 3.41, 3.42, and 3.43 in 'Pixels rate' (Subsection 3.3.2).
`Sort()`	Section 6.3.
`Sum()`	Section 6.3.
`NormPow()`	Eq. 6.2 and 6.3.
`ObjFunc()`	Algorithm. 6.1.

- *Normalized power consumption.* The function `NormPow()` determines the normalized power consumption ($f_3 \in (0,\ 1]$) as a function of β and α as follows:

$$f_3 = \alpha \cdot \beta + (1-\beta)\,, \qquad \text{for SFR,} \tag{6.2}$$

$$f_3 = \alpha \cdot \beta + ((1-\beta)/3)\,, \qquad \text{for FFR.} \tag{6.3}$$

- *Objective Functions.* The procedure for computing the objective functions (f_1, f_2, and f_3, see Section 6.2) for each possible NOP ($\mathbf{x} \in \mathbb{R}^{L+1}$) is represented by the function `ObjFunc()`. The pseudo-code shown in Algorithm 6.1 indicates the exact procedure and it is explained in the next subsection.

6.3.1 Objective Functions

Algorithm 6.1 determines for every single SFR/FFR configuration ($\mathbf{x} \in \mathbb{R}^{L+1}$), the objective vector $\mathbf{f}$. This is done according to the system model presented in Appendix C (Section C.1) and the framework introduced in Subsection 3.3.2.

The steps 1 to 7 correspond to preliminary computations that are based on the functions previously introduced. The goal is determining the rate at pixel level (the vector $\mathbf{r} \in \mathbb{R}^{A}$). In lines 8 to 10, the objective functions are calculated. The average cell capacity (f_1) is calculated by dividing the total aggregate capacity by the number of cells in the system (L). The objective function f_2 that corresponds to the aggregate capacity of the worst 5% pixels is obtained through the function `Sum()`, and finally, the normalized power consumption (f_3) is computed according to (6.2) and (6.3), by means of the function `NormPow()`. The objective vector ($\mathbf{f}$) is returned in line 12.

Algorithm 6.1: Objective functions in static ICIC optimization

Inputs :
$\mathbf{x}(1:L)$: The L classification thresholds. See Figure 6.1.
α, β: Power ratio and bandwidth sharing ($\mathbf{x}(L+1)$). See Figure 2.9.
$\mathbf{P}_{\text{ser}}$ and $\mathbf{P}_{\text{int}}$: Characteristic matrices. See (3.32) and (3.35).
$\mathbf{\Psi}_{\text{u}}$: Average SINR vector. See 3.27.
$\mathbf{G}_j$, $\mathbf{S}_j$, and $\mathbf{S}_j^{\text{c}}$: Segmented matrices.
B, L, and A: System bandwidth, number of cells, and number of pixels.

Output :
$\mathbf{f}$: Objective vector.

```
// Preliminary computations
```

1 $\mathbf{B} \leftarrow$`Bandwidth(`β, B`);` `/* Bandwidth allocation */`
2 $\mathbf{C} \leftarrow$`Class(`$\mathbf{\Psi}_{\text{u}}, \mathbf{x}(1:L)$`);` `/* Pixel classication */`
3 $\mathbf{C}_j \leftarrow$`Segmentation(`$\mathbf{C}$`);` `/* For` $j = 1, 2, 3$. `*/`
4 $\mathbf{\Phi} \leftarrow$`RelCov(`$\mathbf{S}_j$, $\mathbf{C}_j$`);` `/* For` $j = 1, 2, 3$. `*/`
5 $\mathbf{r} \leftarrow$`PixRate(`$\mathbf{B}$, $\mathbf{P}_{\text{ser}}$, $\mathbf{P}_{\text{int}}$, $\mathbf{G}_j$, $\mathbf{S}_j$, $\mathbf{S}_j^{\text{c}}$`);` `/* Rate of each pixel */`
6 $\mathbf{r} \leftarrow$`Sort(`$\mathbf{r}$`);` `/* Sorting (ascending order) */`
7 $k \leftarrow \lceil 0.05 \cdot A \rceil$; `/* Number of 'cell edge pixels' */`

```
// Objective functions
```

8 $f_1 \leftarrow (\mathbf{r} \cdot \mathbf{1})/L$; `/*` f_1`: average cell capacity */`
9 $f_2 \leftarrow$`Sum(`$\mathbf{r}$, k`);` `/*` f_2`: cell edge aggregate capacity */`
10 $f_3 \leftarrow$`NormPow(`α, β`);` `/*` f_3`: normalized power consumption */`

```
// Objective vector
```

11 $\mathbf{f} \leftarrow [\ -f_1,\ \ -f_2,\ \ f_3\ ]$;
12 **return** $\mathbf{f}$;

6.4 Multiobjective Optimization of SFR and FFR

Once defined the method to compute the objective functions (f_1, f_2, and f_3), (6.1) is solved by means of MOEAs. To be precise, by means of the algorithms NSGA-II or SPEA 2 (or both). The proposed framework can be used for both SFR and FFR, just taking into account the particularities of each scheme as it is explicitly indicated. For instance, (3.33) vs. (3.34), (3.38) vs. (3.39), and (6.2) vs. (6.3).

Algorithm 6.2 shows the procedure. Lines 1 to 4 perform preliminary computations. In line 1, the function `PerCellCov()` determines the coverage of each cell according to (C.1) and (C.2) (Appendix C). The average SINR estimation that is required to classify pixels as exteriors ($\mathcal{E}$) or interiors ($\mathcal{I}$) is done in line 2 by means of the function `AvgSINR()` (see Table 6.1). In lines 3 and 4, the functions `TypeOfServer()` and `Segmentation()` determine the type of serving cell of each pixel and perform the segmentation of the matrices $\mathbf{G}$, $\mathbf{S}$, and $\mathbf{S}^{\text{c}}$, respectively. Both procedures appear in Table 6.1.

Algorithm 6.2: Multiobjective framework for static ICIC optimization

Inputs :

Z: Pareto Front estimation. ('0' for NSGA-II, '1' for SPEA 2, '2' for both).
B: System bandwidth.
$P_{\max}$: Available power per cell.
L: Number of cells.
A: Number of pixels in the coverage area.
σ^2: Noise power.
α_{low}, α_{up}, β_{low}, β_{up}, ψ_{low}, ψ_{up}: Design variables bounds.
$\mathcal{O}_{\text{NSGA-II}}$, $\mathcal{O}_{\text{SPEA 2}}$: Configuration of MOEAs.
$\mathbf{p}_{\text{CS-RS}}$: Vector with the power of CS-RS at each cell.
$\mathbf{v}_\phi$: Vector with the azimuth of each cell.
$\mathbf{G}$: Long term channel gain matrix.

Output:

$\mathcal{X}^\star$: Estimated set of nondominated solutions.

```
// Preliminary computations
S, S^c ←PerCellCov(G, p_CS-RS);   /* Per-cell coverage. See Section C.1. */
Ψ_u ←AvgSINR(σ^2, p_CS-RS, G, S, S^c) ;   /* Average SINR. See Table 6.1. */
t ←TypeOfServer(v_φ, S);          /* Type of serving cell. See Table 6.1. */
{G_j, S_j, S_j^c} ←Segmentation(G, S, S^c); /* Segmentation. See Table 6.1. */

// Estimation of nondominated solutions through MOEAs
if Z = 0 then
    X*_NSGA-II ←NSGA-II(O_NSGA-II);          /* NSGA-II. See Section 5.4. */
    X*_SPEA-2 ← ∅;
end
if Z = 1 then
    X*_NSGA-II ← ∅;
    X*_SPEA-2 ←SPEA-2(O_SPEA-2);             /* SPEA 2. See Section 5.5. */
end
if Z = 2 then
    X*_NSGA-II ←NSGA-II(O_NSGA-II);          /* NSGA-II. See Section 5.4. */
    X*_SPEA-2 ←SPEA-2(O_SPEA-2);             /* SPEA 2. See Section 5.5. */
end
X* ←MergePF(X*_NSGA-II ∪ X*_SPEA-2);     /* Set of nondominated solutions. */
```

The estimation of the set of nondominated solutions ($\mathcal{X}^\star$) is done depending on the choice of the decision variable Z. Thus, for $Z = 0$ or $Z = 1$, the set of nondominated solutions is obtained by means of the algorithm NSGA-II or SPEA 2, respectively. This was the initial approach of the research. It was observed that while SPEA-2 provides better distribution of the estimated Pareto Front, NSGA-II is able to achieve better convergence, but only in certain regions of the objective space. Details are provided in the next section. Thus, based on these differences,

the possibility of combining both algorithms was investigated. This corresponds to the option $Z = 2$. If $Z = 2$, the estimation is done by using both algorithms and merging the output of each one (the sets $\mathcal{X}^{\star}_{\text{NSGA-II}}$ and $\mathcal{X}^{\star}_{\text{SPEA 2}}$) by means of the function `MergePF()` as it is indicated in line 17. This function returns a set of Pareto efficient solutions taken from the set that is passed as argument, in this case $\mathcal{X}^{\star}_{\text{NSGA-II}} \cup \mathcal{X}^{\star}_{\text{SPEA-2}}$. This is done by applying the Pareto dominance notion (Section 5.2).

In this manner, the novel approach introduces the idea of using both MOEAs to take advantage of the best features of each of them. Both sets, $\mathcal{X}^{\star}_{\text{NSGA-II}}$ and $\mathcal{X}^{\star}_{\text{SPEA 2}}$ are, by definition, composed of nondominated solutions, but the union of them could contain dominated individuals. Indeed, it is reasonable to expect that, for $Z = 2$, $|\mathcal{X}^{\star}| > |\mathcal{X}^{\star}_{\text{NSGA-II}}|$, $|\mathcal{X}^{\star}| > |\mathcal{X}^{\star}_{\text{SPEA 2}}|$, and $|\mathcal{X}^{\star}| < |\mathcal{X}^{\star}_{\text{NSGA-II}}| + |\mathcal{X}^{\star}_{\text{SPEA 2}}|$. Hence, the option of employing both algorithms offers obtaining more SFR/FFR (Pareto efficient) configurations for the same computational cost. The satisfactory results shown in the next section demonstrate the effectiveness of this new method. Real- and discrete-valued design variables are considered to further illustrate the versatility of the proposed framework.

6.5 Performance Evaluation

In this section, the setting used in numerical evaluations is presented. Subsection 6.5.1 describes the network parameters, configuration of evolutionary algorithms, and the cellular scenario. The reference schemes (benchmarks) are introduced in Subsection 6.5.2. The numerical results corresponding to the optimization of SFR and FFR are analyzed in Subsections 6.5.3 and 6.5.4, respectively.

6.5.1 Settings and Test Case

The set of parameters used in numerical evaluations together with the configuration of the evolutionary algorithms are shown in Table 6.2. A discussion on calibration aspects is provided in Subsection 6.6.1 to explain the calibration process and provide practical guidelines.

In order to prove the effectiveness of the proposed multiobjective framework, a realistic deployment is considered. The test case is the scenario 'MORANS' that is defined in Appendix B (Subsection B.1.2).

6.5.2 Benchmarks and Reference Cases

In order to provide a good perspective of the merit of the proposed framework, this strategy is compared with a wide set of reference schemes including classic resource allocation patterns, baseline SFR/FFR designs, and existing approaches from the literature. The benchmarks are described next.

Table 6.2: Evaluation setting and MOEAs configuration

Network settings and parameters	
Available power per cell	43.00 dBm
System bandwidth (B)	5.40 MHz
Number of cells (L)	60
Number of pixels (A)	288750
CS-RS power ($\mathbf{p}_{\text{CS-RS}}(l)$, $l = 1, 2, \cdots, L$)	18.4 dBm
Bandwidth sharing (β) in SFR optimization	2/3
Power ratio (α) in FFR optimization	0.40
MOEAs configuration	
Population size	600
Max number of generation	2000
Crossover probability	1.0
Mutation probability	$1/(L+1)$=1/61
Termination criterion: relative gain in each f_i	$< 0.01\%/40$ generations
Design variable bounds: ψ_{TH}	[-4.00 8.00] [dB]
Design variable bounds: α (SFR optimization)	[0.15 0.50]
Design variable bounds: β (FFR optimization)	[0.30 0.50]

- *Full reuse* ($\mathbf{x}_{\text{FR}}$): or reuse factor 1, each cell transmits full power over the whole system bandwidth, i.e., full frequency reuse (see FR1 in Figure 2.8). It is worth saying that, 1) this is a common configuration used in real-world deployments, and 2) this benchmark is very often the only one used in related works [63, 250, 251]. Note that user classification is not required in this scheme.

- *Reuse factor* 3 ($\mathbf{x}_{\text{R3}}$): Each cell transmits the available power over a third part of the system bandwidth (see FR3 in Figure 2.8). User classification is not required in this scheme.

- SFR/FFR - *Class proportionality* ($\mathbf{x}^x_{\text{CP}}$): A common SINR threshold (ψ_{TH}) is applied to all cells so that each class has, on average, the same number of users. The average SINR distribution (see the blue curve in Figure 3.15b) is considered to determine ψ_{TH}. Several configurations have been considered and they are indicated by the superindex x.

- SFR/FFR - *Bandwidth proportionality* ($\mathbf{x}^x_{\text{BP}}$): The SINR threshold (ψ_{TH}) guarantees that the number of pixels in each class is proportional to its bandwidth. Similarly to class proportionality, ψ_{TH} holds for all cells and it is computed based on the average SINR distribution of the whole network. Several configurations have been considered and they are indicated by the superindex x.

- *Subband Allocation* ($\mathbf{x}^x_{\text{SA}}$): It corresponds to the best configurations found by means of the subband allocation (local-search-based) algorithms proposed

Table 6.3: Benchmarks configuration and performance.

Scheme	K	α **or** β (SFR/FFR)	ψ_{TH} [dB]	f_1 [Mbps]	f_2 [Mbps]	f_3
Classic configurations						
$\mathbf{x}_{\text{FR}}$	1	NA	NA	9.81	5.70	1.00
$\mathbf{x}_{\text{R3}}$	3	NA	NA	7.40	3.82	1.00
SFR configurations						
$\mathbf{x}_{\text{CP}}^{1}$	3	0.45	3.60	10.97	5.03	0.630
$\mathbf{x}_{\text{CP}}^{2}$	3	0.40	3.60	10.84	5.17	0.600
$\mathbf{x}_{\text{BP}}^{1}$	3	0.46	0.90	9.04	6.73	0.640
$\mathbf{x}_{\text{BP}}^{2}$	3	0.41	0.90	8.92	6.67	0.610
$\mathbf{x}_{\text{SA}}^{1}$	3	0.20	3.00	9.90	6.60	1.000
$\mathbf{x}_{\text{SA}}^{2}$	3	0.50	5.00	12.33	4.09	1.000
$\mathbf{x}_{\text{SA}}^{3}$	4	0.15	2.00	9.69	6.74	1.000
$\mathbf{x}_{\text{SA}}^{4}$	4	0.50	5.00	13.44	3.25	1.000
FFR configurations						
$\mathbf{x}_{\text{BP}}^{1}$	3	0.50	-0.92	7.70	8.16	0.367
$\mathbf{x}_{\text{BP}}^{2}$	3	0.40	-0.08	7.60	7.84	0.360
$\mathbf{x}_{\text{BP}}^{3}$	3	0.33	0.69	7.51	7.65	0.355
$\mathbf{x}_{\text{BP}}^{4}$	3	0.25	1.92	7.64	7.26	0.350
$\mathbf{x}_{\text{SA}}^{1}$	3	0.35	2.00	9.85	5.50	0.425
$\mathbf{x}_{\text{SA}}^{2}$	4	0.35	1.00	8.94	7.03	0.369
$\mathbf{x}_{\text{SA}}^{3}$	4	0.40	0.00	8.03	8.35	0.471

in [63] and [64] for SFR and FFR, respectively. It is worth saying that since these algorithms require as input the number of subbands K, α or β, and ψ_{TH}, more than 150 trials[2] were required to find the configurations achieving the best results. Several configurations have been considered and they are indicated by the superindex x.

The configuration and performance of the benchmarks in terms of f_1, f_2, and f_3 are shown in Table 6.3.

6.5.3 Numerical Results: SFR Optimization

In this subsection, the results corresponding to the optimization of SFR through Algorithm 6.2 are presented. In particular, the novel approach that considers the

[2]The search space was obtained after an initial trial and error procedure required to localize the region of interest, i.e., $K \in \{3, 4\}$, $\psi_{\text{TH}} \in \{-3, -2, \cdots, 6\}$ [dB], $\alpha \in \{0.05, 0.10, \cdots, 0.60\}$, and $\beta \in \{0.15, 0.10, \cdots, 0.60\}$.

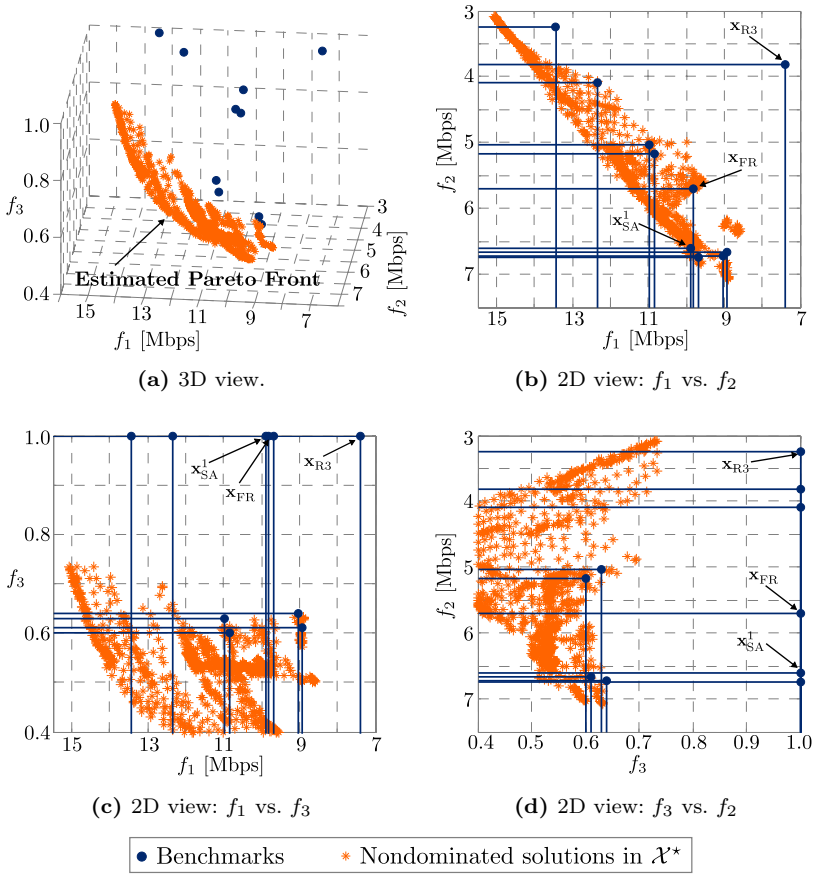

(a) 3D view.

(b) 2D view: f_1 vs. f_2

(c) 2D view: f_1 vs. f_3

(d) 2D view: f_3 vs. f_2

Figure 6.2: Representations of the estimated Pareto Front.

parallel use of two different MOEAs (NSGA-II+SPEA 2) is considered at this instance.

Figure 6.2 shows 3D and 2D visualizations of the estimated Pareto Front ($\mathcal{X}^\star$). Recall that each element of $\mathcal{X}^\star$ represents a Pareto efficient SFR configuration, meaning that no improvement can be made on an objective function without worsen at least another one. In the figure, the images of the nondominated solutions and reference schemes are represented by orange starts and blue circles, respectively.

Figure 6.2a provides a 3D representation of the estimated Pareto Front, from which it can be seen that the benchmarks are all behind the surface created by the images of the elements in $\mathcal{X}^\star$. Given that the convex shape of the Pareto Front points to regions where better values of f_1, f_2, and f_3 are located, the result gives a first insight about the excellent quality of the solutions.

In order to provide a better qualitative perspective of the improvement that can

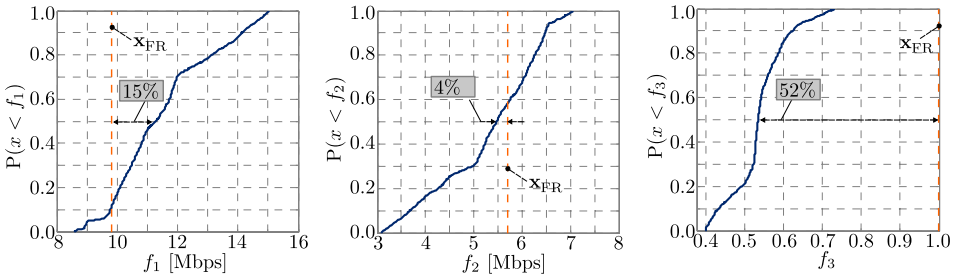

(a) Average cell capacity. **(b)** Cell edge capacity. **(c)** Norm. power consumption.

Figure 6.3: CDF of objective functions of the elements in $\mathcal{X}^\star$.

be achieved, 2D profiles are shown in Figures 6.2b, 6.2c, and 6.2d, for each possible pair of objective functions. 2D profiles are generated by projecting the Pareto Front onto the f_1-f_2, f_1-f_3, and f_2-f_3 planes. They are an alternative representation providing better insights about the tradeoff between each pair of objective functions. In this manner, the operator can decide how much loss in terms of one metric is traded by a more significant gain in terms of another one. For instance, Figure 6.2c shows that small losses in terms of f_1 allow significant energy savings (f_3) while, Figure 6.2b indicates a more linear relationship between f_1 and f_2.

Note that from the perspective of each pair of objective functions, there exist dominated solutions. This is due to the fact that the Pareto dominance is applied considering all the metrics: f_1, f_2, and f_3. In any case, the 2D profiles clearly show that Algorithm 6.2 always succeeds in finding SFR configurations dominating each reference scheme from the perspective of each pair of objective functions. Thus, the intersection of the set of solutions dominating each benchmark in each 2D profile is the set of solutions dominating that reference scheme in the Pareto sense.

Focusing on the spectral efficiency vs. cell edge performance tradeoff (Figure 6.2b), it can be seen that most of the reference cases only offer tradeoffs (improve one performance metric by paying a price in another one) with respect to full reuse ($\mathbf{x}_{\mathrm{FR}}$). However, it is possible through the proposed algorithm to find SFR configurations dominating $\mathbf{x}_{\mathrm{FR}}$, i.e., improving simultaneously all performance metrics. This is very important, because it means that **there is no point in employing full frequency reuse instead of optimized SFR configurations** in the context of realistic deployments. Note that the scheme represented by $\mathbf{x}^1_{\mathrm{SA}}$ (indicated in the figures) is also strictly superior to $\mathbf{x}_{\mathrm{FR}}$ and it is very close to the Pareto Front. However, it is still dominated by some SFR configurations in the set $\mathcal{X}^\star$ in terms of f_1 and f_2, and it is clearly outperformed in terms of energy consumption (see 2D profiles including f_3). Thus, the SFR settings obtained by means of Algorithm 6.2, not only improve all reference cases from the perspective of spectral efficiency and cell edge performance, but also do it reducing the energy consumption.

Figures 6.3 provide a first quantitative point of view of the gains. The CDFs of the objective functions (obtained by means of the elements of $\mathcal{X}^\star$) are shown in

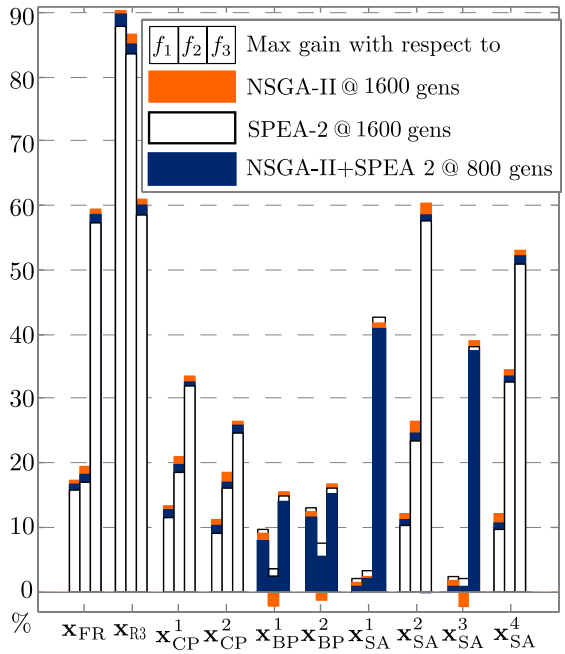

Figure 6.4: Gains obtained by the elements of $\mathcal{X}^\star$.

Figures 6.3a, 6.3b, and 6.3c. This representation is a convenient way of looking at the improvement with respect to any reference case or benchmark. In the figure, the important case of full reuse is shown. The results basically tell that, randomly selecting a solution from the set $\mathcal{X}^\star$ results in an average gain of 15% and 52% with respect to f_1 and f_3, respectively. The average loss of 4% with respect to f_2 just means that in $\mathcal{X}^\star$ there are more solutions with worse values of f_2 than $\mathbf{x}_{\mathrm{FR}}$. Nevertheless, it is important that all the benchmarks are dominated by a non-empty set of SFR configurations, and hence, a mobile operator can select solutions according to its needs. Moreover, obviously the design variable bounds can be redefined to focus the exploration in a certain region of the search space $\mathcal{X}$. The CDFs show the widespread of the estimated Pareto Front, i.e., $f_1 \in [8.5,\ 15]$ (in Mbps), $f_2 \in [3.0,\ 7.0]$ (in Mbps), and $f_3 \in [0.4,\ 0.73]$.

In order to have another quantitative perspective, Figure 6.4 shows average gains that can be achieved by means of the proposed scheme using both MOEAs (option $Z = 2$ in Algorithm 6.2), and each MOEA independently (options $Z = 0$ and $Z = 1$ in Algorithm 6.2). In order to make a fair comparison, the number of generations for NSGA-II and SPEA 2 was doubled with respect to the hybrid case (NSGA-II+SPEA 2). The figure shows the maximum gain in terms of each metric (f_1, f_2 and f_3) and with respect to each benchmark. Note that, after 800 generations[3], the extra gain by running NSGA-II (or SPEA 2) for 800 additional generations is

[3]As it will be shown later on, 800 generations suffices, on average, to fulfill the termination criterion.

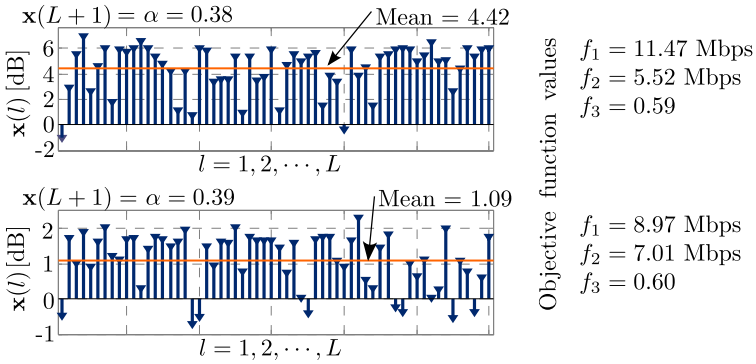

Figure 6.5: Representation of two solutions in $\mathcal{X}^{\star}$.

typically quite small, within 2%. Note that there are benchmarks the algorithm NSGA-II was unable to outperform ($\mathbf{x}^1_{\text{BP}}$, $\mathbf{x}^2_{\text{BP}}$ and $\mathbf{x}^3_{\text{SA}}$), as the performances of these reference cases are located in the boundaries of the Pareto Front. Nowever, these *extreme* solutions are outperformed by SPEA-2 which is able to achieve better diversity than NSGA-II due to its excellent diversity-preserving mechanism.

In the light of the previous results, it was decided to investigate a novel approach based on the joint use of NSGA-II and SPEA-2 by means of the Pareto dominance notion. As the results shown in Figure 6.4 confirm, this method allows **obtaining the best properties of each algorithm** without increasing the computational cost. While NSGA-II is well-known for its excellent convergence, SPEA 2 provides good diversity [228]. Therefore, it is concluded that the performance of the hybrid scheme (NSGA-II+SPEA 2) is superior to the one of each MOEA because it outperforms (without exception) all the benchmarks. Thus, by sacrificing a marginal gain in terms of convergence that is quantified shortly, the hybrid scheme is able to obtain a wide- and well distributed Pareto Front. In addition, the hybrid approach increases significantly the number of nondominated solutions for the same computational cost, this is also quantified shortly.

It is worth noting that, in most of the cases, the gains obtained by the scheme NSGA-II+SPEA 2 at 800 generations are still greater than the ones achieved by SPEA-2 at 1600 generations due to the excellent convergence of NSGA-II at 800 generations. This clearly shows the potential benefit of the proposed scheme as a mean to improve the convergence vs. diversity synergy through the joint use of NSGA-II and SPEA 2.

Focusing on the features of the SFR settings obtained through Algorithm 6.2, Figure 6.5 shows the structure of two elements of $\mathcal{X}^{\star}$. As mentioned before, every single solution is composed of L classification thresholds (one for each cell) plus a global SFR power ratio α. Recall that every SFR configuration belonging to $\mathcal{X}^{\star}$ is, by definition, Pareto efficient, and hence, selecting another element in $\mathcal{X}^{\star}$ always implies a tradeoff. The figure illustrates how different SFR settings featuring more or less the same energy requirement attain different goals. While the upper solution enhances

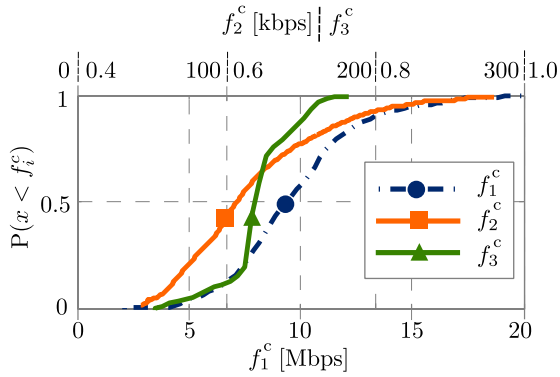

Figure 6.6: Per-cell stattistics: solutions in $\mathcal{X}^\star$.

28% the system capacity with respect to the solution below, the latter increases 27% the capacity in the worst percentile 5 of the coverage area. Nevertheless, in this case, only the upper configuration dominates $\mathbf{x}_{\text{FR}}$, while the lower one only brings a tradeoff. In addition, an increment of the classification thresholds (orange lines indicate mean values) favors, on average, spectral efficiency and penalizes cell edge performance. Thus, the upper configuration outperforms the one below in terms of f_1, while the latter dominates the former in terms of f_2. This goes in line with previous results reported in [45].

Another important point of view is the performance at cell level. Figure 6.6 shows the statistic of *cell-level* versions of f_1, f_2, and f_3: f_1^c, f_2^c, and f_3^c, respectively. In this case, a wide range of values is also obtained for these metrics ($f_1^c \in (2.5,\ 20)$ [Mbps] and $f_2^c \in (60,\ 285)$ [kbps]). Based on these CDFs, it can be concluded that the proposed algorithm is able to find different SFR profiles, all of them achieving network-wide (f_1, f_2, and f_3) gains and different performance at cell level. The fact that the results at cell level can be suboptimal is not necessarily bad because network dynamics (traffic patterns) change from one cell to another, and therefore, having multiple solutions is desirable from a practical standpoint. As it was mentioned, this particular feature of the proposed multiobjective optimization framework becomes one of its major strengths, i.e., it provides mobile operators with a set of pre-calculated SFR operational points that can be applied as required without any *online* computational cost nor heavy intercell signaling overhead.

It is important to stress that global optimization gains come from the fact that the proposed algorithm takes advantage of the differences among cells, and thus, it is expected that higher gains are more feasible under quite unbalanced conditions, otherwise, optimization makes no sense and it is not feasible.

If minimum performances at cell level are required, the proposed methodology allows for any of the following approaches:

- ✓ Selecting elements of $\mathcal{X}^\star$ whose objective function values at cell level are within desired limits,

- ✓ adjusting variable bounds in (6.1) to further localize the stochastic search of the MOEAs, or
- ✓ applying the 'Method of Inequalities' [252], in which an interval of interest is defined as a goal range $[f_{i,\text{low}},\ f_{i,\text{up}}]$ for each objective function f_i. However, this would require to evaluate each performance metric for each cell, and hence, it would increase the overall complexity/cost.

6.5.4 Numerical Results: FFR Optimization

In order to illustrate the versatility of the proposed framework, the results corresponding to the optimization of FFR are presented for the case where only one MOEA is used. The conclusions on the comparative between NSGA-II and SPEA 2 (the cases $Z = 0$, $Z = 1$, and $Z = 2$) are extensible to the case of FFR optimization. Thus, for the sake of brevity, the use of NSGA-II ($Z = 0$) is considered herein.

As it was done in Figure 6.2, now Figure 6.7 shows 3D and 2D representations of the estimated Pareto Front. A similar analysis also holds for this case. The proposed scheme is able to find solutions dominating each benchmark from the perspective of each pair of objective functions in a strict sense, i.e., improving simultaneously f_1, f_2, and f_3. However, in this case, it is notorious the relative position of the full reuse scheme, which is much above of the Pareto Front (see Figure 6.7b). This means that there are only few solutions (6%) improving $\mathbf{x}_{\text{FR}}$ in terms of average cell capacity (f_1), while most of the elements in $\mathcal{X}^\star$ do outperform $\mathbf{x}_{\text{FR}}$ from the cell edge capacity (f_2) viewpoint. The situation is expected given the bandwidth reduction in FFR. In any case, Algorithm 6.2 is able to find solutions strictly better than $\mathbf{x}_{\text{FR}}$, and thus, the algorithm also shows the potential and feasibility of FFR for realistic deployments with irregular cell layouts.

Figures 6.7c and 6.7d show the 2D profiles in which the energy consumption (f_3) is included. In this case, it is evident that this parameter is much less sensitive to variations of $\beta \in [0.3,\ 0.5]$ than in case of SFR/α. Note that for $\beta = 0$ and $\beta = 1$, $f_3 = 1/3$ and $f_3 = \alpha_{\text{FFR}} = 0.4$. Thus, the range of f_3 is smaller than in case of SFR.

The quantitative point of view is provided in Figure 6.8. The figure shows the maximum gains that can be achieved in terms of each objective function and with respect to each benchmark. As mentioned before, the gains in terms of f_1 with respect to $\mathbf{x}_{\text{FR}}$ are much lower (around 5%) than the ones in terms of f_2 and f_3, which go up to 60% and 65%, respectively. The improvement is even greater in case of $\mathbf{x}_{\text{R3}}$, being the gain in terms of aggregate cell edge capacity of around 70%. The gains with respect to the baseline designs range from 5% and 40% in terms of f_1 and 10% to 65% in terms of f_2. All these gains are always accompanied of reductions that go from 2% to 25% in terms of average power consumption (f_3).

Figure 6.9 shows the statistics corresponding to the elements of the set $\mathcal{X}^\star$. Figures 6.9a, 6.9c, and 6.9e, show the statistics of f_1, f_2, and f_3, respectively. Again the analysis is focused on the important case of full reuse ($\mathbf{x}_{\text{FR}}$), but the same analysis holds for the rest of benchmarks. Figure 6.9a indicates that a random

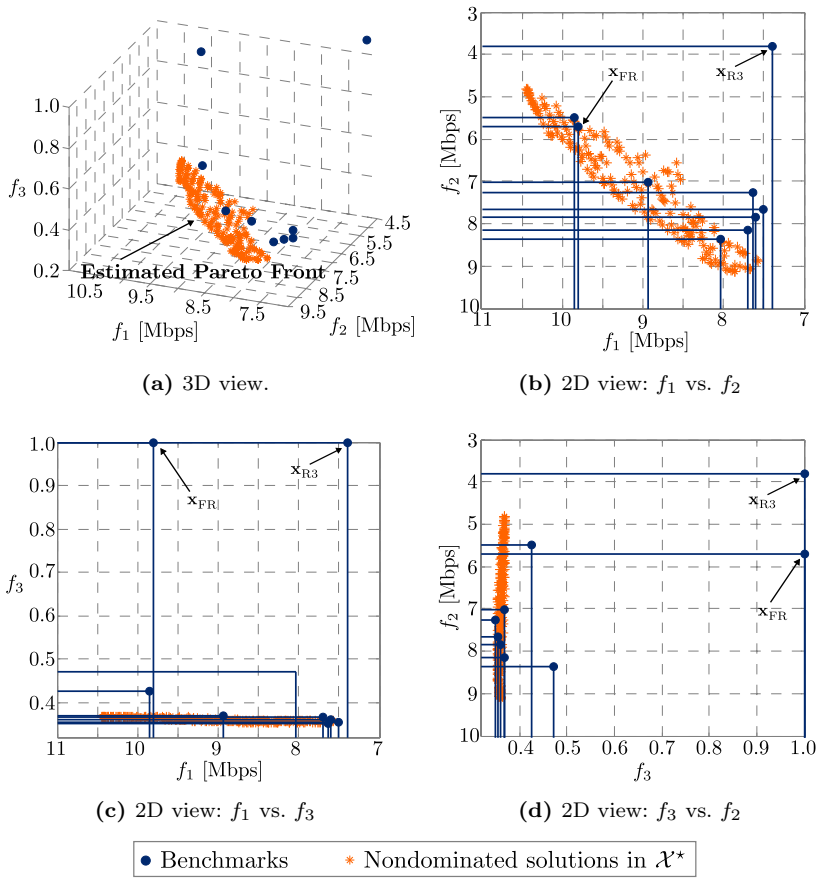

(a) 3D view.

(b) 2D view: f_1 vs. f_2

(c) 2D view: f_1 vs. f_3

(d) 2D view: f_3 vs. f_2

Figure 6.7: Representations of the estimated Pareto Front.

selection of the solutions in $\mathcal{X}^\star$ provides, on average, a loss of 8% in terms of f_1 with respect to $\mathbf{x}_{\text{FR}}$. As it can be seen, only 25% of the elements of $\mathcal{X}^\star$ achieves a higher average cell capacity. Average gains in terms of f_2 and f_3 are in the order of 21% and 64%, respectively.

The corresponding cell-level versions (f_1^c, f_2^c, and f_3^c) are also included and they are shown in Figures 6.9b, 6.9d, and 6.9e (note that the statistic of f_3 is the same statistic than f_3^c). The distribution of β is shown in Figure 6.9f. A very similar loss in terms of cell capacities (f_1^c) is obtained with respect to $\mathbf{x}_{\text{FR}}$ as a consequence of the bandwidth reduction. However, more important from an ICIC point of view, is the average gain of more than 90% in terms of cell edge capacity at each cell, thus confirming the effectiveness of the proposed strategy, also for the case of FFR.

Finally, to close this subsection, the structure of two solutions in $\mathcal{X}^\star$ and its corresponding system and cell level performance are shown in Figure 6.10. It can be seen how two different nondominated solutions result in significantly different

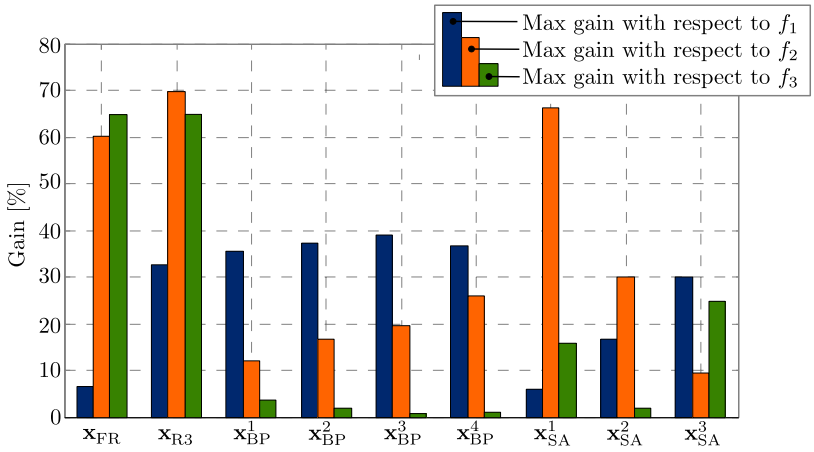

Figure 6.8: Gains obtained by the elements of $\mathcal{X}^{\star}$.

results at cell level. This nondomination relationship does not necessarily holds at cell level because the multiobjective optimization procedure is performed taking into account f_1, f_2, and f_3, but f_1^{c}, f_2^{c}, and f_3^{c}. The figure also indicates average values (orange lines and bold text) in each case. Note that, the upper solution, featuring a higher average classification threshold (ψ_{TH}), favors spectral efficiency, while the one below, with smaller ψ_{TH}, achieves better cell edge performance.

As it can be intuitively inferred from Figure 6.10, it is interesting to study the connections between cell level performances and system oriented metrics. The fact that very dissimilar performance at cell level can result in similar global performances opens the possibility of employing the proposed framework as the starting point of adaptive (low-complexity) ICIC schemes based on SFR or FFR. Given that, according to [253], there are close relationships between multiobjective optimization and multi-agent decision theory, the extension of the framework presented in this thesis seems natural.

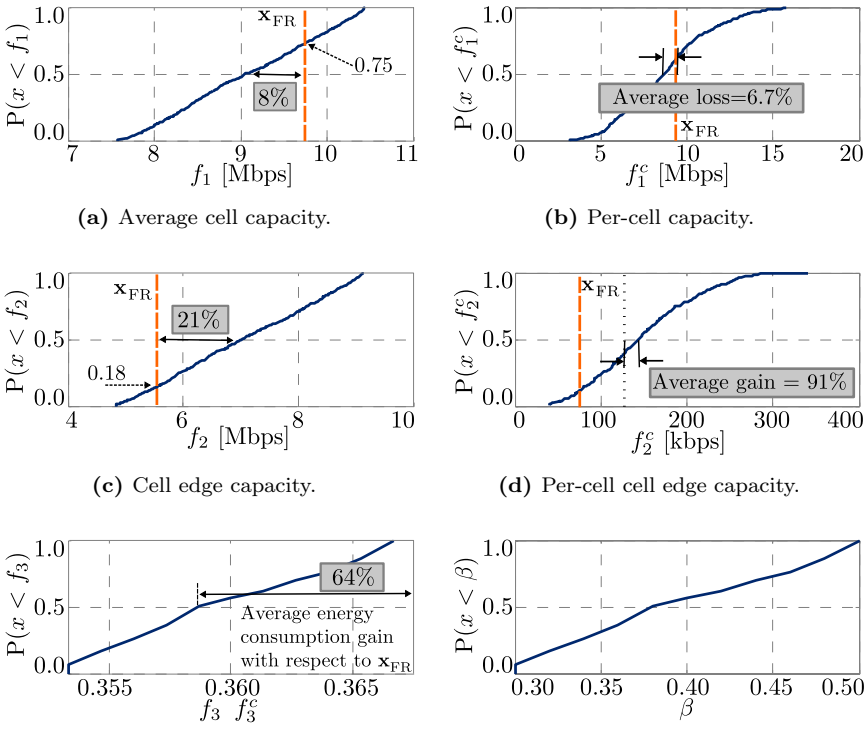

(a) Average cell capacity. **(b)** Per-cell capacity.

(c) Cell edge capacity. **(d)** Per-cell cell edge capacity.

(e) Norm. power consumption. **(f)** Distribution of β in $\mathcal{X}^\star$

Figure 6.9: CDF of objective functions of the elements in $\mathcal{X}^\star$.

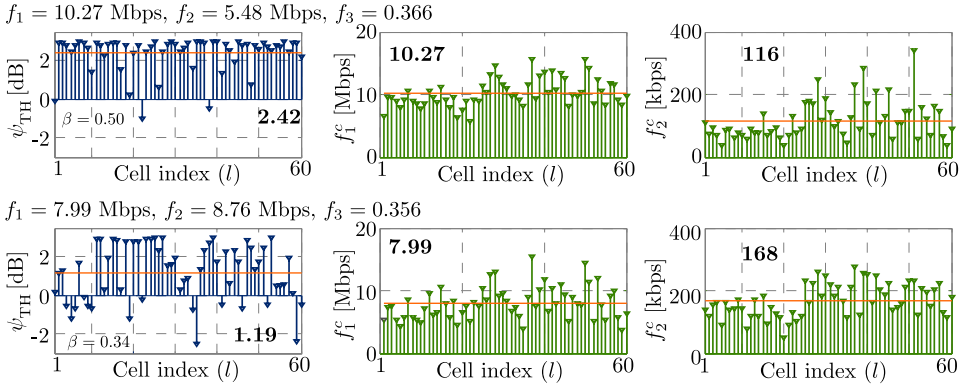

Figure 6.10: Performance of two solutions in $\mathcal{X}^\star$.

6.6 Additional Aspects

The previous section demonstrates the effectiveness and suitability of the novel multiobjective optimization framework in the context of realistic cellular deployments. In addition to those numerical results, additional aspects include the calibration of MOEAs, convergence properties of these algorithms applied to (6.1), feasibility in LTE, and complexity. This section covers all these elements. Most of the discussion apply both to SFR and FFR optimization. Wherever a distinction is required, it will be explicitly indicated.

6.6.1 Calibration of MOEAs

An important aspect of the novel multiobjective optimization scheme is that a calibration is required for the parameters that control the evolutionary algorithms. The objective of this discussion is to give an insight into the matter and derive rules of thumb for an easy adjustment.

Thus, the sensitivity of the results to the inputs (subject to calibration) was studied. These aspects have been investigated considering that, as it was mentioned in Chapter 5, any good MOEA must implement mechanisms to satisfy convergence and distribution requirements.

- ✓ In the context of MOEAs, convergence refers to the ability of the algorithm to get close to the Optimal Pareto Front as soon as possible. Convergence has been speeded up through the use of elitism, a technique by which the algorithm preserves good solutions.

- ✓ The distribution is related to the ability to provide the largest possible set of nondominated solutions and keep them as evenly distributed as possible along the Pareto Front.

The way in which NSGA-II and SPEA 2 implement such desired features is discussed in Chapter 5, however, these mechanisms are summarized in Table 6.4. Thus, the calibration procedure investigates how changes in the parameters that govern the algorithm affect its performance in terms of hypervolume (υ) and nonuniformity index (ϱ), the reader is referred back to Subsection 5.3.2 for their description.

The convergence of MOEAs depends on its operational parameters such as population size, number of generations, crossover and mutation probabilities, crossover and mutation type, and distribution indexes. The following paragraphs aim at highlighting some practical calibration guidelines:

- *Population size*: There is a general consensus about the population size in approaches based on genetic algorithms (such as NSGA-II and SPEA 2). The range to consider during calibration is [20,100] and beyond 100, extra gains are hardly achieved and the same global convergence is obtained [240]. In this sense,

Table 6.4: Main features of NSGA-II and SPEA 2.

	Convergence	**Distribution**
NSGA-II	Nondomination based rank.	Selection based on crowding distance metric.
SPEA-2	Raw fitness assignment process.	Density metric based on distance.

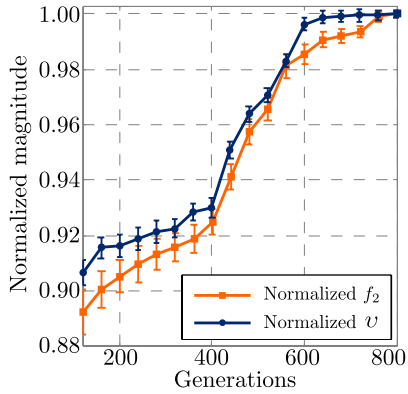

Figure 6.11: Convergence pattern in SFR optimization.

during calibration time it is obtained that the statistical properties of different sets of nondominated solutions (in different executions of the optimization process) converged for a population size of more than 30 individuals. In fact, for sets of cardinality 30, the hypervolume indicator went asymptotically close to a common value and the mean value of nonuniformity was almost constant. Since computation time grows exponentially with this input, the final population size also depends on the problem scale and the computational complexity that can be afforded.

However, in our context: a higher population size allows a smoother Pareto Front, and hence, operators could choose among a more contiguous and denser set of solutions. Thus, taking into account this tradeoff, the results presented herein considered populations of 600 individuals, which surpasses by far any recommendation in the literature.

- *Number of generations and termination criterion*: The number of generations depends on a predefined termination criterion. In this study, the execution of MOEAs finishes when the improvement of each objective function is less than 0.01% after a block of 40 generations. With this approach, the stochastic nature of genetic algorithms is taken into account, thus avoiding a premature termination of the algorithm. This situation could happen if the condition is tested after a small number of generations. Figure 6.11 shows the convergence pattern of Algorithm 6.2 in terms of the slowest objective function (f_2) and the hypervolume indicator (υ). The normalized points in the plot correspond to the average of 50 realizations and error bars are used to represent statistical

reliability [254].

Note that there is a close correlation between the evolution of f_2 and v. This behavior is expected because, as it was explained in Chapter 5, the maximization of the hypervolume is equivalent to the estimation of the Optimal Pareto Front [239]. For the setting employed herein, 800 generations typically suffice to fullfil the termination criterion, but obviously, this figure would vary according to the problem scale (network size) under consideration.

- *Genetic operators*: When real-valued design variables are used, genetic algorithms use simulated binary crossover (see [226, 227, 241, 242]) and polynomial mutation (see [226, 227, 241]) for crossover and mutation, respectively. In case of discrete-valued design variables, Single Point Crossover and Unary Reproduction operators [220] are employed.

  The crossover operator is a key element in the search process, since it defines how flexible the algorithm is to generate new solutions in the search space. On the one hand, simulated binary crossover creates children solutions proportional to the differences in parents, and on the other hand, polynomial mutation uses a certain probability distribution to model the required variations. Both methods require an input denoted as distribution index that is inversely proportional to the creation of children solutions distant to the parents. Thus, distribution indexes are scalars used for tuning both crossover and mutation: n_c and n_m, respectively. These coefficients control the spread of the next generations in the space of solutions, and hence, they govern the convergence-diversity tradeoff of the evolutionary process. Crossover and mutation operators for discrete-valued design variables are simpler and these mechanisms are described in [220].

  In case of highly nonlinear responses, smaller values of crossover and mutation distribution indexes yield good results. The range for this value goes from 0.5 to 500. A value of 20 is selected as a result of a previous calibration process based on small scale experiments, in which the evolution of the hypervolume indicator with the number of generations is analyzed. Figure 6.12 shows average values obtained from 50 independent starting points. As expected, smaller distribution indexes favor better distribution (low nonuniformity). A distribution index of 20 provides the best convergence for the problem under consideration. Indeed, values ranging from 5 to 70 will not have a very different impact. Note that this figure ($n_\mathrm{c} = n_\mathrm{m} = 20$) is the reference value suggested by the creators of the algorithms in their original references [226, 227].

- *Crossover and mutation rate (probabilities)*: These parameters control the rate of evolutionary operations. Recall that 1) crossover is a fundamental process, especially when genetic algorithms preserve elitism, because it guarantees exploring the search space in regions where *good* solutions are more likely to be found, and 2) mutation is an important source of diversity in evolutionary processes.

  Values close to one are suggested in the related literature [226] for crossover rate, while mutation rates around $1/n$, where n is the number of design variables, have been also suggested [226]. In any case, the selection of these parameters

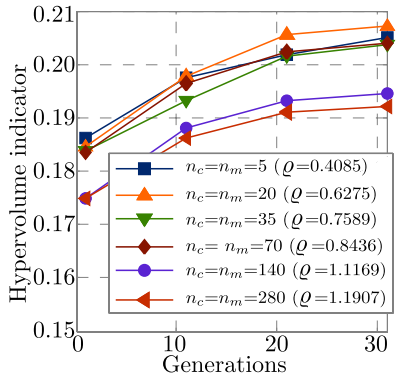

Figure 6.12: Calibration of distribution indexes (SFR optimization).

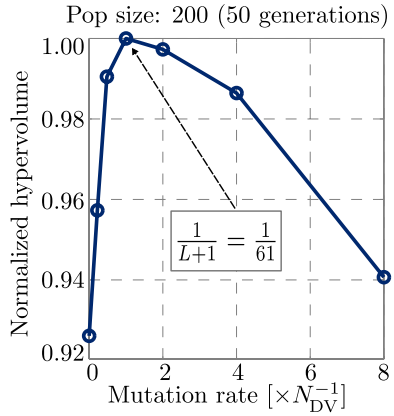

Figure 6.13: Calibration of mutation rate (FFR optimization).

is done following a calibration process. As an example, Figure 6.13 shows the results corresponding to different mutation rate in FFR optimization. Recall that L is number of cells in the network. As it can be seen in the figure, a fine tuning calibration around the reference value $(1/(L+1))$ implies a marginal differences of around 1% in the case of NSGA-II. Thus, one can conclude that the recommendations in the literature are suitable for this particular problem, and hence, crossover and mutation rate are set to 1 and $1/(L+1)$, respectively. These values provide good results for the setting presented herein.

6.6.2 Convergence Properties and Statistical Reliability

The convergence is studied by looking at the evolution of the hypervolume indicator. Figure 6.14 shows the evolution of the hypervolume for NSGA-II and SPEA 2 until 1600 generations for the SFR case. This is done in order to make a fair comparison and to show the advantage of the novel approach (NSGA-II+SPEA 2). In this

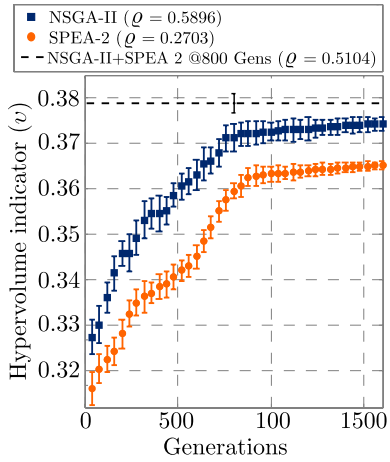

Figure 6.14: Hypervolume evolution and nonuniformity of the Pareto Front

manner, the three cases have the same computational cost in terms of objective function evaluations. The figure also shows the hypervolume figure obtained with the hybrid scheme at 800 generations (when the termination criterion is fulfilled). The experiments were conducted with a population size of 600 individuals. The results represent average values of 50 realizations and error bars are used to represent statistical reliability [254], corresponding to the standard deviation found in each case. It is clear that both algorithms exhibit the expected asymptotic behavior. The ratio between the extra gain (in terms of hypervolume) and the number of additional generations (number of function evaluations) decreases very slowly once a certain quality in the set of solutions is reached. In addition, the legend indicates average nonuniformity figures.

The results show that the average gains in terms of hypervolume are of 0.69% and 3.20% with respect to NSGA-II and SPEA-2, respectively. Since NSGA-II@1600 generations is rather close to Algorithm 6.2 (with $Z = 2$), a statistical analysis is performed to provide further evidence supporting the use of the combined approach.

By using the samples used to estimate the cumulative distribution functions, the Wilcoxon-Mann-Whitney [255] test[4] was performed and the corresponding p-values were obtained (Table 6.5). The results clearly show that the null hypothesis can be rejected in both cases. Indeed, the null hypothesis, i.e., distributions have same median, can be rejected at significance levels much below 0.05, the typical threshold used for statistical significance. Given the previous paragraphs, it can be said that, on average, NSGA-II+SPEA 2@800 generations provides better convergence than NSGA-II@1600 and SPEA-2@1600.

In addition, by means of the merging process based on the Pareto dominance, the hybrid scheme increases the number of nondominated SFR configurations by

[4]Prior to perform Wilcoxon-Mann-Whitney's test, the data was analyzed in order to verify that it does not follow a normal distribution by means of the Shapiro-Wilk's [256] and Kolmogrov-Smirnov-Lilliefors's [257] tests. Normality was always discarded with a significance level of 0.05.

Table 6.5: Wilcoxon-Mann-Whitney's test (U-test).

Test	p-value: Hypervolume	p-value: Nonuniformity
NSGA-II+SPEA 2 vs. NSGA-II	3.30e-10	1.37e-17
NSGA-II+SPEA 2 vs. vs. SPEA-2	7.06e-18	7.06e-18

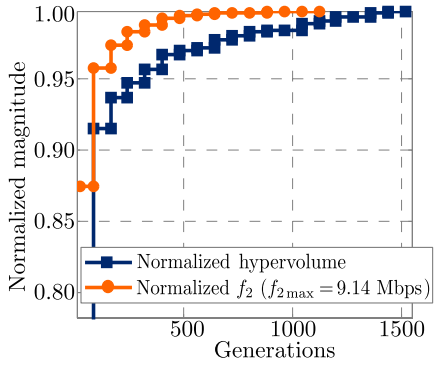

Figure 6.15: Convergence pattern in FFR optimization.

78% (on average). Note that after 800 generations, both NSGA-II and SPEA 2 have an average number of 575 and 581 nondominated solutions respectively. Thus, after merging both sets, through the Pareto dominance notion, an average number of 1068 Pareto efficient configurations is obtained. This represents 78% more than the number of nondominated solutions found by NSGA-II and SPEA-2 after 1600 generations. This is very important from a practical perspective as the improvement of the objective function values is marginal after a certain number of generations. This also explains the gain in terms of hypervolume previously shown.

Finally, Figure 6.15 shows the convergence pattern obtained in FFR optimization. The figure indicates the evolution of the slowest objective function (f_2) and hypervolume indicator (υ). Note that after only 80 generations, both f_2 and υ reached more than 85% of their final value showing excellent convergence, and hence, the accurate calibration of NSGA-II for this problem. It can be seen that after the fulfillment of the termination criterion (typically after 800 generations), the relative improvement in terms of hypervolume is less than 2%, despite that 800 additional generations are run. Therefore, it can be concluded that the ratio between gains and processing cost decreases very fast after the termination criterion meaning that the algorithm reaches a convergence state.

6.6.3 LTE Feasibility and Complexity

Although SFR and FFR are ICIC strategies whose implementation is in essence straightforward, it is advisable to consider the targeted received power when defining the coverage area to be optimized. This is important because SFR and FFR apply some power reduction to the PDSCH in certain parts of the system bandwidth. Besides, since SINR estimations are based on RSs, current values of α must be informed to UEs (by means of user-dedicated signaling [162]) to conveniently take them into account when processing SINR figures and CSI feedback reports (further details are provided in Chapter 4).

Moreover, it is worth saying that, all the processing required to perform the optimization can be done offline.This functionality, is not standardized in the LTE specifications, and hence, it would be an added-value feature that can be offered by vendors.

The complexity of Algorithm 6.2 is mainly set by the complexity associated with the evolutionary mechanisms employed to estimate the Pareto Front. According to [226] and [227], the complexity of NSGA-II and SPEA 2 is $O(MN^2)$ and $O((N + R)^2 \cdot \mathrm{Log}(N + R))$, respectively. The variables N, M, and R correspond to the population size, number of objectives, and the archive size (used to preserve elitism), respectively.

Although, a priori, such complexity looks restrictive, it is important to take into account that after one execution of Algorithm 6.2, the output represents a big set of nondominated (SFR or FFR) configurations. In the stochastic search, near-optimum values for each design variable are found. In contrast, other algorithms such as the one proposed in [63], with an overall complexity bounded by $O(L^2 \cdot K \cdot (K-1)/2)$[5], has the drawback that, since it is local search, global optima cannot be guaranteed, and indeed, a huge number of trials needs to be performed in order to find acceptable results.

Given that these algorithms are different in nature, computational complexity is given in terms of different set of parameters. Therefore, in order to establish some point of comparison, note that in case of Algorithm 6.2, the number of design variables is equal to the number of cells plus one ($N = L + 1$). As it was indicated before, the complexity grows linearly with L. In case of the algorithm proposed in [63], the number of cells L also affects the complexity, but exponentially.

6.7 Concluding Remarks

The performance at cell edges is a critical issue in OFDMA cellular systems such as LTE and LTE-A. In realistic deployments featuring irregular cellular layouts, the performance of baseline design configurations of SFR and FFR and reference schemes such as full reuse is significantly degraded. This chapter presents a novel

[5]Recall that K is the number of subbands in the system bandwidth and that $K-1$ subbands are devoted to cell edges.

multiobjective optimization framework that aims at improving the operation of SFR and FFR in this type of deployments. Given that SFR and FFR constitute the fundamental basis of most static ICIC schemes, the framework is general and easily extensible.

Requiring only commonly available propagation information, the proposed approach is suitable to be applied to any realistic deployment without need for making assumptions on network topology. Moreover, it allows mobile operators to suitably define several performance indicators according to their needs.

The optimization strategy succeeds in finding Pareto efficient configurations enhancing simultaneously all performance metrics with respect to an important group of reference cases, and hence, its effectiveness and suitability has been clearly demonstrated. The main results can be summarized as follows:

- A significant reduction of ICI in cell edge is achieved. This is confirmed by the gains in terms of the capacity of those areas. This is very important because the main target of ICIC techniques is precisely to improve the QoS in zones with low SINR levels. The formulation presented herein optimizes average ICI conditions by means of expressions that consider the resource allocation pattern in SFR and FFR.

- The merit of the proposed scheme is demonstrated as the algorithm is able to find a set of SFR/FFR configurations outperforming schemes existing in the literature, baseline designs, and reference schemes. Moreover, it provides a consistent set of network configurations from which, the operator is able to make a selection according to its needs. Besides, this is done having a clear picture of the different tradeoffs among objectives. As it was mentioned, the methodology by itself opens the door for further research towards SFR/FFR-based adaptive mechanisms.

- The hypothesis formulated in Section 6.1 is verified. Such idea is based on the suitability of the classification threshold (ψ_{TH}) to control the operation of SFR and FFR. This paremater can be adjusted at each cell without impact in terms of ICI at neighbour cells. Thus, it is shown that by adjusting the classification thresholds at cell level, an attractive cost-performance tradeoff is attained. The results also show the suitability of MOEAs in the context of static ICIC optimization, another important conceptual novelty of this research.

- A novel method based on the combination of two different MOEAs is proposed. The approach allows to leverage the best characteristics of each algorithm (NSGA-2 and SPEA 2). In particular, it was shown that the hybrid scheme (NSGA-II+SPEA 2@800 generations) provides better convergence than NSGA-II@1600 and SPEA-2@1600. This result indicates that for the same computational cost (objective function evaluations), the number of nondominated solutions (network configurations) is significantly increased (78% on average) and a more distributed Pareto Front is obtained. Given that after a certain number of generations the improvement of the objective function values is very small (typically less than 1%), the extra number of solutions compensate this

marginal loss as they all contribute to improve the hypervolume indicator. In this manner, gains in terms of hypervolume are also achieved.

- A detailed statistical analysis of the convergence properties of the evolutionary algorithms was performed. The results show the impact of the calibration process on the performance of the proposed strategy, and consequently, a detailed discussion on the matter is provided indicating rules of thumb and practical guidelines.

- As it was indicated in Chapter 3, the consideration of irregular traffic distributions can be done almost directly by simply considering a probability space to weight different zones of the coverage area. Thus, providing the proposed scheme of another interesting practical feature. An example of this is shown in Chapter 8, where the consideration of irregular traffic distributions is mandatory.

- Although multiobjective optimization was performed taking into account system-oriented metrics, the study of the features of the resulting nondominated SFR/FFR configurations showed that such dominance relationships do not hold necessarily at cell level. The performance at cell level is obviously very important and, as such, requires attention. The proposed framework also takes that aspect into account and allows several means to guarantee minimum local performances. However, it should be clearly understood that high global optimization gains typically comes at the expense of local unbalances, being this feature another strength of the proposed algorithm. Indeed, it provides several solutions that, having similar global performances, provide quite different performances at cell level, and hence, the set of solutions can be used by the mobile operator according to its needs or preferences.

- The proposed multiobjective approach has been designed for data channels. However, another very important component of cellular systems such as LTE and LTE-A, is the performance of control channels, which are also affected by the cell edge performance issue. That is the matter of the next chapter.

Chapter 7

ICIC for Control Channels

7.1 Introduction

In previous chapters, it was shown that cell edge performance is especially important in realistic deployments mainly due to the irregularities found in real-world networks. As a result, long tails in SINR distributions are expected because these inhomogeneities cause significant variations in the radio channel quality, both in serving and interfering signals.

The industry recognized this challenge and responded by means of Intercell Interference Coordination (ICIC) techniques aiming at reducing the ICI at cell edges, and so, homogenizing SINR values. An example of such efforts is the novel multiobjective optimization algorithm presented in the previous chapter, whose design is oriented to improve the SINR levels experienced by cell edge users in data channels. In systems such as LTE and LTE-A, the design of those channels allows the implementation of *the adjustments* in terms of transmit power and frequency reuse factor defined in SFR and FFR. Therefore, ICIC is a useful tool to alleviate the cell edge performance issue from the perspective of data channels.

The design of the control channel in LTE, the PDCCH, is less flexible than its data counterpart because it is time-multiplexed, and hence, traditional ICIC schemes such as SFR or FFR (or optimization techniques derived from them as the ones presented in the previous chapter) cannot be applied directly. The situation worsen because the PDCCH operates under full frequency reuse. Thus, cell edge SINR figures are so bad that, even employing robust modulations and coding schemes, the PDCCH would fail [53]. Indeed, it has been shown that the PDCCH acts as a *bottleneck* in certain traffic scenarios and load conditions. To be precise, the PDCCH limitates the system capacity in scenarios with many low-rate users as every single user requires control resources independently of the targeted rate, and hence, they saturate the PDCCH. Most of the works investigating this issue, such as [165, 258], are focused on scenarios limited by an extensive presence of VoIP users. For this

reason, during this dissertation a study on NRT services was done. For the sake of clarity, this study is not included in this chapter. The interested reader can find it in Appendix F. A reading of it will provide a deeper insight on PDCCH capacity issues.

In the light of this situation, LTE-A introduces some mechanisms to protect the PDCCH (subsequently revised). Nevertheless, LTE networks still require some measures to enhance the reliability and capacity of the PDCCH. Therefore, taking into account that conventional ICIC is not an option and the operation of the PDCCH, an adaptation of the solution introduced in the previous chapter is proposed in order to enhance the performance of the PDCCH, and consequently, increase its capacity. As it will be shown shortly, the proposed multiobjective optimization scheme is based on adjustments of the power allocated to the PDCCH at each cell[1].

As an answer to the aforementioned problems in the PDCCH, release 11 introduces the ePDCCH. This new structure is defined to increase the signaling capacity to cope with the increasing amount of control information required to support the set of new features in LTE-A such as wider bandwidths, enhanced downlink and uplink transmission, relaying, support of heterogeneous networks, and machine-to-machine communications, among others [158]. The ePDCCH solves some lacks such as the possibility of employing frequency domain ICIC, and hence, the use of optimization schemes based on the framework presented in the previous chapter seems to be logical. However, the optimization of the ePDCCH poses a new problem. The resources devoted to the ePDCCH need to be borrowed from the PDSCH, and hence, it creates a conflict between the capacity of data and control channels. This tradeoff is carefully considered by the SFR-based optimization scheme presented in this chapter.

The chapter is organized as follows: the next section starts reinforcing the need for ICIC for control channels and providing an overview of related works. The system model and the definition of the performance metrics are explained in Section 7.3. The multiobjective problem formulations are described in Section 7.4. Sections 7.5 and 7.6 present numerical results and convergence aspects. Finally, the chapter is closed with final remarks in Section 7.7.

7.2 The Need for ICIC for Control Channels

The deployment of LTE is growing at a pace never seen before, and according to [1], a similar trend is expected for LTE-A. While the proper operation of LTE strongly relies on the performance of the PDCCH, the new features and enhancements in LTE-A also require a reliable management of the increasing amount of control information.

This section aims at providing the description of the novel strategies for the PDCCH in LTE and the ePDCCH in LTE-A. Recall that a basic description of the structure and operation of these channels was presented in Chapter 2 (Subsection 2.7.1). The following discussion completes the required background and justifies the need for ICIC in control channels.

[1] An extension of this approach for the data channels is presented in Appendix E.

7.2.1 The PDCCH

As it can be seen from Figure 2.16, the PDCCH in one PRB is composed of all subcarriers (except for 2 CS-RS) of the n first OFDM symbols ($n \leq 4$, in the figure $n = 3$). Each PDCCH is transmitted using one or more Control Channel Elements (CCEs), where each CCE contains 9 sets of 4 REs known as Resource Elements Group (REGs). The CCEs are the basic control information unit in LTE. As it was indicated in Chapter 2, the information transmitted over the PDCCH includes downlink (and uplink) scheduling grants, power control commands, and data required to decode and demodulate OFDM symbols in the downlink (encode and modulate in the uplink). Given the importance of such information, a target BLER of 1% is pursued for the PDCCH. Thus, in order to satisfy that requirement, both link adaptation and power control have been defined for the PDCCH [259]. In particular, 4 different PDCCH formats, Aggregation Levels (ALs), have been specified. All of them use QPSK as modulation scheme and 4 different coding rates can be selected based on the target SINR of the AL x (ψ_x^{T}). This is shown in Table C.2[2].

As it was mentioned, the PDCCH is time-multiplexed, and thus, its design is less flexible than the PDSCH which can be multiplexed both in time and frequency. Therefore, traditional ICIC techniques such as SFR and FFR cannot be applied directly to the PDCCH. To be precise, the PDCCH does not support any signaling mechanism to indicate users where to find their control information if those resources were moved dynamically to avoid ICI. Indeed, users must perform a search process to find their control messages, the so-called *blind* detection [159, 162].

On the one hand, increasing the aggregation level implies grouping CCEs in sets of 1, 2, 4, and 8 to increase the robustness (see Table C.2). Since the number of CCEs depends on average SINR values, higher ALs (required at cell edges) increase significantly the consumption of CCEs. On the other hand, power boost is mainly used in coverage-limited scenarios. When signal power is boosted up, ICI is also increased, and hence, improvements are hardly achieved in interference limited environments. In addition, it is worth mentioning that:

1. The PDCCH offers a natural protection against ICI in low load conditions due to the shifted positioning of the CCEs in different cells. However, in case of low-rate services such as voice, many users would saturate the PDCCH, and thus, the interference scenario becomes full reuse.

2. LTE-A provides means to protect the PDCCH. The first option, in the frequency domain, is based on CA [147] and cross carrier scheduling [146]. However, it is not an option for legacy users. The second approach is in the time domain, the use of ABSs. Nevertheless, this alternative severely penalizes the capacity, and hence, it is a solution reserved for HetNets [140, 141].

Given that the PDCCH conveys critical scheduling information to mobile termi-

[2]The extension to other antenna configurations such as MIMO can be done by modifying the SINR thresholds (ψ_x^{T}).

nals, the impact of its limitations (capacity) on system performance has been widely studied in the context of real-time services such as VoIP [165, 258]. Recall that a study of the impact of the capacity constraints of the PDCCH on the provision of QoS for NRT services is presented in Appendix F. In addition, several resource allocation schemes have been proposed including strategies based on power boost [259] and search space redefinitions [260]. However, one important drawback of these schemes is their feasibility as they rely on strong assumptions such as perfect CSI and the restrictive real-time complexity.

Bearing in mind the previous context, the power allocation scheme described in Section 7.4 is proposed as a mean to reduce the consumption of control resources in the network.

7.2.2 The ePDCCH

As it was mentioned earlier, the ePDCCH was introduced to increase the signaling capacity of the system given the increased amount of signaling required to support the new features introduced in LTE-A. The ePDCCH is designed in such a way that frequency domain ICIC can be used. This is done by *inserting* the ePDCCH into the PDSCH. For this reason, an adapation of the strategies previously presented for ICIC for data channels is developed. However, a new tradeoff appears because the ePDCCH take resources normally devoted to users payload, and hence, the increment of the signaling capacity comes at the expense of a reduction in terms of spectral efficiency [45]. Therefore, this important conflict must be carefully considered.

In order to allow frequency domain ICIC, the ePDCCH is based on FDM as it is illustrated in Figure 2.16. Additional Demodulation Reference Signals (DM-RSs) are inserted within the ePDCCH to allow for user-specific beamforming and spatial diversity. Thus, each serving cell configures UE with one or more ePDCCH PRB sets, i.e., a set of contiguous PRBs used to allocate the ePDCCH. This user-specific allocation is transmitted to UE by means of higher layers signaling [261].

The exact position and amount of resources devoted to the ePDCCH can be changed dynamically and it depends on aspects such as system bandwidth, required control capacity and location of the ePDCCH in neighbor cells. Details about the control resource allocation mechanism for the ePDCCH in LTE-A, i.e., how to localize and index the enhanced CCEs (eCCEs) within the PRBs carrying the ePDCCH, can be found in [166, 261]. Note that the eCCEs are an improved version of the CCEs in the PDCCH.

The type of information that is transmitted over the ePDCCH is basically of the same type as in the PDCCH, and consequently, similar reliability requirements are also specified for the ePDCCH. Therefore, ALs are also defined for the ePDCCH as it is shown in Table C.3. In this manner, the consumption of control resources (eCCEs) is also conditioned to the SINR levels. However, in contrast to the PDCCH, that selects the AL based on average (wideband) SINR figures, the aggregation of eCCEs for the ePDCCH is done with CSI at PRB level.

It is worth mentioning that the ePDCCH is compatible with legacy carriers, providing so more signaling capacity. Moreover, it can operate in Multicast-Broadcast Single Frequency Network (MBSFN) subframes [262].

Given its recent appearance (release 11, 2012), few studies about the ePDCCH have been reported. Indeed, most of the work done about the ePDCCH has been focused on comparing its performance with the PDCCH. The recent study presented in [263] demonstrates that the ePDCCH outperforms the PDCCH in terms of achievable SINR levels mainly due to its inherent capability to perform frequency domain resource allocation. The work presented in [264] is concentrated on the design of the search space, i.e., how to allocate the eCCEs in the physical resources devoted for such purpose. Other related works such as [147] and [265], are focused on the mechanisms introduced in the release 10 such as cross carrier scheduling and ABS. To the best of the authors' knowledge, no work has investigated static ICIC for the ePDCCH, and consequently, the suitability of SFR to protect the ePDCCH is studied herein.

7.3 System Model

The system model is the one presented in Appendix C, Section C.1. Moreover, it considers the analytical framework explained in Section 3.3.2.

The proposed scheme requires that all cells in the system are time-synchronized, meaning that the PDCCH is transmitted simultaneously in the network. Nowadays, time synchronization is becoming a trend for operators of systems such as LTE and LTE-A. It is a requirement for important functionalities including MBSFN [262] and other radio resource management techniques such as CoMP [34] and eICIC [141]. There are several feasible alternatives to synchronize distributed clocks with an accuracy of less than one microsecond such as IEEE 1588 [266] and/or Global Positioning System (GPS).

7.3.1 Design Insights

The target of the optimization schemes presented in this chapter is to increase the capacity of the PDCCH and ePDCCH by reducing the average consumption of control resources. Given that the signaling for cell edge users (typically with low average SINR values) is expensive in terms of CCEs and eCCEs (see Tables C.2 and C.3), the proposed strategies aim at minimizing the number of users with such high demand. The previous goal can be attained by improving the radio channel quality at cell edges, and hence, it is expected that the framework developed so far for ICIC can be adapted to these problems.

As it was indicated, the optimization problem for the PDCCH is modeled as power allocation. Note that assuming that the PDCCH is time-synchronized is indeed the worst case scenario. Given this, a expression similar to (3.27) can be used to approximate the SINR levels in the PDCCH. Once the statistic for

those average SINR values ($\psi_{\mathrm{u}}^{\mathrm{PDCCH}}$) is built, the analysis must be focused on the average consumption of CCEs. Since the PDCCH is independent of the PDSCH (see Figure 2.16), no impact on the capacity of the latter is expected.

The analysis for the case of the ePDCCH has some similarities but important differences. Again, the strategies for the ePDCCH are oriented to reduce the consumption of eCCEs. However, the model based on wideband SINR levels is not longer valid because the ePDCCH is allocated within the PDSCH (the data channel). The previous condition has two important implications:

1. A more refined estimation of average SINR values is required. In this study, the use of SFR is proposed to enhance the performance of the ePDCCH. Thus, the statistical framework developed for data channels can be adapted since it predicts average SINR figures in different subbands of the PDSCH that are subject to different resource allocation conditions.
2. Given that the ePDCCH *borrows* resources from the PDSCH, the capacity of the latter is affected. Thus, such impact must be included into the analysis.

In addition to the previous considerations, the power expenditure over the air interface is also studied to include the important energetic perspective. In the next subsection, the performance metrics that are considered in each case are presented together with their corresponding mathematical definition.

7.3.2 Objective Functions

Bearing in mind the design aspects previously discussed, two different sets of performance metrics are required for the PDCCH and ePDCCH. Both sets are presented separately next.

Objective Functions in PDCCH Optimization

The following performance criteria have been considered:

1. Minimization of the **average** CCE **consumption** (f_1): this metric reflects the consumption of control resources network-wide, thus providing a system-oriented perspective.
2. Minimization of the **consumption of** CCEs **in the worst cell** (f_2): this metric reflects the condition of the worst cell in the system. Thus, f_2 introduces fairness among cells as it can be regarded as a min-max model within the whole multiobjective formulation.
3. Minimization of **the transmit power** in the PDCCH (globally) in the system (f_3): the reason of including this metric is twofold. First, reducing the energy expenditure over the air interface. Recall that the PDCCH is always active. Second, minimizing the ICI in the network.

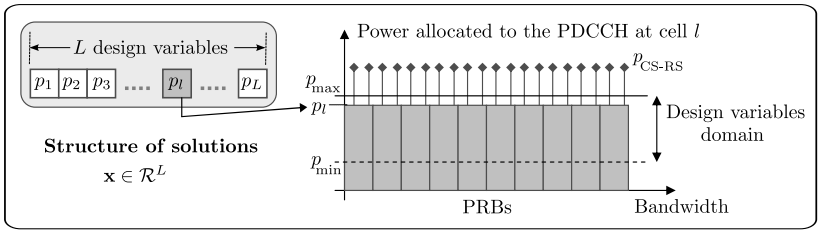

Figure 7.1: Power allocation optimization model for the PDCCH.

The estimation of the previous objectives is based on the statistic of the SINR levels in the PDCCH. Recall that the PDCCH operates under full reuse condition provided the required synchronization. Thus, average SINR levels are obtained by means of an expression similar to (3.27)[3]. In this manner, the vector $\mathbf{\Psi}_{\mathrm{u}}^{\mathrm{PDCCH}} \in \mathbb{R}^A$ that indicates the SINR levels at each pixel, depends on the power allocated to the PDCCH at each cell ($\mathbf{p}^{\mathrm{PDCCH}} \in \mathbb{R}^L$). In order to be consistent with the notation used so far (and for the sake of clarity), let's consider $\mathbf{x} = \mathbf{p}^{\mathrm{PDCCH}}$. Therefore,

$$\mathbf{\Psi}_{\mathrm{u}}^{\mathrm{PDCCH}} = \left[(\mathbf{S} \odot \mathbf{G}) \cdot \mathbf{x}\right] \oslash \left[\left[(\mathbf{S}^{\mathrm{c}} \odot \mathbf{G}) \cdot \mathbf{x}\right] \oplus \sigma^2\right], \tag{7.1}$$

where each element $\mathbf{x}(l)$ (the power allocated to the PDCCH in the l^{th} cell) is bounded, i.e., $\mathbf{x}(l) = p^l \in [\, p_{\min},\ p_{\max}\,],\ \forall\, l = 1, 2, \cdots, L$, as it is shown in Figure 7.1. In this manner, the optimization vector ($\mathbf{x}$) is defined as follows:

$$\mathbf{x} = [\, p^1,\ \ p^2,\ \cdots,\ p^L\,]. \tag{7.2}$$

Once the vector $\mathbf{\Psi}_{\mathrm{u}}^{\mathrm{PDCCH}}$ is obtained, according to (7.1), the empirical CDF of $\psi_{\mathrm{u}}^{\mathrm{PDCCH}}$ in the l^{th} cell ($F^l_{\psi_{\mathrm{u}}^{\mathrm{PDCCH}}}$) can be built. Note that $F^l_{\psi_{\mathrm{u}}^{\mathrm{PDCCH}}}$ is a function of $\mathbf{x}$. This dependence is omitted for the sake of clarity.

Let's denote as ξ^l the average consumption of CCEs in the l^{th} cell. Thus, ξ^l is obtained as follows:

$$\xi^l = \sum_{x=0}^{3} \mathrm{AL}_x \cdot P_x^l, \tag{7.3}$$

where the weights AL_x are indicated in the column 'Format' in Table C.2. The probabilities P_x^l are obtained from the empirical CDFs ($F^l_{\psi_{\mathrm{u}}^{\mathrm{PDCCH}}}$) as follows:

$$P_0^l = 1 - F^l_{\psi_{\mathrm{u}}^{\mathrm{PDCCH}}}\left(\psi_0^{\mathrm{T}}\right), \tag{7.4}$$

$$P_1^l = F^l_{\psi_{\mathrm{u}}^{\mathrm{PDCCH}}}\left(\psi_0^{\mathrm{T}}\right) - F^l_{\psi_{\mathrm{u}}^{\mathrm{PDCCH}}}\left(\psi_1^{\mathrm{T}}\right), \tag{7.5}$$

$$P_2^l = F^l_{\psi_{\mathrm{u}}^{\mathrm{PDCCH}}}\left(\psi_1^{\mathrm{T}}\right) - F^l_{\psi_{\mathrm{u}}^{\mathrm{PDCCH}}}\left(\psi_2^{\mathrm{T}}\right), \tag{7.6}$$

$$P_3^l = F^l_{\psi_{\mathrm{u}}^{\mathrm{PDCCH}}}\left(\psi_2^{\mathrm{T}}\right). \tag{7.7}$$

Note that P_x^l corresponds to the probability of requiring the AL_x in the l^{th} cell.

[3]The estimation of the matrices $\mathbf{G}$, $\mathbf{S}$, and $\mathbf{S}^{\mathrm{c}}$ is indicated in Appendix C (Section C.1).

Thus, the objective functions (f_1, f_2, and f_3) are calculated as follows:

$$f_1(\mathbf{x}) = \frac{1}{L}\sum_{l=1}^{L} \xi^l, \tag{7.8}$$

$$f_2(\mathbf{x}) = \max\left([\ \xi^1,\ \ \xi^2,\ \cdots,\ \xi^L\ ]\right), \tag{7.9}$$

$$f_3(\mathbf{x}) = \frac{1}{(L \cdot p_{\max})} \cdot (\mathbf{x} \cdot \mathbf{1}). \tag{7.10}$$

The dependence of f_1, f_2, and f_3 on $\mathbf{x}$ is also omitted for the sake of clarity.

Objective Functions in ePDCCH Optimization

It is worth recalling that the optimization of the ePDCCH adds another interesting perspective: the impact of allocating resources (normally devoted to data) to control channels on the capacity of data channels. Therefore, in order to provide such *visibility*, the performance assessment is based on the joint optimization of the following metrics:

1. Maximization of the **average cell capacity** (f_1): it corresponds to the same metric f_1 introduced in Section 6.2. In this case, f_1 will be affected by the presence of the ePDCCHs.
2. Maximization of the **capacity of the worst 5% of the coverage area** (f_2): it corresponds to the same metric f_2 introduced in Section 6.2.
3. Minimization of the **average eCCE consumption** (f_3): this metric reflects the impact of the ICI on the radio quality associated to the ePDCCH network-wide. It indicates the average consumption of eCCEs per cell. It would correspond to the metric f_1 in PDCCH optimization (the previous point), however, the consumption will be given in eCCEs rather than CCEs.
4. Minimization of the **worst eCCE consumption** (f_4): it corresponds to the average eCCE consumption in the worst cell of the system, i.e., the most interfered cell. It would correspond to the metric f_2 in PDCCH optimization, although it is given in eCCEs.
5. Maximization of **ePDCCH resources** (f_5): this metric quantifies how much resources (PRBs) are devoted to the ePDCCH, which is independent of the average consumption of eCCEs (f_3 or f_4). As it was mentioned, this objective is in conflict with f_1.
6. Minimization of the **normalized energy consumption** (f_6): it corresponds to the metric f_3 introduced in Section 6.2.

The parameters β_c and α determine how much resources are devoted to the ePDCCH and the power ratio between interior ($\mathcal{I}$) and exterior ($\mathcal{E}$) users, respectively. As it can be seen in Figure 7.2, the resources allocated to the ePDCCH (controlled

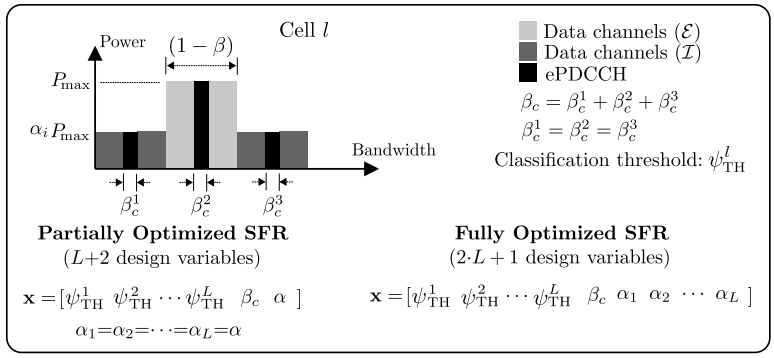

Figure 7.2: SFR-based optimization models for the ePDCCH.

by β_c) are proportionally distributed between the bandwidth portions of each class of users ($\mathcal{E}$ and $\mathcal{I}$). The bandwidth sharing coefficient (β) is kept as an input and its value is set to the minimum value avoiding overlapping between cell edge subbands, thus $\beta = 2/3$. Recall that β determines the bandwidth allocated to the set of interior users (see Figure 2.9).

As it has been indicated, in virtue of the design (FDM-based) of the ePDCCH, the framework previously investigated for ICIC for data channels is applied to this problem. Thus, the optimization of the previous objectives is based on SFR (see Figure 2.9) and it follows an approach similar to the one used in Chapter 6, i.e., fine tuning the operational parameters α and ψ_{TH} at each cell. It is important to recall that in the previous chapter, the parameter α is defined as a global design variable to reduce the computational cost and to favor a better convergence (see Subsection 6.2.1). Experimental trials showed that the gain obtained throught local adjustments of α is very small and it comes at the expense of a significant computational cost increment. The study presented here on the complete problem (data and control channels) demonstrates the previous statement. In order to differenciate this analysis from the case where α is kept as a global design variable, the following nomenclature is introduced: Partially Optimized SFR (POS) and Fully Optimized SFR (FOS). Both models are described in the following points.

1. *Partially Optimized SFR*: In this scheme, there are L local classification thresholds (ψ_{TH}^l) optimized at cell level plus 2 additional network-wide design variables (β_c and α) that are applied globally. This model corresponds to the following mapping: $\mathbf{x} \in \mathbb{R}^{L+2} \rightarrow \mathbf{f} \in \mathbb{R}^6$. Recall that $\mathbf{f}$ is the vector that defines the objective space (see Section 5.2) through of each objective function. The design target of this scheme is achieving a competitive optimization level while keeping the computational complexity as low as possible. For this reason, α and β_c are defined as a network-wide design variable. Thus, the model is similar to the one presented in Chapter 6 for SFR optimization.

2. *Fully Optimized SFR*: This scheme corresponds to the complete study in which the gains achieved by the local optimization of α are investigated. As it was

mentioned in Section 6.2, it will be shown that the improvement obtained by means of this fine tuning is marginal and it comes at the expense of computational cost. Thus, the study considers $2L+1$ design variables, α^l and ψ^l_{TH}, for $l = 1, 2, \cdots, L$, plus β_{c} as global design variable. This model corresponds to the following mapping: $\mathbf{x} \in \mathbb{R}^{2L+1} \rightarrow \mathbf{f} \in \mathbb{R}^6$.

It is important to note that the first model (POS) is a particular case of the second one (FOS), where $\alpha_l = \alpha,\ \forall\ l$. Hence, the more general case is used for both models and the genotype of the decision vector ($\mathbf{x}$) for ePDCCH optimization is as follows:

$$\mathbf{x} = [\ \psi^1_{\mathrm{TH}},\ \ \psi^2_{\mathrm{TH}},\ \cdots\ \psi^l_{\mathrm{TH}},\ \ \beta_{\mathrm{c}},\ \ \alpha_1,\ \ \alpha_2,\ \cdots\ \alpha_l\ ]. \tag{7.11}$$

The steps required to compute the objective functions ($f_1,\ f_2, \cdots f_6$) are indicated in Algorithm 7.1. In the pseudo-code, some of the functions introduced in the previous chapter (see Table 6.1) are also used. Lines 1 to 7 perform preliminary computations by means of the aforementioned functions. In line 8, the vector $\mathbf{v}_\alpha \in \mathbb{R}^L$ is created with the power ratio coefficient (α) corresponding to each cell. The amount of bandwidth devoted to the ePDCCH is indicated by β_{c} in line 9.

A generalized form of the characteristic matrices, similar to (3.32) and (3.35), is built in lines 10-15. Recall that these matrices capture the resource allocation pattern of SFR. In line 16, the bandwidth allocated to each class of users ($\mathcal{E}$ and $\mathcal{I}$) is calculated taking into account the amount of resources devoted to the ePDCCH (given by β_{c}). In line 17, the function `PixRate()` (introduced in Section 6.3) determine the achievable rate at each pixel. Note that the bandwidth matrix ($\mathbf{B}$) passed as argument is computed in line 16, and hence, the effect of β_{c} is included.

In lines 18 and 19, a vector of pointers to CDFs is created. Each of these pointers represents the CDF of each class of user at each cell, and hence, $2L$ pointers are required. In order to generate these CDFs, the average SINR of each pixel (stored in $\mathbf{\Psi}$) is required. In addition, the classification and serving cell of each pixel are required as well. This information is stored in the matrices $\mathbf{C}$ and $\mathbf{S}$, respectively.

In lines 20 and 21, the vector with the rate of each pixel ($\mathbf{r}$) is sorted and the number of pixels that compose the worst 5% of the coverage area is calculated, respectively. Lines 22 to 24 determine the objective functions f_1, f_2, and f_6, similarly as it was done in Chapter 6. However, note that f_6 takes into account the particular value of α at each cell, which is stored in the vector $\mathbf{v}_\alpha$.

The loop enclosed in lines 25 to 36, determines the average eCCE consumption at each cell. The procedure is similar to the one used for the PDCCH in the sense that it is based on average SINR distributions. However, given that SFR is employed, a user classification exist, and thus, the analysis needs to be done independently for each class (the loop enclosing lines 26 to 33). The resulting consumption at cell level, is computed in line 35, where the proportion of exterior and interior users is taken into account to weight the partial result of each class. Once the outer loop is completed, the eCCE consumption of each cell is available and the rest of objective functions (f_3, f_4, and f_5) are calculated according to the expressions in lines 37 to 39. The objective vector ($\mathbf{f}$) is created and returned in lines 40 and 41, respectively.

Algorithm 7.1: Objective functions in ePDCCH optimization

Inputs :

$\mathbf{x}$: Design vector. See (7.11).
$\mathbf{\Psi}_{\mathrm{u}}$: Average SINR vector. According to (3.27).
$\mathbf{G}$, $\mathbf{S}$, and $\mathbf{S}^{\mathrm{c}}$: As indicated in Appendix C (Section C.1).
$\mathbf{v}_{\phi}$: Vector with the azimuth of each cell.
B, L, and A: System bandwidth, number of cells, and number of pixels.

Output :

$\mathbf{f}$: Objective vector.

// Preliminary computations

$\mathbf{S}$, $\mathbf{S}^{\mathrm{c}} \leftarrow$ `PerCellCov(`$\mathbf{G}$, $\mathbf{p}_{\text{CS-RS}}$`);` `/* Per-cell coverage. See Section C.1. */`

$\mathbf{\Psi}_{\mathrm{u}} \leftarrow$ `AvgSINR(`σ^2, $\mathbf{p}_{\text{CS-RS}}$, $\mathbf{G}$, $\mathbf{S}$, $\mathbf{S}^{\mathrm{c}}$`)` ; `/* Average SINR. See Table 6.1. */`

$\mathbf{t} \leftarrow$ `TypeOfServer(`$\mathbf{v}_{\phi}$, $\mathbf{S}$`);` `/* Type of serving cell. See Table 6.1. */`

$\{\mathbf{G}_j, \mathbf{S}_j, \mathbf{S}_j^{\mathrm{c}}\} \leftarrow$ `Segmentation(`$\mathbf{G}$, $\mathbf{S}$, $\mathbf{S}^{\mathrm{c}}$`);` `/* Segmentation. See Table 6.1. */`

$\mathbf{C} \leftarrow$ `Class(`$\mathbf{\Psi}_{\mathrm{u}}, \mathbf{x}(1:L)$`);` `/* Pixel classification */`

$\mathbf{C}_j \leftarrow$ `Segmentation(`$\mathbf{C}$`);` `/* For` $j = 1, 2, 3$. `*/`

$\mathbf{\Phi} \leftarrow$ `RelCov(`$\mathbf{S}_j$, $\mathbf{C}_j$`);` `/* For` $j = 1, 2, 3$. `*/`

$\mathbf{v}_{\alpha} \leftarrow \mathbf{x}(L+2 : 2L+1)$; `/* Vector with the` α`'s. */`

$\beta_{\mathrm{c}} \leftarrow \mathbf{x}(L+1)$; `/* ePDCCH bandwidth. */`

// Generalized characteristic matrices

$P_{\max} \leftarrow P_{\max}^{\mathrm{SC}}$; `/* As defined in (3.29). */`

$$\mathbf{P}_{\mathrm{ser}} = \begin{bmatrix} P_{\max} & P_{\max} & \cdots & P_{\max} \\ \mathbf{v}_{\alpha}(1) \cdot P_{\max} & \mathbf{v}_{\alpha}(2) \cdot P_{\max} & \cdots & \mathbf{v}_{\alpha}(L) \cdot P_{\max} \end{bmatrix}^{\mathrm{T}};$$

for each $s = 0 : ((L/3) - 1)$ **do**

$$\mathbf{P}_{\mathrm{int}}^{\mathrm{base}}(s) = \begin{bmatrix} P_{\max} & \mathbf{v}_{\alpha}(3s) \cdot P_{\max} & \mathbf{v}_{\alpha}(3s) \cdot P_{\max} \\ \mathbf{v}_{\alpha}(3s) \cdot P_{\max} & \mathbf{v}_{\alpha}(3s) \cdot P_{\max} & P_{\max} \\ \mathbf{v}_{\alpha}(3s+1) \cdot P_{\max} & P_{\max} & \mathbf{v}_{\alpha}(3s+1) \cdot P_{\max} \\ P_{\max} & \mathbf{v}_{\alpha}(3s+1) \cdot P_{\max} & \mathbf{v}_{\alpha}(3s+1) \cdot P_{\max} \\ \mathbf{v}_{\alpha}(3s+2) \cdot P_{\max} & \mathbf{v}_{\alpha}(3s+2) \cdot P_{\max} & P_{\max} \\ \mathbf{v}_{\alpha}(3s+2) \cdot P_{\max} & P_{\max} & \mathbf{v}_{\alpha}(3s+2) \cdot P_{\max} \end{bmatrix}^{\mathrm{T}};$$

end

$$\mathbf{P}_{\mathrm{int}} = \left[\mathbf{P}_{\mathrm{int}}^{\mathrm{base}}(0)^{\mathrm{T}} \quad \mathbf{P}_{\mathrm{int}}^{\mathrm{base}}(1)^{\mathrm{T}} \quad \cdots \quad \mathbf{P}_{\mathrm{int}}^{\mathrm{base}}((L/3)-1)^{\mathrm{T}}\right]^{\mathrm{T}};$$

// Bandwidth allocation

$$\mathbf{B} \leftarrow B \cdot [\ ((1-\beta) \cdot (1-\beta_{\mathrm{c}})), \quad (\beta \cdot (1-\beta_{\mathrm{c}}))\ ];$$

Algorithm 7.1.: Continuation.

// Rate of each pixel, see Table 6.1.
$\mathbf{r} \leftarrow$ PixRate($\mathbf{B}$, $\mathbf{P}_{\text{ser}}$, $\mathbf{P}_{\text{int}}$, $\mathbf{G}_j$, $\mathbf{S}_j$, $\mathbf{S}_j^c$);

// Resizing the vector with pointers to per-cell/per-class SINR CDFs.
Resize($\mathbf{P}_{\text{CDF}}$, $2 \cdot L$); /* $\mathbf{P}_{\text{CDF}}$ points to $2L$ CDFs ($\{\mathcal{E},\ \mathcal{I}\} \times L$ cells). */

// Create CDFs of average SINR values: per class and per cell: $F_{\mathcal{E}}^l$ and $F_{\mathcal{I}}^l$ $\forall\ l$.
$\mathbf{P}_{\text{CDF}} \leftarrow$ CreateCDFs($\mathbf{\Psi}_j$, $\mathbf{C}_j$, $\mathbf{S}_j$); /* For $j = 1, 2, 3$. */

$\mathbf{r} \leftarrow$ Sort($\mathbf{r}$); /* Sorting (ascending order)' */

$k \leftarrow \lceil 0.05 \cdot A \rceil$; /* Number of 'cell edge pixels' */

// Objective functions: f_1, f_2, and f_6.

$f_1 \leftarrow (\mathbf{r} \cdot \mathbf{1})\,/L$; /* f_1: average cell capacity */

$f_2 \leftarrow$ Sum($\mathbf{r}$, k); /* f_2: cell edge aggregate capacity */

$f_6 = \frac{1}{L} \sum_{l=1}^{L} (1 - (\beta \cdot (1 - \mathbf{v}_\alpha(l))))$; /* f_6: normalized power consumption */

// For each cell $l = 1, 2, \cdots, L$.
for $l = 1 : L$ **do**
  // For each class ('0' for class $\mathcal{E}$, and '1' for class $\mathcal{I}$).
  for $c = 0 : 1$ **do**
    $F \leftarrow \mathbf{P}_{\text{CDF}}(2l + c - 1)$; /* Average SINR CDF: class c at cell l */
    // Required probabilities: ψ_x^{T} are defined in Table C.3.
    $P_0 \leftarrow 1 - F(\psi_0^{\text{T}})$;
    $P_1 \leftarrow F(\psi_0^{\text{T}}) - F(\psi_1^{\text{T}})$;
    $P_2 \leftarrow F(\psi_1^{\text{T}}) - F(\psi_2^{\text{T}})$;
    $P_3 \leftarrow F(\psi_2^{\text{T}})$;
    // Average eCCE consumption: class c, cell l. AL_x in Table C.3.
    $\mathbf{U}(c) \leftarrow \sum_{x=0}^{3} \text{AL}_x \cdot P_x$;
    // Number of pixels in the class c at cell l.
    $\mathbf{V}(c) \leftarrow (\mathbf{\Phi}(c, l))^{-1}$;
  end
  // The consumption per cell depends on the amount of interior and exterior pixels, and hence, ξ^l depends on the classification threshold (ψ_{TH}^l).
  $\xi^l \leftarrow \left(\frac{\mathbf{V}(0)}{\mathbf{V}(0)+\mathbf{V}(1)} \cdot \mathbf{U}(0)\right) + \left(\frac{\mathbf{V}(1)}{\mathbf{V}(0)+\mathbf{V}(1)} \cdot \mathbf{U}(1)\right)$;
end

// Objective functions: f_3, f_4, and f_5.
$f_3(\mathbf{x}) \leftarrow \frac{1}{L} \sum_{l=1}^{L} \xi^l$; /* f_3: average eCCE consumption */

$f_4(\mathbf{x}) \leftarrow \max\left(\left[\ \xi^1\ \ \xi^2\ \cdots\ \xi^L\ \right]\right)$; /* f_4: worst eCCE consumption */

$f_5 \leftarrow \beta_{\text{c}} \cdot N_{\text{RB}}^{\text{DL}}$; /* f_5: control resources devotes to the ePDCCH */

// Objective vector
$\mathbf{f} \leftarrow [\ -f_1,\ \ -f_2,\ \ f_3,\ \ f_4,\ \ -f_5,\ \ f_6\ ]$;
return $\mathbf{f}$;

The procedure described by Algorithm 7.1, must be executed to estimate the objective vector for every single $\mathbf{x}$, as it is defined in (7.11). Consequently, this procedure must be invoked continuously from the evolutionary algorithm employed to perform the multiobjective optimization.

Having explained the method for computing the required objectives functions for each case (PDCCH and ePDCCH), the multiobjective formulations can be introduced. That is the content of the next section.

7.4 Multiobjective Problem Formulation

This section introduces the multiobjective formulations used for PDCCH and ePDCCH optimization according to the setting previously explained.

Multiobjective Formulation for PDCCH Optimization

The formulation is based on adjustments of the power allocated to the PDCCH locally at each cell as it is shown in Figure 7.1. Thus, each network configuration or solution ($\mathbf{x} \in \mathbb{R}^L$), see (7.2), is represented by a set of L power levels (one for each cell) that must be applied to the REs corresponding to the PDCCH, see Figure 2.16. Thus, the multiobjective problem can be written as follows:

$$\text{minimize} \quad \mathbf{f}(\mathbf{x}) = [\ f_1(\mathbf{x}),\ \ f_2(\mathbf{x}),\ \ f_3(\mathbf{x})\ ], \tag{7.12a}$$

subject to:

$$\mathbf{x}(l)\ \in\ [\ p_{\min},\ p_{\max}\ ],\quad l = 1, 2, \cdots, L, \tag{7.12b}$$

where $p_{\min}$ and $p_{\max}$ are the bounds of the design variables required to define the search space $\mathcal{X}$. Note that the selection of $p_{\min}$ is scenario-dependent and it should be done considering the minimum power level expected to be received. Recall that the mathematical definitions of the objective functions (f_1, f_2, and f_3) in (7.12a) correspond to (7.8), (7.9), and (7.10), respectively. The multiobjective formulation (7.12) allows to reduce the ICI at cell edges, and hence, it minimizes the average consumption of CCEs. Recall that the consumption of control resources is significantly increased by the aggregation levels (AL_2 and AL_3, see Table C.2) assigned to users with low average SINR levels.

Multiobjective Formulation for ePDCCH Optimization

The formulation is based on adjustments of the classification thresholds (ψ_{TH}) and power ratios (α) as it is shown in Figure 7.2. Two different optimization models are considered (POS and FOS, see 'Objective Functions in ePDCCH Optimization' in Subsection 7.3.2). The optimization vector ($\mathbf{x} \in \mathbb{R}^{2L+1}$) as it is defined in (7.11) is

used for both schemes. Thus, the multiobjective problem can be written as follows:

$$\text{minimize} \quad \mathbf{f}(\mathbf{x}) = [\ -f_1(\mathbf{x}),\ -f_2(\mathbf{x}),\ f_3(\mathbf{x}),\ f_4(\mathbf{x}),\ -f_5(\mathbf{x}),\ f_6(\mathbf{x})\ ], \tag{7.13a}$$

subject to:

$$\mathbf{x}(l) \in [\ \psi_{\text{low}},\ \psi_{\text{up}}\ ], \quad l = 1, 2, \cdots, L, \tag{7.13b}$$

$$\mathbf{x}(L+1) \in [\ \beta_{\text{c,low}},\ \beta_{\text{c,up}}\ ], \tag{7.13c}$$

$$\mathbf{x}(l) \in [\ \alpha_{\text{low}},\ \alpha_{\text{up}}\ ], \quad l = L+2, L+3, \cdots, 2L+1, \tag{7.13d}$$

where ψ_{low}, ψ_{up}, $\beta_{\text{c,low}}$, $\beta_{\text{c,up}}$, α_{low}, and α_{up} are the bounds that define the search space ($\mathcal{X}$).

On the Use of MOEAs in PDCCH and ePDCCH Optimization

As the reader has probably inferred, the mathematical structure of the optimization problems (7.12) and (7.13) is similar to (6.1) in Chapter 6. Consequently, in this study the use of MOEAs to explore the domains of the design variables (the set $\mathcal{X}$) is also investigated. Indeed, (7.13) is much more complex than all the previous multiobjective formulations because both the number of design variables and objective functions are doubled.

As it was indicated in Chapter 5, and it was confirmed in Sections 6.5.3 and 6.5.4, the black-box nature of MOEAs makes them suitable to deal with complex objectives such as the ones specified in Algorithm 7.1. In addition, in the light of the excellent convergence properties of the algorithm NSGA-II in problems such as SFR and FFR optimization, it is reasonable to expect that a similar performance would be obtained in this context as well. Therefore, the algorithm NSGA-II (see Section 5.4) is employed to estimate the set of nondominated network configurations ($\mathcal{X}^\star$) both in PDCCH and ePDCCH optimization.

Numerical results are presented in the next section.

7.5 Performance Evaluation

In this section, the whole setting used in numerical evaluations is presented. Subsection 7.5.1 describes the network parameters, configuration of the algorithm NSGA-II, and the cellular scenario. The reference schemes (benchmarks) are introduced in Subsection 7.5.2. Finally, the numerical results corresponding to PDCCH and ePDCCH optimization are analyzed in Subsections 7.5.3 and 7.5.4, respectively.

7.5.1 Settings and Test Case

The set of parameters used in numerical evaluations together with the configuration of the algorithm NSGA-II is shown in Table 7.1. Calibration is done according to

Table 7.1: Evaluation setting and NSGA-II configuration

Network settings and parameters	
Available power per cell	43.00 dBm
System bandwidth (B)	5.40 MHz
Number of cells (L)	60
Number of pixels (A)	288750
CS-RS power ($\mathbf{p}_{\text{CS-RS}}(l), \quad l = 1, 2, \cdots, L$)	18.4 dBm
Bandwidth sharing (β) in ePDCCH optimization	2/3
NSGA-II configuration	
Population size	300
Max number of generation	3000
Termination criterion: relative gain in each f_i	$< 0.001\%$/40 generations
Crossover probability	1.0
PDCCH optimization: mutation probability	$1/(L+2)$
ePDCCH optimization: mutation probability	$1/(2L+1)$
PDCCH optimization: [$p_{\min}$, $p_{\max}$]	[9.16, 17.4] [dBm/15 KHz]
ePDCCH optimization: ψ_{TH}	$\in$ [-4.00 8.00] [dB]
ePDCCH optimization: α	$\in$ [0.15 0.60]
ePDCCH optimization: β_{c}	$\in$ [0.10 0.30]
Type of design variables	Discrete-valued (Res: 2%)

the guidelines explained in Subsection 6.6.1.

In this study, the realistic deployment considered in the previous chapter (the scenario 'MORANS', see Appendix B, Subsection B.1.2) is also considered.

7.5.2 Benchmarks and Reference Cases

For comparison purposes, in case of PDCCH optimization, the solutions obtained through the proposed scheme are compared with the full reuse case, $\mathbf{x}_{\text{FR}}$, i.e., all cells transmit the PDCCH with the same power ($p_{\max}$).

In case of ePDCCH optimization, several benchmarks have been considered. These references include full reuse ($\mathbf{x}^x_{\text{FR}}$), considering different bandwidth allocations (β_{c}) for the ePDCCH, and baseline designs of SFR ($\mathbf{x}^x_{\text{SFR}}$) according to the bandwidth proportionality criterion (see Subsection 6.5.2). Recall that baseline designs are schemes in which the parameter ψ_{TH} is selected according to the SINR statistic observed in the whole coverage area (see the blue pattern in Figure 3.15b). The configurations of these benchmarks together with their corresponding objective function values are shown in Table 7.2.

Table 7.2: Benchmarks used in ePDCCH optimization.

Ref	Type	$\psi_{\mathbf{TH}}$	α	β	$\beta_{\mathbf{c}}$	f_1	f_2	f_3	f_4	f_5	f_6
$\mathbf{x}^1_{\mathrm{FR1}}$	FR	N/A	N/A	N/A	0.10	8.83	5.13	4.25	6.26	3.00	1.00
$\mathbf{x}^2_{\mathrm{FR1}}$	FR	N/A	N/A	N/A	0.20	7.84	4.56	4.25	6.26	6.00	1.00
$\mathbf{x}^3_{\mathrm{FR1}}$	FR	N/A	N/A	N/A	0.30	6.86	3.99	4.25	6.26	9.00	1.00
$\mathbf{x}^1_{\mathrm{SFR}}$	SFR	0.00	0.40	2/3	0.10	5.72	5.84	4.08	5.67	3.00	0.60
$\mathbf{x}^2_{\mathrm{SFR}}$	SFR	0.00	0.40	2/3	0.20	5.14	5.19	4.08	5.67	6.00	0.60
$\mathbf{x}^3_{\mathrm{SFR}}$	SFR	0.00	0.40	2/3	0.30	4.56	4.54	4.08	5.67	9.00	0.60

Units: f_1 [Mbps], f_2 [Mbps], f_3 [eCCE], f_4 [eCCE], f_5 [PRB], f_6 [$\cdot$], ψ_{TH} [dB].

7.5.3 Numerical Results: PDCCH Optimization

Figure 7.3 shows several representations of the obtained Pareto Front. Figure 7.3a corresponds to a 3D visualization of the images of the elements in $\mathcal{X}^\star$. Figures 7.3b, 7.3c, and 7.3d show 2D representations. As it was mentioned, 2D profiles provide better insights about the tradeoff between each pair of metrics. In these profiles, the performance of the baseline design $\mathbf{x}_{\mathrm{FR}}$ is indicated as well as the gains that can be obtained. The proposed algorithm succeeds in finding network settings outperforming the reference scheme with respect to each performance metric. The gains vary from 3.15% to 5.67%, 1.3% to 25.5%, and 38% to 50% in terms of f_1, f_2, and f_3, respectively. Thus, by selecting different solutions from the set $\mathcal{X}^\star$, different tradeoffs among the objective functions can be attained (within the ranges previously indicated). The best solution in terms of f_2 reduces the CCE requirement, on average, one fourth in the worst cell of the system. Moreover, power savings of at least 38% (up to 50%) are always achieved. If one considers that 21% of power transmitted over the air interface is devoted to the PDCCH (3 out of 14 OFDM symbols in the setting employed here), the results indicate that between 8% and 10% of the total radiated power can be saved.

Figure 7.4 illustrates the performance of the solutions in $\mathcal{X}^\star$ at cell level, by showing the cell level version of the objective functions, f_1^c, f_2^c, and f_3^c. Focusing on f_1^c, the results indicate that, although the CCE consumption of some cells are above the average CCE consumption obtained by means of $\mathbf{x}_{\mathrm{FR}}$, **the average at system level (f_1) is always better** as it was shown in Figure 7.3. However, it is worth noting that there are solutions in which the vast majority of cells reduce their consumption of control resources. Such cell-to-cell variability is what allows to the proposed optimization scheme to obtain global gains, and more important, **always reduce the average consumption of** CCEs **in the worst cell**. This feature, and the fact that many Pareto efficient configurations are available, makes possible to tune the network in situations where load unbalances at different cells appear. Given that as all these solutions are calculated offline, no real-time processing cost is required.

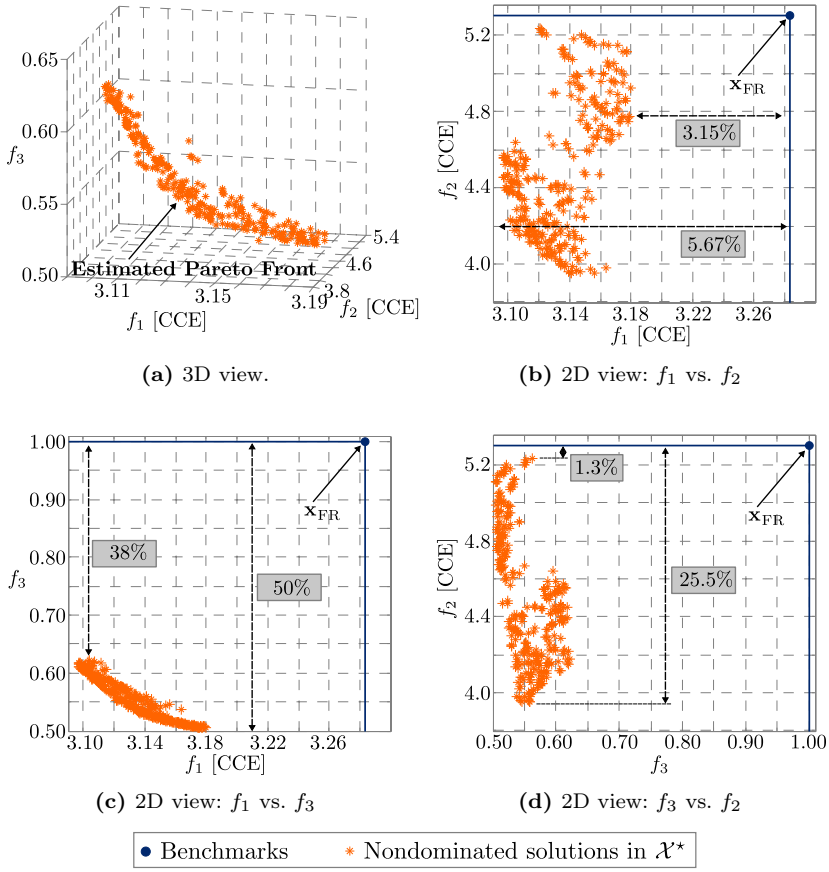

(a) 3D view.

(b) 2D view: f_1 vs. f_2

(c) 2D view: f_1 vs. f_3

(d) 2D view: f_3 vs. f_2

Figure 7.3: Representations of the estimated Pareto Front.

In order to illustrate the previous idea, Figure 7.5 shows the CDF of the average PDCCH SINR ($\psi_{\mathrm{u}}^{\mathrm{PDCCH}}$) at two different cells ($l = 34$ and $l = 37$) when two solutions taken from the set $\mathcal{X}^\star$ ($\mathbf{x}_{\mathrm{A}}$ and $\mathbf{x}_{\mathrm{B}}$), and the benchmark $\mathbf{x}_{\mathrm{FR}}$ are applied. In each case, the average CCE consumption (ξ) according to (7.3) is indicated. It can be seen that switching from $\mathbf{x}_{\mathrm{A}}$ to $\mathbf{x}_{\mathrm{B}}$ increases ξ in cell 37, while the corresponding effect in cell 34 is the opposite, i.e., a reduction of the average consumption of CCEs. In addition, the gains achieved by $\mathbf{x}_{\mathrm{A}}$ and $\mathbf{x}_{\mathrm{B}}$ with respect to $\mathbf{x}_{\mathrm{FR}}$ vary significantly. The gains in terms of ξ with respect to $\mathbf{x}_{\mathrm{FR}}$ are 19% (by $\mathbf{x}_{\mathrm{A}}$) and 16% (by $\mathbf{x}_{\mathrm{B}}$), and 34% (by $\mathbf{x}_{\mathrm{A}}$) and 44% (by $\mathbf{x}_{\mathrm{B}}$) in cells 34 and 37, respectively. Thus, the proposed scheme improves the average CCE consumption globally, while different performances at cell level can be obtained. In this manner, different network configurations can be selected to account with the time-varying nature of the traffic.

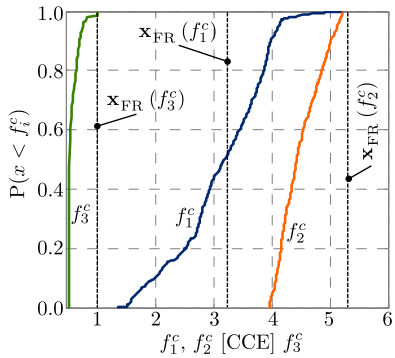

Figure 7.4: Performance at cell level.

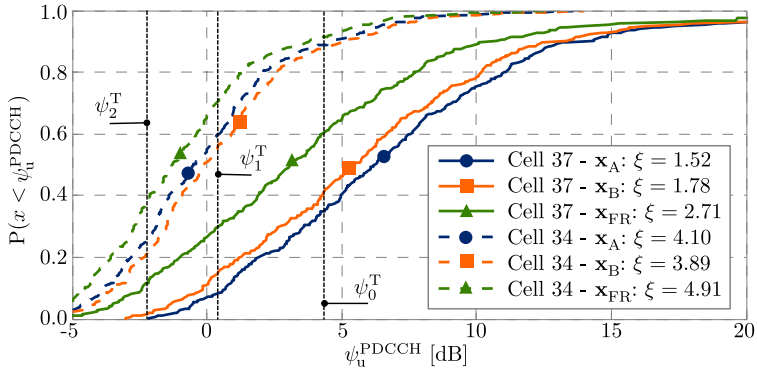

Figure 7.5: Statistic of average PDCCH SINR at cell level (two solutions in $\mathcal{X}^\star$).

7.5.4 Numerical Results: ePDCCH Optimization

Given the high number of objective functions considered for the case of ePDCCH optimization, the main results are presented as CDFs for each performance metric. Such statistics for both optimization models (POS and FOS) are shown in Figure 7.6. The performances of the benchmarks are also indicated (black lines).

The results indicate, on the one hand, that the SFR-based settings obtained through the proposed schemes are able to offer different tradeoffs among f_1, f_2, f_4, and f_5, while on the other hand, the performance in terms of f_3 and f_6 is always enhanced with respect to the benchmarks. Therefore, the solutions in the set $\mathcal{X}^\star$ allow selecting different levels of spectral efficiency (f_1), cell edge performance (f_2), consumption of the worst cell (f_4), or amount of resources allocated to the ePDCCH (f_5), but **always achieving gains in terms of the average consumption of eCCEs and transmitted power** (f_3 and f_6, respectively). As a conclusion, the proposed optimization schemes succeed in reducing significantly the average consumption of control resources (eCCEs), and hence, the signaling capacity of the ePDCCH is increased.

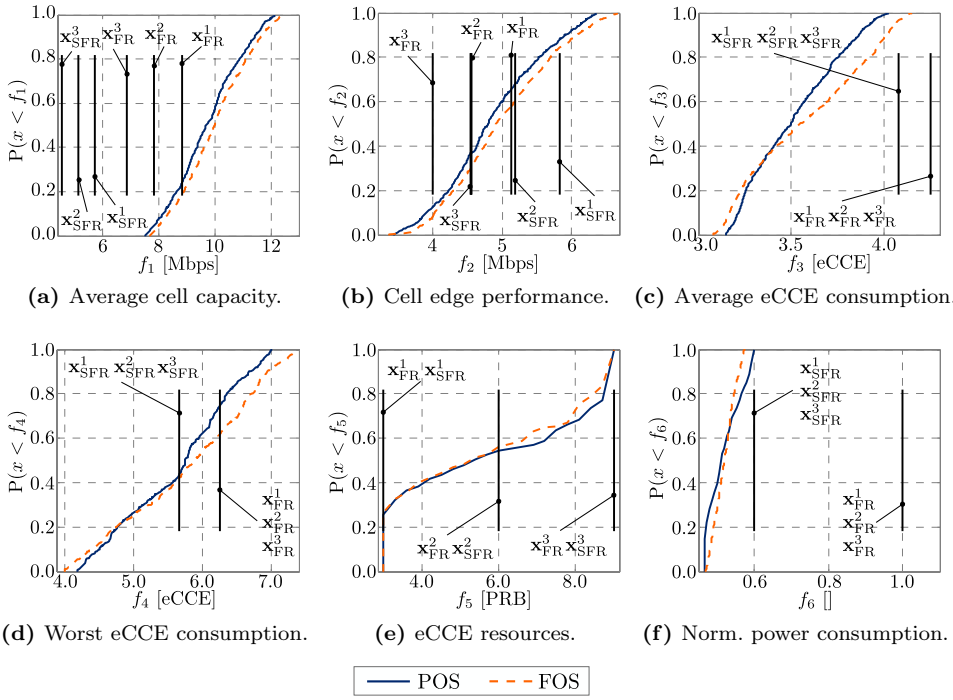

(a) Average cell capacity. **(b)** Cell edge performance. **(c)** Average eCCE consumption.

(d) Worst eCCE consumption. **(e)** eCCE resources. **(f)** Norm. power consumption.

Figure 7.6: Performance of the elements of $\mathcal{X}^\star$ in ePDCCH optimization.

From a comparative perspective, the performance obtained by means of the model FOS is slightly better than the model POS as a result of the more accurate power adjustment. Recall that in FOS, the parameter α is optimized at each cell. In this sense, gains are observed in terms of f_1 and f_2 (Figures 7.6a and 7.6b) as the CDF of the FOS model is completely to the right of the one corresponding to the model POS. Moreover, smaller (better) values of f_3 and f_4 are also attained through the scheme FOS as it is shown in Figures 7.6c and 7.6d. Given that the bounds of the design variables α and β_c are the same in both schemes, the distribution of the amount of resources devoted to the ePDCCH (f_5) and the average power consumption (f_6) are quite similar in both cases as it can be appreciated from Figures 7.6e and 7.6f.

Figure 7.7 shows the gains in terms of each performance metric and with respect to each benchmark. Such gains are computed based on the subsets of solutions dominating each case in the Pareto sense, and hence, no loss is expected. The cardinality of these subsets is indicated in Table 7.3. Thus, the proposed strategies are able to find non-empty sets of configurations dominating each benchmark. The gains shown in Figure 7.7 make evident that significant improvements are obtained with respect to the important case of full reuse (three different values of β_c were considered, see Table 7.2). Both subfigures include an example indicating how they must be read. For instance, focusing on Figure 7.7b and $\mathbf{x}_{\mathrm{FR}}^2$, it has been obtained

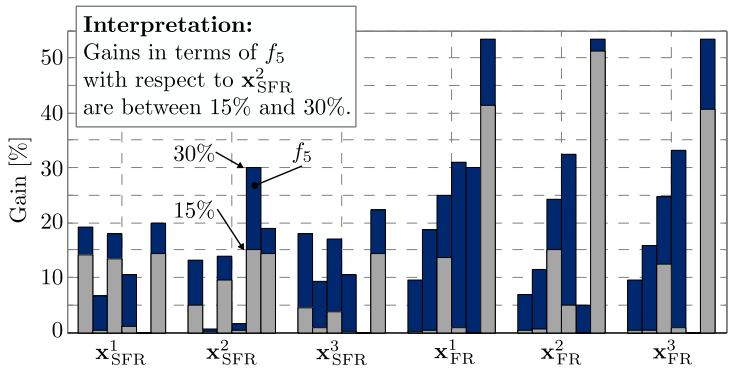

(a) Partially Optimized SFR (POS).

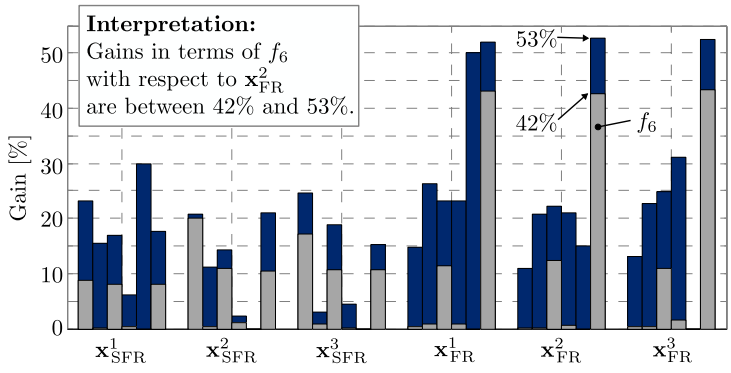

(b) Fully Optimized SFR (FOS).

Figure 7.7: Gains achieved by means of the proposed optimization models.

Table 7.3: Cardinality of the subsets dominating each benchmark.

Model	$\mathbf{x}^1_{\text{FR}}$	$\mathbf{x}^2_{\text{FR}}$	$\mathbf{x}^3_{\text{FR}}$	$\mathbf{x}^1_{\text{SFR}}$	$\mathbf{x}^2_{\text{SFR}}$	$\mathbf{x}^3_{\text{SFR}}$
POS	36	3	22	8	2	10
FOS	47	7	29	13	3	10

that the energy consumption (f_6) can be decreased up to 53% without losses in terms of any other performance metric (there are 7 configurations dominating $\mathbf{x}^2_{\text{FR}}$ in Table 7.3).

Note that the proposed schemes outperform all the benchmarks achieving gains of 20% or more in at least one of the objective functions. These results confirm the effectiveness of the optimization models as they are able to 1) achieve effective ICIC for the ePDCCH (which is evident given the gains in terms of f_3 and f_4), and 2) attain gains in terms of spectral efficiency and cell edge performance (f_1 and f_2, respectively).

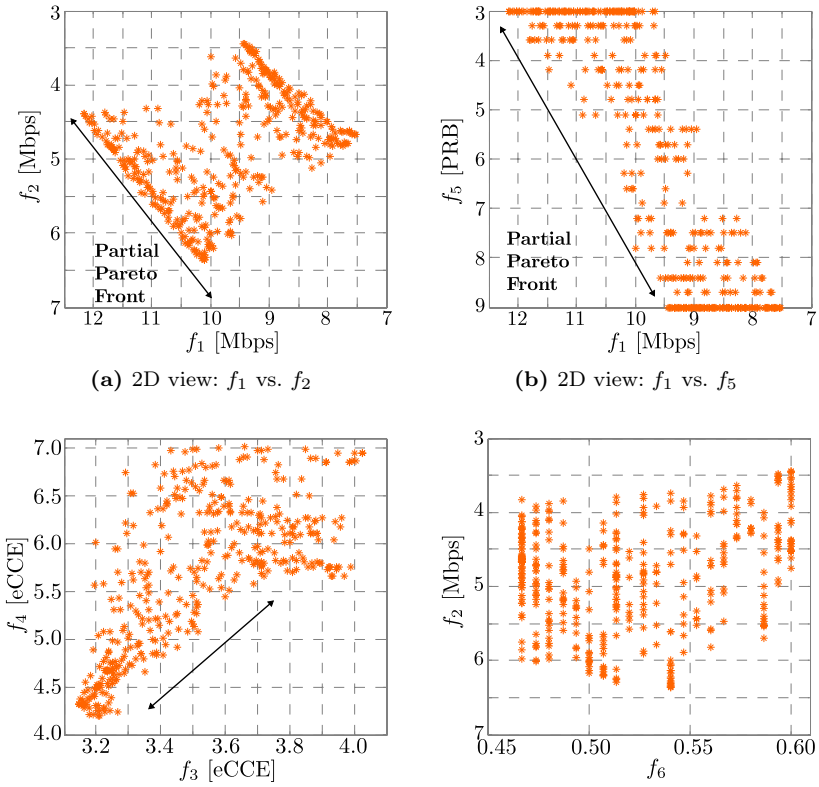

(a) 2D view: f_1 vs. f_2

(b) 2D view: f_1 vs. f_5

(c) 2D view: f_3 vs. f_4

(d) 2D view: f_6 vs. f_2

Figure 7.8: Several 2D views of the obtained Pareto Front (POS model).

In order to provide additional insights on the tradeoff between the performance metrics, 2D profiles are presented in Figure 7.8 for the case of the scheme POS. Similar patterns were obtained for the model FOS. The figure includes 4 different planes out of 15 possible combinations that can be taken from the six objective functions. The profiles correspond to: f_1-f_2, f_1-f_5, f_3-f_4, and f_6-f_2. In the two first cases, it is notorious the conflicting nature of each pair of metrics. Indeed, Figure 7.8a corresponds to the well-known tradeoff between cell edge performance and spectral efficiency. Figure 7.8b illustrates how allocating more resources to the ePDCCH (increasing β_c) tends to penalize the overall network capacity (the capacity of the PDSCH). The next case, shown in Figure 7.8c, suggests that SFR settings attaining better average eCCE consumption are also able to minimize the consumption of control resources in the worst cell of the system, which is not evident from the analogy that could be made *a priori* with the tradeoff f_1-f_2. Finally, Figure 7.8d illustrates a case where a metric (f_2) is plotted as a function of the normalized power consumption (f_6). In this case no evident connection can be inferred between them, despite it could be expected that decreasing α would benefit the cell edge performance. The situation can be explained because Pareto dominance include

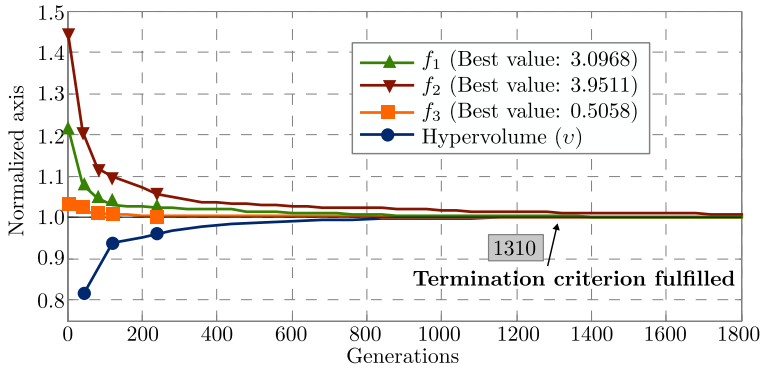

Figure 7.9: Convergence pattern in PDCCH optimization.

other metrics that depends on other (independent) parameters such as β_c, and hence, the expected tradeoff is not reflected in the 2D profile. Nevertheless, the idea is to illustrate how much complex the analysis of the problem becomes by adding additional objectives to the multiobjective formulation. This is a consequence of the Pareto dominance relationships in a high-dimensional (more than 3) objective space. In any case, all the metrics considered are mandatory to get sure that the resulting configurations provide actual gains without losing sight of the important objectives related to the capacity of the data channel (f_1 and f_2).

7.6 Convergence and Feasibility Aspects

In this section, the convergence pattern of the algorithm NSGA-II for PDCCH and ePDCCH optimization is presented.

Figure 7.9 shows the evolution of the normalized hypervolume (υ) and each objective function. It was found that the termination criterion is fulfilled, on average, after 1310 generations. It can be noticed that, after only 750 generations, all the indicators are within 98% of their final value. This means that the algorithm reaches a convergence state relatively fast taking into account the amount of generations required to meet the termination criterion.

Similarly, Figure 7.10 illustrates the convergence pattern of both optimization schemes (POS and FOS) in terms of the hypervolume indicators (υ) for the case of ePDCCH optimization. It can be seen that initially the convergence of FOS is slower than POS. This is due to the higher number of design variables that need to be adjusted in FOS. However, after a certain number of generations (approx. 500), FOS features better convergence, explaining so the differences in performance previously found. However, it is worth mentioning that both schemes are valid since there are cases in which the computational cost is a limiting factor, for instance, in very large scale scenarios, and hence, a 3% in convergence can be traded by an interesting saving of 26% in computational cost that can be achieved by means of POS.

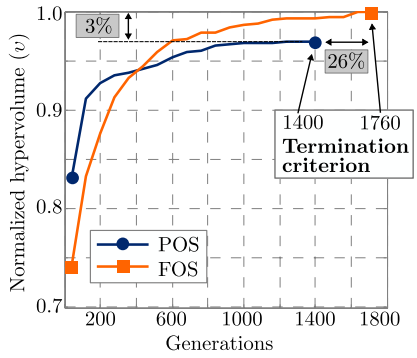

Figure 7.10: Convergence pattern in ePDCCH optimization.

Both schemes, POS and FOS, are compatible with the mechanisms already defined in LTE-A. As it was mentioned previously, the allocation of the ePDCCH to users is dynamic, and hence, the allocation of the amount of resources indicated by the parameter β_c is already considered in the technical specifications (see [261] for details). A similar reasoning applies to the power adjustments specified by the paremeter α. Thus, the way in which the proposed models are implemented depends on the vendor but no change with respect to the standard is required.

7.7 Concluding Remarks

The performance of cellular systems such as LTE and LTE-A strongly depends on the reliability of the control channels that convey the critical user-specific information. In practice, it is commonly believed that since control channels are designed to be more robust than data channels, no additional measures need to be taken. However, the consumption of control resources is linked to the average radio channel quality, and hence, cell edge users penalize significantly the capacity of the control channels.

In addition, previous studies have shown how the PDCCH acts as a *bottleneck* in scenarios with many real-time (low-rate) users. In the light of this situation, the new frequency-multiplexed ePDCCH was incorporated in LTE-A to increase the signaling capacity of the system.

This chapter investigates multiobjective ICIC optimization frameworks to improve the performance of both structures: the PDCCH and ePDCCH. In the first case, the capacity of the PDCCH was enhanced by reducing the areas of the network where high aggregation levels are required. The previous was accomplished by means of a strategy that optimizes the power allocated to the PDCCH at each cell. The problem in ePDCCH optimization is much more complicated because resources from the data channels are borrowed from, and hence, the impact of the capacity of these channels must be considered. Given that the ePDCCH is frequency-multiplexed, frequency domain ICIC can be applied to it. The schemes presented in this chapter

investigate the use of SFR to protect the ePDCCH and so, increase its capacity. The two different schemes presented are largely based on the framework introduced in previous chapters, although with the required adaptations.

Given that these solutions are based on the statistical framework presented in Chapter 3, they can be used in any realistic deployment. The novel strategies are able to find network configurations providing significant enhancements to the capacity of the control channels without a negative impact on the performance of the data channels. Moreover, the core-processing can be done offline and the output is composed of many near-optimal solutions that jointly optimize all the performance criteria. After evaluating the merit of the novel strategies, the main conclusions can be summarized as follows:

- Both global and local improvements are only achievable by improving the radio channel conditions at cell edges as these areas represent a severe penalty in terms of the consumption of control resources. Thus, ICIC for control channels is both relevant and required.
- The rigid design of the PDCCH does not allow applying an ICIC strategy properly said. However, the formulation presented in this chapter captures the essence of the problem and it takes an ICIC-oriented approach by focusing on improving the bottom tail of the resulting average SINR distributions. This provides, on average, a reduction of the consumption of control resources.
- The ePDCCH, being inserted within the PDSCH, allows for ICIC. Thus, two SFR-based schemes were developed. By adjusting the classification thresholds (ψ_{TH}) at each cell and the power ratio (α) locally and globally, configurations that increase the capacity of the ePDCCH were obtained.
- The use of MOEAs in the context of ICIC for control channels was investigated. The results and experience obtained during the research indicate that appropriate calibration results both in effective optimization and good convergence. As it was mentioned earlier, in problems such as the one studied herein, the use of exact or deterministic optimization techniques is not possible without relaxing the problem. Thus, in order to keep expressions that capture accurately the behavior of the ICI, metaheuristic procedures (MOEAs) based on global stochastic search has been successfully employed. The main advantage of the method resides on the fact that a good picture of the tradeoffs and several solutions are obtained. Interestingly, it is found that reducing the average consumption of eCCEs (network-wide) does not implies necessarily a payoff in terms of the consumption of the worst cell.

Finally, it is important to remark that the implementation and use of the solutions obtained through the novel strategies are transparent in system such as LTE and LTE-A. Indeed it does not require either any change with respect to the current specifications or assume any particular interworking with other network functionalities. The optimization models capture the network geometry and focus on the optimization of long term ICI conditions, thus, they feature an attractive tradeoff between performance and feasibility.

Chapter 8

Further Improvements to Energy Efficiency

8.1 Introduction

Along the previous chapters, the proposed ICIC strategies included the energetic perspective by minimizing power requirements in the air interface. As it was indicated in Chapter 2, this is an increasingly important aspect in the context of wireless networks, but it is often missed in ICIC solutions. Nevertheless, although the optimization models presented so far for ICIC reduce significantly the transmitted power, the corresponding energy saving only represents a very small fraction of the overall power consumption at base stations. Thus, in order to achieve a more graspable improvement in terms of energy saving, additional measures need to be taken. This chapter takes the efforts a step further by extending and adapting the ICIC models presented in previous chapters to the emerging field of CSO. As it will be shown shortly, there are interesting connections between this framework and ICIC. Therefore, the experience and knowledge previously obtained were successfully applied in CSO. The study, developed at Carleton University, Canada, was framed in the context of the project '5G+', the largest collaborative research project between academia and industry in Canada on 5G wireless networks[1].

Today, nobody can deny the explosive growth of the wireless network industry. The rising cost of energy and the increased environmental awareness have created the urgent need for developing energy efficient *green* communications [248]. This requires close interactions between different (previously independent) frameworks towards this common objective. Thus, this Ph.D. dissertation also aims at getting ICIC closer to this transversal goal, and consequently, the scope has been not limited

[1]The project is funded by the Ontario Ministry of Economic Development and Innovation's ORF-RE (Ontario Research Fund - Research Excellence) program, Huawei Canada, Telus, and Carleton University.

to include energy efficient aspects into the optimization formulations, but also to develop energy saving schemes inspired by ICIC models. This is the case of the CSO proposal presented in this chapter.

The next section introduces the context of green communications and the different approaches that are being investigated. Among them, CSO is without a doubt, one of the most promising strategies, and as such, it has captured great attention in the last few years. The section introduces the most fundamental aspects of this framework. Next, in Section 8.3, a survey of relevant contributions is provided. Based on this review, several research gaps were identified, and eventually, they turned into a multiobjective optimization scheme for CSO in dense cellular networks. The details of the novel system and method are explained in Section 8.4. Performance evaluations based on system level simulations are presented in Section 8.5. The results include a comparative analysis with previous proposals. Finally, the chapter is closed with a discussion about the advantages of this approach and conclusions.

8.2 Green Communications and Cell Switch Off

According to [267], Information and Communications Technologies (ICT) is a growing sector that has an important share of the overall green house gas emissions. Thus, as an important component of ICTs, wireless communications networks are concerned with strategies to reduce the energy consumption not only for environmental aspects but also for economical reasons. In this scenario, the cellular communications industry is growing exponentially worldwide. Thus, *green* communications and energy efficiency are now very important issues for mobile operators. To cope with this issue, the research community has addressed the problem from different angles and a variety of proposals has been presented. In the context of cellular systems, the proposals can be classified as follows:

1. *Cell Layout Adaptation*: This family of strategies includes algorithms and schemes in which the cell coverage pattern is modified dynamically. Within this category, strategies designed for HetNets have been studied [268]. These schemes have proven to be an interesting alternative to improve the energy efficiency of cellular networks by means of cell-breathing-like mechanisms. However, from an energy consumption point of view, the value of these algorithms is limited. Another approach is the use of relays [269], but in this case, energy efficiency gains are only possible in cases where the power consumed by relaying is significantly low compared to direct links.

   In addition to these schemes, algorithms whose idea is to exploit temporal and spatial variations of traffic to turn off base stations in which a significant part of resources are idle have been proposed. This paradigm is called CSO and preliminary works such as [270] showed that the power consumption can be significantly improved in dense deployments. In these scenarios, energy savings between 25% and 60% can be obtained [271]. Thus, the framework presented herein is inspired by this approach. An introduction to CSO is provided shortly.

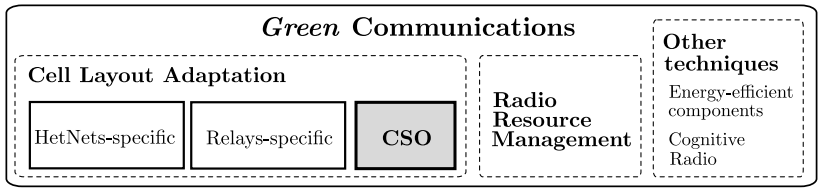

Figure 8.1: Techniques enabling energy efficient and green communications.

2. *Radio Resource Management*: This family includes several energy-efficient transmission techniques and radio resource allocation algorithms. Interesting surveys on this type of contributions can be found in [272, 273].

3. *Other approaches*: Additional strategies include Cognitive Radio (CR) based schemes and research towards energy efficient components such as power amplifiers and cooling systems. Potential applications of CR for green communications are discussed in [274]. Research focused on energy-efficient components is another highly active area. An interesting example can be found in [275].

A big picture of the context of green communications is illustrated in Figure 8.1. Additional material related to techniques enabling energy-efficient communications in wireless networks can be found in [246–248] and the references therein.

8.2.1 Cell Switch Off Basics

The CSO problem has its origin in the need for energy-efficient wireless networks. Initial approaches to green communicationswere were oriented towards minimizing the radiated power, which in turns reduces the electromagnetic pollution and its potential risks on human health. Unfortunately, between 50% to 80% of the energy consumption in wireless networks takes place on the radio access infrastructure, specifically at base stations [276]; being this consumption independent of the traffic load. Therefore, the idea of **switching off lightly loaded base stations** has been considered recently as *the alternative* to achieve significant energy savings. Interesting CSO contributions are surveyed in the next section.

Problem Statement

The CSO problem consists in determining the largest set of cells that can be switched off without compromising the Quality of Service (QoS) provided to users.

Theoretical aspects

- *Energy savings and deployment density*. It is well-known that, the denser the cellular deployments is, the higher the energy saving that can be achieved [277].

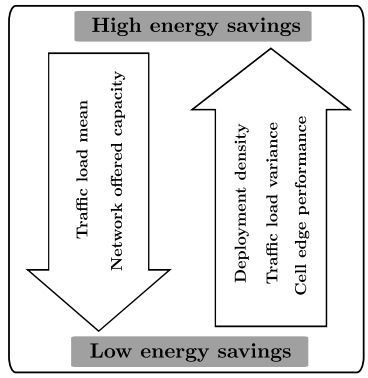

Figure 8.2: Energy saving tradeoffs. Arrows indicate increments of the variables.

Recall that cellular networks are dimensioned to meet traffic demand in the busy hour, and hence, most of the resources are underutilized. Thus, the dense cell deployment is the natural context to test the performance of CSO.

- *Energy savings and traffic behavior.* The amount of energy saving is proportional to the variance-to-mean ratio of the traffic load (in time and space) [277].
- *Energy savings and network capacity.* In general, the higher the number of active cells, the higher the network capacity, which is a direct consequence of the frequency reuse. Therefore, energy saving and offered capacity are conflicting objectives in the context of CSO.
- *Energy savings and ICIC.* In OFDMA, the higher the frequency reuse, the worse the radio quality at cell edges as more ICI is created. Thus, intuitively, it can be concluded that less active cells create less ICI, and hence, the radio channel quality of cell edge users can be improved more easily.

The previous tradeoffs are illustrated in Figure 8.2.

Practical aspects

- *Coverage.* This is an important aspect that must be taken into account. The term 'coverage' refers to the fraction of the serving area in which the network is able to provide services. In general, coverage depends on two variables: the received signal power (sensitivity) and SINR (inversely proportional to the amount of ICI). Thus, any given point of the serving area is said to be in coverage outage (hereafter outage), if the minimum requirement in terms of 1) the received power from the serving cell ($P_{\min}^{\mathrm{Rx}}$), and 2) SINR ($\psi_{\min}$), are not met. Coverage analysis in CSO is crucial due to the fact that many coverage holes can appear as base stations are switched off.
- *Switch on/off transitions.* From a practical perspective, minimizing the number of transitions is advisable. Switching on/off base stations is far from being a

simple procedure, and indeed, this process must be gradual and controlled as it has been pointed out in [278, 279]. Moreover, a large number of transitions could result in a high number of network-triggered handovers with a negative impact on other RRM functionalities.

- *Solution architecture*. Although centralized solutions provide more stability than distributed mechanisms, they require that information from all over the network is transmitted to a centralized unit. Depending on the type/amount of data, network size, and operation time scale, feasibility and complexity could become difficult issues to deal with. Thus, distributed and semidistributed solutions are preferred.

- *Additional aspects*. Other practical aspects such as emergency switch-on mechanisms, improved migration (handover) procedures [280], pilot power adaptation, and control channels reliability are also interesting features to consider. A discussion about these aspects can be found in [281, 282].

8.3 Related Work

The literature review presented herein includes relevant contributions presented recently. Given the diversity among existing studies, it is difficult to establish common points for comparison. Thus, the following criteria have been considered:

- *C1*: It indicates the type of tool used in the resolution of the problem: analytical tools, heuristics, metaheuristics.

- *C2*: It indicates the type of architecture of each proposal: distributed, semidistributed, or centralized.

- *C3*: It indicates whether coverage/outage aspects are considered. Coverage aspects include a minimum SINR or the receiver's sensitivity, i.e., the minimum required power.

- *C4*: It indicates whether a realistic ICI model is used. A strong assumption that can be easily found is the computation of SINR values considering all cells as active, even after swithching off some of them. Somehow this invalidates part of the outcomes. C4 indicates whether this assumption has been considered.

- *C5*: It indicates whether practical aspects such as the number of transitions, stability, intercell signaling, real time complexity, or computational cost are analyzed.

- *C6*: It indicates the traffic model.

Table 8.1 shows a comparative assessment based on the previous criteria, referred to as *Cx*. As it can be seen, no proposal meets all these criteria. Note that typically the works propose heuristics to tackle the CSO problem (C1), sometimes preceded

Table 8.1: Summary of CSO proposals and contributions

Ref.	Context	C1	C2	C3	C4	C5	C6
[283]	CSO	Heuristic	CE	×	×	P	Full buffer
[284]	CSO	Analytical	CE	P	×	×	Full buffer
[285]	Planning: how to deploy cell for minimizing energy consumption	Analytical	NA	P	×	NA	NA
[286]	CSO	Heuristic	CE	×	×	×	Poisson
[287]	Cell size adaptation	Heuristic	CE	×	×	×	Full buffer
[288]	An interesting RRM strategy for energy savings	Heuristic	CE	×	×	×	Poisson
[289]	CSO	Heuristic	Both	×	×	✓	Full buffer
[277]	CSO	Analytical	CE	×	×	×	Poisson
[290]	CSO	Analytical	CE	×	P	×	Full buffer
[291]	CSO	Heuristic	CE	×	P	P	Full buffer
[292]	CSO	Heuristic	CE	P	P	×	Full buffer
[293]	CSO	Heuristic	CE	×	✓	P	Realistic
[294]	CSO	Heuristic	SD	×	×	P	Realistic
[295]	Cell size adaptation	Heuristic	Both	×	×	×	Realistic
[296]	CSO	Heuristic	CE	×	×	×	Full buffer
[297]	CSO	Heuristic	CE	×	×	×	Full buffer
[298]	CSO	Heuristic	CE	×	×	×	Several models
[299]	Impact of power reduction on coverage and capacity	Analytical	NA	✓	✓	NA	Full buffer

P: Partially CE: Centralized SD: Semidistributed DI: Distributed

by analytical formulations used as starting point. This clearly indicates the practical approach followed by many authors, in contrast to the vast majority of resource allocation schemes that rely on optimization formulations.

As it can be seen, the majority of schemes require centralized operation (C2). This is expected given the nature of CSO, i.e., a certain global knowledge is required in order to determine which base stations can be switched off.

From the comparative analysis, it is also clear that coverage analysis is often missed (C3). Moreover, the survey also reveals that ICI models (C4) are not so accurate, which is done mainly to make the mathematical treatment feasible. Sometimes, these type of assumptions could lead to erroneous conclusions, especially in a CSO-ICIC scenario. Regarding this aspect, the author believe that ICI must be modeled accurately since it is the main capacity-limiting factor in cellular systems, and in the particular case of CSO, **ICI conditions vary drastically as cells are switched on/off**. The author also believes that, a joint ICIC-CSO framework is an interesting research line. However, it is worth saying that incorporating this feature into the picture makes the problem extremely complicated.

Feasibility aspects (C5) are also forgotten most of the time. Despite it is a very important element, the vast majority of the studies do not pay great attention to implementation. Indeed, statistics of the number of handovers or required number of transitions rarely appear.

Finally, full buffers is usually considered as traffic model (C6). Only few works incorporate more realistic patterns.

In the light of the previous findings, it can be concluded that 1) there is a good room for improvement in the context of CSO, and 2) ICIC notions can (and should) be incorporated within these formulations. The next section provides a description of the framework developed for CSO in dense cellular networks.

8.4 Framework Description

The main research objective of this work is to design a scheme that can take advantage of the well-known behavior of traffic both in space and time to reduce the energy expenditure in the radio access network. Rather than following the conventional, but hardly feasible, user-oriented approach in which an optimization procedure needs to be performed for every discrete realization of users, this framework aims at employing the statistical behavior of the traffic. In this manner, by means of multiobjective optimization, a set of *high quality* (Pareto efficient[2]) network configurations is found. These network configurations, understood as any possible combination of active and inactive cells, provide a near-optimum tradeoff between the number of active cells and average system capacity.

[2]An introduction to multiobjective optimization is provided in Chapter 5.

Design insights

First, some definitions and conventions need to be introduced:

- *Network Operation Point* (NOP): In this context, a NOP is any possible state of the network in terms of active and non-active (switched off) cells. Thus, a network composed of L cells, has $(2^L - 1)$ NOPs, being each of them represented by a binary string $\mathbf{x} \in \{0,1\}^L$ of length L. All possible solutions form the set $\mathcal{X}$ with $|\mathcal{X}| = (2^L - 1)$. If the i^{th} element of $\mathbf{x}$ is equal to 1, the i^{th} cell is active, otherwise it is switched off.
- *Network Energy Level* (NEL): The NEL is defined as the number of active cells in a NOP, i.e., the sum of the '1's in any CSO network configuration. Thus, the j^{th} NEL can be understood as the set $\mathcal{X}_j$ defined as the set of all the solutions in which j cells are active. Thus, $\mathcal{X}_j = \{\mathbf{x} \in \mathcal{X} \mid \mathbf{x} \cdot \mathbf{1} = j\}$.
- *Snapshot*: A snapshot corresponds to any possible state of the network in terms of active users. It is assumed that the location of users at any given time follows a spatial traffic distribution $\mathbf{\Gamma}$. The vector $\mathbf{\Gamma} \in \mathbb{R}^A$ indicates the probability (in the event of a new a user) of each pixel having the user on it, and hence, $\mathbf{\Gamma} \cdot \mathbf{1} = 1$. Since the traffic behavior is statistically well-known to the mobile operators, it is reasonable to assume that $\mathbf{\Gamma}$ is known. The assumption is commonly found in CSO literature [277, 291, 294, 296, 297].

The research objectives can be summarized as follows:

1. *Minimize overall network power expenditure.* To that end, the underlying intuition is to find the minimum set of active cells that provides a certain QoS.
2. *Prioritize zones in which traffic load is concentrated.* The idea is to give higher importance to cells providing better capacity to areas in which users are more likely to appear. This is done by weighting each pixel according to $\mathbf{\Gamma}$. Thus, a novel metric: *the weighted network capacity*, is proposed aiming at focusing the exploration of the search space ($\mathcal{X}$) in regions where such network configurations can be found.
3. *Find near-optimal* NOPs ($\mathcal{X}^\star$): The idea is to find, for each NEL, the NOP that maximizes the weighted network capacity. In principle, the solutions belonging to the set $\mathcal{X}^\star$ would provide good QoS, on average, to users located/distributed according to $\mathbf{\Gamma}$. Thus, the set $\mathcal{X}^\star$, composed of solutions that are $\mathbf{\Gamma}$-specific, is obtained by considering the tradeoff between the number of switched off cells and aggregate network capacity. As these criteria are conflicting objectives, multiobjective optimization represents a convenient approach to investigate CSO through the Pareto dominance notion. This hypothesis is confirmed by the results presented in Section 8.5.
4. *Robustness and feasibility*: The design should be flexible to be applied to any network topology. In addition, the operation should be done in time scales of

tens of minutes or hours as the traffic patterns ($\mathbf{\Gamma}$'s) can be considered fairly constant during time intervals with arbitrarily small duration [277, 294]. In addition, no interworking with other RRM entities must be assumed in order to allow for transparent implementation.

5. *Low complexity*: The real time complexity should be minimized. In the CSO scheme presented here, the optimization procedure is done offline. Such processing requires, on the one hand, a radio characterization of the coverage area, and on the other hand, the knowledge of $\mathbf{\Gamma}$, both typically available. Thus, the solutions can be stored in databases and/or look-up tables and they can be used in real-time operation with minimal effort.

8.4.1 System Model

The system model is described in Appendix C, Section C.1. In addition, each cell transmits all its available power equally distributed over the system bandwidth, i.e., full frequency reuse.

Recall that the vector $\mathbf{x}$ is a binary string indicating which cells are active and which ones are switched off. Taking this into account, the average CS-RS received power, indicated in (C.1), can be generalized by considering the vector $\mathbf{x}$ as follows:

$$\mathbf{R}_{\text{CS-RS}} = \mathbf{G} \cdot \text{diag}\left(\mathbf{p}_{\text{CS-RS}} \odot \mathbf{x}\right). \tag{8.1}$$

Note that (C.1) and (8.1) are equivalent if all the cells are active. Thus, the cell coverage pattern, i.e., the area associated to each cell (given by the matrix $\mathbf{S}$, see Section C.1) becomes a function of $\mathbf{x}$. However, for the sake of clarity, that dependence is omitted.

According to the system model, the vector $\mathbf{p}_{\text{PDSCH}}$ indicates the transmitted power over the data channel (the PDSCH) at each cell. Without loss of generality, it is assumed that $\mathbf{p}_{\text{PDSCH}}(l)$ is the same for all $l = 1,\ 2,\ \cdots,\ L$ and that $\mathbf{p}_{\text{PDSCH}} = \mathbf{p}_{\text{CS-RS}}$ (see Appendix C). Recall that coverage criteria are taken into account. In this manner, the vector $\mathbf{\Psi} \in \mathbb{R}^A$ representing the average SINR at each pixel is given by:

$$\mathbf{\Psi} = \left[(\mathbf{S} \odot \mathbf{G}) \cdot (\mathbf{p}_{\text{PDSCH}} \odot \mathbf{x})\right] \oslash \left[\left[(\mathbf{S}^{\text{c}} \odot \mathbf{G}) \cdot (\mathbf{p}_{\text{PDSCH}} \odot \mathbf{x})\right] \oplus \sigma^2\right]. \tag{8.2}$$

Recall that $\odot$, $\oslash$, and $\oplus$ indicate Hadamard (pointwise) operations and σ^2 is the noise power. Note that the definition of $\mathbf{\Psi}$ captures the actual ICI generated in the network as only active cells are taken into account. Without loss of generality, it has been assumed that collisions (among active cells) occur with probability 1 as CSO schemes tend to concentrate traffic in few cells. Nevertheless, load factors $< 100\%$ can be introduced easily in the system model [300].

In order to take coverage aspects into account, it is assumed that the a^{th} pixel is in outage if the following conditions are not met:

- Minimum received power: $\mathbf{R}_{\text{CS-RS}}(a, l^{\star}) \geq P_{\min}^{\text{Rx}}$.
- Minimum SINR: $\mathbf{\Psi}(a) \geq \psi_{\min}$.

The spectral efficiency of each pixel is stored in the vector $\mathbf{H} \in \mathbb{R}^{A}$, which is obtained by computing a non-decreasing function of the SINR. To capture the level of sensitivity with respect to the SINR variations, the Shannon's formula is considered. Thus, allowing a certain abuse of notation, the following expressing can be written:

$$\mathbf{H} = \log_2(1 + \mathbf{\Psi}). \tag{8.3}$$

In order to take into account the coverage criteria and penalize solutions with coverage holes, the spectral efficiency of the a^{th} pixel is computed according to the following rule:

$$\mathbf{H}(a) = \mathrm{u}(\mathbf{\Psi}(a) - \psi_{\min}) \cdot \mathrm{u}\left(\mathbf{R}_{\text{CS-RS}}(a, l^{\star}) - P_{\min}^{\text{Rx}}\right) \cdot \log_2(1 + \mathbf{\Psi}(a)), \tag{8.4}$$

where $\mathrm{u}(\,)$ is the unit step function (see Apendix A).

8.4.2 Performance metrics

The main target in any CSO scheme is minimizing energy consumption subject to QoS constraints. In this manner, two objectives are considered:

1. *The minimization of the number of active cells* (f_1). This metric was considered because the major part of the energy consumption is proportional to the number of active cells. This expression can be easily generalized to the case where different cells have different energy expenditure by considering the minimization of a weighted sum. The assumption is largely adopted in the literature [283, 295]. Note that f_1 is equivalent to the NEL of each solution $\mathbf{x}$. Thus, f_1 is defined as follows:

$$f_1 = \mathbf{x} \cdot \mathbf{1}. \tag{8.5}$$

2. *The maximization of the weighted network capacity* (f_2): This metric is based on the expected value of the spectral efficiency at pixel level but **including the effect of the traffic distribution $\mathbf{\Gamma}$**. In this manner, it represents the weighted sum of the pixel's throughputs. Given that the contribution of the pixels out of coverage is not considered, see (8.4), this metric takes into account information about the offered traffic and coverage level provided by each NOP. Thus, for any given solution $\mathbf{x}$, the metric is defined as follows:

$$f_2 = (B \cdot A) \cdot \left[\left[(\mathbf{H} \odot \mathbf{\Gamma})^{\mathrm{T}} \cdot \mathbf{S}\right] \odot \mathbf{n}\right] \cdot \mathbf{1}. \tag{8.6}$$

Equation 8.6 deserves some comments. The vector $\mathbf{H} \odot \mathbf{\Gamma}$ contains the weighted spectral efficiency of each pixel as the *nominal* one is scaled by $\mathbf{\Gamma}$. The intuition is to give more importance to the $\mathbf{x}$'s that are expected to provide better spectral efficiency

to the zones with more concentrated traffic load. The constant A corresponds to the number of pixels and it is used to normalize the obtained capacity to the reference case where all the pixels have the same probability, i.e., $\mathbf{\Gamma}(a) = 1/A \ \ \forall a$. The vector $\mathbf{n} \in \mathbb{R}^L$ contains the inverse of the sum of each column in $\mathbf{S}$, i.e., the number of pixels served by each cell. It is assumed that each pixel is served by one cell at a time. This vector is used to distribute the capacity of each cell evenly over its coverage area, i.e., the bandwidth is shared equally by the pixels belonging to each cell. This improves the fairness in the long run similar to the proportional fairness policy that tends to share the resources equally among users as time passes. This fairness notion results in decreasing the individual rates as the number of users increases. This effect is also captured by $\mathbf{n}$ as the bandwidth per pixel is inversely proportional to the pixels associated with each cell.

8.4.3 Multiobjective Problem Formulation

In order to 1) capture the tradeoff between the number of active cells (f_1) and aggregate network capacity (f_2), and 2) obtain more than one single network configuration for each traffic profile $\mathbf{\Gamma}$, the use of multiobjective optimization has been investigated. The multiobjective optimization problem can be formulated as follows:

$$\begin{aligned} \text{minimize} \quad & [\ f_1(\mathbf{x}),\ -f_2(\mathbf{x})\ ], && \text{(8.7a)} \\ \text{subject to:} \quad & \\ & \frac{(\mathbf{v}^{\mathrm{T}} \cdot \mathbf{1})}{A} \leq \kappa_{\mathrm{COV}}, && \text{(8.7b)} \\ & \mathbf{x} \in \{0,1\}^L,\ \mathbf{x} \neq \mathbf{0}. && \text{(8.7c)} \end{aligned}$$

Problem 8.7 defines the multiobjective framework considered herein. The objective functions in (8.7a), f_1 and f_2, are defined by (8.5) and (8.6), respectively. Constraints 8.7b and 8.7c correspond to the coverage criterion and the feasible set ($\mathcal{X}$), respectively. The binary vector $\mathbf{v} \in \{0,1\}^A$ indicates the outage pattern associated to each solution $\mathbf{x}$. Therefore, if the a^{th} pixel is in outage, $\mathbf{v}(a) = 1$, and 0 otherwise. The parameter κ_{COV} is an operator-defined figure indicating how much (coverage) outage is allowed.

Problem 8.7 corresponds to a combinatorial optimization task that belongs to the class NP-complete, and hence, an optimal solution cannot be found in polynomial time. Thus, in order to solve it efficiently, two different approaches has been considered:

1. *Stochastic search*: This is done by means of the algorithm NSGA-II (see Section 5.4). The use of MOEAs is also considered in the context of CSO given the similarities between the frameworks investigated for ICIC (Chapters 6 and 7) and the combinatorial formulation required for CSO. Indeed, the particularities found in this context makes even more advisable to use MOEAs because the inherent tradeoff between the aggregate capacity and the number of active

cell is suitable to be exploited by means of multiobjective techniques and the Pareto efficiency concept. Moreover, the very complex structure of the weighted network capacity (8.6) together with its combinatorial nature makes impossible to address this problem by means of traditional optimization tools without relaxation. The results presented later on confirm that the proposed method is a convenient approach to CSO featuring several interesting advantages with respect to previous proposals[3].

2. *Minimum distance algorithm*: As it was mentioned, the need for minimizing the number of transitions is very important from a practical perspective. With this requirement in mind, a novel heuristic is also proposed. The algorithm aims at finding a collection of NOPs, one for each NEL, featuring 1) the minimum distance property, and 2) acceptable performance. In this context, the word 'distance' refers to the Hamming distance (d_{H}), i.e., the number of positions in which the corresponding symbols in two different solutions are different. In this manner, for two solutions $\mathbf{x}_i$ and $\mathbf{x}_j$ in a set $\mathcal{X}^{\star}_{\mathrm{md}}$ featuring the minimum distance property, the following implication always holds:

$$d_{\mathrm{H}}\left(\mathbf{x}_i, \mathbf{x}_j\right) = 1 \Rightarrow \left|\left(\mathbf{x}_i \cdot \mathbf{1}\right) - \left(\mathbf{x}_j \cdot \mathbf{1}\right)\right| = 1. \tag{8.8}$$

Algorithm 8.1 is used for finding the set $\mathcal{X}^{\star}_{\mathrm{md}}$. Initially, the algorithm determines the best NOP with NEL = 1 ($\mathbf{x}_1$) in lines 3-9. Then, in lines 11-19, for each successive NEL (NEL = 2, 3, ..., L), the algorithm finds the best cell that should be activated (resulting in the solution $\mathbf{x}_j$), such that 1) the Hamming distance with the previous solution $\mathbf{x}_{j-1}$ is one, and 2) the function f_2 is maximized. In this manner, each solution that is added to the set $\mathcal{X}^{\star}_{\mathrm{md}}$ provides the biggest increment in terms of f_2 with respect to the one previously added and only one cell needs to be turned on, i.e., only one transition.

It is worth saying that the two previous methodologies can be used to estimate the set of Pareto efficient solutions $\mathcal{X}^{\star}$. Both approaches build a set composed of solutions with different NELs, and hence, different values of f_2. This is accomplished in case of stochastic search by means of the Pareto dominance notion[4], while in case of the minimum distance algorithm, the heuristic is explicitly designed to do that. Note that, in case of the minimum distance algorithm, $\mathcal{X}^{\star} = \mathcal{X}^{\star}_{\mathrm{md}}$ and $|\mathcal{X}^{\star}| = L$. The second condition, in general, cannot be guaranteed by means of stochastic search. This depends on the level of diversity achieved by the MOEA. Indeed, having $|\mathcal{X}^{\star}| = L$ is very important because it indicates the best distribution of the elements of $\mathcal{X}$, i.e., one solution for each NEL.

[3]The multiobjective method has been patented and filed by Huawei Canada, see [P1].

[4]Recall that f_1 is equivalent to the NEL of each solution $\mathbf{x}$, see (8.5), and hence, the Pareto efficiency concept (see Section 5.2) guarantees that two solutions in $\mathcal{X}^{\star}$ cannot have the same NEL. However, it is possible to obtain solutions with the same NEL for different traffic profiles ($\mathbf{\Gamma}$).

Algorithm 8.1: A method for finding a minimum distance set.

input :
$\mathcal{X}_1$: Set of NOPs with NEL=1, $\mathcal{X}_1 = \{\mathbf{x} \in \mathcal{X} \mid \mathbf{x} \cdot \mathbf{1} = 1\}$, $|\mathcal{X}_1| = L$.
output:
$\mathcal{X}^{\star}_{\mathrm{md}}$: A set of L NOPs featuring minimum distance.

```
// Initiates the capacity variable;
C* ← 0;
// Initiates the output set;
X*_md ← ∅;
// Looking for the best NOP with NEL = 1;
for each x ∈ X_1 do
    // Get the weighted network capacity;
    C_x ← f_2(x);
    // Look for the best initial point;
    if C_x > C* then
        // Updates the best value;
        C* ← C_x;
        // Update the best NOP with NEL = 1;
        x_1 ← x;
    end
end
// Updates the output;
X*_md ← X*_md ∪ {x_1};
// Looking for the rest of NOPs, NEL > 1;
for each j = 2 : L do
    // Initiates the capacity variable;
    C* ← 0;
    // Look for the best new active cell;
    for each x ∈ X_j | d_H(x, x_{j-1}) = 1 do
        // Get the Weighted Network Capacity;
        C_x ← f_2(x);
        // Look for the best new member;
        if C_x > C* then
            // Updates the best value;
            C* ← C_x;
            // Update the best NOP with NEL = j;
            x_j ← x;
        end
    end
    // Updates the output;
    X*_md ← X*_md ∪ {x_j};
end
```

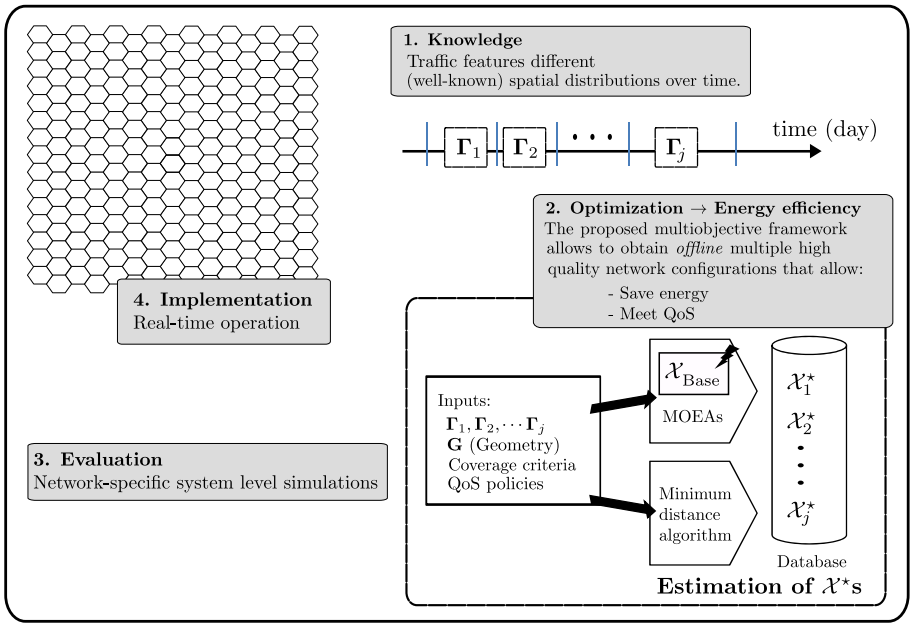

Figure 8.3: Conceptual design of the proposed framework.

8.4.4 Overall Architecture

Figure 8.3 illustrates the conceptual design of the proposed framework. The framework relies on the knowledge of traffic behavior both in time and space. By means of different traffic distributions ($\mathbf{\Gamma}_j$), the spatial component of the traffic at different moments of the day can be captured. These patterns can be considered fairly constant during time intervals whose duration can be arbitrarily small [277, 294].

Thus, starting from the knowledge of $\mathbf{\Gamma}$, a set of Pareto Efficient NOPs (with respect to f_1 and f_2, see Equations 8.5 and 8.6) can be obtained through MOEAs or Algorithm 8.1. It is important to say that $\mathcal{X}^\star$ is specific to $\mathbf{\Gamma}$, and hence, a traffic pattern $\mathbf{\Gamma}_j$ results in its corresponding set $\mathcal{X}_j^\star$.

The set $\mathcal{X}^\star$ is composed of several NOPs. Thus, an interesting question is about what configuration should be used at any given time. The answer requires introducing another element: the traffic intensity λ expressed in arrivals/sec. In general, the solution that must be applied depends on the traffic load because each element of $\mathcal{X}^\star$ provides a different aggregate throughput. However, higher network throughput requires more active cells, and consequently, more energy consumption. This is the fundamental tradeoff inspiring the multiobjective CSO approach.

Note that, by modulating λ by means of $\mathbf{\Gamma}$, different arrival rates λ_x result at different zones of the coverage area, thus modeling the behavior of the traffic realistically. This idea is illustrated in Figure 8.4.

A very nice feature of this framework is that the evaluation of the different

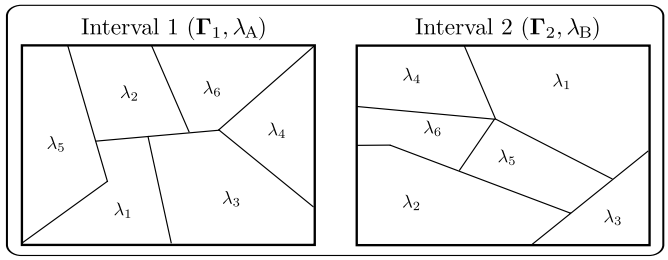

Figure 8.4: Realistic/irregular traffic patterns.

NOPs in the set $\mathcal{X}^\star$ can be done offline by means of system level simulations based on network operators' interests. In this manner, different QoS criteria, scheduling policies and traffic load patterns can be considered and evaluated independently.

In real time operation, provided a certain level of coordination among cells and basic pattern recognition techniques, it is possible to determine the current status of the network in terms of traffic distribution ($\mathbf{\Gamma}$) and load (λ). Thus, the selection and application of the configurations previously calculated and tested (the elements of the sets $\mathcal{X}_j^\star$ corresponding to each possible $\mathbf{\Gamma}_j$, see Figure 8.3) can be done with minimal real-time effort.

Obviously, each set $\mathcal{X}_j^\star$ mus be evaluated offline by means of system level simulations (for different traffic intensities) to determine the load that each solution can support subject to the QoS policies.

The next section presents the results corresponding to each of the processes described so far: the estimation of the set $\mathcal{X}^\star$ (by means of the two approaches presented before) and system level simulations.

8.5 Results

8.5.1 Test Case and Evaluation Setting

The test case is the scenario 'Small-dense' described in Appendix B, Subsection B.1.3. In order to emulate traffic unbalances, a particular spatial traffic distribution ($\mathbf{\Gamma}$) is required. Figure 8.5 illustrates the particular realization of $\mathbf{\Gamma}$ used for numerical evaluations. It is worth saying that the pattern shown in the figure is generated by means of the same bidimentional model used for shadowing, which is described in Appendix B, Section B.3. However, some parameters such as the correlation distance are adjusted to properly scale to the size of the network. As it can be seen, the traffic distribution pattern features a certain spatial correlation similar to traffic behavior. Note that red areas have around 10 times more probability of having traffic than blue areas, and hence, distributing users according to $\mathbf{\Gamma}$ results in a non uniform traffic distribution.

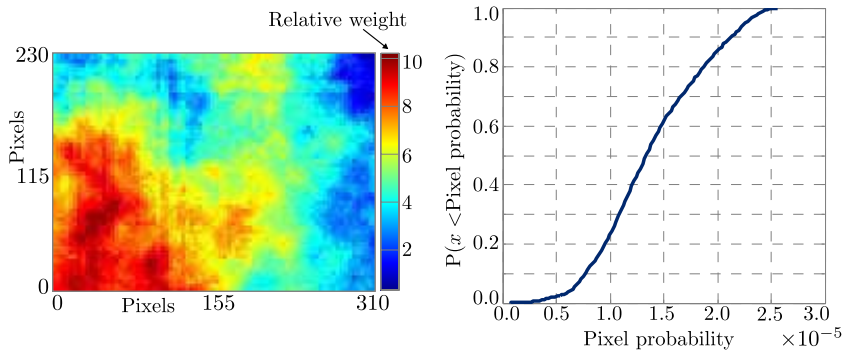

(a) Non uniform traffic distribution. **(b)** CDF of the probability of each pixel.

Figure 8.5: Spatial traffic distribution.

Table 8.2: Coverage constraints used in numerical evaluations.

Parameter	Value
Minimum SINR ($\psi_{\min}$)	-7.0 dB
Minimum received power ($P_{\min}^{\mathrm{Rx}}$)	-123 dBm
Outage threshold (κ_{COV})	2.0 %

The coverage constraints are shown in Table 8.2. The next subsection discusses and illustrates the impact of such parameters.

8.5.2 Impact of Coverage Constraints

In order to show the impact of coverage constraints, a random NOP ($\mathbf{x}_{\mathrm{R}}$) is evaluated according to the formulation presented in Section 8.4. The solution $\mathbf{x}_{\mathrm{R}}$ belongs to the NEL = 38 (38 out of the 54 cells are active) and it is as follows:

$\mathbf{x}_{\mathrm{R}}$=[1 1 1 0 1 1 0 1 1 0 1 0 1 1 0 1 1 1 1 1 1 1 1 0 1 1 1 0 1 0 1 0 1 1 0 1 0 0 0 1 1 0 1 1 1 1 1 1 0 0 1 1 1 1 1]$^{\mathrm{T}}$

As it can be seen in Table 8.3, more rigid coverage constraints result not only in greater outage but also lower values of the objective function f_2 as the spectral efficiency of outage pixels is discarded, see (8.4). Recall that along the optimization process, NOPs resulting in outage values larger than κ_{COV} (the operator-defined threshold) are also considered out of the feasible set.

Table 8.3: Evaluation of $\mathbf{x}_{\mathrm{R}}$ under different coverage constraints.

Constraints set 1	**Constraints set 2**
$\psi_{\min}$ = -7.0 dB $P_{\min}^{\mathrm{Rx}}$ = -123.00 dBm	$\psi_{\min}$ = -3.0 dB $P_{\min}^{\mathrm{Rx}}$ = -90.00 dBm
$f_1(\mathbf{x}_{\mathrm{Ref}}) = 38$ $f_2(\mathbf{x}_{\mathrm{Ref}}) = 536.68$ [Mbps]	$f_1(\mathbf{x}_{\mathrm{Ref}}) = 38$ $f_2(\mathbf{x}_{\mathrm{Ref}}) = 529.07$ [Mbps]
SINR outage = 0.02% Received power outage = 0.00% Total outage = 0.02%	SINR outage = 4.49% Received power outage = 4.20% Total outage = 4.49%

8.5.3 Multiobjective Optimization

As previously indicated, the estimation of the set $\mathcal{X}^{\star}$ has been investigated by means of two approaches. In this subsection, the merit of both alternatives is compared. It is important to recall that the calibration of the algorithm NSGA-II is done as in previous chapters. General guidelines are provided in Subsection 6.6.1.

Modified Initial Generation: Improved Convergence and Distribution

An improvement is proposed for the initial population in order to favor both convergence and distribution (better diversity). Bearing in mind the definition of the objective functions, it is expected that the estimated Pareto will be composed of at most L solutions, one for each NEL. The idea is to include the *extreme* solutions (the ones in the borders of the Pareto Front) from the very begining of the stochastic search. Thus, adding the solution with all the cells active implies having the upper limit of the Pareto Front. The lower limit is expected to be a solution with only one active cells, and so, the L solutions with NEL = 1 are included as well. Thus, the set $\mathcal{X}_{\mathrm{Base}}$ of configurations added to the initial generation is defined as follows:

$$\mathcal{X}_{\mathrm{Base}} = \{\mathbf{x} \in \mathcal{X} \mid \mathbf{x} \cdot \mathbf{1} = 1\} \cup \{\mathbf{x} \in \mathcal{X} \mid \mathbf{x} \cdot \mathbf{1} = L\}. \tag{8.9}$$

In this manner, the fact of having the extreme solutions in the initial population is exploit to complete the estimated Pareto Front from its limits by means of the genetic mechanisms (crossover and mutation).

A comparative study between the proposed initial population and the default (random) population is presented in Figure 8.6. The comparison is based on a population size of 110 individuals. Figure 8.6a shows a representation of the estimated Pareto Front (the images of the elements in $\mathcal{X}^{\star}$) for each case. On the one hand, the proposed modified initial generation succeeds in finding one solution for each NEL, i.e., the best possible diversity in terms of the number of members of the Pareto Front (54 Pareto efficient NOPs). On the other hand, the search starting from a random generation not only requires 24% more generations to converge, see Figure 8.6b,

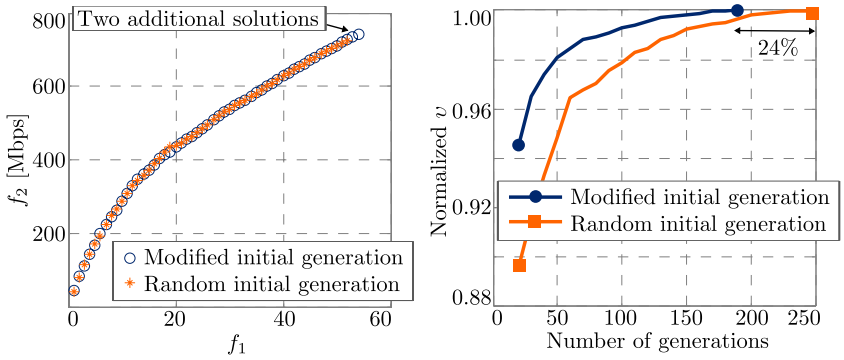

(a) Estimated Pareto Front. **(b)** Evolution of the hypervolume.

Figure 8.6: Performance gains through the improved initial generation.

but also fails in finding a complete Pareto Front, indeed, only 52 NOPs were found. This clearly indicates that the proposed modified initial generation represents an enhancement with respect to the baseline as both convergence and distribution are improved.

Stochastic Search vs. Algorithm 8.1

The merit of each approach can be estimated through direct comparison. Two aspects must be considered, the quality of the estimated Pareto Fronts and the complexity. The asymptotic complexity of Algorithm 8.1 is $\mathcal{O}(L^2)$, while the asymptotic complexity of the algorithm NSGA-II is $\mathcal{O}(K \cdot L^2)$. Recall that L is the number of cells in the system and K corresponds to number of objective functions. Thus, at least in terms of asymptotic complexity there is not big difference because in this formulation $K = 2$.

Let's consider that the sets $\mathcal{X}^{\star}_{\text{SS}}$ and $\mathcal{X}^{\star}_{\text{MD}}$ correspond to the sets of nondominated solutions found by means of stochastic search (by employing the algorithm NSGA-II) and the minimum distance heuristic (Algorithm 8.1), respectively. Thus, looking at the number of objective function evaluations, Algorithm 8.1 requires $\frac{L\cdot(L+1)}{2}$ operations to find the nondominated set $\mathcal{X}^{\star}_{\text{MD}}$, while NSGA-II requires $(N_{\text{pop}} \times N_{\text{gens}})$ operations to estimate $\mathcal{X}^{\star}_{\text{SS}}$. N_{pop} and N_{gens} are the population size and number of generations till the termination criterion, respectively. Note that in practice, a *good* termination criterion typically results in that $(N_{\text{pop}} \times N_{\text{gens}}) \gg \frac{L\cdot(L+1)}{2}$[5]. In any case, it is expected that the additional computational cost required in the stochastic search approach achieves better NOPs.

Figure 8.7 shows a comparison between $\mathcal{X}^{\star}_{\text{SS}}$ and $\mathcal{X}^{\star}_{\text{MD}}$. Figure 8.7a shows the corresponding Pareto Fronts in terms of the images f_1 and f_2. Note that the quality

[5]In the numerical assessment presented herein, $N_{\text{pop}} \times N_{\text{gens}} = 100 \times 190 = 20900$, while $\frac{L\cdot(L+1)}{2} = \frac{54\cdot(54+1)}{2} = 1485$.

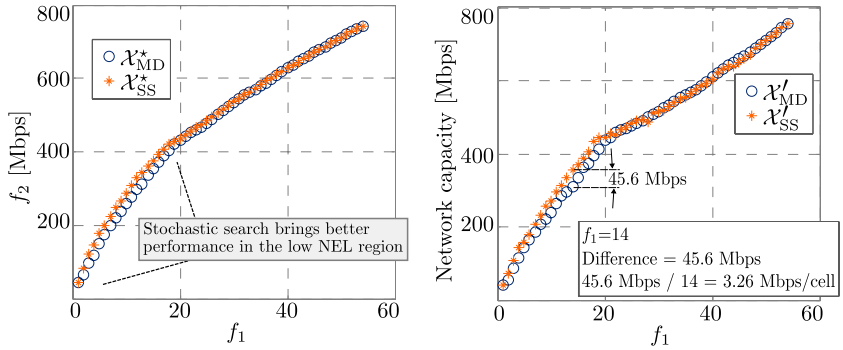

(a) f_1 vs f_2. **(b)** f_1 vs real capacity.

Figure 8.7: Comparison: Stochastic search vs. minimum distance algorithm.

of the solutions with $f_1 \geq 20$ is almost the same. However, for NOPs in the low NEL region ($f_1 < 20$), the solutions found by means of the algorithm NSGA-II are better. Given that f_2, the weighted network capacity, scales the spectral efficiency with $\mathbf{\Gamma}$, it is also interesting to look at the network capacity according to the conventional definition (without any weighting). The result is shown in Figure 8.7b. Again, the solutions in $\mathcal{X}^\star_{\text{SS}}$ also outperform the ones in $\mathcal{X}^\star_{\text{MD}}$ in terms of network capacity for the low NEL region. Taking as example the solutions with $f_1 = 14$, the difference in terms of network capacity is 45.6 Mbps, but as only 14 cells are active, a substantial gain of 3.26 Mbps/cell is obtained. This clearly illustrates the gain in terms of quality that can be achieved by means of MOEAs.

Moreover, it is worth noting that, taking into account the number of objective function evaluations required to meet the termination criterion and the size of the search space ($\mathcal{X}$), it can be concluded that the use of NSGA-II in conjunction with f_1 and f_2 accomplish a highly efficient exploration of the search space because only $\frac{N_{\text{pop}} \times N_{\text{gens}}}{2^L} = 1.16 \times 10^{-10}\%$ of the domain need to explored to obtain a good estimation of the set $\mathcal{X}^\star$.

Up to now, two different methods for finding the set of Pareto efficient solutions in terms of the metrics f_1 and f_2 have been presented. However, in order to shed light into the practical value of the solutions in the set $\mathcal{X}^\star$, system level simulations are presented.

8.5.4 System Level Simulations

General Setting and Methodology

System level simulations are based on Monte Carlo experiments. The results compile statistics taken from 100 independent experiments, each of which has a duration of 3600 s. The rest of the setting is explained in the following points:

- *Users*: Users are allocated in the coverage area according to the spatial traffic distribution $\mathbf{\Gamma}$ (see Figure 8.5a). It is assumed that a new user appears in the system (in some point of the coverage area) every 75 ms (on average). This inter arrival time is modeled as an exponentially distributed random variable with mean $1/\lambda = 0.075$ s. Each user remains in the network during a certain session time that is also modeled as an exponentially distributed random variable with mean $1/\mu = 60$ s. Therefore, the average number of users in the system (M_{avg}) can be obtained by means of the Little's formula as follows:

$$M_{\text{avg}} = \frac{\lambda}{\mu}. \tag{8.10}$$

  The target rate is (r_{T}) is equal to 250 kbps and link performance is calculated with the Shannon's formula (see Appendix A).

- *QoS*: At every QoS checking interval, the target QoS policy is said to be fulfilled if at least 97.5% of users obtain a rate equal to r_{T}. The impact of other values for the target QoS is presented in Subsection 8.5.5.

- *Scheduling*: The scheduling policy that have been considered in the simulations is referred to as 'Best first'. It is described next:

  - *Best first*: At each cell, the users are sorted according their average radio channel quality (spectral efficiency). Then, starting from the best user, each one is granted with the bandwidth required to obtain an instantaneous rate equal to r_{T}. Only users that receive enough bandwidth to achieve r_{T} are scheduled.

  In Subsection 8.5.5, a comparative study among the scheduling disciplines is presented to clarify the impact of other scheduling policies. However, the studies presented in the current subsection are just for the 'best first' case which is shown to have the highest number of satisfied users.

The results presented in this section are grouped in two types:

- *NOP selection based on NEL sorting*: In this study, at every QoS checking interval, all the solutions within the set of nondominated solutions, either $\mathcal{X}^{\star}_{\text{SS}}$ or $\mathcal{X}^{\star}_{\text{MD}}$, are evaluated. The solution with the lowest NEL that is able to satisfy the QoS policy is selected. The idea is to create an statistic about the solutions that fulfill the QoS policy and simultaneously achieve the higher energy consumption saving. To determine the *winning* solution at each time, a binary search algorithm can be used[6]. The QoS checking interval is one second.

- *Single NEL performance evaluation*: One single solution is applied statically to study its performance without the possibility of switching to another solution. Obviously, the solution that is applied is selected by taking into account the results from the previous analysis, i.e., the NOP selection based on NEL sorting (binary search).

[6]The complexity of the binary search algorithm is $\mathcal{O}(\log(n))$. As a reference, a search in an array of 50000 elements takes, on average, 26 iterations. The sort can be done offline.

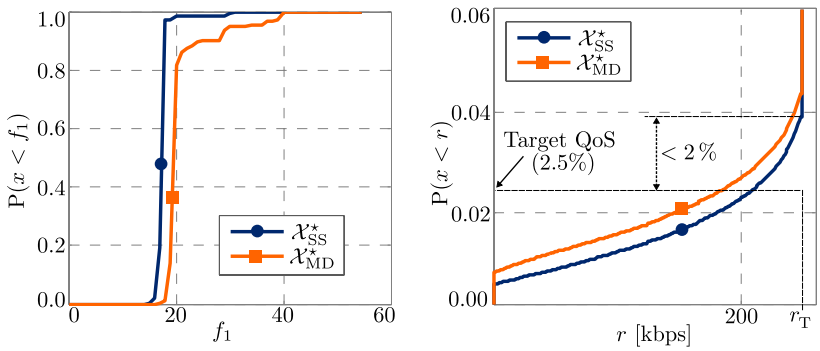

(a) CDF of the lowest NEL selection. **(b)** CDF of users rate.

Figure 8.8: Performance of the sets of nondominated solutions.

Performance Evaluation of NOP Selection Based on NEL Sorting

System level simulations can be used to complete the performance comparison between the sets $\mathcal{X}^\star_{SS}$ and $\mathcal{X}^\star_{MD}$. Figure 8.8 illustrates the NOP selection based on binary search considering the 'Best first' scheduling policy. Figure 8.8a shows that by using the set $\mathcal{X}^\star_{SS}$, the selected NOP almost always has a NEL between 15 and 29, while the use of $\mathcal{X}^\star_{MD}$ results in NOPs with NELs between 17 and 40. This is a direct consequence of the difference in terms of aggregate capacity between the solutions in both sets. Clearly, $\mathcal{X}^\star_{SS}$ requires, on average, less active cells to meet the QoS criterion, and hence, its performance is better than $\mathcal{X}^\star_{MD}$ from the energy saving point of view. Figure 8.8b shows the resulting user rates. Also from this perspective, $\mathcal{X}^\star_{SS}$ performs better. The small deviation (less than 2%) with respect to the target QoS (97.5% of users with a rate $\geq r_T$) is due to the fact that the user rate (r) reflects the average rate of each user taking into account the whole session period. Note that if a user, due to the network dynamism (users coming in and out), does not receive r_T in at least one scheduling interval, then its rate will be lower than r_T. Recall that 1) the scheduling policy only assigns the instantaneous rates in the set $\{0, r_T\}$, and 2) NOP selection based on NEL sorting guarantees the QoS policy at each interval, but this policy could imply that the sets of satisfied and unsatisfied users can be different at different scheduling intervals.

Another comparative study is shown in Figure 8.9. Figure 8.9a illustrates the effect of ICI when more cells are active. Recall, that in this part of the analysis all NOPs in $\mathcal{X}^\star$ are evaluated, and hence, statistics are collected for each NEL. As expected, average SINR levels are worse as more cells are active. However, it is interesting to note that the solutions in $\mathcal{X}^\star_{SS}$ provide small improvements in this sense, meaning that they are also better from the ICIC point of view. The average QoS level of each NEL is shown in Figure 8.9b. The result is interesting because suggest that, for any given traffic distribution pattern and load level, there is a certain NOP that provides the desired QoS (with high probability), and hence, solutions with

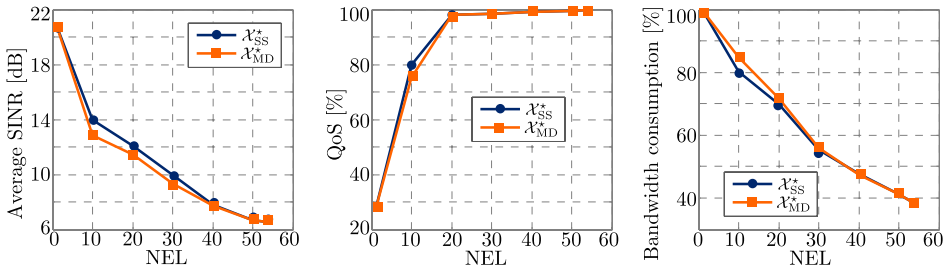

(a) Average SINR. **(b)** QoS. **(c)** Bandwidth consumption.

Figure 8.9: Performance of the sets of nondominated solutions.

NEL above that point result in idle capacity, and consequently, energy wasting. This perspective is important because it means that network capacity and offered QoS should be characterized in terms of $\mathbf{\Gamma}$ and λ.

Finally, Figure 8.9c shows the average per-cell bandwidth consumption as a function of the NEL. It is found that the lower the number of active cells, the higher the average per-cell bandwidth consumption due to the traffic concentration.

Given that $\mathcal{X}^{\star}_{\mathrm{SS}}$ achieves better performance, the rest of results are based on this set and the subscript 'SS' is omitted for the sake of clarity.

Results for Single NEL Performance Evaluation

Given that the NEL sorting selection indicated that the NOP with NEL=18 is selected most of the time, it results interesting to investigate what happens if that configuration is applied and kept fixed during an interval of time in which $\mathbf{\Gamma}$ is constant. The idea is to show that it is not necessary to change the network configuration every second (as it was done previously in simulations by means of the NOP selection based on NEL sorting) to achieve the desired QoS level.

Figure 8.10 presents the result. Interestingly, the degradation in terms of QoS with respect to NOP selection based on NEL sorting is minimal, while the gain from the feasibility point of view is significant because applying one single solution *statically* implies that no cell needs to be switched on/off.

The statistic of users rate (r) is shown in Figure 8.10a. Thus, the system level simulations confirm that $\mathbf{x}_{18}$ succeeds in achieving an acceptable performance as only less than 2.5% users do not receive the target rate (r_{T}), and hence, it can be said that the desired rate was delivered, on average, to more than 97.5% of users.

From the QoS perspective, Figure 8.10b shows that only 5% of the time, the global QoS is below the required threshold. However, this small tradeoff can be afforded in the light of the excellent performance in terms of user rates and the significant energy saving. Note that NEL = 18 implies that 66% of the network can be switched off. Moreover, during the interval in which the NOP is applied, no

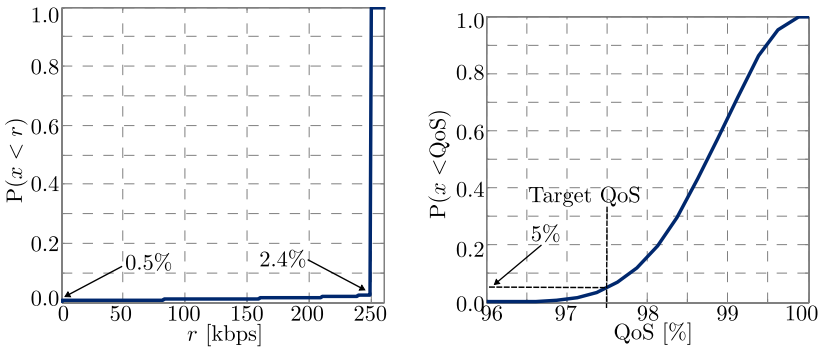

(a) Users rate. **(b)** QoS.

Figure 8.10: Single NEL performance evaluation (NEL=18).

transition would be required, and hence, he number of handovers is also minimized to the number of handovers required due to mobility.

Thus, as a conclusion, the proposed methodology accomplishes all the design targets: **good performance and feasibility**. Based on the statistics collected from the lowest NEL selection analysis part, the mobile operator can select a NOP (that most of the time provides the desired QoS such as $\mathbf{x}_{18}$) and apply it conveniently during an interval of time in which the traffic is distributed according to $\mathbf{\Gamma}$. As it was mentioned aerlier, this can be done by means of pattern recognition techniques that are out of the scope of this thesis.

Performance Comparison with Previous Proposals

In order to provide another perspective of the merit of the proposed CSO framework, a performance comparison with reference schemes is shown. Reference schemes taken from the literature include: the *Cell Zooming* algorithm proposed in [295] and the *Improved Cell Zooming* scheme presented in [283]. The *Cell Zooming* algorithm tries to swicth off cell with low traffic starting from the lowest loaded. If at least one user of a cell can not be re-associated, the execution of the algorithm finishes. In contrast, the *Improved Cell Zooming* tries to switch off every cell in the network before terminating.

Figure 8.11a illustrates the average power consumption (in terms of NEL) versus system load. Recall that the NEL is equivalent to the value of f_1 of the solution selected at each QoS checking interval, and therefore, its mean value determines the energy saving that can be obtained, on average, with each scheme. As it can be seen, the proposed multiobjective framework outperforms the reference schemes, being the gains with respect to the closest benchmark between 6% and 30%. Besides to that, the good efficiency of the solutions in $\mathcal{X}^\star$ becomes evident when looking to the QoS provided to users. Figure 8.11b shows that when the system goes to the overload

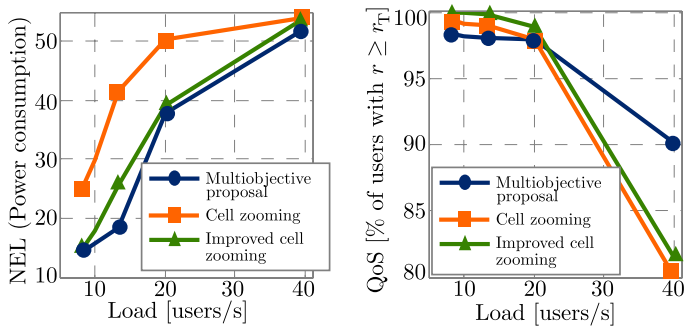

(a) NEL selection vs. system load **(b)** QoS vs. system load

Figure 8.11: Performance comparison among several CSO schemes.

region (40 new users per second in the network) the proposed framework minimizes the QoS degradation by improving 8% the QoS with respect to the improved cell zooming scheme.

Table 8.4 provides additional performance figures including the average number of transitions and handovers per QoS checking interval. In this manner, the feasibility perspective can also be considered. Recall that transitions refer to the number of cells that should be switched on/off by selecting another network configuration. As it was mentioned, this is important because a high number of transitions results in a undesirable number of network-triggered handovers. The first row shows the merit of the solution with $f_1 = 18$ ($\mathbf{x}_{18}$). As it was mentioned, the performance degradation with respect to the NOP selection based on NEL sorting is minimal, while the gains from the feasibility point of view are significant as no cell needs to be switched on/off. Note that the NOP selection based on NEL sorting has been include for comparative purposes because evaluating such QoS at that small time scales is not practical due to the computational cost and the required signaling overhead. Thus, the gains with respect to the benchmarks in terms of power consumption ($> 50\%$), number of handovers ($> 85\%$), and transitions ($> 87\%$) are remarkable, being this feasibility aspect one of the most attractive features of the proposed multiobjective CSO framework.

Note that, although reference schemes are very close to 100% in term of QoS, this comes at the expense of the need for more active cells, and hence, less energy saving. In addition, as those schemes explore the whole search space continuously, it is expected that the number of transitions, and consequently, handovers, is also very high as it was shown in Table 8.4. Thus, it is verified that the **proposed scheme provides a much better tradeoff between performance, feasibility, and complexity**.

The next subsection includes complementary, though interesting, results.

Table 8.4: Additional performance indicators ($\lambda_{\text{avg}} = 0.075$ s)

Scheme	NEL	QoS	Handovers	Transitions
$\mathbf{x}_{18} \in \mathcal{X}^{\star}$	18.00	97.81	0.00	0.00
NOP selection based on NEL sorting	18.47	98.74	7.14	0.31
Cell zooming [295]	41.45	99.05	57.56	3.47
Improved cell zooming [283]	25.36	99.87	80.14	7.47

8.5.5 Additional perspectives

To close this section, a comparative study among scheduling policies is presented. As it was commented, the idea is to evaluate the impact of this important functionality of the performance of the proposed CSO strategy. To be precise, illustrate the fact that different schedulers imply different NELs, and hence, the gains of a CSO algorithm should be given with respect to a scheduling discipline and QoS parameters.

Besides the 'best first' policy, the following scheduling strategies are also considered:

- *Best first*: At each cell, the users are sorted according their average radio channel quality (spectral efficiency). Then, starting from the best user, each one is granted with the bandwidth required to obtain an instantaneous rate equal to r_{T}. Only users that receive enough bandwidth to achieve r_{T} are scheduled.

- *Random*: The policy is similar to the previous. However, users are served in a random order. Similarly, users that cannot be assigned with enough bandwidth are left out of the scheduling at that moment.

- *Fair*: At each cell, the bandwidth is equally shared among active users. Each user receives exactly the same bandwidth, and hence, instantaneous rates depends on the spectral efficiency of each user.

In addition, the impact of other parameters is analyzed. Figure 8.12 illustrates the impact of the scheduling and system load on the performance of the NOPs found through the proposed framework. The analysis was carried out by means of the NOP selection based on NEL sorting.

Figure 8.12a shows that the 'Best first' policy achieves the lowest NEL selection. From this point of view, the performance of the 'Random' scheme typically results in the choice of NOPs with NEL$>$ 30, and hence, this policy does no favor the main goal of CSO. Even worse is the performance of the 'Fair' policy that almost invariantly requires to have all cells active to fulfill the desired QoS.

Looking at the problem from the users rate standpoint as illustrated in Figure 8.12b reveals the 'Best first' scheduling also provides a convenient tradeoff

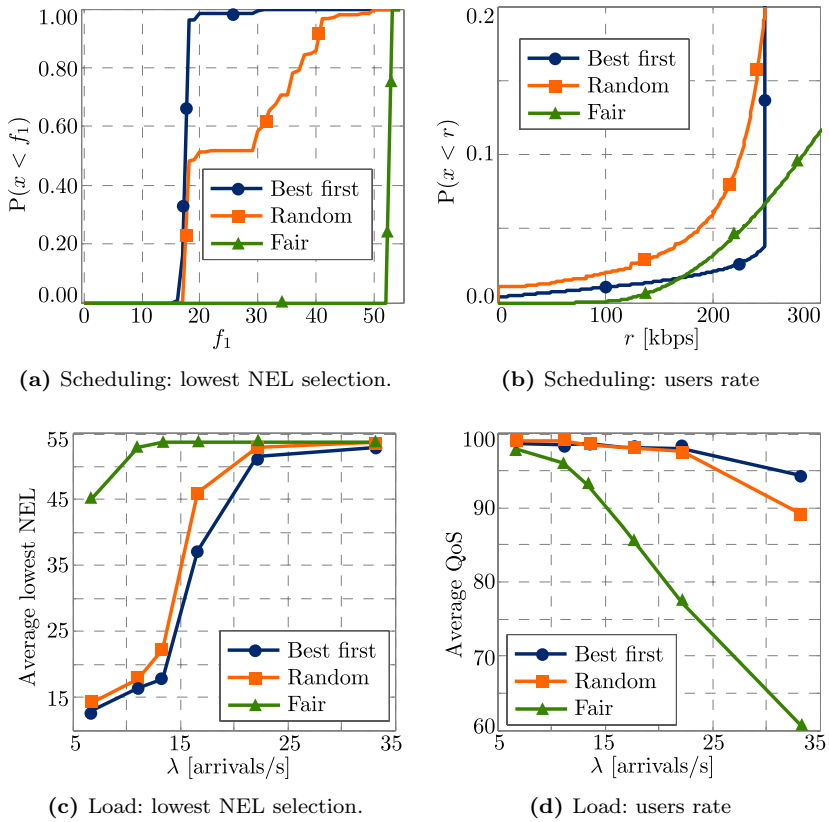

(a) Scheduling: lowest NEL selection.

(b) Scheduling: users rate

(c) Load: lowest NEL selection.

(d) Load: users rate

Figure 8.12: Effect of scheduling and system load.

between energy saving and fairness, being the policy that achieves the highest energy saving, and at the same time, it provides a very good fairness level because the vast majority of users get the target rate while only a marginal fraction gets smaller figures.

Figures 8.12c and 8.12d illustrate the effect of system load on the lowest NEL selection and offered QoS, respectively. As expected, it is found that the higher the system load in terms of average arrivals per second, the higher the average NEL that is required to fulfill the QoS target. Figure 8.12c indicates that, for a given QoS requirement, there is a certain traffic load after which, no energy saving is feasible. A complementary view of this result is provided in Figure 8.12d, where it is also confirmed that traffic load is a context variable of utmost relevance in CSO. Thus, the results of the studies indicate that, in the context of CSO, several perspective of the problem must be considered. This is precisely another strength of the multiobjective framework presented herein, i.e., it allows decoupling the CSO from other context variables and studying their impact independently.

Finally, Figure 8.13 shows the effect of the target rate and QoS. It is evident

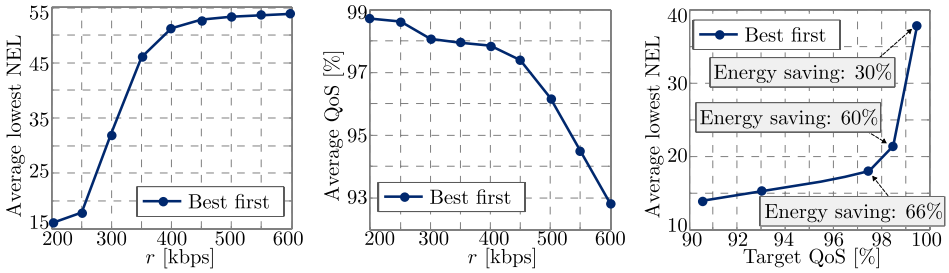

(a) Target rate: lowest NEL. **(b)** Target rate: QoS **(c)** Target QoS: lowest NEL.

Figure 8.13: Effect of target rate and QoS.

that the selection of r_T has a great influence on the amount of energy that can be saved. Looking at Figures 8.13a and 8.13b, it can be seen that while moving from 200 kbps to 250 kbps only implies moving the average NEL selection from 16 to 18, the same increment from 250 to 300 kbps implies a more considerable energy expenditure because the average lowest NEL goes from 18 to 32. Similarly, the target QoS, see Figure 8.13c, is another important parameter that must be carefully calibrated because small deviations result in significant changes in terms of the number of active cells. As a conclusion, it can be said that, in addition to a good CSO strategy, selecting operational parameters properly also plays a very important role in CSO. Consequently, a well designed CSO strategy is useless if the setting is not properly calibrated by means of the corresponding network-specific studies. In these analysis, the impact of the rest of network and QoS parameters must be considered.

8.6 Concluding Remarks

CSO is a paradigm that has gained popularity is the last few years as it has been shown to be an effective approach to reduce the energy consumption in cellular networks. By extending the multiobjective models previously employed in ICIC to this emerging field, a novel CSO has been developed and several aspects of this problem have been investigated. The research has revealed that exploiting the tradeoff between aggregate network capacity and the number of active cells is a natural and effective way to reduce the complexity of this difficult problem. This approach allows for achieving the main goal: reduce energy consumption without penalizing QoS. The studies have remarked the need for carefull calibration as an important requirement to maximize the profit.

The proposed framework has the following desirable features:

- ✓ *Robustness*: It makes no assumption on network topology nor QoS policies. Indeed, it focuses on providing the best spectral efficiency (with the minimum energy consumption) to the areas in which higher traffic load is expected.

- ✓ *Feasibility*: The proposed scheme does not require any new additional functionality. The operation could be done in a time scale of tens of minutes or hours as $\mathbf{\Gamma}$ typically does not change drastically over time. In addition, no interworking with other RRM entities is assumed, and hence, integration in existing (operative) networks is transparent.
- ✓ *Real time complexity and scalability*: The real time complexity is minimum since the optimization task is done offline. Such processing requires, on the one hand, a radio characterization of the coverage area, and on the other hand, the knowledge of the traffic behavior. Note that an interesting feature of the proposed scheme, in contrast to user-oriented approaches, is that the real-time complexity does not depend on the network load, i.e., the number of users in the system.

The conclusions can be summarized as follows:

- The proposed framework is a new approach to analyze the CSO problem by 1) explicitly considering the spatial traffic distribution, and 2) introducing a weighted network capacity metric that prioritizes cells providing better capacity to zones where traffic is concentrated.
- The network characterization in terms of a set of near-optimal NOPs (that are traffic-profile-specific) is addressed by means of two different approaches: stochastic search (through MOEAs) and a minimum distance heuristic. Both algorithms are based on the inherent tradeoff between energy consumption (NEL) and aggregate capacity. In this manner, the method proposed here only operates with a reduced number of CSO configurations. The fact that the solutions are computed offline makes the proposed scheme suitable for distributed implementations. The results indicates that the proposed strategy offers a convenient tradeoff in terms of complexity, performance, and feasibility.

- System level trials confirm that the performance obtained is excellent. In addition, it clearly outperforms reference schemes both in terms of achievable gains and feasibility/complexity. Although achievable energy savings are, in general, network dependent, the proposed framework provides a suitable way to observe the impact of parameters such as target rate (r_{T}) and the scheduling policy on the performance of the CSO strategy.

Potential extensions of this work include:

- Investigate and integrate traffic patterns recognition schemes that can operate efficiently in conjunction with proposed CSO model in real-world implementations.

Chapter 9

Final Considerations, Conclusions and Future Works

The extended mobility is the main advantage of cellular networks. This fundamental aspect has promoted that mobile devices including smartphones, tablets, and notebooks are becoming the preferred way to access the Internet. This situation is pressing the industry because the number of users of cellular networks has grown exponentially, and hence, in order to keep up in this competitive market, operators must guarantee seamless coverage and excellent QoS to their users.

In current (and future) cellular technologies such as LTE and LTE-A, ICIC has been identified as a key framework to meet the challenges posed by this evolving context. Thus, the objective of this Ph.D. thesis is to make a solid contribution to the theory of static ICIC and its feasibility for implementation in real-world cellular deployments. Based on the study of the state of the art, a set of research opportunities were identified, and consequently, new methods of analysis, strategies of optimization, and guidelines have been presented with the goal of improving network performance. The current dissertation contributes with solid arguments and novel optimization schemes to make static ICIC more attractive. The research methodology comprised a combination of mathematical models, optimization techniques, and system level simulations.

The novelties presented in this Ph.D. thesis include not only developments of static ICIC mechanisms for data and control channels but also efforts towards further improvements of the energy efficiency perspective. Thus, the framework developed for ICIC has been successfully applied to investigate traffic-driven multiobjective optimization strategies for CSO.

On the Feasibility of Static ICIC Schemes in Real-World Deployments.

Currently, the research on ICIC is far from being finished. Mobile operators, industry, and academia are working on developing effective and feasible solutions. In this context, static ICIC stands out as an attractive alternative to deal with the cell edge performance issue in OFDMA-based cellular networks due to their low complexity.

The research work presented in this Ph.D. thesis started investigating efficient and flexible models to study the performance and feasibility of static ICIC techniques in cellular deployments featuring arbitrary network topologies. The proposed statistical model takes into account the network geometry to predict the long term (average) behavior of ICI. It can be regarded as a type of planning scheme for ICIC. The analysis revealed that the operation of SFR and FFR can be described in terms of two subsystems: the class of interior and exterior users. This approach is convenient because it allows for a deeper understanding of the impact of the operational parameters of SFR and FFR on the system. This knowledge proved to be key in the design of the optimization schemes subsequently developed.

By means of this method, it is possible to study the performance of SFR and FFR in any arbitrary network topology without the need for computationally-heavy system level simulations. The model provides convenient performance patterns in the form of 2D maps that can be used by mobile operators to obtain an easy visual-assessment of the configuration that should be applied to the network. Moreover, different criteria can also be defined in a flexible manner.

The performance of SFR and FFR has been analyzed in the context of both synthetic and realistic deployments. It was found that while in synthetic scenarios they provide a convenient way to adjust the tradeoff between spectral efficiency and cell edge performance, in a real-world context, the performance of baseline design configurations is poor in the sense that no attractive tradeoff can be attained. This conclusion was also verified by means of system level simulations.

The reason of such poor results in irregular topologies stems from the fact that, in this type of scenarios, SINRs distributions and cell edge sizes vary significantly from one cell to another, and hence, applying the same configuration globally clearly leads to performances that are far from optimal. In this manner, the need for optimization in such contexts is demonstrated. Moreover, it is worth saying that based on the analysis carried out by means of the proposed method, several insights into how to perform the required optimization have also been obtained. Thus, local adjustments of the parameters α and β are not recommended due to practical difficulties. On the one hand, increasing α implies more ICI in neighbor cells and decreasing it could result in coverage holes. On the other hand, adjusting β (even globally) implies a precise coordination among cells to avoid undesired inter-class bandwidth overlapping. The study revealed that the classification threshold (ψ_{TH}) is the best candidate to achieve the required local tuning. First, changing this parameter is transparent as it would only require to modify the scheduling policy (an operator-defined rule). Second, ψ_{TH} can be adjusted independently at each cell without impact on neighboring ones.

Besides the need for optimization in realistic deployments, it was also identified that the interworking between static ICIC schemes and other network functionalities such as CSI feedback is not considered within the specifications. Indeed, LTE just provides a certain support so that every vendor/operator configures its particular ICIC option. CSI feedback is a very important and fundamental piece in wireless communications; as such, its design must be done considering an adequate interworking with other network entities. Thus, two novel CSI feedback schemes, suitable to operate in conjunction with SFR and FFR, have been developed. ICIC-SEQ and ICIC-LOC exploit the typical resource allocation pattern of SFR and FFR to improve the accuracy of the CSI feedback process. To be precise, refining the estimation of the wideband CQI figure, which is done focusing each user on the subbands of interest in the system bandwidth. The novel proposals provide significant gains in terms of overall QoS, average user rates, and cell edge performance. Moreover, they are suitable for practical implementation in LTE systems and their requirement of uplink overhead is minimal compared to native LTE schemes and existing proposals from the literature. UE performing CSI feedback according to the novel strategies can coexist transparently with legacy users. Based on the performance analysis, the following rules of thumb are advised:

- ✓ A way to improve the performance of CSI feedback schemes is not necessarily through more uplink overhead. Instead, more accurate and better localized channel quality estimations suffice to achieve desired results.
- ✓ In scenarios with traffic of type full buffer such as FTP, transmission errors must be avoided. Thus, channel quality estimations based on average figures are recommended in order to minimize the number of retransmissions.
- ✓ In scenarios with bursty traffic such as HTTP, a more *aggressive* channel quality estimation, i.e., narrow band estimations (based on short-term samples), can be afforded because a certain number of transmissions errors are compensated by retransmission capabilities such as HARQ, without a negative impact on the overall QoS.

ICIC for Data and Control Channels in LTE/LTE-A based on MOEAs.

As it was suggested by the results of the first studies, the performance of SFR and FFR can be optimized by adjusting the configuration of these schemes locally at each cell. This type of optimization problems (combinatorial or not) typically belong to the class NP-Complete, and hence, deterministic methods or exact procedures are not an option.

The use of MOEAs has been investigated taking into account the particularities required for static ICIC optimization. In this context, MOEAs offer the following advantages:

- ✓ The possibility to study the problem as it is, without the need for incurring in system simplifications or assumptions to make the mathematical treatment

feasible. This is possible thanks to the black-box nature of this type of metaheuristic that does not require any particular condition on objective functions such as linearity, convexity, or differentiability.

✓ A complete picture of the tradeoffs among objective functions. Therefore, it is possible to detect when a slight loss in one objective allows very high gains in others, and hence, different configurations can be selected in a clever way.

✓ Multiobjective optimization brings as output several network configurations rather than one single solution. These solutions feature Pareto efficiency, and hence, they represent different tradeoffs among the objectives and allow mobile operators to select the network setting best fitting their needs.

✓ They are able to find good (near-optimal) solutions by efficiently exploring complex n-dimensional search spaces.

The proposed multiobjective optimization strategies are based on the statistical framework developed during the initial stage of the research. Thus, they aim at optimizing expected values, i.e., the minimization of average ICI levels. The method achieves an attractive tradeoff between effectiveness and feasibility as significant reductions of ICI levels in cell edge areas are achieved. Moreover, the formulation based on the optimization of the classification threshold (ψ_{TH}) at each cell confirms the hypothesis that this parameter is the best option to deal with the spectral efficiency vs. cell edge performance tradeoff.

The main conclusions can be summarized as follows:

- Initially the work dealt with the adaptation of NSGA-II and SPEA-2 to the current optimization problem. The proposed schemes succeed in finding SFR and FFR configuration that outperform schemes from the state-of-the-art along with baseline designs of SFR/FFR and basic reference schemes (reuse 1 and 3).

- Next, a novel hybrid scheme is designed. It considers the use of two different MOEAs (NSGA-II + SPEA 2) and it provides both better convergence and distribution than each of them separately. This was verified under fair experiments subject to the same computational cost in terms of objective function evaluations. Moreover, another important practical advantage is is an increase in the number of Pareto efficient network configurations, 78% on average.

- The convergence properties of the evolutionary algorithms have been studied by means of statistical methods. The results show the importance of an accurate calibration process, and hence, practical guidelines and rules of thumb for an easy adjustment were derived for the optimization problem under consideration.

- The study of the features of the resulting nondominated SFR/FFR configurations showed that such dominance relationships do not hold necessarily at cell level. The performance at cell level is obviously very important and, as such, requires attention. The proposed framework also takes that aspect into account

and allows several means to guarantee minimum local performances. However, it should be clearly understood that high global optimization gains typically comes at the expense of local unbalances. This can be seen as a strength of the method given that it provides means to select network configurations fulfilling the requirements of each cell.

Besides the development of ICIC strategies for data channels, optimization schemes for control channels have also been investigated. The performance of cellular systems such as LTE and LTE-A strongly depends on the reliability of the control channels as they convey the critical user-specific information. Both for the PDCCH and ePDCCH, the consumption of control resources is overloaded by cell edge users requiring higher aggregation levels. Thus, ICIC can be employed to reduce the needs of these users, and so, increase the signaling capacity of the system. The novel strategies are based on the statistical framework presented in Chapter 3, and therefore, they can also be used in any realistic deployment.

Previous studies have shown that the PDCCH limits network capacity in scenarios with many low-rate users (either RT or NRT). LTE-A introduces some features to further protect the PDCCH, but additional measures are still required. The PDCCH is time-multiplexed, and hence, frequency domain ICIC cannot be applied. In this manner, a solution based on the optimization of the power allocated to the PDCCH at each cell was designed. The proposed formulation takes an ICIC-oriented approach by focusing on improving the bottom tail of the resulting average SINR distributions. In this manner, it results in reductions of the average consumption of control resources. Given that the design of this strategy assumes full frequency reuse, it is clearly extensible to data channels as well. Such adaptation has been proposed for SON and it is shown in Appendix E.

The design of the ePDCCH is much more flexible than the PDCCH. Thus, frequency domain ICIC can be used. Given this, an adaptation of the static ICIC strategies previously designed for data channels has been investigated. However, ICIC optimization for the ePDCCH is more complicated because the resources devoted to this channel are borrowed from the PDSCH (the data channel). Thus, increasing the signaling capacity implies reducing the resources devoted to users payload. The proposed optimization strategy does take this tradeoff into account by adding the required objective functions. The optimized network configurations allow gains with respect to baseline designs and reference schemes.

It is important to mention that, under this general optimization framework that includes both control and data channels, the marginal gains obtained by means of local adjustments of α was investigated. It is concluded that this improvement is not worth given the significant complexity cost that is required.

A Step Forward Towards *Greener* Cellular Networks.

As final objective of the research presented in this Ph.D. thesis, studies focused on network energy efficiency have been conducted. Thus, the multiobjective optimization

schemes introduced previously for ICIC have been extended and adapted to the framework of CSO. CSO is a paradigm that has gained popularity in the last few years as it has been shown to be an effective approach to reduce the energy consumption in cellular networks.

The studies reveal that there are interesting connections between ICIC and CSO, and hence, the tradeoff between aggregate network capacity and the number of active cells has been successfully exploited by means of the Pareto dominance notion. To be precise, the main idea is to take advantage of the fact that decreasing the number of active cells reduces ICI. However, the decision of which cells must remain active depends on the spatial traffic distribution. This is accomplished by means of a weighted network capacity metric that prioritizes cells providing better capacity to zones where traffic is concentrated.

The proposed multiobjective optimization method, based on evolutionary optimization, allows for achieving significant energy savings without penalizing QoS. The core processing, i.e., the network characterization in terms of a set of near-optimal NOPs that are traffic-profile-specific, is done offline, and thus, the novel optimization scheme does not require real-time computational cost. Moreover, an analysis (based on system level simulations) of this set of Pareto efficient NOPs allows to determine the network configuration that is selected most of the time for a given spatial traffic distribution, load, and QoS policy. It is shown that by applying this configuration *statically*, it is not necessary to change the NOP continuously in order to achieve the desired QoS level. This implies a significant gain from the feasibility point of view because applying one single setting implies minimizing the number of transitions: no cell needs to be switched on/off. Moreover, the merit of the proposed CSO solution has been shown by comparing it with schemes taken from the literature. The novel multiobjective provides higher energy savings and better QoS. In this manner, it is concluded that the novel method provides an excellent tradeoff between performance, feasibility, and complexity.

Finally, the studies also point out the need for a careful selection of network parameters such as target rate as they have a great influence on the performance of the CSO scheme. From this part of the analysis, it is concluded that even a well designed CSO strategy results in highly suboptimal performances if those figures are not carefully chosen.

Future Research Lines.

In the current context of exponential grow in mobile data traffic, there is a consensus about the next challenge, increasing capacity in a factor 1000x. Among the different challenges that this goal has, providing better coverage and user experience for cell edge users still is a priority. ICIC mechanisms should be extended to fit in the new technological developments. In the light of the conclusions and the experienced obtained so far, future research items include:

- Research towards pattern recognition schemes to be used in the frameworks

presented in this thesis as a mean to develop feasible dynamically self-tuned ICIC strategies.

- With radio link performance getting closer and closer to the Shannon limit, extreme densification of networks and hierarchical topologies appears to be a clear trend towards the 1000x objective. Therefore, investigate the potentials of the proposed ICIC framework in hyper dense network deployments and HetNets seems to be a logical direction.
- The current work is general enough to consider other likely scenarios such as the uplink counterpart of the problem.

Appendices

Appendix A

Notation

The following tables contain the notation and symbols used throughout the document. For convenience, the overall notation has been divided into (1) system model and operational parameters, (2) performance metrics and, (3) functions and transformations.

The following symbols have global scope. However, sub- and super-indices are used to denote different instances of the same measure. For instance, while η always denotes a measure of spectral efficiency, the symbol η^x could correspond to the spectral efficiency of a user x. The meaning of the indices is either evident from the context or explicitly indicated.

The following matrix convention is adopted. For the vector $\mathbf{v}$ and the matrix $\mathbf{V}$, $\mathbf{v}(x)$ and $\mathbf{V}(x, y)$ correspond to the x^{th} element and the element in the x^{th} row and y^{th} column, respectively. These inclusion relationships will be always evident from the context as vectors and matrices are written in **bold** while functions and transformations are not.

System model and operational parameters

A	Number of area elements or pixels in which the coverage area is divided.
B	System bandwidth.
$\mathcal{B}$	Set of subbands in the system bandwidth.
$\mathcal{B}_l^{\text{A}}$	Set of subbands that the l^{th} cell is allowed to use.
$\mathcal{B}_{l,\mathcal{I}}^{\text{R}},\ \mathcal{B}_{l,\mathcal{E}}^{\text{R}}$	SFR/FFR: Set of subbands reserved for each class of users in the l^{th} cell.
$B_{l,\mathcal{I}},\ B_{l,\mathcal{E}}$	SFR/FFR: Bandwidth reserved for each class of users in the l^{th} cell.
$\mathcal{E},\ \mathcal{I}$	Sets of central and cell edge users.
$\mathbf{G}$	Long term channel gain (inverse of large scale fading) matrix ($\mathbf{G} \in \mathbb{R}^{A \times L}$ or $\mathbf{G} \in \mathbb{R}^{M \times L}$).

$g_{m,l}^{n,sc}$	Channel gain (inverse of large plus small scale fading) of user m with cell l in RB n and subcarrier sc.
J	LTE: Number of bandwidth parts in the system bandwidth.
$l,\ L$	Indices for cells and total number of cells. Thus, $l = 1, 2, \cdots, L$.
$\hat{l}$	Index of serving cell.
$m,\ M$	Indices for UEs and total number of users. Thus, $m = 1, 2, \cdots, M$.
N_{J}	LTE: Number of consecutive subbands in each bandwidth part.
$N_{\mathrm{RB}}^{\mathrm{DL}}$	LTE: Number of resource elements in the system bandwidth.
N_{SB}	LTE: Number of subbands in the system bandwidth.
$N_{\mathrm{sc}}^{\mathrm{RB}}$	LTE: Number of subcarriers per resource element.
$N_{\mathrm{symb}}^{\mathrm{DL}}$	LTE: Number of OFDM symbols per slot.
$\mathbf{n}$	The inverse of the number of pixels associated to each cell ($\mathbf{n} \in \mathbb{R}^L$).
$P_{\max}$	Maximum power available at each cell.
$P_{\min}^{\mathrm{Rx}}$	Receivers sensitivity.
$P_l^{n,sc}$	Power transmitted by cell l in RB n and subcarrier sc.
$\mathbf{p}$	Vector to indicate a set of transmited powers ($\mathbf{p} \in \mathbb{R}^L$).
$\mathcal{P}$	LTE: An arbitrary set of PRBs.
$\mathcal{P}_s$	LTE: An arbitrary set of (contiguous) PRBs in the s^{th} subband.
$\mathcal{P}_{i,j}$	LTE: i^{th} subband within the j^{th} bandwidth part.
$\mathbf{R}$	Matrix to indicate a set of received powers ($\mathbf{R} \in \mathbb{R}^{A \times L}$ or $\mathbf{R} \in \mathbb{R}^{M \times L}$).
$\mathbf{S},\ \mathbf{S}^{\mathrm{c}}$	Binary coverage matrix and its complement. ($\mathbf{S},\ \mathbf{S}^{\mathrm{c}} \in \{0,1\}^{A \times L}$ or $\mathbf{S},\ \mathbf{S}^{\mathrm{c}} \in \{0,1\}^{M \times L}$), see Appendix C, Section C.1.
$\mathbf{v}$	Binary vector to indicate outage in pixels ($\mathbf{v} \in \{0,1\}^A$). '1' = outage.
$\mathbf{x},\ \mathcal{X}$	A generic solution vector and the set of multiple solutions. The dimension of $\mathbf{x}$ is always clear from the context, otherwise indicated.
α	SFR/FFR: Power ratio. Ratio between the power assigned to cell edge users and central users.
β	SFR/FFR: Bandwidth sharing coefficient. Fraction of the system bandwidth assigned to central users.
$\mathbf{\Gamma}$	Generic probability space used to describe the traffic (load) distribution spatially in the network.
Δ_{X}	LTE: Content of the CSI feedback report type X.
δ_{X}	LTE: Uplink overhead of the CSI feedback report type X.
Θ	LTE: A CQI value.
κ	An arbitrary constant: $\kappa \in \mathbb{R}^+$.
λ	Traffic intensity [arrivals per second].
σ^2	Thermal noise power.
$\psi_{\min}$	Minium SINR threshold to establish a radio link.
ψ_{TH}	SFR/FFR: SINR threshold used to classify users.

Performance metrics and objective functions

C	Capacity or aggregate sum rate.
F_X	Cumulative Distribution Function of the random variable X.
F'_X	Probability Mass Function of the random variable X.
f_i	The i^{th} objective function in multiobjective formulations.
r	Users or pixels rate.
$\hat{x}$	Normalized value of the variable x.
η, $\mathbf{H}$	Spectral efficiency: scalars and matrices, respectively.
ξ	Average consumption of control resources (CCEs or eCCEs).
ϱ	Non-uniformity index.
υ	Hypervolume indicator.
ψ, $\mathbf{\Psi}$	SINR values: scalars and matrices, respectively.
$\jmath$	Jain's index.

Functions and/or transformations

$d_{\text{H}}(\mathbf{x}_1, \mathbf{x}_2)$	Hamming distance between the binary strings $\mathbf{x}_1$ and $\mathbf{x}_2$.
$\log_2(1+\psi)$ [bps/Hz]	Shannon's formula for spectral efficiency.
$\text{u}(\,)$	Unit step function. $\text{u}(z) = 1$ if $z \geq 0$, 0 otherwise.
$\Theta = \Lambda(\psi_{\text{eff}})$	Mapping from effective SINR (ψ_{eff}) to CQI (Θ).

Appendix B

Simulation Scenarios

This appendix presents a description of the simulation scenarios considered in this thesis. The description includes basic features that include topology, number of cells and propagation model, leaving aspects that are particular to each study such as system bandwidth/power configuration to be indicated in the corresponding chapters. In addition, a description of the traffic models and the generation of large and small scale fading is also included.

B.1 Cellular scenarios

Two different antennas have been used: a synthetic antenna defined in [175] and a commecial antenna [301]. In the document, these antennas are referenced to as 'M.2135' and 'Kathrein', respectively. The main features of the antennas are shown in Table B.1. Vertical and horizontal radiation patterns are shown in Figures B.1 and B.2, respectively.

Table B.1: Main features of the antennas.

Antenna	**Gain [dBi]**	**3 dB beam (H/V)**	**Front-to-back ratio [dB]**
M.2135	17.00	70°/15°	20 dB
Kathrein	19.33	65°/4°	>25 dB

In this thesis, several cellular scenarios have been considered. The first one is a synthetic (hexagonal) layout similar to the one proposed by ITU in [175] as a reference for evaluation of radio interface technologies for IMT-Advanced. The second scenario is a realistic cellular network covering the city of Vienna and its

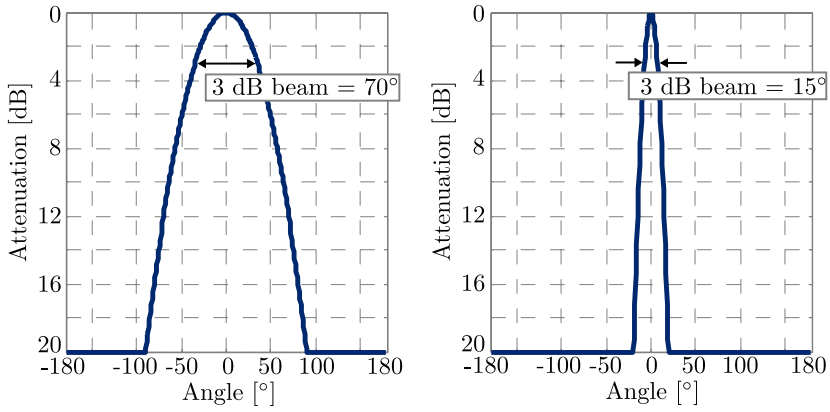

(a) Horizontal. **(b)** Vertical.

Figure B.1: Radiation pattern of antenna M.2135.

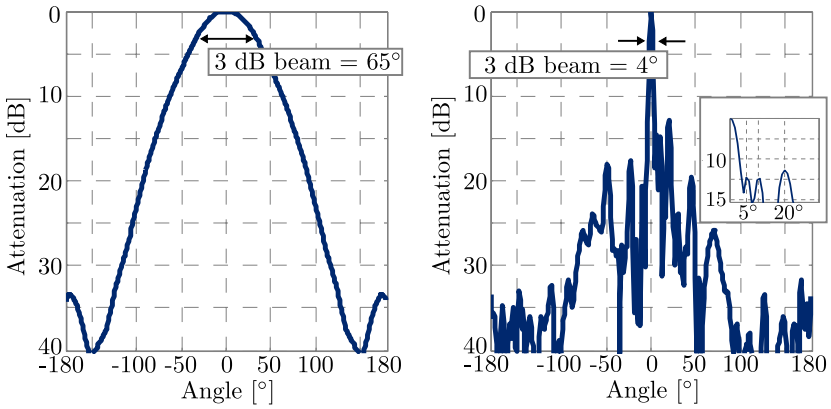

(a) Horizontal. **(b)** Vertical.

Figure B.2: Radiation pattern of antenna Kathrein

surroundings. The term 'realistic' is used in the sense that the digital elevation model and sites/cells parameters have been obtained from the MORANS initiative [302]. This activity was framed within the European COST 273 Action and aimed at providing common system simulation environments so that different researchers can compare results. In addition to the previous test cases, a small/dense deployment was considered for the studies about CSO, which require a deployment that is small in size but with high density of eNBs. However, before presenting the description of each scenario, Table B.2 shows a set of parameters that are common to all of them.

Table B.2: Parameters common to all scenarios/studies.

Parameter	Value
Thermal noise power (σ^2)	–174 dBm/Hz
UE noise figure	7 dB
Pixels resolution	5 m/pixel (square pixels)
Available power per cell ($P_{\max}$)	43.0 dBm
Carrier frequency	2.140 GHz
Large and small scale fading	As indicated in Section B.3

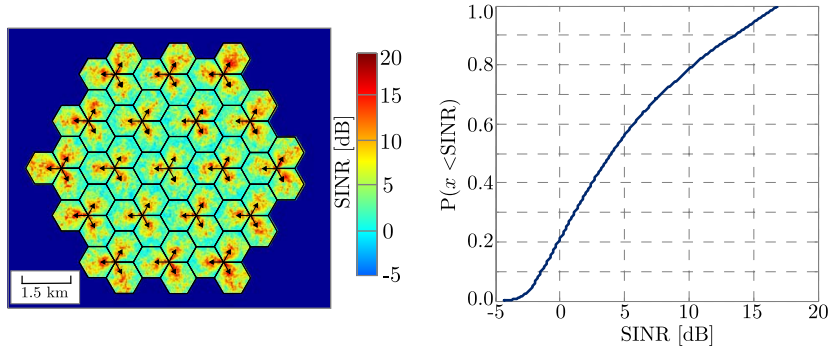

(a) Cellular layout and average SINR map. **(b)** CDF of the average SINR.

Figure B.3: Synthetic cellular layout.

B.1.1 Synthetic Test Case

The synthetic scenario is a 3GPP based urban/macrocellular network. The scenario features an hexagonal grid with 57 cells in 19 trisectorial sites. The sites are separated by a distance of 1.5 km. The scenario is assumed to be flat, i.e., no elevation model is considered and the antennas are all at a height of 25 m and downtilted 6°. Propagation was modelled according to the 3GPP urban macrocellular model as defined [303]. In the document, the scenario is referred to as scenario 'Synthetic'. The cellular layout with the average SINR map under full frequency reuse (the condition assumed for cell selection) and the CDF of this variable are shown in Figure B.3.

B.1.2 Realistic Test Case

The realistic scenarios considered in this thesis are based on one of the reference scenarios defined within the MORANS initiative [302]. In particular, the one covering the city of Vienna. The scenario is built upon real world information including geo-localization-data for the sites, clutter definition (traffic information), realistic elevation model, sites features/configuration and propagation based on in-field measurements. This realistic test case is composed of 211 sites in which 628 cells

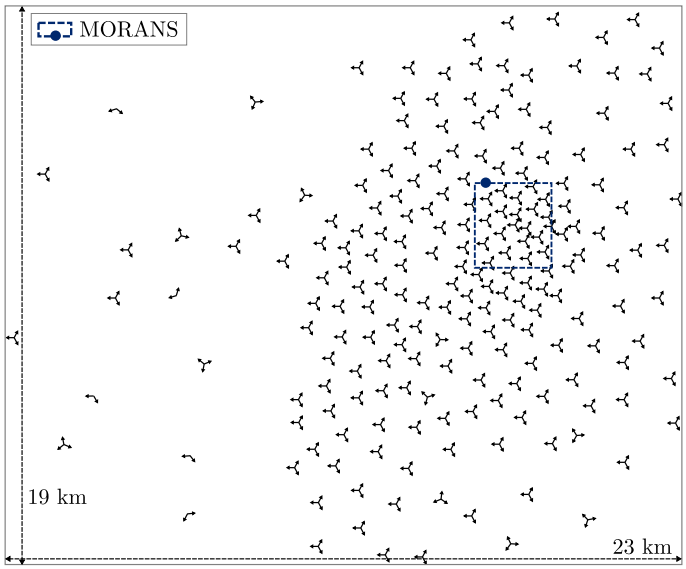

(a) Cellular layout.

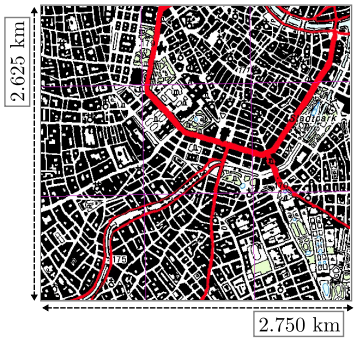

(b) Subscenario MORANS.

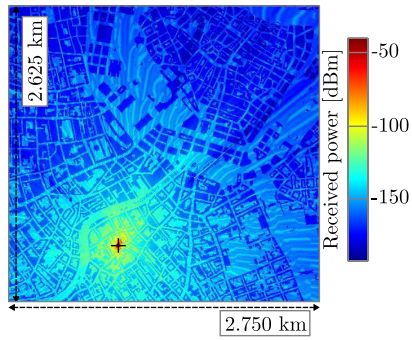

(c) Realistic propagation

Figure B.4: MORANS reference test case: Vienna.

provide service to a zone of 19×23 km^2. Given the realistic nature of this scenario, sites features such as azimuth, antennas height and downtilts are specific for each transmitter. Figure B.4 illustrates several aspects of this scenario. The cellular layout of the whole reference test case is shown in Figure B.4a, where the subscenario used for numerical evaluations is indicated. The area corresponding to this subscenario is accurately characterized in terms of ICI by means of the empirical propagation model COST 231-Walfish-Ikegami [304]. As an example, Figure B.4b shows the topografical information of the subscenario 'MORANS' and Figure B.4c depicts the propagation pattern for one reference site.

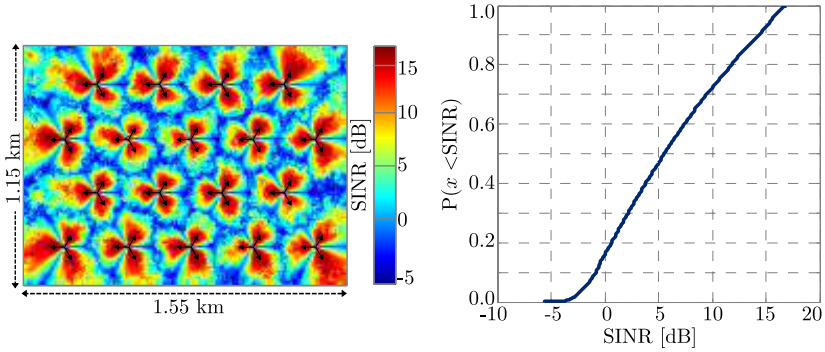

(a) Cellular layout and average SINR map. **(b)** CDF of the average SINR.

Figure B.5: Small and dense deployment.

Table B.3: Summary of cellular test cases.

Scenario	Layout/ISD	Sites/cells	Antenna/height	Area
Synthetic	Hexagonal/1.5 km	19/57	Kathrein/25 m	37.02 km^2
MORANS	Irregular/Variable	20/60	Kathrein/Variable	20.79 km^2
Small-dense	Hexagonal/300 m	18/54	M.2135/15 m	1.78 km^2

B.1.3 Small Dense Test Case

The scenario is a small dense deployment which extension is comparable to a campus such as Carleton University. To be precise, the scenario is composed of 18 trisectorial sites with 54 cells and, without loss of generality, the sites are uniformly distributed over a flat area of 1.55×1.15 km^2. The propagation model is the one proposed in ITU-R M.2135 for urban microcellular deployments [175]. Sites height is 15 m and the downtilt of antennas is 12°. In the document, the scenario is referred to as scenario 'Small-dense'. The cellular layout with the average SINR map and the CDF of this variable are shown in Figure B.5.

Table B.3 summarizes the main features of the cellular test cases.

B.2 Traffic Models

Four different traffic models are considered: Hypertext Transfer Protocol (HTTP), File Transfer Protocol (FTP), Voice over Internet Protocol (VoIP) and full buffers. Traffic models for HTTP (web browsing sessions) and FTP (file transfers) are defined in [57]. The traffic model for VoIP was taken from [175].

A brief description of these models is provided.

Table B.4: Traffic models parameters.

Traffic	Parameters/Distributions
HTTP	Main object size: Truncated Lognormal (mean: 10710 bytes, standard deviation: 25032 bytes) Embedded object size: Truncated Lognormal (mean: 7758 bytes, standard deviation: 126168 bytes) Number of embedded objects: Truncated Pareto (mean: 5.64) Reading time: Exponential (mean: 30 s) Parsing time: Exponential (mean: 0.13 s)
FTP	File size: Truncated Lognormal (mean: 2 Mbytes, standard deviation: 0.722 Mbytes) Reading time: Exponential (mean: 180 s)
VoIP	Adaptive Multi-Rate (AMR) audio codec. Source rate: 12.2 kbps Activity factor: 50 % Voice packets: 40 bytes every 20 ms Silence packets: 15 bytes every 160 ms

- *HTTP*. Sessions are divided into ON/OFF periods representing web-page downloads and intermediate reading times, where the web-page downloads are referred to as packet calls. These ON and OFF periods are a result of human interaction.
- *FTP*. In FTP applications, a session consists of a sequence of file transfers, separated by reading times. The size of the transfers is typically much bigger than in HTTP sessions.
- *VoIP*. The model is based on a two-state Markov Chain such that each user remains, on average, 50% of the session time generating VoIP packets.
- *Full buffers*. It is assumed that there is always traffic awaiting for transmission.

Table B.4 summarizes the main parameters of the stochastic models used for each service. Figure B.6 illustrates a typical realization of each type of traffic.

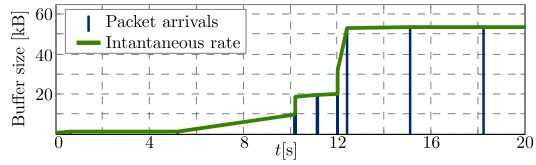

(a) HTTP.

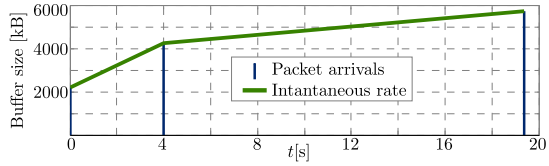

(b) FTP.

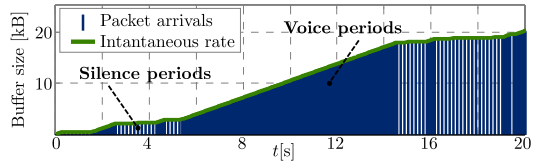

(c) VoIP.

Figure B.6: A realization of the stochastic models for realistic traffic.

B.3 Large and Small Scale Fading

The large scale fading (shadowing) is based on multiple correlated layers according to the bidimentional model proposed in [305]. By means of this model, a common shadowing value is assigned to each pixel with respect to each cell. In this manner, the actual behavior of shadowing can be captured, i.e., nearby users have correlated values. Table B.5 shows the parameters employed in the generation of correlated shadowing layers. As an example, one small layer of 64×64 pixels is shown in Figure B.7.

The small scale fading (frequency selective fading) is generated according to [306]. Since this computation is very time consuming, its use is based on pre-generated traces. In addition, in order to be consistent with the LTE numerology, an extended channel model featuring a tap resolution of 32.55 ns was selected, see [178] for details. Table B.5 shows the parameters employed in the generation of the small scale fading. Figure B.8 shows a small representation of the channel used in dynamic system level simulations.

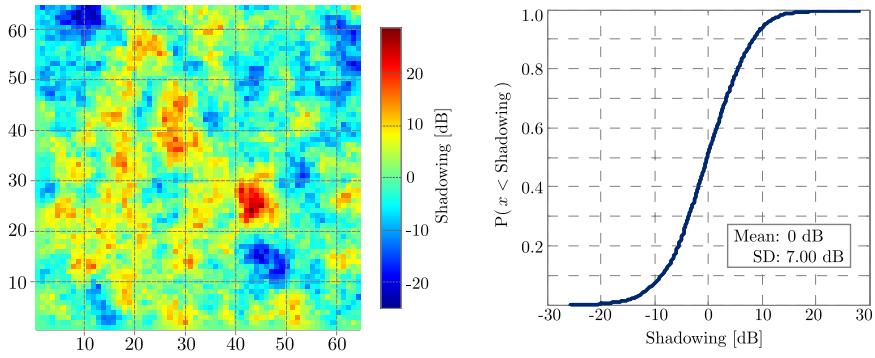

(a) A simple shadowing map. **(b)** CDF of shadowing.

Figure B.7: A bidimentional shadowing pattern.

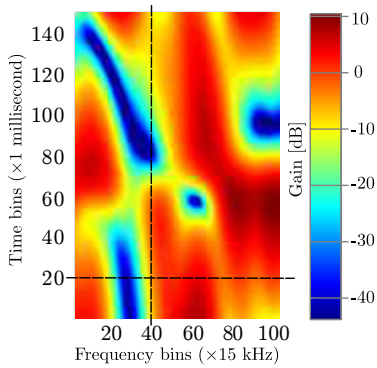

(a) A channel snapshot.

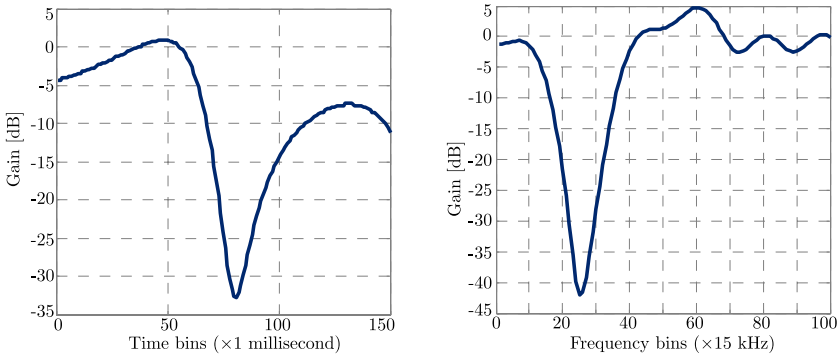

(b) A temporal cut. **(c)** A frequency cut.

Figure B.8: A representation of the channel used in dynamic system level simulations.

Table B.5: Shadowing parameters.

Parameter	Value
Mean	0 dB
Standard deviation	7 dB
Correlation between layers	0.5
Decorrelation distance	20 m
Resolution (square pixels)	5 m/pixel

Table B.6: Frequency selective fading and channel model parameters.

Parameter	Value
Bins bandwidth	15 kHz (Subcarriers separation in LTE)
FFT size	2048
Doppler frequency	5.94 Hz (Speed: 3 km/h)
Sampling frequency	1000 Hz (One value each millisecond)
Channel model	ITU - Extended Pedestrian B [178]

Appendix C

Evaluation settings and LTE parameters

This appendix presents the configurations and models used for numerical evaluations and/or simulations. LTE settings and parameters are also included. The appendix is based on the general notation previously defined in Appendix A whose reading can be considered complementary and recommended.

C.1 System model

The system model considers the downlink of an OFDMA cellular network based on LTE. The network is composed of L cells and the coverage area is divided in A small area elements (pixels). It is assumed that within each pixel, the average received power from each cell is constant and hence, average SINR figures are also constant within each pixel. Received power is measured in the central point of each pixel.

The system bandwidth is B [Hz] and it is composed of $N_{\text{RB}}^{\text{DL}}$ RBs, each of which is divided into $N_{\text{sc}}^{\text{RB}}$ consecutive subcarriers of 15 kHz. The total available power per cell is $P_{\max}$. The way in which the power is distributed among the different RBs is explicitly indicated where it is required.

The radio characterization of the network is given by the matrix $\mathbf{G}$ containing the net large scale fading, i.e. it accounts for propagation loss, antenna gain, and shadowing. The vectors $\mathbf{p}_{\text{CS-RS}}$ and $\mathbf{p}_{\text{PDSCH}}$ indicate the power transmited (per subcarrier) at each cell in CS-RS and the PDSCH, respectively. Without loss of generality, it is assumed that the power allocated to CS-RS is the same at each cell, in this manner, $\mathbf{p}_{\text{CS-RS}}(l) = P_{\max}/(N_{\text{RB}}^{\text{DL}} \cdot N_{\text{sc}}^{\text{RB}}) \quad \forall\, l = 1,\ 2,\ \cdots,\ L$.

Cell selection is based on the average CS-RS received power that is given by the following expression:

$$\mathbf{R}_{\text{CS-RS}} = \mathbf{G} \cdot \text{diag}\left(\mathbf{p}_{\text{CS-RS}}\right) \tag{C.1}$$

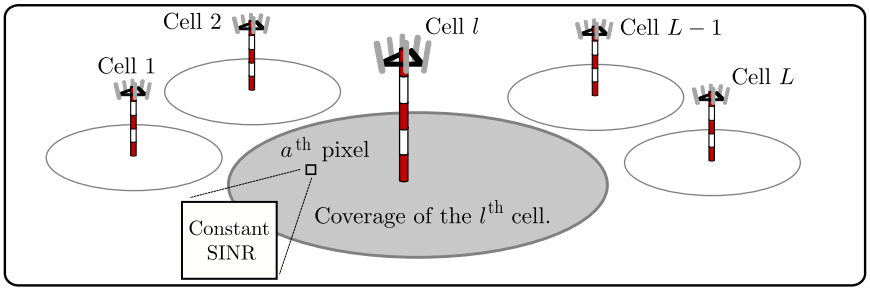

Figure C.1: A pictorial representation of the system model.

Thus, the pixel a (a^{th} row in $\mathbf{R}_{\text{CS-RS}}$) is served by cell $l^\star$, if and only if:

$$l^\star = \underset{l\in\{1,2,\dots,L\}}{\text{argmax}} \; \mathbf{R}_{\text{CS-RS}}(a,l) \tag{C.2}$$

Based on Equations C.1 and C.2, the binary coverage matrices $\mathbf{S}$, $\mathbf{S}^{\text{c}} \in \mathbb{R}^{A\times L}$ can be easily obtained. If a is served by $l^\star$, then $\mathbf{S}(a,l^\star)=1$. $\mathbf{S}^{\text{c}}$ is the binary complement of $\mathbf{S}$. Note that, the cell coverage pattern, implicitly defined in $\mathbf{S}$, is a function of $\mathbf{p}_{\text{CS-RS}}$. The vector $\mathbf{n}\in\mathbb{R}^L$ contains the inverse of the sum of each column in $\mathbf{S}$, i.e., the number of pixels associated to each cell.

The vector $\mathbf{\Gamma}\in\mathbb{R}^A$ indicates the probability of each pixel of having a user on it. Therefore $\mathbf{\Gamma}^{\text{T}}\cdot\mathbf{1}=1$. Note that, in the particular case where users are uniformly distributed in the coverage area, each element $\gamma_i\in\mathbf{\Gamma}$ is equal to $1/A$.

Finally, it is assumed that each pixel (or user) can be served only by one cell. A pictorial representation of the system model is shown in Figure C.1.

C.2 Modulation and Coding Schemes

Table C.1 shows the modulation and coding rate used in LTE for the PDSCH. Tables C.2 and C.3 show the transmission formats used in LTE for the PDCCH [307] and the ePDCCH [308], respectively. Target SINR values were computed to achieve a target BLER of 1% according to [174, 177]. Single Input Single Output (SISO) is assumed.

Table C.1: MCS used in LTE system level simulations.

Index	Modulation	Coding rate	Index	Modulation	Coding rate
0	QPSK	0.12	14	16QAM	0.54
1	QPSK	0.16	15	16QAM	0.60
2	QPSK	0.19	16	16QAM	0.64
3	QPSK	0.25	17	64QAM	0.43
4	QPSK	0.30	18	64QAM	0.46
5	QPSK	0.37	19	64QAM	0.51
6	QPSK	0.44	20	64QAM	0.55
7	QPSK	0.52	21	64QAM	0.60
8	QPSK	0.59	22	64QAM	0.65
9	QPSK	0.67	23	64QAM	0.70
10	16QAM	0.33	24	64QAM	0.75
11	16QAM	0.37	25	64QAM	0.80
12	16QAM	0.43	26	64QAM	0.85
13	16QAM	0.48	27	64QAM	0.89

Table C.2: Transmission formats for the PDCCH.

Format	Modulation	CCEs	Coding rate	Target SINR (ψ_x^{T}) [dB]
0 (AL_0)	QPSK	1	2/3	$\psi_0^{\mathrm{T}} = 4.40$
1 (AL_1)	QPSK	2	1/3	$\psi_1^{\mathrm{T}} = 0.40$
2 (AL_2)	QPSK	4	1/6	$\psi_2^{\mathrm{T}} = -2.10$
3 (AL_3)	QPSK	8	1/12	$< \psi_2^{\mathrm{T}}$

Table C.3: Transmission formats for the ePDCCH.

Format	Modulation	CCEs	Coding rate	Target SINR (ψ_x^{T}) [dB]
0 (AL_0)	QPSK	1	2/3	$\psi_0^{\mathrm{T}} = 9.25$
1 (AL_1)	QPSK	2	1/3	$\psi_1^{\mathrm{T}} = 2.50$
2 (AL_2)	QPSK	4	1/6	$\psi_2^{\mathrm{T}} = -0.50$
3 (AL_3)	QPSK	8	1/12	$< \psi_2^{\mathrm{T}}$

C.3 Channel State Feedback

Table C.4 indicates the CQI definition for CSI feedback. Tables C.5, C.6, C.7, C.8 and C.9 show several LTE specifications related to periodic and aperiodic CSI reporting in LTE.

Table C.4: Definition of the CQIs in LTE.

Index	**Modulation**	**Coding rate×1024**	**Target SINR ($\psi_x^{\mathbf{T}}$) [dB] (BLER = 10%)**
0		Out of range	
1	QPSK	78	$\psi_1^{\mathrm{T}} = -7.05$
2	QPSK	120	$\psi_2^{\mathrm{T}} = -5.20$
3	QPSK	193	$\psi_3^{\mathrm{T}} = -3.10$
4	QPSK	308	$\psi_4^{\mathrm{T}} = -1.15$
5	QPSK	449	$\psi_5^{\mathrm{T}} = 0.70$
6	QPSK	602	$\psi_6^{\mathrm{T}} = 2.70$
7	16QAM	378	$\psi_7^{\mathrm{T}} = 4.30$
8	16QAM	490	$\psi_8^{\mathrm{T}} = 6.30$
9	16QAM	616	$\psi_9^{\mathrm{T}} = 8.10$
10	64QAM	466	$\psi_{10}^{\mathrm{T}} = 9.20$
11	64QAM	567	$\psi_{11}^{\mathrm{T}} = 10.8$
12	64QAM	666	$\psi_{12}^{\mathrm{T}} = 12.7$
13	64QAM	772	$\psi_{13}^{\mathrm{T}} = 14.70$
14	64QAM	873	$\psi_{14}^{\mathrm{T}} = 16.80$
15	64QAM	948	$\psi_{15}^{\mathrm{T}} = 19.00$

Table C.5: Subband size vs. system bandwidth.

System bandwidth ($N_{\mathbf{RB}}^{\mathbf{DL}}$)	**Subband size (k)**
6-7	Wideband CQI only
8-10	4
11-26	4
27-63	6
64-110	8

Table C.6: Subband size and bandwidth parts vs. system bandwidth.

System bandwidth ($N_{\mathbf{RB}}^{\mathbf{DL}}$)	**Subband size (k)**	**Bandwidth parts (J)**
6-7	Wideband CQI only	1
8-10	4	1
11-26	4	2
27-63	6	3
64-110	8	4

Table C.7: Subband size and number of preferred subbands vs. system bandwidth.

System bandwidth ($N_{\mathbf{RB}}^{\mathbf{DL}}$)	**Subband size (k)**	**Preferred subbands (M)**
6-7	Wideband CQI only	Wideband CQI only
8-10	2	1
11-26	2	3
27-63	3	5
64-110	4	6

Table C.8: Differential encoding for LTE-HLC aperiodic CSI reporting.

Subband CQI reports are encoded differentially with respect to the wideband CQI using 2 bits as follows: Subband differential CQI offset = Subband CQI − Wideband CQI (Θ_{WB}) Possible values are $\{\leq -1,\ 0,\ +1,\ \geq +2\}$

Table C.9: Differential encoding for LTE-UESEL CSI aperiodic/periodic reporting.

Subband CQI reports are encoded differentially with respect to the wideband CQI using 2 and 3 bits (aperiodic and periodic) as follows: Differential CQI = CQI of the best M subbands − Wideband CQI (Θ_{WB}) Aperiodic reporting values are $\{\leq +1,\ +2,\ +3,\ \geq +4\}$ Periodic reporting values are $\{\leq -4,\ -3,\ -2,\ -1,\ 0,\ +1,\ +2,\ \geq +3\}$

Appendix D

Simulation Platform

The complexity of cellular systems such as LTE and LTE-A often makes unfeasible to investigate the impact of many RRM algorithms on high level system- and user-oriented metrics by means of analytical methods. However, the study by means of software tools allows accurate modeling of almost every single aspect of complex technologies such as LTE. Therefore, simulation tools are highly valued by researchers and engineers working on cellular systems.

In parallel to the research work corresponding to this Ph.D. thesis, the author developed a complete and flexible LTE-based system level simulation environment to facilitate the study and analysis of the schemes and innovations presented in the document. This appendix provides a general description of the main features of this research tool.

D.1 Architecture

The architecture of the network simulator is shown in Figure D.1. As it can be seen, the simulation environment is composed of three main components:

1. *Core processing software*. It was completely developed in C++ [309] and it implements all the network functionalities and additional features that have been needed during the research. These elements include functional aspects of LTE and LTE-A that were required for each study and complementary modules to analyze or generate additional data that was also used in system level simulations.

2. *Graphical user interface* (GUI). This visual interface has been developed in Visual Basic® [310] and it allows a visual and easy configuration of experiments and studies as well as the processing and analysis of results.

3. *Data repository*. It is composed of a database and a set raw files with infor-

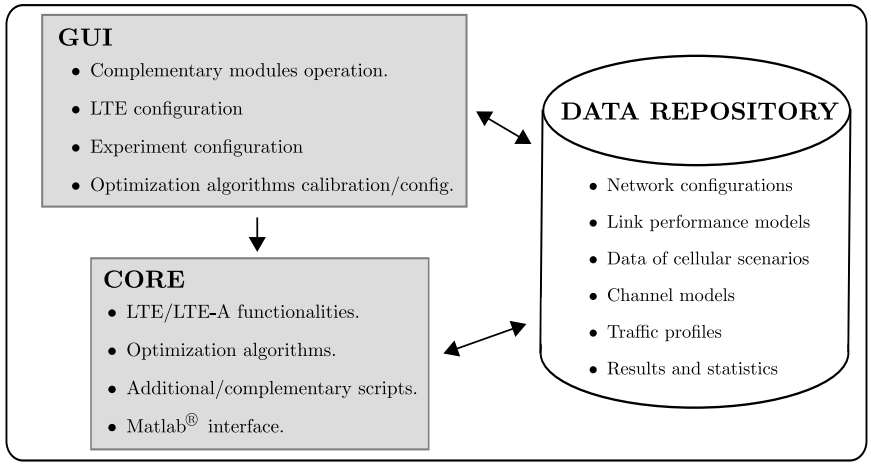

Figure D.1: Architecture of the simulation environment.

mation related to network configurations, traffic profiles, channel and link performance models, results and statistics, and data of cellular scenarios, among others.

D.2 Description of the Main Features

In this section, a general description of the main features and capabilities of the simulation environment is presented. The next points summarize the most important features:

- ✓ *Flexible configuration of system level simulations.* The GUI allows for an easy/visual inspection of the overall setting that is used in system level simulations. As it is illustrated in in Figure D.2a, the GUI provides means to inspect and modify LTE/LTE-A parameters such as the OFDMA setting, power and bandwidth allocation, HARQ and CSI feedback, among others. By means of controls provided by the GUI, static ICIC schemes or CSI feedback schemes can be flexibly configured, thus facilitating the research activity. Similarly, other parameters related to particular preferences of each study including mobility models, scheduling policies, user allocation methods, duration of experiments, number of trials (for standard Montecarlo experiments), and the cellular scenario can also be configured.

  It is important to remark that all the strategies and optimization algorithms presented in this Ph.D. thesis have been implemented and evaluated by means of this tool.

- ✓ *Complementary modules.* In addition to the control panel, the GUI also provides access to additional, though very useful, functionalities (see Figure D.2b)

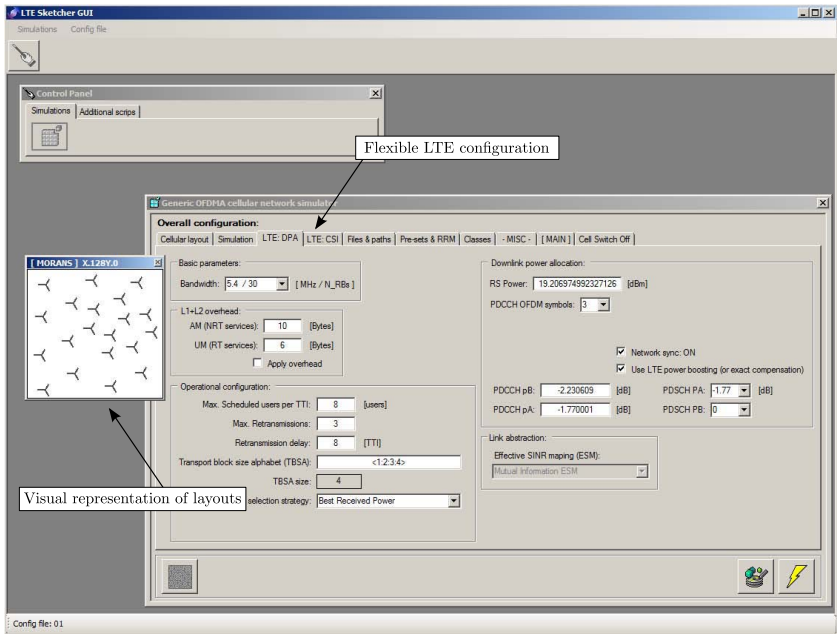

(a) Configuration of system level simulations.

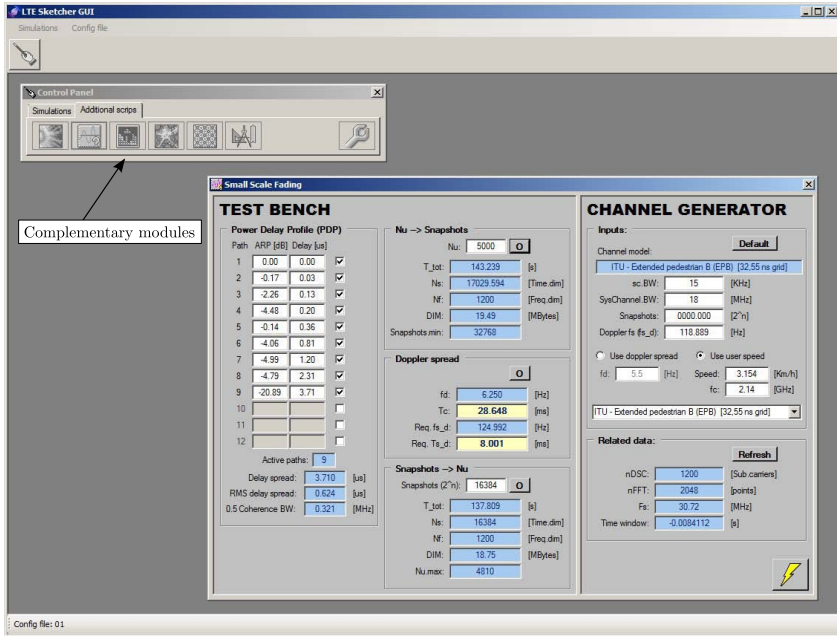

(b) Complementary modules.

Figure D.2: Several views of the GUI.

that have been included as in-built modules within the simulation environment. They allow to study/create antenna's propagation patterns, channel models, realistic traffic traces, and large scale fading effects, among others.

✓ *Radio Resource Management.* The core processing module has been designed in a flexible manner such that every single RRM entity can be modified and configured independently. Thus, the cross-impact and interworking among functionalites such as ICIC algorithms, CSI feedback, and scheduling can be studied conveniently. Moreover, the widely use of C++ allows for a direct integration of cutting-edge and reliable routines and external programming resources, such as Numerical Recipes® [311] that guarantees the minimum processing cost.

✓ *Compatibility and calibration.* The data repository stores information of several *standardized* cellular scenarios (test cases) such as MORANS (see Subsection B.1.2), but in general, any particular data can be loaded and integrated. This is important to obtain reproducible and comparable results. Moreover, the model used to define the scenarios allows for flexible implementation of almost any possible cellular layout without contraints nor limitations of scale. In this sense, the extension to hierarchical architectures (HetNets) can be done without significant effort. Moreover, previously (external) calibrated data can be also easily integrated and used. For instance, data for shadowing patterns or look-up tables for link performance abstraction.

✓ *Further enhancements.* The open and modular architecture that has been followed during the development of this simulation environment allows for extensions to investigate the interworking of LTE and LTE-A with other technologies such as WLANs.

Appendix E

A SON Scheme based on Power Planning

Besides to the initial planning, dimensioning, installation, testing and preliminary optimization, the operation and management of complex systems such as LTE and LTE-A include performance monitoring, troubleshooting, **post-launch optimization** and maintenance. These activities are both time-consuming and highly complex. Very often, human intervention in these processes results in inaccuracies that lead to QoS degradations. Therefore, the only way to deal with this challenge is by means of more automated and autonomous systems such as SON. SON allows addressing this problem in an effective and cost-efficient manner minimizing human intervention.

This appendix presents a multiobjective optimization scheme based on power planning that is suitable to be used in SON. The proposed multiobjective scheme is based on the framework introduced in Chapter 3 and it aims at reconfiguring the average transmission power at each cell as a mean to adaptively tune the network to traffic load unbalances. Several levels of adaptation are obtained by identifying solutions capturing the best possible tradeoff between spectral efficiency, cell edge performance and the minimization of the transmitted power.

E.1 Self-Organizing Networks: An Introduction

The focus of SON are autonomous network deployment, performance optimization and dynamic adaptation to environmental changes such as variations in traffic load. Thus, in SON, one or more configuration parameters are independent and dynamically modified at each base station to reduce operational costs and improve network performance [312].

The main functionalities of SON can be classified as:

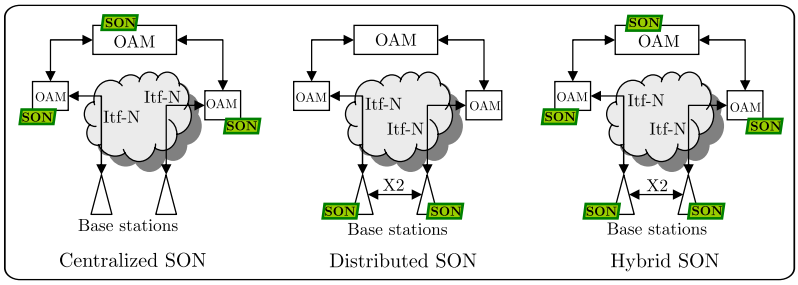

Figure E.1: SON architectures.

1. *Self-configuration*: it refers to the set of mechanisms or procedures by which a new base station is automatically installed and configured.

2. *Self-optimization*: it includes means by which both mobile devices and base stations dynamically tune the network based on measurements, performance metrics or any other information that can be used to enhance the network operation.

3. *Self-healing*: it encompasses functions that aim at automatic detection and localization of failures. It also include recovering and fallback procedures.

According to the location of the optimization algorithms, SON can be divided into three classes: Centralized SON, Distributed SON and Hybrid SON. Figure E.1 illustrates the different architectures for SON.

1. *Centralized SON*: in this kind of solutions, the optimization algorithms are executed in a small number of locations in the network. The Operation and Maintenance (OAM) subsystem is responsible for collecting and processing such information.

2. *Distributed SON*: the optimization algorithms are executed in each base station or in many locations in the network.

3. *Hybrid SON*: in this type of SON, some decisions are taken in a centralized manner, while others are executed in each base station.

E.1.1 Representative Contributions

In the context of OFDMA systems such as LTE and LTE-A, significant efforts are being devoted to SON. Remarkable contributions addressing aspects such as adaptive interference coordination [313], load balancing [314], coverage/capacity optimization [315], energy saving [316], and mobility and handover optimization [317] have been presented.

In addition, it is worth mentioning that the research on SON is especially active in the context of HetNets, where this feature plays a crucial role in the

optimization of such hierarchical deployments. Relevant and interesting resource allocation contributions include [318, 319].

E.2 Proposed SON Scheme

E.2.1 System Model

The system model is the one presented in Appendix C, Section C.1.

The novel framework aims at adjusting the transmit power for the data channels at each cell. In the proposed scheme, full frequency reuse is assumed. Therefore, the vector $\mathbf{x} \in \mathbb{R}^L$ indicates the power that must be applied in the PRBs of each cell as it is indicated in Figure E.2. Note that each element of $\mathbf{x}$ ($\mathbf{x}(l),\ l = 1, 2, \cdots, L$) is bounded to the interval $[\ p_{\min},\ p_{\max}\ ]$. This approach is convenient because different configurations only require adjusting one single parameter: the power of the PDSCH, and hence, the real-time cost is minimal. In addition, the highly critical configuration of control channels does not need to be altered as it would be the case if the cell coverage pattern were modified, for instance, if CS-RS power were modified.

In this study, the use of the objectives functions f_1, f_2, and f_3, as they are defined in Section 6.2 is proposed. Thus, the optimization scheme aims at the joint optimization of the following criteria:

1. Maximization of average cell capacity (f_1). This performance indicator provides the system-oriented perspective.
2. Maximization of the capacity of the worst 5% of the network coverage area, typically users at cell edge (f_2). This metric introduces fairness.
3. Minimization of transmitted power (f_3). This figure includes the energy efficient point of view.

The evaluation of the objective functions is done in terms of the power allocation vector ($\mathbf{x}$). Once the cell coverage pattern (the matrices $\mathbf{S}$ and $\mathbf{S}^{\mathrm{c}}$) are computed according to the procedure indicated in Section C.1, the resulting average SINR (ψ_{u}) at each pixel can be obtained by using an expression similar to (3.27), therefore,

$$\mathbf{\Psi}_{\mathrm{u}} = [(\mathbf{S} \odot \mathbf{G}) \cdot \mathbf{x}] \oslash \left[\, [(\mathbf{S}^{\mathrm{c}} \odot \mathbf{G}) \cdot \mathbf{x}] \oplus \sigma^2 \,\right]. \tag{E.1}$$

Given $\mathbf{\Psi}_{\mathrm{u}} \in \mathbb{R}^A$, the spectral efficiency of each pixel is obtained by means of the Shannon's formula. Thus, the vector $\mathbf{H} \in \mathbb{R}^A$ is given by:

$$\mathbf{H} = \log_2 (1 + \mathbf{\Psi}_{\mathrm{u}}). \tag{E.2}$$

Under the assumption of full frequency reuse and equal resource sharing among pixels, the rate of each pixel (the vector $\mathbf{r} \in \mathbb{R}^A$) can be obtained as follows:

$$\mathbf{r} = B \cdot ((\mathbf{S} \cdot \mathbf{\Phi}) \odot \mathbf{H}). \tag{E.3}$$

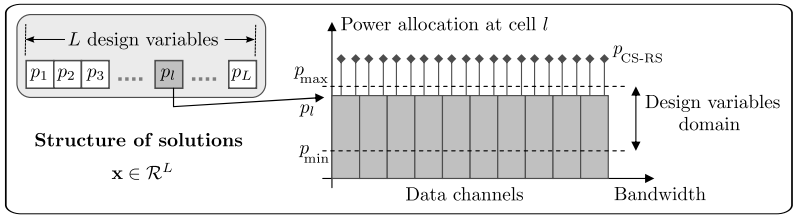

Figure E.2: Codification of network configurations.

The vector $\mathbf{\Phi} \in \mathbb{R}^L$ contains the inverse of the number of pixels associated to each cell, and hence, $\mathbf{\Phi} = \mathbf{1} \oslash \left(\mathbf{S}^{\mathrm{T}} \cdot \mathbf{1}\right)$. The objective functions are calculated according to the following expressions:

$$f_1 = (\mathbf{r} \cdot \mathbf{1})\,/L, \tag{E.4}$$

$$f_2 = \texttt{Sum(Sort(r), } 0.05 \cdot A \texttt{)}, \tag{E.5}$$

$$f_3 = (\mathbf{x} \cdot \mathbf{1})\,/\,(L \cdot p_{\max})\,. \tag{E.6}$$

The functions `Sort()` and `Sum()` are introduced in Section 6.3. The function `Sort()` sorts a vector in ascending order, while the function `Sum()` determines the sum of the first k elements of the vector that is passed as argument. Note that in (E.5), $k = 0.05 \cdot A$, and hence, f_2 represents the aggregate capacity of the worst 5% of the coverage area.

E.2.2 Multiobjective Problem Design

The proposed multiobjective problem formulation can be written as follows:

$$\underset{\mathbf{x}}{\text{minimize}} \quad \mathbf{f}(\mathbf{x}) = [\ -f_1(\mathbf{x}),\ \ -f_2(\mathbf{x}),\ \ f_3(\mathbf{x})\ ], \tag{E.7a}$$

subject to:

$$\mathbf{x}(l)\ \in\ [\ p_{\min},\ p_{\max}\ ], \quad l = 1, 2, \cdots, L, \tag{E.7b}$$

where $p_{\min}$ and $p_{\max}$ are the bounds of the design variables. Recall that the selection of $p_{\min}$ is scenario dependent and it should be done considering the minimum power level expected to be received at each pixel. In this study, (E.7) is solved by means of the algorithm NSGA-II (see Section 5.4) for the reasons that were explained in Subsections 5.3.1 and Section 6.4. In summary, the ability of this type of multiobjective-metaheuristic procedures to explore objective spaces whose mathematical structure does not allow the use of exact/deterministic procedures. Moreover, as it was shown in Chapters 6, 7, and 8, NSGA-II has excellent convergence properties in problems similar to (E.7).

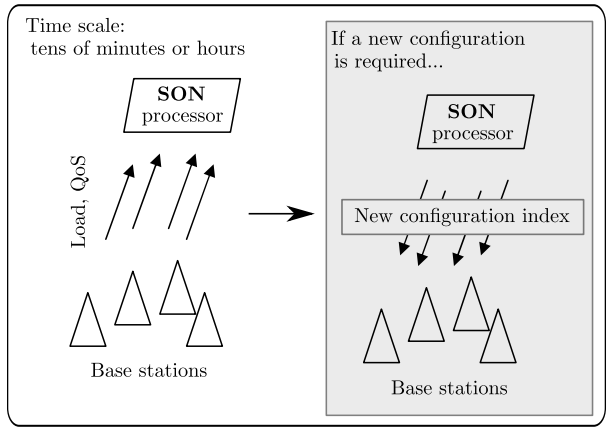

Figure E.3: Proposed operation: continuous monitoring of the network.

E.2.3 Conceptual Design

Figure E.3 illustrates the implementation of the proposed SON framework, whose most important features are described in the following points:

- From users point of view, neither additional functionality is required nor control information is needed to be transmitted over the air interface.

- The operation time scale is in the order of tens of minutes or hours depending on network dynamism.

- Each base station would transmit basic information about its current traffic load and QoS to several SON processors that control clusters of cells. Thus, implementation is semidistributed. The previous data can be transmitted by means of indexes indicating discrete traffic load levels and current QoS. For this, few bits suffices, lets say 3 bits (8 states) to indicate the status in terms of load and QoS. The information can be transmitted through the interface X2 being the intercell overhead negligible given the operation time scale.

- Each SON processor determines, based on the information coming from base stations, whether another configuration is required to better tune the network (or the cluster) according to current status. Recall that the network configurations (solutions in the set X.) are computed and evaluated offline and stored in databases (look-up tables).

- Finally although the implementation of the proposed scheme would be a vendor-specific feature (added value), it is worth saying that some aspects of power setting changes are indicated with the specifications of LTE or LTE-A [162, 217], and hence, not new functionality need to be indicated to do that.

Table E.1: Evaluation setting and NSGA-II configuration

Network settings and parameters	
Available power per cell	43.00 dBm
System bandwidth (B)	5.40 MHz
Number of cells (L)	60
Number of pixels (A)	288750
CS-RS power ($\mathbf{p}_{\text{CS-RS}}(l), \quad l = 1, 2, \cdots, L$)	18.4 dBm
Bandwidth sharing (β) in ePDCCH optimization	2/3
NSGA-II configuration	
Population size	150
Max number of generation	1000
Termination criterion: relative gain in each f_i	$< 0.01\%/40$ generations
Crossover probability	1.0
Mutation probability	$1/L$
Type of design variables	Discrete-valued (Res: 2%)
$[\ p_{\min},\ p_{\max}\ ]$	[9.16, 17.4] [dBm/15 KHz]

E.3 Performance Evaluation

In this section, performance evaluation results are presented. Given that convergence and calibration aspects have been addressed in Chapters 6, 7, and 8, only the most basic results are shown.

E.3.1 Multiobjective Optimization

The set of parameters used in numerical evaluations together with the configuration of the algorithm NSGA-II is shown in Table E.1. Calibration was done according to the guidelines explained in Subsection 6.6.1.

The performance of the proposed framework is analyzed/compared with the case where each cell transmits (selfishly) at maximum power over its available bandwidth. Thus, the reference scheme ($\mathbf{x}_{\text{FR}}$) is defined as follows:

$$\mathbf{x}_{\text{FR}} = \left[\ p_{\max}^{(1)}, \quad p_{\max}^{(2)}, \quad \cdots, \quad p_{\max}^{(L)} \ \right]^{\text{T}}.$$

Figure E.4 shows several views of the estimated Pareto Front. In the figures, the reference scheme ($\mathbf{x}_{\text{FR}}$) is also indicated in dark blue. Focusing on the 2D profiles (Figures E.4b E.4c, and E.4d), it can be clearly observed how the proposed optimization framework always succeeds in finding network configurations dominating the reference scheme from the perspective of each pair of objective functions. Recall that the intersection of the set of solutions dominating each baseline design in each

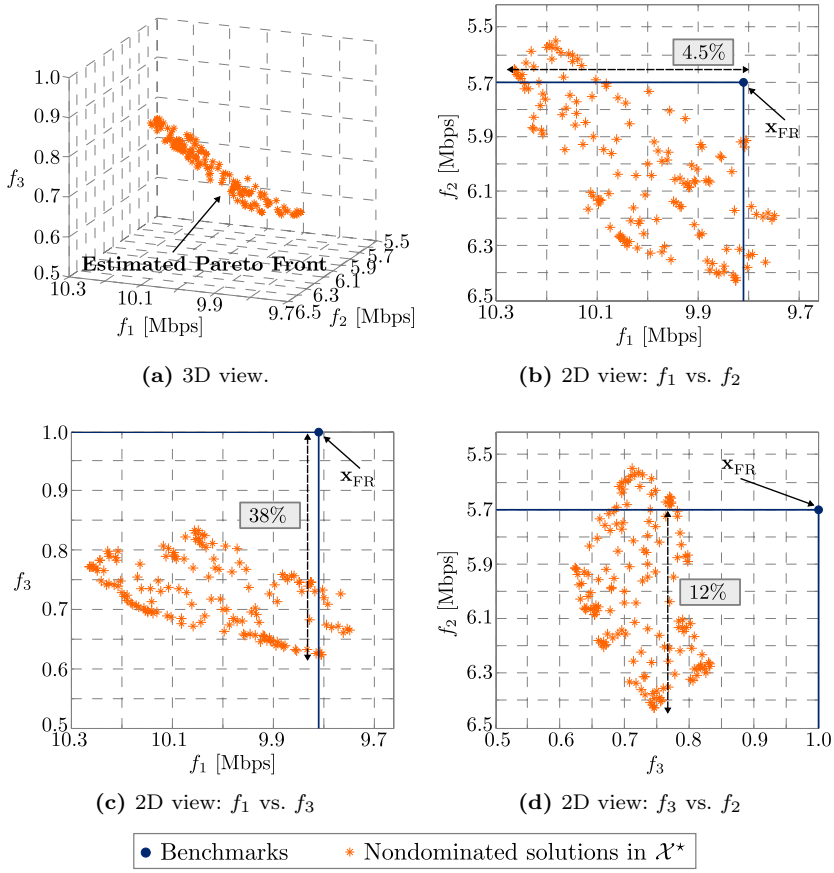

(a) 3D view.

(b) 2D view: f_1 vs. f_2

(c) 2D view: f_1 vs. f_3

(d) 2D view: f_3 vs. f_2

Figure E.4: Representations of the estimated Pareto Front.

2D profile correspond to the set of solutions that dominates $\mathbf{x}_{\mathrm{FR}}$ in the Pareto sense. In the example shown, the cardinality of such set is 97 which means that 64% of the population become into solutions dominating $\mathbf{x}_{\mathrm{FR}}$. However, the size of such set can be increased by changing the number of individuals in the population at the expense of more objective function evaluations per generation.

In the light of the previous results, it can be concluded that the proposed multiobjective scheme is also effective to improve not only the performance of SFR and FFR, but also classic schemes such as full reuse. The extension to other cases including reuse factor 3 is straightforward.

Finally, Figure E.5 indicates both system and cell level performance of two Pareto efficient solutions ($\mathbf{x}_1$ and $\mathbf{x}_2$) and the reference scheme ($\mathbf{x}_{\mathrm{FR}}$). Recall that from the system point of view, $\mathbf{x}_1$ and $\mathbf{x}_2$ are Pareto efficient, and hence, switching from one to another always implies a tradeoff. For instance, the configuration $\mathbf{x}_1$ increases 4.6% the average cell capacity with respect to $\mathbf{x}_2$, which in turn improves the cell

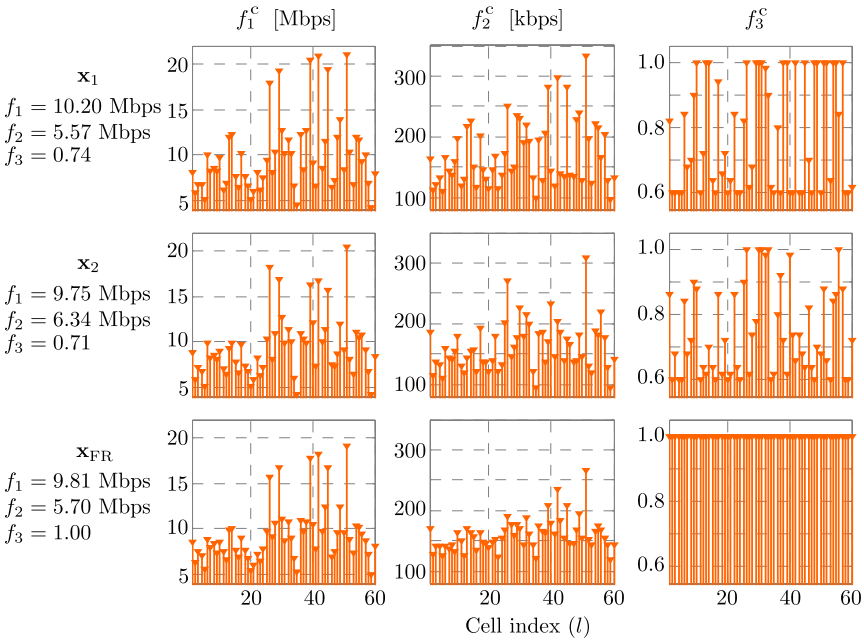

Figure E.5: Performance at cell level of two nondominated solutions.

edge performance and energy consumption 13% and 4%, respectively.

Regarding the suitability of the proposed scheme for SON, it can be seen that both $\mathbf{x}_1$ and $\mathbf{x}_2$ results in quite different performances at cell level which is precisely the desired feature to compensate load unbalances from cell to cell. By recognizing average traffic profiles in the network the operator can look for the appropriate solution in databases and apply the selected network configuration with minimal intercell signaling and computational cost.

Appendix F

Impact of PDCCH Capacity Limitations on the QoS

One of the main issues associated to dynamic scheduling is the high amount of signaling overhead required to provide users with resource allocation information. While the impact of control channel limitations on LTE VoIP capacity has been widely studied [165, 258], the tradeoffs associated to the use of control resources and the provision of QoS for NRT services has been omitted in current literature.

Only few works, such as [307, 320], addressing such issue have been presented. The study presented here also deals with the same framework, nevertheless it differs from them in that a pure QoS-oriented scheduler [215] (fed by a CQI-based channel quality reporting scheme) explicitly designed for multi-service environments is considered. Thus the impact of PDCCH resources consumption on performance is evaluated for different levels of QoS (measured in terms of offered bit rates).

F.1 Interworking Description

In this work, the downlink of an LTE-based cellular network that largely follows the LTE specifications [159] was considered. As in Chapter 4, the scheduling implementation corresponds to the Capacity-driven Resource Allocation (CRA) scheduler proposed in [215]. The CRA scheduler dynamically controls the resource sharing among flows in order to satisfy the maximum number of users according to the QoS criterion of each service. The system performance depends on the following inputs: operational configuration of the scheduler, users channel status given by CSI reports, and HARQ acknowledgments. This interworking is shown in Figure F.1. Two different parameters of the CRA scheduler are considered:

1. Target bit rate (r_{T}): the target throughput the scheduler tries to deliver to each user in the system.

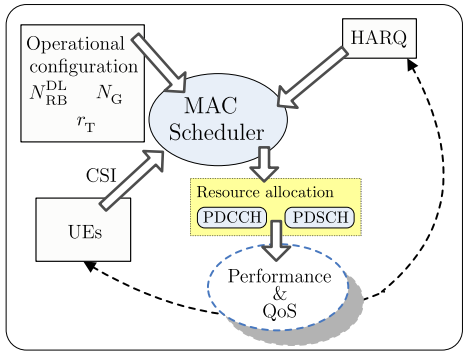

Figure F.1: System interworking.

2. Scheduling set size (N_G): the maximum number of downlink grants the scheduler is allowed to make at each TTI per cell.

The allocation of control resources is done as explained in Subsection 7.2.1, i.e., the number of control resources allocated to each user depends on the average radio channel quality (wideband SINR) (see also Table C.2). The allocation of data resources depends on the CRA scheduler. Thus, the output (and hence the overall system performance) includes the actual resource allocation which comprises how both PDCCH and PDSCH resources are going to be shared among users.

Recall that, as it was indicated in 'The user plane and the control plane' in Subsection 2.7.1, The DCI carries downlink (and uplink) scheduling assignments, power control commands, and additional information required to decode and demodulate data symbols in the downlink (encode and modulate data symbols in the uplink). In addition to the DCI, also the Control Format Indicator (CFI) and HARQ indicator (HI) are transmitted over the first OFDMA symbols of every frame, although through different physical channels: the Physical Control Format Indicator Channel (PCFICH) and Physical HARQ Indicator Channel (PHICH), respectively. Since resource consumption of both CFI and HI is variable [161, 162], a practical rule of thumb is to assume that the amount of resources devoted to the DCI is approximately equal to $k = 4/5$ of the total PDCCH capacity [258]. In this study, only downlink is considered, so it is assumed that only 50% of the resources devoted to the PDCCH are available. The rest of resources are reserved to uplink grants. The minimum resource unit allocated to one single user for control signaling is a CCE. Thus, an upper bound for the number of avaiable CCEs (N_{CCE}^{Max}) is given by:

$$N_{CCE}^{Max} = \frac{1}{2} \cdot \frac{k \cdot n \cdot N_{SC}}{4 \cdot N_{REG}}, \tag{F.1}$$

where the parameter n indicates how many OFDM symbols are dedicated to the PDCCH ($n \in \{1, 2, 3, 4\}$]). The parameters N_{REG} and N_{SC} correspond to the number of REGs per CCE and the number of subcarriers in the system bandwidth, respectively. It can be noted that N_{SC} depends on the number of resource blocks (N_{RB}^{DL}), indeed $N_{SC} = 12 \cdot N_{RB}^{DL}$.

Table F.1: Simulation Parameters and Evaluation Setting.

Parameter	**Value/assumption**
Test cases (scenarios)	'Synthetic' (see Section B.1).
System bandwidth (B)	5.4 MHz, ($N_{\mathrm{RB}}^{\mathrm{DL}} = 30$).
System load	$20 \times L$ users (20 users per cell (on average)).
PDCCH OFDM symbols (n)	3.
Scheduler	CRA scheduler [215].
Traffic model	Full Buffers.
CSI feedback	CQI-based, one CQI per RB.
Mobility model	Urban vehicular [173]
Link Abstraction	Mutual Information Equivalent SINR Mapping [174].
Transmission mode	Single-antenna port.

F.2 Impact of PDCCH Capacity Constraints

F.2.1 Evaluation Setting

This study was conducted by means of LTE-based system level simulations. The general setting is the one described in Subsection 3.4.2. The results were collected from Monte Carlo experiments with uniform randomly spread users. They compile statistics from 500 independent experiments each of which has a duration of 60 s (6×10^4 TTIs). Simulation parameters common to all scenarios are indicated in Table B.2. Additional parameters and assumptions considered for this study are shown in Table F.1.

F.2.2 Numerical Results

In order to determine the impact of PDCCH resources consumption on the QoS experienced by users, different independent experiments were performed. As mentioned, the study has two degrees of freedom: the maximum number of users that can be scheduled per TTI/cell (N_{G}) and the offered bit rate (r_{T}).

Scheduler Operation and CCE Consumption

The general operation of the CRA scheduler is illustrated by means of the CDFs of the user rates r for different values of r_{T} and $N_{\mathrm{G}} = 4$. Figure F.2 shows the basic principle of the CRA scheduler, where only the minimum amount of resources required to achieve the target bit rate is allocated to users. It can be seen that the lower the value of r_{T}, the higher the percentage of users achieving such rate. Given this, the effect of N_{G} is studied next.

In order to illustrate the pace at which PDCCH resources are used, the CDF of the number of CCEs per TTI/cell (N_{CCE}) as a function of N_{G} (assuming that

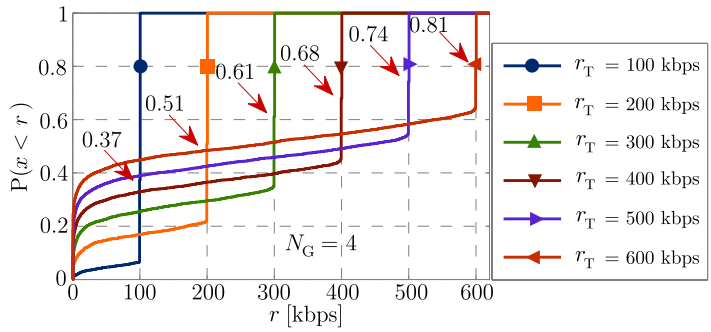

Figure F.2: CRA scheduler operation: CDF of user rates.

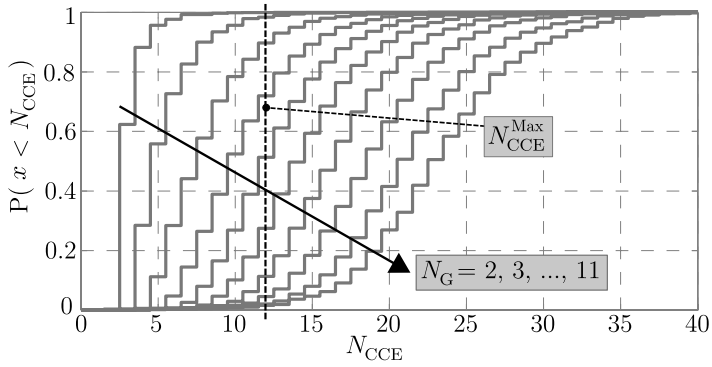

Figure F.3: CCE Consumption: $r_{\mathrm{T}} = 100$ kbps.

resources for PDCCHs are never fully consumed) is shown in Figure F.3. The dashed black line indicates the value of $N_{\mathrm{CCE}}^{\mathrm{Max}}$ for the setting under consideration, see (F.1). This is important because in practice, schedulers are forced to verify the availability of PDCCH resources before schedule each user. It can be seen that if a blocking probability of around 5-10% due to PDCCH capacity were allowed, then the choice of $N_{\mathrm{G}} = 3$-4 would be required. However, as it will be shown shortly, this limitation plays an important role in the provisioning of QoS for NRT services.

User Satisfaction Ratio

Figure F.4 shows the user satisfaction probability. Note that $N_{\mathrm{G}} \in \{2, 3, ..., 11\}$ and $R_{\mathrm{T}} \in \{100, 200, ..., 600\}$. Any point in the surface can be understood as the probability of a user to obtain a throughput at least equal to r_{T}. For low values of r_{T} the system capacity is clearly limited by the amount of available PDCCH resources, and hence, the overall satisfaction level is directly proportional to the number of users the scheduler can attend. It is assumed that resources for PDCCHs are never fully consumed in order to determine when this constrain is a limiting factor (bearing in mind the value of $N_{\mathrm{CCE}}^{\mathrm{Max}}$ previously computed). This behaviour goes in the line with results reported for VoIP in [165], specifically for the case of dynamic scheduling.

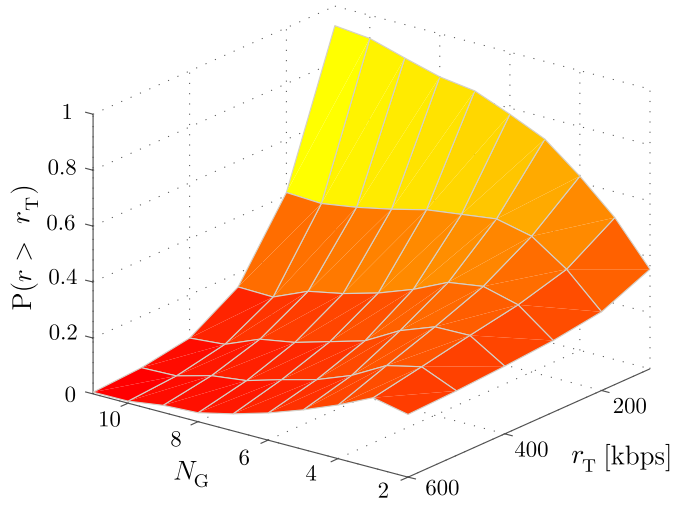

Figure F.4: User satisfaction probability.

In this case VoIP is a service demanding very low bit rates and the **the capacity is effectively limited by the number of control resources**. As r_{T} grows, the optimum value of N_{G} becomes smaller. This is due to the fact that the CRA scheduler operates in such a way as to maximize the number of satisfied flows. Therefore, for high values of r_{T}, overall satisfaction becomes inversely proportinal to N_{G}, i.e., an opposite behaviour compared to cases where r_{T} is small. It is important to recall that the system capacity is, according to [215], a function of the load and traffic mix. Consequently, the result shown in Figure F.4 clearly suggests that in order to let the system operate efficiently from the radio resource allocation perspective, it is important to characterize the system taking into account the traffic features (offered QoS and expected load), scheduling policy, and availability of resources available for PDCCH. Thus, given the constraint seen in the previous subsection (N_{G} = 3-4), the impact of the PDCCH capacity would not be harmful if high values of r_{T} were pursued, while for low values of r_{T} the system capacity would be penalized.

Bibliography

[1] T. Loozen, R. Murdoch, and S. Orr, *Mobile Web Watch 2013*. Accenture, 2013. Technical Report. Available online at: www.accenture.com.

[2] M. L. Roberts, M. A.Temple, R. F. Mills, and R. A. Raines, "Evolution of the Air Interface of Cellular Communications Systems Toward 4G Realization," *IEEE Communication Surveys & Tutorials*, vol. 8, no. 1, pp. 2–23, Jan. 2006.

[3] N. Himayat, S. Talwar, A. Rao, and R. Soni, "Interference Management for 4G Cellular Standards," *IEEE Communications Magazine*, vol. 48, no. 8, pp. 86–92, Aug. 2010.

[4] Ericsson, NTT DoCoMo, *R1-060586: Downlink and Uplink Intercell Interference Coordination/Avoidance*. 3GPP, Feb 2006. Radio Access Network (RAN) Working Group 1, Meeting #44: Denver, USA.

[5] A. Bahai, B. Saltzberg, and M. Ergen, *Multi-Carrier Digital Communications: Theory and Applications of OFDM*. Springer, 2nd ed., 2004.

[6] K. Son, Y. Yi, and S. Chong, "Adaptive Multi-Pattern Reuse in Multi-Cell Networks," in *Proc. of 7th International Symposium on Modeling and Optimization in Mobile, Ad Hoc, and Wireless Networks (WiOPT 2009)*, Seoul (Korea), Jun. 23–27, 2009.

[7] S. Sadr, A. Anpalagan, and K. Raahemifar, "Radio Resource Allocation Algorithms for the Downlink of Multiuser OFDM Communication Systems," *IEEE Communication Surveys & Tutorials*, vol. 11, no. 3, pp. 92–106, 3^{rd} Quarter 2009.

[8] M. Salem, A. Adinoyi, M. Rahman, H. Yanikomeroglu, D. Falconer, Y.-D. Kim, E. Kim, and Y.-C. Cheong, "An Overview of Radio Resource Management in Relay-Enhanced OFDMA-Based Networks," *IEEE Communication Surveys & Tutorials*, vol. 12, no. 3, pp. 422–438, 3^{rd} Quarter 2010.

[9] B. Sklar, "Rayleigh Fading Channels in Mobile Digital Communication Systems. Part I: Characterization," *IEEE Communications Magazine*, vol. 35, no. 7, pp. 90–100, Jul. 1997.

[10] *TR 25.814 (Release 7) - Physical Layer Aspects for Evolved Universal Terrestrial Radio Access (UTRA).* 3GPP Technical Report. Available online at: www.3gpp.org.

[11] *TR 36.814 (Release 9) - Further Advancements for E-UTRA Physical Layer Aspects.* 3GPP Technical Report. Available online at: www.3gpp.org.

[12] R. Bosisio and U. Spagnolini, "Interference Coordination vs. Interference Randomization in Multicell 3GPP LTE System," in *Proc. of IEEE Wireless Communications and Networking Conference (WCNC 2008)*, Las Vegas (United States), Mar. 31–Apr. 3, 2008.

[13] E. Dahlman, S. Parkvall, and J. Sköld, *4G LTE/LTE-Advanced for Mobile Broadband.* Elsevier, 1st ed., 2004.

[14] D. Khan and B. Priyanto, "Performance Evaluation of Frequency Hopping Schemes in UTRA-ITE Uplink," in *Proc. of IEEE Annual IEEE Conference 2008*, Aalborg (Denmark), Feb. 15–26, 2008.

[15] I. Kim, Y. Han, Y. Kim, and S. C. Bang, "Sequence Hopping Cell Search Scheme for OFDM Cellular Systems," *IEEE Transactions on Wireless Communications*, vol. 7, no. 7, pp. 1483–1489, May. 2008.

[16] K. Chang, P. Ho, and Y. Choi, "Signal Design for Reduced Complexity and Accurate Cell Search/Synchronization in OFDM-Based Cellular Systems," *IEEE Transactions on Vehicular Technology*, vol. 61, no. 9, pp. 4170–4175, Jul. 2012.

[17] F. Lu, T. Komine, T. Suzuki, and M. Sawahashi, "CAZAC Sequence Hopping for Physical Uplink Control Channel of LTE," in *Proc. of IEEE 68th Vehicular Technology Conference (VTC 2008 Fall)*, Calgary (Canada), Sep. 21–24, 2008.

[18] H. A. Ngo and L. Hanzo, "Area Spectral Efficiency of Soft Decision Space–Time–Frequency Shift-Keying-Aided Slow Frequency Hopping Multiple Access," *IEEE Transactions on Vehicular Technology*, vol. 61, no. 3, pp. 1433–1439, Jan. 2012.

[19] G. Boudreau, J. Panicker, N. Guo, R. Chang, N. Wang, and S. Vrzic, "Interference Coordination and Cancellation for 4G Networks," *IEEE Communications Magazine*, vol. 47, no. 4, pp. 74–81, Apr. 2009.

[20] M.-X. Chang and Y.-T. Su, "Blind and Semiblind Detections of OFDM Signals in Fading Channels," *IEEE Transactions on Communications*, vol. 52, no. 5, pp. 744–754, May. 2004.

[21] Y. Léost, M. Abdi, R. Richter, and M. Jeschke, "Interference Rejection Combining in LTE Networks," *Bell Labs Technical Journal*, vol. 17, no. 1, pp. 25–49, Jun. 2012.

[22] H. Maleki, S. Jafar, and S. Shamai, "Retrospective Interference Alignment Over Interference Networks," *IEEE Journal of Selected Topics in Signal Processing*, vol. 6, no. 3, pp. 228–240, May. 2012.

[23] S. Sen, N. Santhapuri, R. Choudhury, and S. Nelakuditi, "Successive Interference Cancellation: Carving Out MAC Layer Opportunities," *IEEE Transactions on Mobile Computing*, vol. 12, no. 2, pp. 346–357, Feb. 2013.

[24] N.-D. Dao, J. Soler-Garrido, R. Cepeda, Y. Sun, and W. H. Chin, "Design and Evaluation of Antenna Selection Methods for Interference Rejection Combining," *IEEE Transactions on Wireless Communications*, vol. 11, no. 8, pp. 2751–2759, Aug. 2012.

[25] Z. Zeng, D. Xiao, and X. Han, "Adaptive IRC Algorithm to Overcome Intercell Interference in Uplink LTE System," in *Proc. of International Conference on Multimedia Technology (ICMT 2011)*, Zurich (Switzerland), Jun. 27–28, 2011.

[26] J. Axnas, Y.-P. Wang, M. Kamuf, and N. Andgart, "Successive Interference Cancellation Techniques for LTE Downlink," in *Proc. of IEEE 22nd International Symposium on Personal, Indoor and Mobile Radio Communications (PIMRC 2011)*, Toronto (Canada), Sep. 11–14, 2011.

[27] Z. Bai, J. Berkmann, C. Spiegel, T. Scholand, G. Bruck, C. Drewes, B. Gunzelmann, and P. Jung, "On MIMO with Successive Interference Cancellation Applied to UTRA LTE," in *Proc. of 3rd International Symposium on Communications, Control and Signal Processing (ISCCSP 2008)*, St. Julians (Malta), Mar. 12–14, 2008.

[28] L. Dong, Z. Song, L. Wenxin, and W. Wenbo, "A Frequency Reuse Partitioning Scheme with Successive Interference Cancellation for OFDMA Uplink Transmission," in *Proc. of IEEE 20th International Symposium on Personal, Indoor and Mobile Radio Communications (PIMRC 2009)*, Tokyo (Japan), Sep. 13–16, 2009.

[29] R. Ghaffar and R. Knopp, "Fractional Frequency Reuse and Interference Suppression for OFDMA Networks," in *Proc. of 8th International Symposium on Modeling and Optimization in Mobile, Ad Hoc, and Wireless Networks (WiOPT 2010)*, Avignon (France), May. 31–Jun. 4, 2010.

[30] V. Cadambe and S. Jafar, "Interference Alignment and Degrees of Freedom of the K -User Interference Channel," *IEEE Transactions on Information Theory*, vol. 54, no. 8, pp. 3425–3441, Aug. 2008.

[31] J. Reitterer and M. Rupp, "Interference Alignment in UMTS Long Term Evolution," in *Proc. of European Conference on Signal Processing (EUSIPCO 2011)*, Barcelona (Spain), Aug. 29–Sep. 2, 2011.

[32] M. Maso, M. Debbah, and L. Vangelista, "A Distributed Approach to Interference Alignment in OFDM-Based Two-Tiered Networks," *IEEE Transactions on Vehicular Technology*, vol. 62, no. 5, pp. 1935–1949, Jun. 2013.

[33] C. Zhou, W. Chen, and Z. Chen, "Combination of Interference Alignment and Beamforming in Cellular Networks," in *Proc. of 6th International ICST*

Conference on Communications and Networking in China (CHINACOM 2011), Harbin (China), Aug. 17–19, 2011.

[34] R. Irmer, H. Droste, P. Marsch, M. Grieger, G. Fettweis, S. Brueck, H.-P. Mayer, L. Thiele, and V. Jungnickel, "Coordinated Multipoint: Concepts, Performance, and Field Trial Results," *IEEE Communications Magazine*, vol. 49, no. 2, Feb. 2011.

[35] Y. Cheng, M. Pesavento, and A. Philipp, "Joint Network Optimization and Downlink Beamforming for CoMP Transmissions Using Mixed Integer Conic Programming," *IEEE Transactions on Signal Processing*, vol. 61, no. 16, pp. 3972–3987, Aug. 2013.

[36] V. Annapureddy, A. El Gamal, and V. Veeravalli, "Degrees of Freedom of Interference Channels With CoMP Transmission and Reception," *IEEE Transactions on Information Theory*, vol. 58, no. 9, pp. 5740–5760, Sep. 2012.

[37] D. Choi, D. Lee, and J. Lee, "Resource Allocation for CoMP With Multiuser MIMO OFDMA," *IEEE Transactions on Vehicular Technology*, vol. 60, no. 9, pp. 4626–4632, Nov. 2011.

[38] D. Lee, H. Seo, B. Clerckx, E. Hardouin, D. Mazzarese, S. Nagata, and K. Sayana, "Coordinated Multipoint Transmission and Reception in LTE-Advanced: Deployment Scenarios and Operational Challenges," *IEEE Communications Magazine*, vol. 50, no. 2, pp. 148–155, Feb. 2012.

[39] D. Lopez-Perez, I. Guvenc, G. de la Roche, M. Kountouris, T. Quek, and J. Zhang, "Enhanced Intercell Interference Coordination Challenges in Heterogeneous Networks," *IEEE Wireless Communications*, vol. 18, no. 3, pp. 22–30, Sep. 2011.

[40] R. Kwan and C. Leung, "A Survey of Scheduling and Interference Mitigation in LTE," *Journal of Electrical and Computer Engineering*, vol. 2010, no. 273486, pp. 1–10, Aug. 2010.

[41] M. Necker, "Interference Coordination in Cellular OFDMA Networks," *IEEE Network*, vol. 22, no. 6, pp. 12–19, Dec. 2008.

[42] A. Hamza, S. Khalifa, H. Hamza, and K. Elsayed, "A Survey on Inter-Cell Interference Coordination Techniques in OFDMA-Based Cellular Networks," *IEEE Communication Surveys & Tutorials*, vol. PP, no. 99, pp. 1–29, Mar. 2013.

[43] C. Kosta, B. Hunt, A. U. Quddus, and R. Tafazolli, "On Interference Avoidance Through Inter-Cell Interference Coordination (ICIC) Based on OFDMA Mobile Systems," *IEEE Communication Surveys & Tutorials*, vol. 15, no. 3, pp. 973–995, Jul. 2013.

[44] G. Fodor, C. Koutsimanis, A. Rácz, N. Reider, A. Simonsson, and W. Muller, "Intercell Interference Coordination in OFDMA Networks and in the 3GPP Long Term Evolution System," *Journal of Communications*, vol. 4, no. 7, pp. 445–453, Aug. 2006.

[45] T. Novlan, R. Ganti, A. Ghosh, and J. Andrews, "Analytical Evaluation of Fractional Frequency Reuse for OFDMA Cellular Networks," *IEEE Transactions on Wireless Communications*, vol. 10, no. 12, pp. 4294—4305, Dec. 2011.

[46] Y. Yu, E. Dutkiewicz, X. Huang, M. Mueck, and G. Fang, "Performance Analysis of Soft Frequency Reuse for Inter-cell Interference Coordination in LTE Networks," in *Proc. of 10th International Symposium on Communications and Information Technologies (ISCIT 2010)*, Tokyo (Japan), Oct. 26–29, 2010.

[47] P. Lee, T. Lee, J. Jeong, and J. Shin, "Interference Management in LTE Femtocell Systems Using Fractional Frequency Reuse," in *Proc. of 12th International Conference on Advanced Communication Technology (ICACT 2010)*, Gangwon-Do (Korea), Feb. 7–10, 2010.

[48] Y. Zhao, X. Fang, X. Hu, Z. Zhao, and Y. Long, "Fractional Frequency Reuse Schemes and Performance Evaluation for OFDMA Multi-hop Cellular Networks," in *Proc. of 5th International Conference on Testbeds and Research Infrastructures for the Development of Networks Communities and Workshops (TridentCom 2009)*, Washington DC (United States), Mar. 6–8, 2009.

[49] Z. Qin, Z. Zhong, R. Xu, and G. Bai, "System Performance of Soft Frequency Reuse in LTE Railway Networks," in *Proc. of 11th IEEE International Conference on Signal Processing (ICSP 2012)*, Beijing (China), Oct. 21–25, 2012.

[50] P. Godlewski, M. Maqbool, M. Coupechoux, and J.-M. Kélif, "Analytical Evaluation of Various Frequency Reuse Schemes in Cellular OFDMA Networks," in *Proc. of 3rd International Conference on Performance Evaluation Methodologies and Tools*, Athens (Greece), Oct. 20–24, 2008.

[51] G. Fodor, "Performance Analysis of a Reuse Partitioning Technique for OFDM Based Evolved UTRA," in *Proc. of 14th IEEE International Workshop on Quality of Service (IWQoS 2006)*, New Haven (United States), Jun. 19–21, 2006.

[52] M. Porjazoski and B. Popovski, "Analysis of Intercell Interference Coordination by Fractional Frequency Reuse in LTE," in *Proc. of International Conference on Software, Telecommunications and Computer Networks (SoftCOM 2010)*, Split (Croatia), Sep. 23–25, 2010.

[53] Fujitsu, *Enhancing LTE Cell-Edge Performance via PDCCH ICIC*, 2011. Technical Report. Available online at: us.fujitsu.com/telecom.

[54] IEEE 802.16 Broadband Wireless Access Working Group, *Fractional Frequency Reuse in Uplink*. IEEE, 2008. Technical Report C802.16m-08/782. Available online at: www.ieee802.org.

[55] Y. M. Kwon, O. K. Lee, J. Y. Lee, and M. Y. Chung, "Power Control for Soft Fractional Frequency Reuse in OFDMA System," in *Proc. of International*

Conference on Computational Science and Its Applications (ICCSA 2010), Fukuoka (Japan), Mar. 23–26, 2010.

[56] D. Kim, J. Y. Ahn, and H. Kim, "Downlink Transmit Power Allocation in Soft Fractional Frequency Reuse Systems," *ETRI Journal*, vol. 33, no. 1, pp. 1–5, Feb. 2011.

[57] *TR 25.892 (Release 6) - Feasibility Study for Orthogonal Frequency Division Multiplexing (OFDM) for UTRAN Enhancement.* 3GPP Technical Report. Available online at: www.3gpp.org.

[58] K. T. Kim and S. K. Oh, "An Incremental Frequency Reuse Scheme for an OFDMA Cellular System and its Performance," in *Proc. of IEEE 67th Vehicular Technology Conference (VTC 2008 Spring)*, Marina Bay (Singapore), May. 11–14, 2008.

[59] Z. Xie and B. Walke, "Resource Allocation and Reuse for Inter-cell Interference Mitigation in OFDMA based Communication Networks," in *Proc. of 5th Annual ICST Wireless Internet Conference (WICON 2010)*, Marina Bay (Singapore), Mar. 1–3, 2010.

[60] A. Najjar, N. Hamdi, and A. Bouallegue, "Fractional Frequency Reuse Scheme with Two and Three Regions For Multi-cell OFDMA Systems," in *Proc. of 17th Telecommunications Forum (TELFOR 2009)*, Belgrade (Serbia), Nov. 24–26, 2009.

[61] C.-S. Chiu and C.-C. Huang, "Combined Partial Reuse and Soft Handover in OFDMA Downlink Transmission," in *Proc. of IEEE 67th Vehicular Technology Conference (VTC 2008 Spring)*, Marina Bay (Singapore), May. 11–14, 2008.

[62] T. Bonald and N. Hegde, "Capacity Gains of Some Frequency Reuse Schemes in OFDMA Networks," in *Proc. of IEEE Global Telecommunications Conference (GLOBECOM 2009)*, Hawaii (United States), Nov. 30–Dec. 4, 2009.

[63] L. Chen and D. Yuan, "Soft Frequency Reuse in Large Networks with Irregular Cell Pattern: How Much Gain to Expect?," in *Proc. of IEEE 20th International Symposium on Personal, Indoor and Mobile Radio Communications (PIMRC 2009)*, Tokyo (Japan), Sep. 13–16, 2009.

[64] L. Chen and D. Yuan, "Generalizing FFR by Flexible Sub-Band Allocation in OFDMA Networks with Irregular Cell Layout," Sydney (Australia), Apr. 18–21, 2010.

[65] Z. Li, Y. Wang, and D. Yang, "A Hybrid Inter-cell Interference Mitigation Scheme for OFDMA System," in *Proc. of 11th IEEE Singapore International Conference on Communication Systems (ICCS 2008)*, Guangzhou (China), Nov. 19–21, 2008.

[66] V. Corvino, D. Gesbert, and R. Verdone, "A Novel Distributed Interference Mitigation Technique using Power Planning," in *Proc. of IEEE Wireless Communications and Networking Conference (WCNC 2009)*, Budapest, Hungary. Apr. 5–8, 2009.

[67] C. Nie, P. Liu, and S. Panwar, "Interference Management using Frequency Planning in an OFDMA Based Wireless Network," in *Proc. of IEEE Wireless Communications and Networking Conference (WCNC 2011)*, Cancun, Mexico. Mar. 28–31, 2011.

[68] Y. Pei, H. Tian, T. Wu, and Y. Wang, "Frequency Planning Scheme Based on Interference Coordination for OFDM-Relay Systems," *IEEE Communication Letters*, vol. 15, no. 1, Jan. 2011.

[69] B. Fan, Y. Qian, K. Zheng, and W. Wang, "A Dynamic Resource Allocation Scheme Based on Soft Frequency Reuse for OFDMA Systems," in *Proc. of IEEE International Symposium on Microwave, Antenna, Propagation and EMC Technologies for Wireless Communications (MAPE 2007)*, Hangzhou (China), Aug. 16–17, 2007.

[70] M. Rahman and H. Yanikomeroglu, "Enhancing Cell-edge Performance: A Downlink Dynamic Interference Avoidance Scheme with Inter-cell Coordination," *IEEE Transactions on Wireless Communications*, vol. 9, no. 4, pp. 1414–1425, Apr. 2010.

[71] Z. Xie and B. Walke, "Frequency Reuse Techniques for Attaining Both Coverage and High Spectral Efficiency in OFDMA Cellular Systems," in *Proc. of IEEE Wireless Communications and Networking Conference (WCNC 2010)*, Sydney (Australia), Apr. 18–21, 2010.

[72] L. Liu, G. Zhu, and D. Wu, "Interference Management Based on Enhanced Fractional Frequency Reuse in OFDMA Networks," in *Proc. of 7th International Conference on Wireless Communications, Networking and Mobile Computing (WiCOM 2011)*, Wuhan (China), Sep. 23–25, 2011.

[73] D. Bilios, C. Bouras, V. Kokkinos, A. Papazois, and G. Tseliou, "A Performance Study of Fractional Frequency Reuse in OFDMA Networks," in *Proc. of 5th Joint IFIP Wireless and Mobile Networking Conference (WMNC 2012)*, Bratislava (Slovakia), Sep. 19–20, 2012.

[74] X. Zhang, C. He, L. Jiang, and J. Xu, "Inter-cell Interference Coordination based on Softer Frequency Reuse in OFDMA Cellular Systems," in *Proc. of International Conference on Neural Networks and Signal Processing (ICNNSP 2008)*, Nanjing (China), Jun. 7–11, 2008.

[75] M. Rahman, H. Yanikomeroglu, and W. Wong, "Interference Avoidance with Dynamic Inter-Cell Coordination for Downlink LTE System," in *Proc. of IEEE Wireless Communications and Networking Conference (WCNC 2009)*, Budapest, Hungary. Apr. 5–8, 2009.

[76] L. Venturino, N. Prasad, and X. Wang, "Coordinated Scheduling and Power Allocation in Downlink Multicell OFDMA Networks," *IEEE Transactions on Vehicular Technology*, vol. 58, no. 6, pp. 2835–2848, Jul. 2009.

[77] M. Katoozian, K. Navaie, and H. Yanikomeroglu, "Utility-based Adaptive Radio Resource Allocation in OFDM Wireless Networks with Traffic Prioritization," *IEEE Transactions on Wireless Communications*, vol. 8, no. 1, pp. 66–71, Jan. 2009.

[78] S. Kiani, G. Oien, and D. Gesbert, "Maximizing Multicell Capacity Using Distributed Power Allocation and Scheduling," in *Proc. of IEEE Wireless Communications and Networking Conference (WCNC 2007)*, Hong kong, Mar. 11–15, 2007.

[79] S. Zheng, H. Tian, Z. Hu, L. Chen, and J. Zhu, "QoS-Guaranteed Radio Resource Allocation with Distributed Inter-Cell Interference Coordination for Multi-Cell OFDMA System," in *Proc. of IEEE 71st Vehicular Technology Conference (VTC 2010 Spring)*, Taipei (Taiwan), May. 16–19, 2010.

[80] T. Kolding, F. Frederiksen, and A. Pokhariyal, "Low-Bandwidth Channel Quality Indication for OFDMA Frequency Domain Packet Scheduling," in *Proc. of 3rd International Symposium on Wireless Communication Systems (ISWCS 2006)*, Valencia (Spain), Sep. 5–8, 2006.

[81] Y. Xue, C. Yin, G. Yue, and D. Liu, "A QoS-Aware Resource Allocation Scheme with Limited Feedback in Downlink OFDMA Systems," in *Proc. of 5rd International Conference on Wireless Communications, Networking and Mobile Computing (WiCOM 2009)*, Beijing (China), Sep. 24–26, 2009.

[82] S.-E. Elayoubi, B. Fourestie, and X. Auffret, "On the Capacity of OFDMA 802.16 Systems," in *Proc. of IEEE International Conference on Communications (ICC 2006)*, Istanbul (Turkey), Jun. 11–15, 2006.

[83] I. Koutsopoulos and L. Tassiulas, "Cross-Layer Adaptive Techniques for Throughput Enhancement in Wireless OFDM-Based Networks," *IEEE/ACM Transactions on Networking*, vol. 14, no. 5, pp. 1056–1066, Oct. 2006.

[84] M. Necker, "Integrated Scheduling and Interference Coordination in Cellular OFDMA Networks," in *Proc. of IEEE 4th International Conference on Broadband Communications, Networks and Systems (BROADNETS 2007)*, Raleigh (United States), Sep. 10–14, 2007.

[85] Q. D. La, Y. H. Chew, and B. H. Soong, "An Interference-Minimization Potential Game for OFDMA-Based Distributed Spectrum Sharing Systems," *IEEE Transactions on Vehicular Technology*, vol. 60, no. 7, pp. 3374–3385, Sep. 2011.

[86] Z. Han, Z. Ji, and K. Liu, "Fair Multiuser Channel Allocation for OFDMA Networks Using Nash Bargaining Solutions and Coalitions," *IEEE Transactions on Communications*, vol. 53, no. 8, pp. 1366–1376, Aug. 2005.

[87] Q. Ni and C. Zarakovitis, "Nash Bargaining Game Theoretic Scheduling for Joint Channel and Power Allocation in Cognitive Radio Systems," *IEEE Journal on Selected Areas in Communications*, vol. 30, no. 1, pp. 70–81, Jan. 2012.

[88] Y. Xing, C. N. Mathur, M. Haleem, R. Chandramouli, and K. Subbalakshmi, "Dynamic Spectrum Access with QoS and Interference Temperature Constraints," *IEEE Transactions on Mobile Computing*, vol. 6, no. 4, pp. 423–433, Apr. 2007.

[89] Y. Chen, K. H. Teo, S. Kishore, and J. Zhang, "Inter-Cell Interference Management in WiMAX Downlinks by A Stackelberg Game between BSs," in *Proc. of IEEE International Conference on Communications (ICC 2008)*, Beijing (China), May. 19–23, 2008.

[90] M. Rahman and H. Yanikomeroglu, "Inter-Cell Interference Coordination in OFDMA Networks: A Novel Approach Based on Integer Programming," in *Proc. of IEEE 71st Vehicular Technology Conference (VTC 2010 Spring)*, Taipei (Taiwan), May. 16–19, 2010.

[91] R. Combes, Z. Altman, M. Haddad, and E. Altman, "Self-Optimizing Strategies for Interference Coordination in OFDMA Networks," in *Proc. of IEEE International Conference on Communications (ICC 2011)*, Kyoto (Japan), Jun. 5–9, 2011.

[92] B. Krasniqi and C. Mecklenbrauker, "Maximization of the Minimum Rate by Geometric Programming for Multiple Users in Partial Frequency Reuse Cellular Networks," in *Proc. of IEEE 74th Vehicular Technology Conference (VTC 2011 Fall)*, San Francisco (United States), Sep. 5–8, 2011.

[93] T. Quek, Z. Lei, and S. Sun, "Adaptive Interference Coordination in Multi-Cell OFDMA Systems," in *Proc. of IEEE 20th International Symposium on Personal, Indoor and Mobile Radio Communications (PIMRC 2009)*, Tokyo (Japan), Sep. 13–16, 2009.

[94] M. Dirani and Z. Altman, "A cooperative Reinforcement Learning approach for Inter-Cell Interference Coordination in OFDMA Cellular Networks," in *Proc. of 8th International Symposium on Modeling and Optimization in Mobile, Ad Hoc, and Wireless Networks (WiOPT 2010)*, Avignon (France), May. 31–Jun. 4, 2010.

[95] P. Vlacheas, E. Thomatos, K. Tsagkaris, and P. Demestichas, "Autonomic Downlink Inter-cell Interference Coordination in LTE Self-Organizing Networks," in *Proc. of 7th International Conference on Network and Service Management (CNSM 2011)*, Paris (France), Oct. 24–28, 2011.

[96] M. Gary and D. Johnson, *Computers and Intractability: A Guide to the Theory of NP-completeness*. WH Freeman and Company, 1st ed., 1978.

[97] M. Duque-Anton, D. Kunz, and B. Ruber, "Channel assignment for cellular radio using simulated annealing," *IEEE Transactions on Vehicular Technology*, vol. 42, no. 1, pp. 14–21, Feb. 1993.

[98] S. Ghosh, B. Sinha, and N. Das, "Channel Assignment Using Genetic Algorithm based on Geometric Symmetry," *IEEE Transactions on Vehicular Technology*, vol. 52, no. 4, pp. 860–875, Jul. 2003.

[99] K. Smith and M. Palaniswami, "Static and Dynamic Channel Assignment Using Neural Networks," *IEEE Journal on Selected Areas in Communications*, vol. 15, no. 2, pp. 238–249, Apr. 1997.

[100] K. Son, S. Chong, and G. Veciana, "Dynamic Association for Load Balancing and Interference Avoidance in Multi-cell Networks," *IEEE Transactions on Wireless Communications*, vol. 8, no. 7, pp. 3566–3576, Jul. 2009.

[101] B. Krasniqi, M. Wrulich, and C. Mecklenbrauker, "Network-load dependent Partial Frequency Reuse for LTE," in *Proc. of 9th International Symposium on Communications and Information Technologies (ISCIT 2009)*, Incheon (Korea), Sep. 28–30, 2009.

[102] F. Bernardo, R. Agustí, J. Pérez-Romero, and O. Sallent, "Dynamic Spectrum Assignment in Multicell OFDMA Networks Enabling a Secondary Spectrum Usage," *IEEE Communications Magazine*, vol. 9, no. 11, pp. 1502–1519, Nov. 2009.

[103] A. Stolyar and H. Viswanathan, "Self-Organizing Dynamic Fractional Frequency Reuse in OFDMA Systems," in *Proc. of 27th Annual Joint Conference of the IEEE Computer and Communications Societies (INFOCOM 2008)*, Phoenix (United States), Apr. 13–18, 2008.

[104] K. Samdanis and A. Aghvami, "Load Balancing Through Dynamic Partitioning for Hierarchical Cellular Networks," in *St. Petersburg (Russia), Jun. 16–Jun. 19, 2008*, St. Petersburg (Russia), Jun. 16–Jun. 19, 2008.

[105] F. Xiangning, C. Si, and Z. Xiaodong, "An Inter-Cell Interference Coordination Technique Based on Users' Ratio and Multi-Level Frequency Allocations," in *Proc. of 3rd International Conference on Wireless Communications, Networking and Mobile Computing (WiCOM 2007)*, Shanghai (China), Sep. 21–23, 2007.

[106] L. Li, D. Liang, and W. Wang, "A Novel Semi-Dynamic Inter-Cell Interference Coordination Scheme Based on User Grouping," in *Proc. of IEEE 70th Vehicular Technology Conference (VTC 2009 Fall)*, Anchorage (United States), Sep. 20–23, 2009.

[107] S. Kumar, G. Monghal, J. Nin, I. Ordas, K. Pedersen, and P. Mogensen, "Autonomous Inter Cell Interference Avoidance under Fractional Load for Downlink Long Term Evolution," in *Proc. of IEEE 69th Vehicular Technology Conference (VTC 2009 Spring)*, Barcelona (Spain), Apr. 26–29, 2009.

[108] C. G. Gerlach, I. Karla, A. Weber, L. Ewe, H. Bakker, E. Kuehn, and A. Rao, "ICIC in DL and UL with network distributed and self‐organized resource assignment algorithms in LTE," *Bell Labs Technical Journal*, vol. 15, no. 3, pp. 43–62, Dec. 2010.

[109] D. Kimura, Y. Harada, and H. Seki, "Self-Optimizing Strategies for Interference Coordination in OFDMA Networks," in *Proc. of IEEE 73rd Vehicular*

Technology Conference (VTC 2011 Spring), Budapest (Hungary), May. 15–18, 2011.

[110] G. Li and H. Liu, "Downlink Radio Resource Allocation for Multi-Cell OFDMA System," *IEEE Transactions on Wireless Communications*, vol. 5, no. 12, pp. 3451–3459, Dec. 2006.

[111] A. B. Sediq, R. Schoenen, H. Yanikomeroglu, G. Senarath, and Z. Chao, "A Novel Distributed Inter-cell Interference Coordination Scheme based on Projected Subgradient and Network Flow Optimization," in *Proc. of IEEE 22nd International Symposium on Personal, Indoor and Mobile Radio Communications (PIMRC 2011)*, Toronto (Canada), Sep. 11–14, 2011.

[112] Z. Liang, Y. Chew, and C. C. Ko, "A Linear Programming Solution to Subcarrier, Bit and Power Allocation for Multicell OFDMA Systems," Las Vegas (United States), Mar. 31–Apr. 3, 2008.

[113] R. Chang, Z. Tao, J. Zhang, and C.-C. Kuo, "Multicell OFDMA Downlink Resource Allocation Using a Graphic Framework," *IEEE Transactions on Vehicular Technology*, vol. 58, no. 7, pp. 3494–3507, Sep. 2009.

[114] J. Ellenbeck, C. Hartmann, and L. Berlemann, "Decentralized Inter-cell Interference Coordination by Autonomous Spectral Reuse Decisions," in *Proc. of 14th European Wireless Conference (EW 2008)*, Prague (Czech Republic), Jun. 22–25, 2008.

[115] Z. Shen, J. Andrews, and B. Evans, "Optimal Power Allocation in Multiuser OFDM Systems," in *Proc. of IEEE Global Telecommunications Conference (GLOBECOM 2003)*, San Francisco (United States), Dec. 1–5, 2003.

[116] A. Gjendemsjo, D. Gesbert, G. Oien, and S. Kiani, "Optimal Power Allocation and Scheduling for Two-Cell Capacity Maximization," in *Proc. of 4th International Symposium on Modeling and Optimization in Mobile, Ad Hoc, and Wireless Networks (WiOPT 2006)*, Boston (United States), Apr. 3–6, 2006.

[117] M. Boghe, J. Gross, and A. Wolisz, "Optimal Power Masking in Soft Frequency Reuse Based OFDMA Networks," in *Proc. of 15th European Wireless Conference (EW 2009)*, Aalborg (Denmark), May. 17–20, 2009.

[118] M. C. Necker, "A Novel Algorithm for Distributed Dynamic Interference Coordination in Cellular Networks," *PIK-Praxis der Informationsverarbeitung und Kommunikation*, vol. 34, no. 2, pp. 97–101, Dec. 2011.

[119] K. Son, S. Lee, Y. Yi, and S. Chong, "Practical Dynamic Interference Management in Multi-Carrier Multi-Cell Wireless Networks: A Reference User Based Approach," in *Proc. of 8th International Symposium on Modeling and Optimization in Mobile, Ad Hoc, and Wireless Networks (WiOPT 2010)*, Avignon (France), May. 31–Jun. 4, 2010.

[120] D. Kun, T. Hui, L. Xingmin, , and S. Qiaoyun, "A Distributed Inter-Cell Interference Coordination Scheme in Downlink Multicell OFDMA Systems," in *Proc. of IEEE 7th IEEE Consumer Communications and Networking Conference (CCNC 2010)*, Las Vegas (United States), Jan. 9–12, 2010.

[121] I. Fraimis, V. Papoutsis, and S. Kotsopoulos, "A Distributed Radio Resource Allocation Algorithm with Interference Coordination for Multi-cell OFDMA Systems," in *Proc. of IEEE 21st International Symposium on Personal, Indoor and Mobile Radio Communications (PIMRC 2010)*, Istanbul (Turkey), Sep. 26–29, 2010.

[122] S. Ko, H. Seo, H. Kwon, and B. G. Lee, "Distributed Power Allocation for Efficient Inter-cell Interference Management in Multi-cell OFDMA Systems," in *Proc. of 16th Asia-Pacific Conference on Communications (APCC 2010)*, Auckland (New Zealand), Oct. 31–Nov. 3, 2010.

[123] Q. La, Y. Chew, and B.-H. Soong, "An Interference Minimization Game Theoretic Subcarrier Allocation Algorithm for OFDMA-Based Distributed Systems," in *Proc. of IEEE Global Telecommunications Conference (GLOBECOM 2009)*, Hawaii (United States), Nov. 30–Dec. 4, 2009.

[124] H. G. Myung, J. Lim, and D. J. Goodman, "Single Carrier FDMA for Uplink Wireless Transmission," *IEEE Vehicular Technology Magazine*, vol. 1, no. 3, pp. 30–38, Sep. 2006.

[125] Z. Meng and W. Jiang, "A Novel Uplink Inter-Cell Interference Management Method for TD-LTE System," *China Communications*, vol. 8, no. 2, pp. 173–180, Mar. 2011.

[126] A. Simonsson and A. Furuskar, "Uplink Power Control in LTE - Overview and Performance," in *Proc. of IEEE 68th Vehicular Technology Conference (VTC 2008 Fall)*, Calgary (Canada), Sep. 21–24, 2008.

[127] M. Lema, M. García-Lozano, S. Ruiz, and J. Olmos, "On the Performance of LTE UL Power Control in Realistic Conditions," *Lecture Notes of the Institute for Computer Sciences, Social-Informatics and Telecommunications Engineering (LNICST)*, vol. 58, pp. 142–155, Sep. 2012.

[128] R. Madan and S. Ray, "Uplink Resource Allocation for Frequency Selective Channels and Fractional Power Control in LTE," in *Proc. of IEEE International Conference on Communications (ICC 2011)*, Kyoto (Japan), Jun. 5–9, 2011.

[129] P. Hosein, "Uplink power control and interference management for the support of QoS applications," in *Proc. of IEEE 21st International Symposium on Personal, Indoor and Mobile Radio Communications (PIMRC 2010)*, Istanbul (Turkey), Sep. 26–29, 2010.

[130] B. Muhammad and A. Mohammed, "Uplink Closed Loop Power Control for LTE System," in *Proc. of 6th International Conference on Emerging Technologies (ICET 2010)*, Islamabad (Pakistan), Oct. 18–19, 2010.

[131] M. Porjazoski and B. Popovski, "Impact of Fractional Frequency Reuse on LTE Performances in Uplink," in *Proc. of IEEE 26th Convention of Electrical and Electronics Engineers in Israel (IEEEI 2010)*, Eilat (Israel), Nov. 17–20, 2010.

[132] A. Mahmud and K. Hamdi, "Uplink Analysis for FFR and SFR in Composite Fading," in *Proc. of IEEE 23rd International Symposium on Personal, Indoor and Mobile Radio Communications (PIMRC 2012)*, Sydney (Australia), Sep. 9–12, 2012.

[133] B. Rengarajan, A. Stolyar, and H. Viswanathan, "Self-organizing Dynamic Fractional Frequency Reuse on the Uplink of OFDMA Systems," in *Proc. of 44th Annual Conference on Information Sciences and Systems (CISS 2010)*, Princeton (United States), Mar. 17–19, 2010.

[134] S. Sun, Q. Gao, Y. Peng, Y. Wang, and L. Song, "Interference Management Through CoMP in 3GPP LTE-Advanced Networks," *IEEE Wireless Communications*, vol. 20, no. 1, pp. 59–66, Feb. 2013.

[135] Y. Liu and P. Chen, "Joint Scheduling for MU-CoMP in Uplink LTE-advanced Systems," in *Proc. of IEEE 14th International Conference on Communication Technology (ICCT 2012)*, Chengdu (China), Oct. 19–21, 2012.

[136] S. Yang, Q. Cui, X. Huang, and X. Tao, "An Effective Uplink Power Control Scheme in CoMP Systems," in *Proc. of IEEE 72nd Vehicular Technology Conference (VTC 2010 Fall)*, Ottawa (Canada), Sep. 6–9, 2010.

[137] D. Jiang, Q. Wang, J. Liu, G. Liu, and C. Cui, "Uplink Coordinated Multi-Point Reception for LTE-Advanced Systems," in *Proc. of 5rd International Conference on Wireless Communications, Networking and Mobile Computing (WiCOM 2009)*, Beijing (China), Sep. 24–26, 2009.

[138] T. Novlan and J. Andrews, "Analytical Evaluation of Uplink Fractional Frequency Reuse," *IEEE Transactions on Wireless Communications*, vol. 61, no. 5, pp. 2098–2108, May. 2011.

[139] A. Damnjanovic, J. Montojo, Y. Wei, T. Ji, T. Luo, M. Vajapeyam, T. Yoo, O. Song, and D. Malladi, "A Survey on 3GPP Heterogeneous Networks," *IEEE Wireless Communications*, vol. 18, no. 3, pp. 10–21, Jun. 2011.

[140] S. Vasudevan, R. Pupala, and K. Sivanesan, "Dynamic eICIC - A Proactive Strategy for Improving Spectral Efficiencies of Heterogeneous LTE Cellular Networks by Leveraging User Mobility and Traffic Dynamics," *IEEE Transactions on Wireless Communications*, vol. PP, no. 99, pp. 1–14, Jun. 2013.

[141] S. Deb, P. Monogioudis, J. Miernik, and J. Seymour, "Algorithms for Enhanced Inter-Cell Interference Coordination (eICIC) in LTE HetNets," *IEEE/ACM Transactions on Networking*, vol. PP, no. 99, pp. 1–14, Jan. 2013.

[142] M. Y. Umair, D. Xiao, Y. Dongkai, and F. Fanny, "Identification of Interferers in Het-Net in LTE-A Systems Based on FeICIC with Cell Range Expansion," in *Proc. of International Conference of Information and Communication Technology (ICoICT 2013)*, Bandung (Indonesia), Mar. 20–22, 2013.

[143] E. Makled, A. Ibrahim, A. Darwish, and H. Elgebaly, "Non-Unanimous Power Inter-Cell Interference Coordination in Heterogeneous Networks," in *Proc. of IEEE 75th Vehicular Technology Conference (VTC 2012 Spring)*, Yokohama (Japan), May. 6–9, 2012.

[144] N. Saquib, E. Hossain, and D. I. Kim, "Fractional Frequency Reuse for Interference Management in LTE-Advanced Hetnets," *IEEE Wireless Communications*, vol. 20, no. 2, pp. 113–122, Apr. 2013.

[145] A. Latrach, R. Nasri, and S. Affes, "Downlink Interference Cancellation Strategy for Shared-Spectrum LTE HetNet," in *Proc. of 9th Wireless Communications and Mobile Computing Conference (IWCMC 2013)*, Cagiari (Italy), Jul. 1–5, 2013.

[146] M. Iwamura, K. Etemad, M.-H. Fong, R. Nory, and R. Love, "Carrier Aggregation Framework in 3GPP LTE-Advanced," *IEEE Communications Magazine*, vol. 48, no. 8, pp. 60–67, Jun. 2010.

[147] Y. Yan, A. Li, A. Harada, and H. Kayama, "Enhanced Downlink Control Channel Resource Allocation Algorithm for Cross-Carrier Scheduling in LTE-Advanced Carrier Aggregation System," in *Proc. of IEEE 73rd Vehicular Technology Conference (VTC 2011 Spring)*, Budapest (Hungary), May. 15–18, 2011.

[148] C. Sun, J. Jiang, L. Huang, and G. Lu, "Component Carrier Selection and Interference Coordination for Carrier Aggregation System in Heterogeneous Networks," in *Proc. of IEEE 14th International Conference on Communication Technology (ICCT 2012)*, Chengdu (China), Oct. 19–21, 2012.

[149] K. Zheng, F. Hu, L. Lei, and W. Wang, "Interference Coordination Between Femtocells in LTE-Advanced Networks with Carrier Aggregation," in *Proc. of 5th International ICST Conference on Communications and Networking in China (CHINACOM 2010)*, Beijing (China), Aug. 25–27, 2010.

[150] I. Hwang, B. Song, and S. Soliman, "A Holistic View on Hyper-dense Heterogeneous and Small Cell Networks," *IEEE Communications Magazine*, vol. 51, no. 6, pp. 20–27, Jun. 2013.

[151] C. Jiming, W. Peng, and Z. Jie, "Adaptive Soft Frequency Reuse Scheme for In-building Dense Femtocell Networks," *China Communications*, vol. 10, no. 1, pp. 44–55, Jan. 2013.

[152] K. Balachandran, J. Kang, K. Karakayali, and K. Rege, "Cell Selection with Downlink Resource Partitioning in Heterogeneous Networks," in *Proc. of IEEE International Conference on Communications (ICC 2011)*, Kyoto (Japan), Jun. 5–9, 2011.

[153] V. Capdevielle, A. Feki, and E. Sorsy, "Joint Interference Management and Handover Optimization in LTE Small Cells Network," in *Proc. of IEEE International Conference on Communications (ICC 2012)*, Ottawa (Canada), Jun. 10–15, 2012.

[154] J. Hoydis, S. ten Brink, and M. Debbah, "Massive MIMO in the UL/DL of Cellular Networks: How Many Antennas Do We Need?," *IEEE Journal on Selected Areas in Communications*, vol. 31, no. 2, pp. 160–171, Feb. 2013.

[155] O. Aliu, A. Imran, M. Imran, and B. Evans, "A Survey of Self Organisation in Future Cellular Networks," *IEEE Communication Surveys & Tutorials*, vol. 15, no. 1, pp. 336–361, Feb. 2012.

[156] F. Dominique, C. G. Gerlach, N. Gopalakrishnan, A. Rao, J. P. Seymour, R. Soni, A. Stolyar, H. Viswanathan, C. Weaver, and A. Weber, "Self-Organizing Interference Management for LTE," *Bell Labs Technical Journal*, vol. 15, no. 3, pp. 19–42, Dec. 2010.

[157] H. Sidi, R. El-Azouzi, and M. Haddad, "Fractional Frequency Reuse Stackelberg Model for Self-Organizing Networks," in *Proc. of IFIP Wireless Days (WD 2011)*, Niagara Falls (Canada), Oct. 10–12, 2011.

[158] S. Sesia, I. Toufik, and M. Baker, *The UMTS Long Term Evolution: From Theory to Practice*. John Wiley & Sons, 2nd ed., 2011.

[159] *TS 36.201 (Release 8) - LTE Physical Layer - General Description*. 3GPP Technical Specification. Available online at: www.3gpp.org.

[160] *TS 36.300 (Release 8) - Evolved Universal Terrestrial Radio Access (E-UTRA) and Evolved Universal Terrestrial Radio Access Network (E-UTRAN) - Overall Description*. 3GPP Technical Specification. Available online at: www.3gpp.org.

[161] *TS 36.211 (Release 8) - Physical Channels and Modulation*. 3GPP Technical Specification. Available online at: www.3gpp.org.

[162] *TS 36.213 (Release 8) - Physical Layer Procedures*. 3GPP Technical Specification. Available online at: www.3gpp.org.

[163] *TS 36.420 (Release 9) - X2 General Aspects and Principles*. 3GPP Technical Specification. Available online at: www.3gpp.org.

[164] *TS 36.423 (Release 9) - X2 Application Protocol (X2AP)*. 3GPP Technical Specification. Available online at: www.3gpp.org.

[165] J. Puttonen, H.-H. Puupponen, K. Aho, T. Henttonen, and M. Moisio, "Impact of Control Channel Limitations on the LTE VoIP Capacity," in *Proc. of 9th International Conference on Networks (ICN 2010)*, Nanjing (French Alps), Apr. 11–16, 2010.

[166] *TS 36.211 (Release 11) - Physical Channels and Modulation*. 3GPP Technical Specification. Available online at: www.3gpp.org.

[167] J. G. Andrews, F. Baccelli, and R. K. Ganti, "A New Tractable Model for Cellular Coverage," in *Proc. of 48th Annual Allerton Conference on Communication, Control, and Computing*, Illinois (United States), Sep. 29–Oct. 1, 2010.

[168] J.-M. Kelif and E. Alman, "Downlink Fluid Model of CDMA Networks," in *Proc. of IEEE 61st Vehicular Technology Conference (VTC 2005 Spring)*, Stockholm (Sweden), May. 30–Jun. 1, 2005.

[169] J.-M. Kelif, M. Coupechoux, and P. Godlewski, "Effect of Shadowing on Outage Probability in Fluid Cellular Radio Networks," in *Proc. of 6th International Symposium on Modeling and Optimization in Mobile, Ad Hoc, and Wireless Networks (WiOPT 2008)*, Berlin (Germany), Mar. 31–Apr. 4, 2008.

[170] H. ElSawy, E. Hossain, and M. Haenggi, "Stochastic Geometry for Modeling, Analysis, and Design of Multi-Tier and Cognitive Cellular Wireless Networks: A Survey," *IEEE Communication Surveys & Tutorials*, vol. 15, no. 3, pp. 996–1019, Jun. 2013.

[171] M. Haenggi, J. Andrews, F. Baccelli, O. Dousse, and M. Franceschetti, "Stochastic Geometry and Random Graphs for the Analysis and Design of Wireless Networks," *IEEE Journal on Selected Areas in Communications*, vol. 27, no. 7, pp. 1029–1046, Sep. 2009.

[172] R. Jain, *The Art of Computer Systems Performance Analysis*. John Wiley & Sons, 1st ed., 1991.

[173] Correia, Luis M. *et al.*, *Identification of Relevant Parameters for Traffic Modelling and Interference Estimation*. Information Society Technologies (IST), Nov. 2001. Tech. Rep. available as IST-2000-28088-MOMENTUM-D21-PUB.

[174] IEEE 802.16 Broadband Wireless Access Working Group, *Link Performance Abstraction for ML Receivers based on RBIR Metrics*. IEEE, 2008. Technical Report C802.16m-08/119. Available online at: www.ieee802.org.

[175] Radiocommunication Sector, *Guidelines for Evaluation of Radio Interface Technologies for IMT-Advanced*. ITU, 2008. Technical Report ITU-R M.2135.

[176] Wireless World Initiative New Radio (WINNER+), *Calibration for IMT-Advanced Evaluations*, 2010. Public document, Project number: CELTIC/CP5-026.

[177] K. Brueninghaus, D. Astely, T. Salzer, S. Visuri, A. Alexiou, S. Karger, and G.-A. Seraji, "Link Performance Models for System Level Simulations of Broadband Radio Access Systems," in *Proc. of IEEE 16th International Symposium on Personal, Indoor and Mobile Radio Communications (PIMRC 2005)*, Berlin (Germany), Sep. 11–14, 2005.

[178] T. Sorensen, P. Mogensen, and F. Frederiksen, "Extension of the ITU Channel Models for Wideband (OFDM) Systems," in *Proc. of IEEE 62th Vehicular Technology Conference (VTC 2005 Fall)*, Dallas (United States), Sep. 25–28, 2005.

[179] J. Olmos, A. Serra, S. Ruiz, M. García-Lozano, and D. González G, "Exponential Effective SIR Metric for LTE Downlink," in *Proc. of IEEE 20th International Symposium on Personal, Indoor and Mobile Radio Communications (PIMRC 2009)*, Tokyo (Japan), Sep. 13–16, 2009.

[180] D. Tse and P. Viswanath, *Fundamentals of Wireless Communication*. Cambridge University Press, 1st ed., 2005.

[181] M. Agarwal, D. Guo, and M. Honig, "Limited-Rate Channel State Feedback for Multicarrier Block Fading Channels," *IEEE Transactions on Information Theory*, vol. 56, no. 12, pp. 6116–6132, Dec. 2010.

[182] Qualcomm Europe, *R1-072731: Scheduling Requests Using CQI*. 3GPP, Jun 2007. Radio Access Network (RAN) Working Group 1, Meeting #49bis: Orlando, USA.

[183] Alcatel-Lucent, *R1-072924: Incremental CQI Feedback Scheme and Simulation Results*. 3GPP, Jun 2007. Radio Access Network (RAN) Working Group 1, Meeting #49bis: Orlando, USA.

[184] Nokia Siemens Networks, *R1-073662: CQI per PRB versus per Group of Best PRBs*. 3GPP, Aug 2007. Radio Access Network (RAN) Working Group 1, Meeting #50: Athens, Greece.

[185] Texas Instruments, *R1-080207: CQI Reporting Procedure for E-UTRA*. 3GPP, Jan 2008. Radio Access Network (RAN) Working Group 1, Meeting #51bis: Sevilla, Spain.

[186] Texas Instruments, *R1-080208: Differential CQI Definition for E-UTRA*. 3GPP, Jan 2008. Radio Access Network (RAN) Working Group 1, Meeting #51bis: Sevilla, Spain.

[187] Ericsson, *R1-080887: CQI Measurement Methodology*. 3GPP, Feb 2008. Radio Access Network (RAN) Working Group 1, Meeting #52: Sorrento, Italy.

[188] Panasonic, *R1-090250: HARQ Protocol Handling of CQI-only Reports*. 3GPP, Jan 2009. Radio Access Network (RAN) Working Group 1, Meeting #55bis: Ljubljana, Slovenia.

[189] NEC Group, *R1-090303: Correction to rhoA Definition for CQI Calculation*. 3GPP, Jan 2009. Radio Access Network (RAN) Working Group 1, Meeting #55bis: Ljubljana, Slovenia.

[190] Alcatel-Lucent, *R1-090394: CQI and CSI Feedback Compression*. 3GPP, Jan 2009. Radio Access Network (RAN) Working Group 1, Meeting #55bis: Ljubljana, Slovenia.

[191] Sharp, *R1-092103: Control Overhead Analysis on Aperiodic PUSCH*. 3GPP, May 2009. Radio Access Network (RAN) Working Group 1, Meeting #57: San Francisco, CA, United States.

[192] Panasonic, HTC, *R1-101262: Aperiodic CQI Reporting for Carrier Aggregation*. 3GPP, Feb 2010. Radio Access Network (RAN) Working Group 1, Meeting #60: San Francisco, CA, United States.

[193] Samsung, *R1-102186: Aperiodic CQI Activation in CA*. 3GPP, Apr 2010. Radio Access Network (RAN) Working Group 1, Meeting #60bis: Beijing, China.

[194] Samsung, *R1-103187: LTE-A Dynamic Aperiodic SRS - Triggering, Duration, Timing, and Carrier Aggregation*. 3GPP, Apr 2010. Radio Access Network (RAN) Working Group 1, Meeting #61: Montreal, Canada.

[195] Panasonic, HTC Corporation, *R1-103761: Aperiodic CQI Reporting for Carrier Aggregation*. 3GPP, Jul 2010. Radio Access Network (RAN) Working Group 1, Meeting #61bis: Dresden, Germany.

[196] Huawei, *R1-110015: Remaining Issues in Aperiodic CQI-only PUSCH*. 3GPP, Jan 2011. Radio Access Network (RAN) Working Group 1, Meeting #63bis: Dublin, Ireland.

[197] Huawei, HiSilicon, *R1-110021: Open Issues for Aperiodic and Periodic CSI Reporting*. 3GPP, Jan 2011. Radio Access Network (RAN) Working Group 1, Meeting #63bis: Dublin, Ireland.

[198] Samsung, *R1-110078: Simultaneous PUSCH and PUCCH Transmissions in case of Aperiodic CSI*. 3GPP, Jan 2011. Radio Access Network (RAN) Working Group 1, Meeting #63bis: Dublin, Ireland.

[199] HTC, *R1-122323: CQI Definition and Feedback Reduction Mechanism for CoMP*. 3GPP, May 2012. Radio Access Network (RAN) Working Group 1, Meeting #69: Prague, Czech Republic.

[200] HTC, *R1-122628: Periodic and Aperiodic CSI Feedback Modes for DL CoMP*. 3GPP, May 2012. Radio Access Network (RAN) Working Group 1, Meeting #69: Prague, Czech Republic.

[201] Hitachi Ltd, *R1-122699: CQI Estimation for CoMP*. 3GPP, May 2012. Radio Access Network (RAN) Working Group 1, Meeting #69: Prague, Czech Republic.

[202] Qualcomm, *R1-122777: CQI definition for downlink CoMP*. 3GPP, May 2012. Radio Access Network (RAN) Working Group 1, Meeting #69: Prague, Czech Republic.

[203] S. Donthi and N. Mehta, "Joint Performance Analysis of Channel Quality Indicator Feedback Schemes and Frequency-Domain Scheduling for LTE," *IEEE Transactions on Vehicular Technology*, vol. 60, no. 7, pp. 3096–3109, Sep. 2011.

[204] S.-H. Hur and B. Rao, "Sum Rate Analysis of a Reduced Feedback OFDMA Downlink System Employing Joint Scheduling and Diversity," *IEEE Transactions on Signal Processing*, vol. 60, no. 2, pp. 862–876, Feb. 2012.

[205] N. Varanese, J. Vicario, and U. Spagnolini, "On the Asymptotic Throughput of OFDMA Systems with Best-M CQI Feedback," *IEEE Communication Letters*, vol. 1, no. 3, pp. 145–148, Jun. 2012.

[206] Jian Su and Bin Fan and Kan Zheng and Wenbo Wang, "A Hierarchical Selective CQI Feedback Scheme for 3GPP Long-Term Evolution System," in *Proc. of IEEE International Symposium on Microwave, Antenna, Propagation and EMC Technologies for Wireless Communications (MAPE 2007)*, Hangzhou (China), Aug. 16–17, 2007.

[207] Motorola, *R1-051334: CQI Feedback Scheme for EUTRA*. 3GPP, Nov 2005. Radio Access Network (RAN) Working Group 1, Meeting #43: Seoul, Korea.

[208] M. Mecking, "Resource Allocation for Fading Multiple-Access Channels with Partial Channel State Information," in *Proc. of IEEE International Conference on Communications (ICC 2002)*, New York (United States), Apr. 28–May. 2, 2002.

[209] M. Ouyang and L. Ying, "On Scheduling in Multi-channel Wireless Downlink Networks with Limited Feedback," in *Proc. of 47th Annual Allerton Conference on Communication, Control, and Computing*, Illinois (United States), Sep. 30–Oct. 2, 2009.

[210] H. Ganapathy and C. Caramanis, "Queue-based Sub-carrier Grouping for Feedback Reduction in OFDMA Systems," in *Proc. of 31th Annual Joint Conference of the IEEE Computer and Communications Societies (INFOCOM 2012)*, Orlando (United States), Mar. 25–30, 2012.

[211] J. Chen, R. Berry, and M. Honig, "Limited Feedback Schemes for Downlink OFDMA Based on Sub-channel Groups," *IEEE Journal on Selected Areas in Communications*, vol. 26, no. 8, pp. 1451–1461, Oct. 2008.

[212] R. Agarwal, V. Majjigi, Z. Han, R. Vannithamby, and J. Cioffi, "Low Complexity Resource Allocation with Opportunistic Feedback over Downlink OFDMA Networks," *IEEE Journal on Selected Areas in Communications*, vol. 26, no. 8, pp. 1462–1472, Oct. 2008.

[213] Y.-J. Choi and S. Bahk, "Partial Channel Feedback Schemes Maximizing Overall Efficiency in Wireless Networks," *IEEE Transactions on Wireless Communications*, vol. 7, no. 4, pp. 1306–1314, Apr. 2008.

[214] A. Gopalan, C. Caramanis, and S. Shakkottai, "On Wireless Scheduling With Partial Channel-State Information," *IEEE Transactions on Information Theory*, vol. 58, no. 1, pp. 403–420, Jan. 2012.

[215] F. R. Marques, S. Wänstedt, F. R. Porto, and W. C. Freitas, "Scheduling for Improving System Capacity in Multiservice 3GPP LTE," *Journal of Electrical and Computer Engineering*, vol. 2010, no. 819729, pp. 1–16, Jun. 2010.

[216] A. Furuskär and J. Zander, "Multiservice Allocation for Multiaccess Wireless Systems," *IEEE Transactions on Wireless Communications*, vol. 4, no. 1, pp. 174–184, Jan. 2005.

[217] *TS 36.331 (Release 8) - Radio Resource Control (RRC) Protocol Specification*. 3GPP Technical Specification. Available online at: www.3gpp.org.

[218] Michael Pilegaard Hansen, *Metaheuristics for Multiple Objective Combinatorial Optimization*. PhD thesis, Technical University of Denmark, Mar 1998.

[219] Y. Sawaragi, I. Hirotaka, and T. Tanino, *Theory of Multiobjective Optimization*. Academic Press, Inc., 1st ed., 1985.

[220] T. Weise, *Global Optimization Algorithms - Theory and Application*. Self-published, 2nd ed., 2009. Online available at http://www.it-weise.de/.

[221] S. Finch, *Transitive Relations, Topologies and Partial Orders*, Jun. 2003. Tech. Rep. available online at http://algo.inria.fr/csolve/posets.pdf.

[222] B. R. Jones, W. A. Crossley, and A. S. Lyrintzis, "Aerodynamic and Aeroacoustic Optimization of Rotorcraft Airfoils via a Parallel Genetic Algorithm," *Journal of Aircraft*, vol. 37, no. 6, pp. 1088–1096, Nov. 2000.

[223] M. P. Fourman, "Compaction of Symbolic Layout Using Genetic Algorithms," in *Proc. of the 1st International Conference on Genetic Algorithms*, Pittsburgh (United States), Jul. 24-26, 1985.

[224] P. E. Gill and E. Wong, *Sequential Quadratic Programming Methods*. Department of Mathematics, University of California, Aug. 2010. Tech. Rep. NA-10-03.

[225] C. A. Coello, G. B. Lamont, and D. A. Van Veldhuizen, *Evolutionary Algorithms for Solving Multi-Objective Problems*. Springer: Genetic and Evolutionary Computation Series, 2nd ed., 2007.

[226] K. Deb, A. Pratap, S. Agarwal, and T. Meyarivan, "A Fast and Elitist Multiobjective Genetic Algorithm: NSGA-II," *IEEE Transactions on Evolutionary Computation*, vol. 6, no. 2, pp. 182–197, Apr. 2002.

[227] E. Zitzler, M. Laumanns, and L. Thiele, *SPEA2: Improving the Strength Pareto Evolutionary Algorithm*. Swiss Federal Institute of Technology (ETH) Zurich, May. 2001. Tech. Rep. TIK-Report 103.

[228] E. Zitzler, K. Deb, and L. Thiele, "Comparison of Multiobjective Evolutionary Algorithms: Empirical Results," *Evolutionary Computation*, vol. 8, no. 2, pp. 173–195, Mar. 2000.

[229] T. Sen, F. M. Raiszadeh, and P. Dileepan, "A Branch-and-Bound Approach to the Bicriterion Scheduling Problem Involving Total Flowtime and Range of Lateness," *Management Science*, vol. 34, no. 2, pp. 254–260, Feb. 1988.

[230] R. L. Carraway, T. L. Morin, and H. Moskowitz, "Generalized Dynamic Programming for Multicriteria Optimization," *European Journal of Operational Research*, vol. 44, no. 1, pp. 95–104, Jan. 1990.

[231] F. Glover and M. Laguna, *Tabu Search*. Kluwer, 1st ed., 1997.

[232] S. Kirkpatrick, D. G. Jr., and M. P. Vecchi, "Optimization by Simmulated Annealing," *Science*, vol. 220, no. 4598, pp. 671–680, May. 1983.

[233] R. Poli, J. Kennedy, and T. Blackwell, "Particle Swarm Optimization," *Swarm Intelligence*, vol. 1, no. 1, pp. 33–57, Jun. 2007.

[234] T. Parks, A. Suppapitnarn, K. A. Seffen, and P. J. Clarkson, "A Simulated Annealing Algorithm for Multiobjective Optimization," *Engineering Optimization*, vol. 33, no. 1, pp. 59–85, Jan. 2000.

[235] X. Yu and M. Gen, *Introduction to Evolutionary Algorithms*. Springer, 1st ed., 2010.

[236] E. Zitzler and L. Thiele, "Multiobjective Optimization Using Evolutionary Algorithms - A Comparative Case Study," in *Proc. of 5th International Conference on Parallel Problem Solving from Nature PPSN (PPSN V)*, Amsterdam (The Netherlands), Sep. 27-30, 1998.

[237] Q. Yang and S. Ding, "Novel Algorithm to Calculate Hypervolume Indicator of Pareto Approximation Set," *Advanced Intelligent Computing Theories and Applications*, vol. 2, no. 99, pp. 235–244, Jan. 2007.

[238] R. M. Solovay, "A Model of Set-theory in which Every Set of Reals is Lebesgue Measurable," *The Annals of Mathematics*, vol. 92, no. 1, pp. 1–56, Jul. 1970.

[239] M. Fleischer, "The Measure of Pareto Optima Applications to Multi-objective Metaheuristics," in *Proc. of 2nd International Conference on Evolutionary Multi-Criterion Optimization (EMO 2003)*, Faro (Portugal), Apr. 8-11, 2003.

[240] J. C. Spall, *Introduction to Stochastic Search and Optimization*. Wiley-Interscience, 1st ed., 2003.

[241] H.-G. Beyer and K. Deb, "On Self-adaptive Features in Real-parameter Evolutionary Algorithms," *IEEE Transactions on Evolutionary Computation*, vol. 5, no. 3, pp. 250–270, Jun. 2001.

[242] K. Deb and R. B. Agrawal, "Simulated Binary Crossover for Continuous Search Space," *Complex Systems*, vol. 9, no. 1, pp. 115–148, Jan. 1995.

[243] N. Srinivas and K. Deb, "Multiobjective Optimization using Nondominated Sorting in Genetic Algorithms," *Evolutionary Computation*, vol. 2, no. 3, pp. 221–248, Oct. 1994.

[244] E. Zitzler and L. Thiele, *An Evolutionary Algorithm for Multiobjective Optimization: The Strength Pareto Approach*. Swiss Federal Institute of Technology (ETH) Zurich, May. 1998. Tech. Rep. TIK-Report 43.

[245] K. Dehnad, "Density Estimation for Statistics and Data Analysis," *Technometrics*, vol. 29, no. 4, pp. 495–495, Nov. 1987.

[246] T. Chen, Y. Yang, H. Zhang, H. Kim, and K. Horneman, "Network Energy Saving Technologies for Green Wireless Access Networks," *IEEE Wireless Communications*, vol. 18, no. 5, pp. 30–38, Oct. 2011.

[247] T. Han and N. Ansari, "On Greening Cellular Networks via Multicell Cooperation," *IEEE Wireless Communications*, vol. 20, no. 1, pp. 82–89, Feb. 2013.

[248] Z. Hasan, H. Boostanimehr, and V. Bhargava, "Green Cellular Networks: A Survey, Some Research Issues and Challenges," *IEEE Communication Surveys & Tutorials*, vol. 13, no. 4, pp. 524–540, Nov. 2011.

[249] L. Correia, D. Zeller, O. Blume, D. Ferling, Y. Jading, I. Godor, G. Auer, and L. Van Der Perre, "Challenges and Enabling Technologies for Energy Aware Mobile Radio Networks," *IEEE Communications Magazine*, vol. 48, no. 11, pp. 66–72, Nov. 2010.

[250] Y. Xiang, J. Luo, and C. Hartmann, "Inter-cell Interference Mitigation Through Flexible Resource Reuse in OFDMA Based Communication Networks," in *Proc. of 13th European Wireless Conference (EW 2007)*, Paris (France), Apr. 1–4, 2007.

[251] I. Fraimis, V. Papoutsis, and S. Kotsopoulos, "A Decentralized Subchannel Allocation Scheme with Inter-Cell Interference Coordination (ICIC) for Multi-Cell OFDMA Systems," in *Proc. of IEEE Global Telecommunications Conference (GLOBECOM 2010)*, Miami (United States), Dec. 6–10, 2010.

[252] V. Zakian, "New Formulation for the Method of Inequalities," *Proc. of the Institution of Electrical Engineers*, vol. 126, no. 6, pp. 579–584, Jun. 1979.

[253] G. Scutari, D. Palomar, F. Facchinei, and J. shi Pang, "Convex Optimization, Game Theory, and Variational Inequality Theory," *IEEE Signal Processing Magazine*, vol. 27, no. 3, Mar. 2010.

[254] F. Fidler and G. R. Loftus, "Why Figures with Error Bars Should Replace p Values," *Journal of Psychology*, vol. 17, no. 1, pp. 27–37, Jun. 2009.

[255] H. B. Mann and D. R. Whitney, "On a Test of Whether one of Two Random Variables is Stochastically Larger than the Other," *The Annals of Mathematical Statistics*, vol. 18, no. 1, pp. 50–60, Mar. 1947.

[256] S. Shapiro and M. Wilk, "An Analysis of Variance Test for Normality (Complete Samples)," *Biometrika*, vol. 52, no. 3-4, pp. 591–611, Dec. 1965.

[257] H. Lilliefors, "On the Kolmogorov-Smirnov Test for Normality with Mean and Variance Unknown," *Journal of the American Statistical Association*, vol. 62, no. 318, pp. 399–402, Jun. 1967.

[258] F. Capozzi, D. Laselva, F. Frederiksen, J. Wigard, I. Kovacs, and P. Mogensen, "UTRAN LTE Downlink System Performance under Realistic Control Channel Constraints," in *Proc. of IEEE 70th Vehicular Technology Conference (VTC 2009 Fall)*, Anchorage (United States), Sep. 20–23, 2009.

[259] Y. Fan and M. Valkama, "Efficient Control Channel Resource Allocation for VoIP in OFDMA-Based Packet Radio Networks," *EURASIP Journal on Wireless Communications and Networking*, vol. 2011, no. 1, pp. 1–12, Feb. 2011.

[260] Y. Chen, "Resource Allocation for Downlink Control Channel in LTE Systems," in *Proc. of 7th International Conference on Wireless Communications, Networking and Mobile Computing (WiCOM 2011)*, Wuhan (China), Sep. 23–25, 2011.

[261] *TS 36.213 (Release 11) - Physical Layer Procedures*. 3GPP Technical Specification. Available online at: www.3gpp.org.

[262] *TS 22.146 (Release 8) - Multimedia Broadcast/Multicast Service*. 3GPP Technical Specification. Available online at: www.3gpp.org.

[263] M. Einhaus, C. Wengerter, J. Ohlhorst, and S. Feng, "Performance Study of an Enhanced Downlink Control Channel Design for LTE," in *Proc. of IEEE 75th Vehicular Technology Conference (VTC 2012 Spring)*, Yokohama (Japan), May. 6–9, 2012.

[264] W. Yi, Z. Hua, and W. Jianming, "The Search Space Design for enhanced Downlink Control Channel in LTE-Advanced System," in *Proc. of 8th International Conference on Wireless and Mobile Communications (ICWMC 2012)*, Venice (Italy), Jun. 24–29, 2012.

[265] Y. Zhu, A. Li, and A. Harada, "Novel Method to Improve Control Channel Reliability in LTE-Advanced Heterogeneous Network," in *Proc. of IEEE 76th Vehicular Technology Conference (VTC 2012 Fall)*, Québec City (Canada), Sep. 3–6, 2012.

[266] "IEEE Standard for a Precision Clock Synchronization Protocol for Networked Measurement and Control Systems," *IEEE Std 1588-2008 (Revision of IEEE Std 1588-2002)*, Jul. 2008.

[267] International Telecommunication Union (ITU), *ICTs and Climate Change*, 2007. Technology Watch Report 3.

[268] H. Claussen, L. T. W. Ho, and F. Pivit, "Effects of Joint Macrocell and Residential Picocell Deployment on the Network Energy Efficiency," in *Proc. of IEEE 19th International Symposium on Personal, Indoor and Mobile Radio Communications (PIMRC 2008)*, Cannes (France), Sep. 15–18, 2008.

[269] D. Cao, S. Zhou, C. Zhang, and Z. Niu, "Energy Saving Performance Comparison of Coordinated Multi-Point Transmission and Wireless Relaying," in *Proc. of IEEE Global Telecommunications Conference (GLOBECOM 2010)*, Miami (United States), Dec. 6–10, 2010.

[270] F. Richter, A. Fehske, and G. Fettweis, "Energy Efficiency Aspects of Base Station Deployment Strategies for Cellular Networks," in *Proc. of IEEE 70th Vehicular Technology Conference (VTC 2009 Fall)*, Anchorage (United States), Sep. 20–23, 2009.

[271] M. Marsan, S. Buzzi, D. Ciullo, and M. Meo, "Optimal Energy Savings in Cellular Access Networks," in *Proc. of IEEE International Conference on Communications (ICC 2009)*, Dresden (Germany), Jun. 14–18, 2009.

[272] G. Li, Z. Xu, C. Xiong, C. Yang, S. Zhang, Y. Chen, and S. Xu, "Energy-efficient Wireless Communications: Tutorial, Survey, and Open Issues," *IEEE Wireless Communications*, vol. 18, no. 6, pp. 28–35, Dec. 2011.

[273] D. Feng, C. Jiang, G. Lim, J. Cimini, L.J., G. Feng, and G. Li, "A Survey of Energy-efficient Wireless Communications," *IEEE Communication Surveys & Tutorials*, vol. 15, no. 1, pp. 167–178, Feb. 2013.

[274] J. Palicot, "Cognitive Radio: An Enabling Technology for the Green Radio Communications Concept," in *Proc. of 5th Wireless Communications and Mobile Computing Conference (IWCMC 2009)*, Leipzig (Germany), Jun. 21–24, 2009.

[275] C. Han, T. Harrold, S. Armour, I. Krikidis, S. Videv, P. M. Grant, H. Haas, J. Thompson, I. Ku, C.-X. Wang, T. A. Le, M. Nakhai, J. Zhang, and L. Hanzo, "Green Radio: Radio Techniques to Enable Energy-efficient Wireless Networks," *IEEE Communications Magazine*, vol. 49, no. 6, pp. 46–54, May. 2011.

[276] I. Humar, X. Ge, L. Xiang, M. Jo, M. Chen, and J. Zhang, "Rethinking Energy Efficiency Models of Cellular Networks with Embodied Energy," *IEEE Network*, vol. 25, no. 2, pp. 40–49, Mar. 2011.

[277] E. Oh and B. Krishnamachari, "Energy Savings through Dynamic Base Station Switching in Cellular Wireless Access Networks," in *Proc. of IEEE Global Telecommunications Conference (GLOBECOM 2010)*, Miami (United States), Dec. 6–10, 2010.

[278] M. Marsan, S. Buzzi, D. Ciullo, and M. Meo, "Switch-Off Transients in Cellular Access Networks with Sleep Modes," in *Proc. of IEEE International Conference on Communications (ICC 2011)*, Kyoto (Japan), Jun. 5–9, 2011.

[279] A. Conte, A. Feki, S. Buzzi, D. Ciullo, M. Meo, and M. Ajmone Marsan, "Cell Wilting and Blossoming for Energy Efficiency," *IEEE Wireless Communications*, vol. 18, no. 5, pp. 50–57, Oct. 2011.

[280] J. Zhou, M. Li, L. Liu, X. She, and L. Chen, "Energy Source Aware Target Cell Selection and Coverage Optimization for Power Saving in Cellular Networks," in *Proc. of 2010 IEEE/ACM International Conference on Green Computing and Communications (GreenCom 2010)*, Hangzhou (China), Dec. 18–20, 2010.

[281] L. Saker and S. Elayoubi, "Sleep Mode Implementation Issues in Green Base Stations," in *Proc. of IEEE 21st International Symposium on Personal, Indoor and Mobile Radio Communications (PIMRC 2010)*, Istanbul (Turkey), Sep. 26–29, 2010.

[282] S.-E. Elayoubi, L. Saker, and T. Chahed, "Optimal Control for Base Station Sleep Mode in Energy Efficient Radio Access Networks," in *Proc. of 30th Annual Joint Conference of the IEEE Computer and Communications Societies (INFOCOM 2011)*, Shanghai (China), Apr. 10–15, 2011.

[283] F. Alaca, A. B. Sediq, and H. Yanikomeroglu, "A Genetic Algorithm based Cell Switch-Off Scheme for Energy Saving in Dense Cell Deployments," in *Proc. of IEEE Global Telecommunications Conference (GLOBECOM 2012)*, Anaheim (United States), Dec. 3–7, 2012.

[284] L. Xiang, F. Pantisano, R. Verdone, X. Ge, and M. Chen, "Adaptive Traffic Load-Balancing for Green Cellular Networks," in *Proc. of IEEE 22nd International Symposium on Personal, Indoor and Mobile Radio Communications (PIMRC 2011)*, Toronto (Canada), Sep. 11–14, 2011.

[285] Y. Wu and Z. Niu, "Energy Efficient Base Station Deployment in Green Cellular Networks with Traffic Variations," in *Proc. of IEEE International Conference on Communications in China (ICCC 2012)*, Beijing (China), Aug. 15–17, 2012.

[286] A. Bousia, E. Kartsakli, L. Alonso, and C. Verikoukis, "Energy Efficient Base Station Maximization Switch Off Scheme for LTE-Advanced," in *Proc. of IEEE 17th IEEE International Workshop on Computer Aided Modeling and Design of Communication Links and Networks (CAMAD 2012)*, Barcelona (Spain), Sep. 17–19, 2012.

[287] T. Han and N. Ansari, "Optimizing Cell Size for Energy Saving in Cellular Networks with Hybrid Energy Supplies," in *Proc. of IEEE Global Telecommunications Conference (GLOBECOM 2012)*, Anaheim (United States), Dec. 3–7, 2012.

[288] S. Morosi, E. Del Re, and P. Piunti, "Traffic Based Energy Saving Strategies for Green Cellular Networks," in *Proc. of 18th European Wireless Conference (EW 2012)*, Poznan (Poland), Apr. 18–20, 2012.

[289] S. Zhou, J. Gong, Z. Yang, Z. Niu, and P. Yang, "Green Mobile Access Network with Dynamic Base Station Energy Saving," in *Proc. of ACM 15th Annual International Conference on Mobile Computing and Networking (MobiCom 2009)*, Beijing (China), Sep. 20–25, 2009.

[290] R. Litjens and L. Jorguseski, "Potential of Energy-Oriented Network Optimisation: Switching Off Over-Capacity in Off-Peak Hours," in *Proc. of IEEE 21st International Symposium on Personal, Indoor and Mobile Radio Communications (PIMRC 2010)*, Istanbul (Turkey), Sep. 26–29, 2010.

[291] J. Gong, S. Zhou, Z. Niu, and P. Yang, "Traffic-Aware Base Station Sleeping in Dense Cellular Networks," in *Proc. of 18th IEEE International Workshop on Quality of Service (IWQoS 2010)*, Beijing (China), Jun. 16–18, 2006.

[292] T. Kang, X. Sun, and T. Zhang, "Base Station Switching Based Dynamic Energy Saving Algorithm for Cellular Networks," in *Proc. of 3rd IEEE International Conference on Network Infrastructure and Digital Content (ICNIDC 2012)*, Beijing (China), Sep. 21–23, 2012.

[293] L. Saker, S.-E. Elayoubi, and T. Chahed, "Minimizing Energy Consumption via Sleep Mode in Green Base Station," in *Proc. of IEEE Wireless Communications and Networking Conference (WCNC 2010)*, Sydney (Australia), Apr. 18–21, 2010.

[294] C. Peng, S.-B. Lee, S. Lu, H. Luo, and H. Li, "Traffic-Driven Power Saving in Operational 3G Cellular Networks," in *Proc. of ACM 17th Annual International Conference on Mobile Computing and Networking (MobiCom 2011)*, Las Vegas (United States), Sep. 19–23, 2011.

[295] Z. Niu, Y. Wu, J. Gong, and Z. Yang, "Cell Zooming for Cost-Efficient Green Cellular Networks," *IEEE Communications Magazine*, vol. 48, no. 11, pp. 74–79, Nov. 2010.

[296] L. Sanchez and L. Munoz, "Energy Efficiency of Simple ON/OFF Scheme in Mobile Cellular Networks," *Electronic Letters*, vol. 46, no. 20, pp. 1404–1405, Sep. 2010.

[297] R. Li, Z. Zhao, X. Zhou, and H. Zhang, "Energy Savings Scheme in Radio Access Networks via Compressive Sensing-based Traffic Load Prediction," *Transactions on Emerging Telecommunications Technologies*, vol. PP, no. 99, pp. 1–11, Aug. 2012.

[298] S. Morosi, P. Piunti, and E. D. Re, "Sleep Mode Management in Cellular Networks: A Traffic Based Technique Enabling Energy Saving," *Transactions on Emerging Telecommunications Technologies*, vol. PP, no. 99, pp. 1–11, Jan. 2013.

[299] J.-M. Kelif, M. Coupechoux, and F. Marache, "Limiting Power Transmission of Green Cellular Networks: Impact on Coverage and Capacity," in *Proc. of IEEE International Conference on Communications (ICC 2010)*, Cape Town (South Africa), May. 23–27, 2010.

[300] I. Siomina and D. Yuan, "Analysis of Cell Load Coupling for LTE Network Planning and Optimization," *IEEE Transactions on Wireless Communications*, vol. 11, no. 6, pp. 2287–2297, Jun. 2012.

[301] Kathrein Inc., *800 10271 Tri-sector Antenna - Technical Specifications.* Available online at: www.kathrein-scala.com.

[302] R. Verdone, H. Buehler, N. Cardona, A. Munna, R. Patelli, S. Ruiz, P. Grazioso, A. Zanella, A. Eisenblätter, and H. Geerdes, *MORANS White Paper - Update.* COST 273, Athens (Greece), Rep. available as TD(04)062, Jan. 26–28, 2004.

[303] *TR 25.942 - RF System Scenarios.* 3GPP Technical Report. Available online at: www.3gpp.org.

[304] *Urban Transmission Loss Models for Mobile Radio in the 900- and 1,800 MHz Bands (Revision 2).* COST 231, The Hague (The Netherlands), Rep. available as TD(90)119, Sep., 1991.

[305] R. Fraile, O. Lázaro, and N. Cardona, *Two Dimensional Shadowing Model.* COST 273, Prague (Czec Republic), Rep. available as TD(03)171, Sep. 24–26, 2003.

[306] D. Young and N. Beaulieu, "The Generation of Correlated Rayleigh Random Variates by Inverse Discrete Fourier Transform," *IEEE Transactions on Communications*, vol. 48, no. 7, pp. 1114–1127, Jul. 2000.

[307] D. Laselva, F. Capozzi, F. Frederiksen, K. Pedersen, J. Wigard, and I. Kovacs, "On the Impact of Realistic Control Channel Constraints on QoS Provisioning in UTRAN LTE," in *Proc. of IEEE 70th Vehicular Technology Conference (VTC 2009 Fall)*, Anchorage (United States), Sep. 20–23, 2009.

[308] HTC, *R1-122331: eREG and eCCE Definitions for ePDCCH.* 3GPP, May 2012. Radio Access Network (RAN) Working Group 1, Meeting #69: Prague, Czech Republic.

[309] A. Stevens, *Teach Yourself C++.* Wiley, 7th ed., 2003.

[310] D. Chapman, *Teach Yourself Visual C++ 6 in 21 days.* Sams, Macmillan Computer Publishing, 1st ed., 1998.

[311] W. H. Press, S. A. Teukolsky, W. T. Vetterling, and B. P. Flannery, *Numerical Recipes, The Art of Scientific Computing.* Cambridge University Press, 3rd ed., 2007.

[312] M. M. S. Marwangi, N. Fisal, S. K. S. Yusof, R. Rashid, A. Ghafar, F. Saparudin, and N. Katiran, "Challenges and Practical Implementation of Self-Organizing Networks in LTE/LTE-Advanced Systems," in *Proc. of International Conference on Information Technology and Multimedia (ICIM 2011)*, Kuala Lumpur (Malaysia), Nov. 14–16, 2011.

[313] X. Li, H. Jin, J. Jiang, S. Hou, M. Peng, and G. Wang, "A Gradient Projection based Self-Optimizing Algorithm for Inter-cell Interference Coordination in Downlink OFDMA Networks," in *Proc. of 7th International ICST Conference on Communications and Networking in China (CHINACOM 2012)*, Kunming (China), Aug. 8–10, 2012.

[314] W. Bo, S. Yu, Z. Lv, and J. Wang, "A Novel Self-Optimizing Load Balancing Method Based on Ant Colony in LTE Network," in *Proc. of 8th International Conference on Wireless Communications, Networking and Mobile Computing (WiCOM 2012)*, Shanghai (China), Sep. 21–23, 2012.

[315] A. Temesvary, "Self-Configuration of Antenna Tilt and Power for Plug & Play Deployed Cellular Networks," in *Proc. of IEEE Wireless Communications and Networking Conference (WCNC 2009)*, Budapest, Hungary. Apr. 5–8, 2009.

[316] K. Samdanis and M. Brunner, "Self-Organized Network Management Functions for Relay Enhanced LTE-Advanced Systems," in *Proc. of IEEE 22nd International Symposium on Personal, Indoor and Mobile Radio Communications (PIMRC 2011)*, Toronto (Canada), Sep. 11–14, 2011.

[317] T. Komine, T. Yamamoto, and S. Konishi, "A Proposal of Cell Selection Algorithm for LTE Handover Optimization," in *Proc. of 17th IEEE Symposium on Computers and Communications (ISCC 12)*, Cappadocia (Turkey), Jul. 1–4, 2012.

[318] I.-H. Hou and C. S. Chen, "An Energy-Aware Protocol for Self-Organizing Heterogeneous LTE Systems," *IEEE Journal on Selected Areas in Communications*, vol. 31, no. 5, pp. 937–946, May. 2013.

[319] B. Soret, H. Wang, K. Pedersen, and C. Rosa, "Multicell Cooperation for LTE-Advanced Heterogeneous Network Scenarios," *IEEE Wireless Communications*, vol. 20, no. 1, pp. 27–34, Feb. 2013.

[320] D. Villa, C. Castellanos, I. Kovacs, F. Frederiksen, and K. Pedersen, "Performance of Downlink UTRAN LTE under Control Channel Constraints," in *Proc. of IEEE 67th Vehicular Technology Conference (VTC 2008 Spring)*, Marina Bay (Singapore), May. 11–14, 2008.

Publications of the author.

[J1] **D. González G**, M. García-Lozano, S. Ruiz, and J. Olmos, "On the Need for Dynamic Downlink Intercell Interference Coordination for Realistic Long Term Evolution Deployments," *Wireless Communications and Mobile Computing*, pp. 1–26, Feb. 2012.

[J2] **D. González G**, M. García-Lozano, S. Ruiz, and J. Olmos, "Improving the Interplay between Periodic Channel State Information Feedback and Static Intercell Interference Coordination in LTE," *Journal of Communications* (Special Issue on Interference Management for 4G Networks), vol. 7, no. 9, pp. 660–675, Sep. 2012.

[J3] **D. González G**, M. García-Lozano, S. Ruiz, and D. Lee, "Optimization of Soft Frequency Reuse for Irregular LTE Macrocellular Networks," *IEEE Transactions on Wireless Communications*, vol. 12, no. 5, pp. 2410–2423, May. 2013.

[J4] **D. González G**, M. García-Lozano, S. Ruiz, and D. Lee, "A Metaheuristic based Downlink Power Allocation for LTE/LTE-A Cellular Deployments," *Wireless Networks*, Accepted for publication, Sep. 2013.

[**J5**] **D. González G**, M. García-Lozano, S. Ruiz, María A. Lema, and D. Lee, "Multiobjective Optimization of Fractional Frequency Reuse for Irregular OFDMA Macrocellular Deployments," *Telecommunication Systems*, Accepted for publication, Oct. 2013.

[**P1**] **D. González G**, H. Yanikomeroglu, and G. Senarath, "A System and Method for a Multiobjective Framework for Cell Switch-Off in Dense Cellular Networks." US Provisional Patent Application, Serial no: 61847403, Filed by Huawei, Canada. Application date: Jul. 2013.

[**B1**] N. Cardona, J. Olmos, J. Monserrat, M. García-Lozano (ed.), *3GPP LTE: Hacia la 4G móvil* (in Spanish). Barcelona, Spain: Marcombo, S.A., 1st ed., 2011. Chapter entitled: *Gestión de Recursos Radio* (Radio Resource Management).

[**B2**] R. Santos, A. Block, and V. Rangel (ed.), *Broadband Wireless Access Networks for 4G: Theory, Application and Experimentation.* Hershey (PA), United States: IGI Global, 1st ed., 2013. Chapter entitled: *Aperiodic ICIC-Oriented CSI Reporting for LTE Networks*.

[**LN1**] **D. González G**, M. García-Lozano, S. Ruiz, and J. Olmos, "Static Inter-Cell Interference Coordination Techniques for LTE Networks: A Fair Performance Assessment," in *Multiple Access Communications* (A. Vinel, B. Bellalta, C. Sacchi, A. Lyakhov, M. Telek, and M. Oliver, eds.), vol. 6235 of *Lecture Notes in Computer Science*, pp. 211–222, Springer Berlin Heidelberg, 2010.

[**LN2**] **D. González G**, M. García-Lozano, S. Ruiz, and J. Olmos, "On the Performance of Static Inter-cell Interference Coordination in Realistic Cellular Layouts," in *Mobile Networks and Management* (K. Pentikousis, R. Agüero, M. García-Arranz, and S. Papavassiliou, eds.), vol. 68 of *Lecture Notes of the Institute for Computer Sciences, Social Informatics and Telecommunications Engineering*, pp. 163–176, Springer Berlin Heidelberg, 2011.

[**C1**] **D. González G**, S. Ruiz, M. García-Lozano, J. Olmos, and A. Serra, "System Level Evaluation of LTE Networks with Semidistributed Intercell Interference Coordination," in *Proc. of IEEE 20th International Symposium on Personal, Indoor and Mobile Radio Communications (PIMRC 2009)*, Tokyo (Japan), Sep. 13–16, 2009.

[**C2**] **D. González G**, V. Corvino, S. Ruiz, J. Olmos, M. García-Lozano, and R. Verdone, "Downlink Resource Allocation in LTE: Centralized vs. Distributed Approach," in *Proc. of Joint COST2100/NEWCOM++ Workshop on Radio Resource Allocation for LTE*, Vienna (Austria), Sep. 30, 2009.

[**C3**] **D. González G**, M. García-Lozano, V. Corvino, S. Ruiz, and J. Olmos, "Performance Evaluation of Downlink Interference Coordination Techniques in LTE Networks," in *Proc. of IEEE 72nd Vehicular Technology Conference (VTC 2010 Fall)*, Ottawa (Canada), Sep. 6–9, 2010.

[**C4**] **D. González G**, M. García-Lozano, S. Ruiz, and J. Olmos, "Static Inter-Cell Interference Coordination Techniques for LTE Networks: A Fair Performance

Assessment," in *Proc. of 3rd Int. Workshop on Multiple Access Communications (MACOM 2010)*, Barcelona (Spain), Sep. 13–14, 2010.

[C5] **D. González G**, M. García-Lozano, S. Ruiz, and J. Olmos, "On the Performance of Static Inter-cell Interference Coordination in Realistic Cellular Layouts," in *Proc. of 2nd Int. ICST Conference on Mobile Networks and Management (MONAMI 2010)*, Santander (Spain), Sep. 22–24, 2010.

[C6] **D. González G**, M. García-Lozano, S. Ruiz, and J. Olmos, "An Analytical View of Static Intercell Interference Coordination Techniques in OFDMA Networks," in *Proc. of IEEE Wireless Communications and Networking Conference Workshops (WCNCW 2012)*, Paris (France), Apr. 1–4, 2012.

[C7] **D. González G**, M. García-Lozano, S. Ruiz, and J. Olmos, "Improving Channel State Information Feedback for Static Intercell Interference Coordination in LTE," in *Proc. of IEEE International Conference on Communications (ICC 2012)*, Ottawa (Canada), Jun. 10–15, 2012.

[C8] **D. González G**, M. García-Lozano, S. Ruiz, and J. Olmos, "On the Role of Downlink Control Information in the Provision of QoS for NRT Services in LTE," in *Proc. of IEEE 75th Vehicular Technology Conference (VTC 2012 Spring)*, Yokohama (Japan), May. 6–9, 2012.

[C9] **D. González G**, M. García-Lozano, S. Ruiz, J. Olmos, and D. Lee, "Optimization of Realistic Full Frequency Reuse OFDMA-based Cellular Networks," in *Proc. of IEEE 23rd International Symposium on Personal, Indoor and Mobile Radio Communications (PIMRC 2012)*, Sydney (Australia), Sep. 9–12, 2012.

[C10] **D. González G**, M. García-Lozano, S. Ruiz, and D. Lee, "Improving Soft Frequency Reuse for Realistic OFDMA-based Cellular Deployments," in *Proc. of IEEE Global Telecommunications Conference (GLOBECOM 2012)*, Anaheim (United States), Dec. 3–7, 2012.

[C11] **D. González G**, M. García-Lozano, S. Ruiz, M. Lema, and D. Lee, "Adapting Fractional Frequency Reuse to Realistic OFDMA Cellular Networks," in *Proc. of 6th Joint IFIP Wireless and Mobile Networking Conference (WMNC 2013)*, Dubai (United Arab Emirates), Apr. 23–25, 2013.

[C12] **D. González G**, M. García-Lozano, and S. Ruiz, "Power Allocation for the PDCCH in LTE: A Way to Increase its Capacity in Realistic Deployments," in *Proc. of Wireless Personal Multimedia Communications Symposium (WPMC 2013)*, Atlantic City (United States), Jun. 24–27, 2013.

[C13] **D. González G**, M. García-Lozano, and S. Ruiz, "Intercell Interference Coordination for the ePDCCH in LTE-Advanced Macrocellular Deployments," in *Proc. of 9th International Conference on Wireless and Mobile Communications (ICWMC 2013)*, Nice (France), Jul. 21–26, 2013.

[**CA1**] **D. González G**, S. Ruiz, J. Olmos, M. García-Lozano, and A. Serra, "Link and System Level Simulation of Downlink LTE," COST 2100, Braunschweig (Germany), Rep. available as TD(09)734, Feb. 16–18, 2009.

[**CA2**] **D. González G**, M. García-Lozano, S. Ruiz, and J. Olmos, "Performance Evaluation of Static Intercell Interference Coordination in Realistic Cellular Layouts," COST 2100, Aalborg (Denmark), Rep. available as TD(10)11053, Jun. 2–4, 2010.

[**CA3**] **D. González G**, M. García-Lozano, S. Ruiz, and J. Olmos, "A Novel ICIC-Oriented Channel State Information Feedback Scheme for Aperiodic Reporting in LTE," COST IC1004, Barcelona (Spain), Rep. available as TD(12)03038, Feb. 8–10, 2012.

[**CA4**] **D. González G**, M. García-Lozano, S. Ruiz, and J. Olmos, "Impact of Downlink Signaling Capacity Constraints on the Provision of QoS in LTE," COST IC1004, Lisbon (Portugal), Rep. available as TD(11)02041, Oct. 19–21, 2011.